HEMATITE - BARITE ALTERATION IN THE OWEN CONGLOMERATE, NORTH LYELL, TASMANIA

b y

Ian M Hart

Thesis submitted in partial fulfillment of the requirements for the degree of Masters of Economic Geology

National Key Centre for Ore Deposit and Exploration Studies

Geology Department,

University of Tasmania

October, 1993

ABSTRACT

The North Lyell mine area is located within the Mt. Read volcanics adjacent to the north-south trending Great Lyell Fault (GLF). It was one of the more copper rich deposits within the Mt. Lyell mining field having produced 5mt of ore with 5.3% Cu, 33 g/t Ag and 0.4 g/t Au. The main zone of mineralisation at North Lyell is located near the intersection of the GLF with the WNW trending North Lyell Fault. Although most of the bornite mineralisation at North Lyell occurred within the volcanics, there was bornite recognised within the Cambrian-Ordovician siliciclastic conglomerate which is also adjacent to the GLF.

The timing of alteration/mineralisation at North Lyell is reflected in the extent and style of alteration observed within the overlying conglomerates, sandstones and limestones. Extensive hematisation with associated barite occurs along the GLF between the volcanics and sediments. The hydrothermal hematisation associated with the mineralisation at North Lyell and Lyell Tharsis extends for some distance into the sediments. As the fluids progressed through the North Lyell system their compositions were modified by their interaction with the various host lithologies, producing distinct alteration assemblages within the surrounding units. Three main geochemical associations related to the alteration can be recognised in the North Lyell area; phosphate-hematite (Fe_2O_3+P_2O_5+La+Sb), sericite (K_2O+Al_2O_3+Cr+Rb) and barite (Ba+Sr+Sb). The barite assemblage is the least dispersed, being confined to the main fluid conduits and wallrocks.

The change in alteration styles from the weakly acidic, reduced sulphide rich volcanic environment, to the highly oxidised conditions within the conglomerate is reflected in the 'dumping' of hematite and pyrite on the GLF boundary. Computer modelling of the fluids show that this redox front alone cannot account for the observed mineralisation at North Lyell. The most successful mechanism for metal deposition was a thermal gradient coupled with the redox boundary. A fluid dominated system with input from the oxidised brines of the Owen Conglomerate produced an assemblage representative of the North Lyell mineralisation.

The recognition of detrital hematite clasts adjacent to the Haulage Unconformity, coupled with the concept of metal deposition in a relatively shallow environment, suggests the hydrothermal enrichment at North Lyell took place during Late Cambrian-Early Ordovician sedimentation.

TABLE OF CONTENTS

INTRODUCTION

The Mt Lyell Cu field lies on the eastern boundary of the north-south trending Cambrian Mt Read volcanics and consists of 20 pyritic-copper orebodies contained within a zone of intense sericite-quartz-chlorite-pyrite alteration. They occur predominantly within the mafic-felsic Central Volcanic Sequence on the faulted boundary with the overlying siliciclastic Owen Conglomerate. The orebodies are distributed between Mt. Lyell and Mt Owen, within Comstock and Linda valleys and together comprise one of the largest Cu producing fields in Australia. Since its discovery in 1833, recorded production figures from the field stand at 1.25 mt Cu, 740,000 kg Ag and 42,250 kg Au from 104 mt of ore (recorded production to July 1989)(Hills, 1990).

The North Lyell orebody occurs near the intersection of the N-S trending Great Lyell Fault and the NE-SW trending North Lyell Fault and transgresses the contact between the Cambrian volcanics and Ordovician conglomerate. The bulk of the mineralisation occurred within the Cambrian volcanics, however, alteration related to the mineralisation can be found within the overlying Ordovician conglomerate beds (Markham, 1968) and can be traced for some distance away from the mineralisation.

A small amount of high grade Cu mineralisation has been reported within the Owen Conglomerate at North Lyell (Wade and Solomon, 1959; Sillitoe, 1985), with the overlying conglomerate and sandstone units exhibiting a well defined zonation of alteration minerals. The bornite rich North Lyell deposit was one of the richest within the Mt. Lyell field, producing 5 mt of ore containing an average of 5.3% Cu, 33 g/t Ag and 0.4 g/t Au. Recorded production of metals (to July 1989) from North Lyell is 256 679 tonnes Cu, 161 906 kg Ag and 1 877 kg Au (Hills, 1990).

This mineralisation and alteration within the Late Cambrian to Ordovician Owen Conglomerate suggests a sole Cambrian volcanogenic mineralising event related to late stages of Mt Read volcanism is unlikely, unless deposition of the Owen Conglomerate occurred more quickly than previously thought, or there was a second phase of hydrothermal activity. For North Lyell and the other comparable high grade deposits, most authors currently accept a secondary Devonian mineralising event associated with the Tabberabberan orogeny, enriching a pre-existing Cambrian volcanogenic deposit (eg. Hendry, 1972, 1981; Solomon et al, 1987; Arnold, 1985 and Sillitoe, 1985). A Cambrian volcanogenic component to the mineralisation is suggested by subaqueous exhalative sulphide lenses at Tasman and Crown Lyell Extended. Markham (1968) noted the similarities in 'primary banding, macrofolding and deformation, and

recrystallisation structures of the sulphide minerals' between the Rosebery deposit and Tasman and Crown Lyell Extended. Pb isotope data from Tasman and Crown Lyell Extended plot directly on top of the Cambrian Rosebery and Hercules analyses (Gulson and Porritt, 1987; Gulson and Vaasjoki, 1987). A secondary hydrothermal overprint of this volcanogenic mineralisation is suggested by the presence of high grade Cu mineralisation within the conglomerates overlying and faulted against the volcanics.

There is strong hematite/barite alteration developed around the North Lyell and Lyell Tharsis deposits within the Owen Conglomerate, which is closely associated with the Cu mineralisation. The proximity of the hematitic oxidised conglomerate to the reduced pyritic environment of the volcanics suggests the presence of a narrow redox front associated with the faulted boundary (ie. the Great Lyell Fault). Hydrothermal fluids derived from the volcanics would have a similarly reduced character. If these fluids were carrying any metals, a sudden transition to a more oxidised environment may produce high grade mineralisation similar to that observed at North Lyell. Associated with this mineralisation will be a significant alteration halo which may extend through the stratigraphy to give an indication of the mineralisation timing. Zonation of alteration within the volcanics has been investigated by numerous authors (Wade and Solomon, 1958; Solomon, 1964; Green, 1971; Walshe, 1971; Reid, 1975; Walshe, 1977 and Hendry, 1981), although the effects of the hydrothermal alteration within the relatively fresh Owen Conglomerate and overlying sediments has never been analysed.

The aims of this study are to investigate the zonation of the alteration within the Owen Conglomerate adjacent to the North Lyell mineralisation (both along strike and across strike) and to use textural evidence from the altered Owen Conglomerate and associated rocks to establish the age of the associated North Lyell mineralisation. Thermodynamic computer modelling programs (CHILLER, SOLVEQ and GEOCAL) were also utilised to establish the composition of the alteration fluids and their predicted influence upon the sedimentary stratigraphy surrounding North Lyell. From this information and previously published data it is intended to produce a genetic model for mineralisation at Mt. Lyell.

PREVIOUS LITERATURE

The Mt Lyell field has been extensively studied since its discovery in 1883 with numerous models being proposed for the origin of the deposits. In the late 1800's Dr J.R. Robertson noted the similarities of the deposit to that of the Tharsis copper mine

in Spain (Blainey, 1954). A complete description of the Mt. Lyell deposit was not produced until J.W. Gregory (1905) proposed a Devonian, hydrothermal replacement model (after pervasive alteration of the Cambrian volcanics), associated with granite emplacement. This Devonian replacement model held sway for many years, being supported by such authors as Loftus Hills (1927), Nye et al (1934), Edwards (1939), Conolly (1947), Solomon (1957), and Wade and Solomon (1958). Regional studies of the area by Carey (1953) and Bradley, (1954, 1956, 1957) also concluded the deposits were of a Devonian, granitic hydrothermal origin within Cambrian volcanics, with emphasis on the structural control of the orebodies.

The first paper to suggest a Cambrian volcanogenic origin for the majority of the mineralisation was put forward by Hall and Solomon (1962) and supported by Campana and King (1963), Solomon (1964) and Solomon and Elms (1965). This was further expanded by Solomon (1967, 1969), using evidence from the Mid Cambrian Owen Conglomerate and Ordovician Gordon Limestone. Other authors to support the Cambrian volcanogenic model include Green (1971), Walshe (1971), Jago et al (1972), Corbett et al (1974), Bryant (1975), Reid (1975) and Solomon and Carswell (1989).

Geochemistry and mineralogy of the deposit was discussed by many authors including Loftus Hills (1967), Loftus Hills and Solomon (1967), Loftus Hills et al (1969), Markham (1963, 1968), Markham and Lawrence (1965), Markham and Otteman (1968), Walshe (1977), and Eastoe et al (1987). Walshe and Solomon (1981) proposed a subaerial depositional environment with a later hydrothermal event, Hendry (1972, 1981) examined the geochemistry and suggested a Cambrian subaqueous volcanogenic event with a Devonian remobilisation which was supported by Solomon et al (1987). Work by Arnold (1985) and Sillitoe (1985) suggests a Late Cambrian dual syngenetic - exhalative, epigenetic - replacement event is unlikely (ie. not just Cambrian mineralisation), with a possible Devonian remobilisation of the Cambrian mineralisation favoured.

Tectonics, structure, stratigraphy and mineralisation have been discussed by Corbett (1979,1981), Cox (1979, 1981), Solomon (1981) and Collins and Williams (1986). A more regional overview has been provided by authors such as Williams et al (1975), Whitford and Wallace (1984), Corbett and Lees (1987), and Corbett et al (1989). Several noteworthy papers were included in a special edition of Economic Geology (v. 87, 1992) devoted entirely to Tasmanian geology and mineral deposits, including Corbett et al, Crawford et al, and McPhie and Allen. A good general description of the Mt Lyell deposits and their history is provided by Hills, (1990).

REGIONAL GEOLOGY

The Mt. Lyell deposits occur on the west coast of Tasmania within rocks of the Mt Read Volcanics (MRV), which have been dated as Middle to Late Cambrian (McDougall and Leggo, 1965; Jago, 1979; and Adams et al, 1985). This N-S trending belt of lavas and volcaniclastic rocks forms the eastern margin of a group of Cambrian sediments which infills the elongate trough (Dundas Trough) between the eastern Precambrian Tyennan Block and the Precambrian Rocky Cape region to the west (Figure 1). The volcanic belt is bisected by the NNE trending Henty Fault Zone (HFZ) which separates a northwestern sequence hosting the mainly stratiform Pb-Zn-Au-Ag-Cu rich deposits of Hellyer, Rosebery and Que River, and a southeastern sequence containing the mainly Cu-Au-Ag rich Mt Lyell deposits (Campana et al, 1958; Solomon, 1981, and Eastoe et al, 1987).

The volcanic belt is composed of an eastern, relatively massive, lava rich zone with numerous intrusions and a wider western zone of volcano-sedimentary sequences rich in volcaniclastic mass flow sandstones and breccia (Corbett, 1992). Most sequences are thought to be deposited in submarine environments below wave base (McPhie and Allen, 1992), in young, orogenic continental margins (Solomon, 1981, Whitford and Wallace, 1984). The early volcanism was dominated by rhyolites-dacites followed by a period of andesitic-basaltic volcanism which was coincident with a period of active extension and rifting (Corbett, 1992). The deposits at Hellyer and Que River and some Mt. Lyell deposits were formed during this period. The last stage of volcanism within the belt was dominated by felsic, crystal and pumice rich mass flow deposits (Corbett, 1992).

On the southeastern side of the Henty fault, the volcanics have been divided into several groups (Corbett et al, 1974, Corbett and Lees, 1987; Corbett et al 1989 and Corbett, 1992) which include the basal clastic Sticht Range beds included with the Eastern quartz porphyritic sequence which underlies and interfingers with the 'Yolande River Sequence'. This sequence similarly underlies and interfingers with the 'Central Volcanic Complex' (CVC), and they are all overlain by the 'Tyndall Group' volcaniclastics. Cambrian granitoid bodies intrude the CVC at Mt Darwin and the Eastern Sequence at Mt Murchison (McDougall and Leggo, 1965; Black and Adams, 1980; Adams et al, 1985 and Corbett, 1992) and have been dated as 510 and 524±15 Ma respectively (Adams et al, 1985; McDougall and Leggo, 1965). There is some geophysical evidence for a continuous Cambrian granitoid ridge beneath Mt. Lyell linking Mt Darwin and Mt Murchison (Payne, 1991; Leaman and Richardson, 1989).

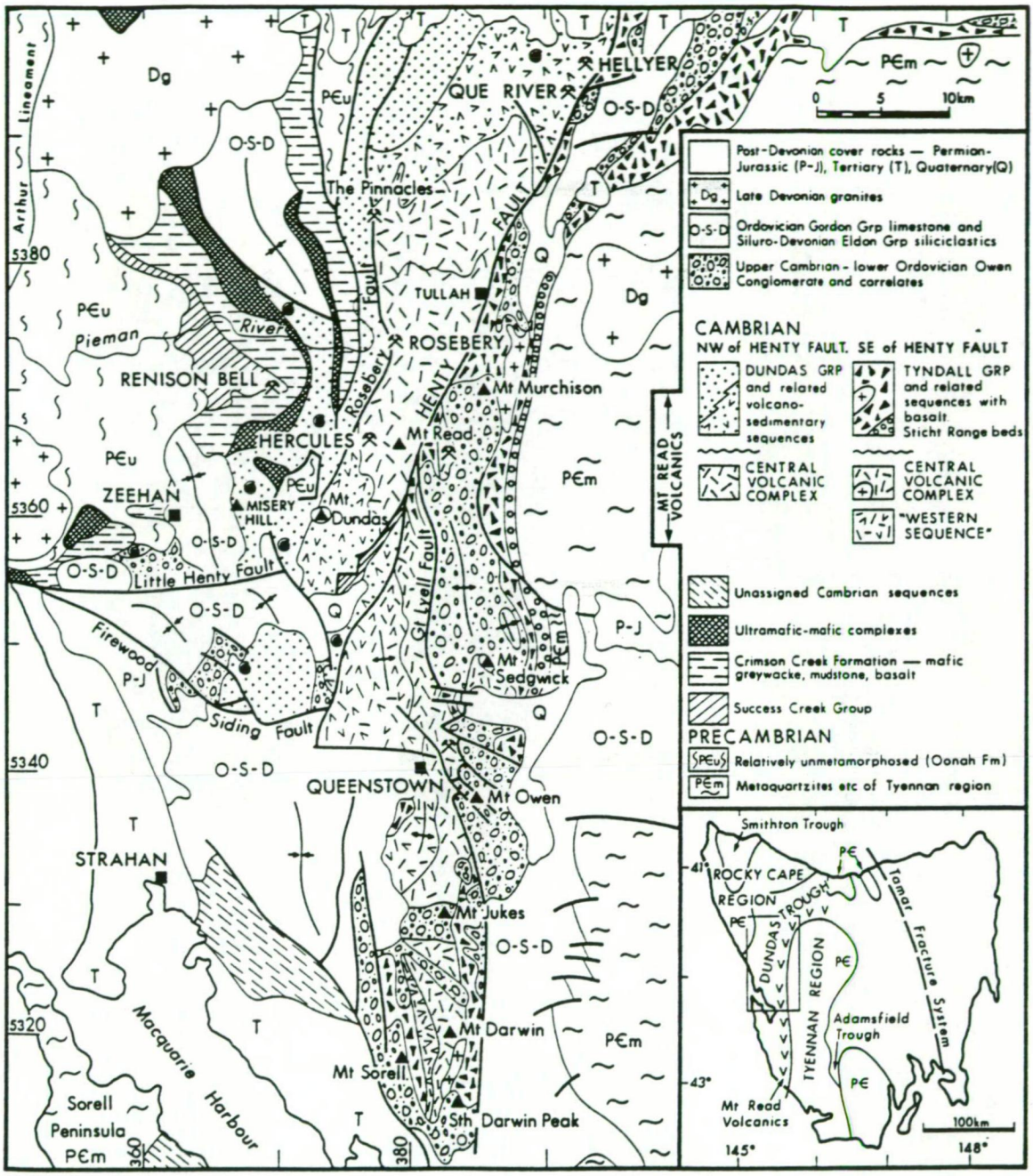

Figure 1 - General geology of central western Tasmania between Hellyer and Mt. Darwin showing Mt. Read Volcanics belt, Owen Conglomerate and associated sequences in the Dundas Trough, after Corbett and Solomon (1989).

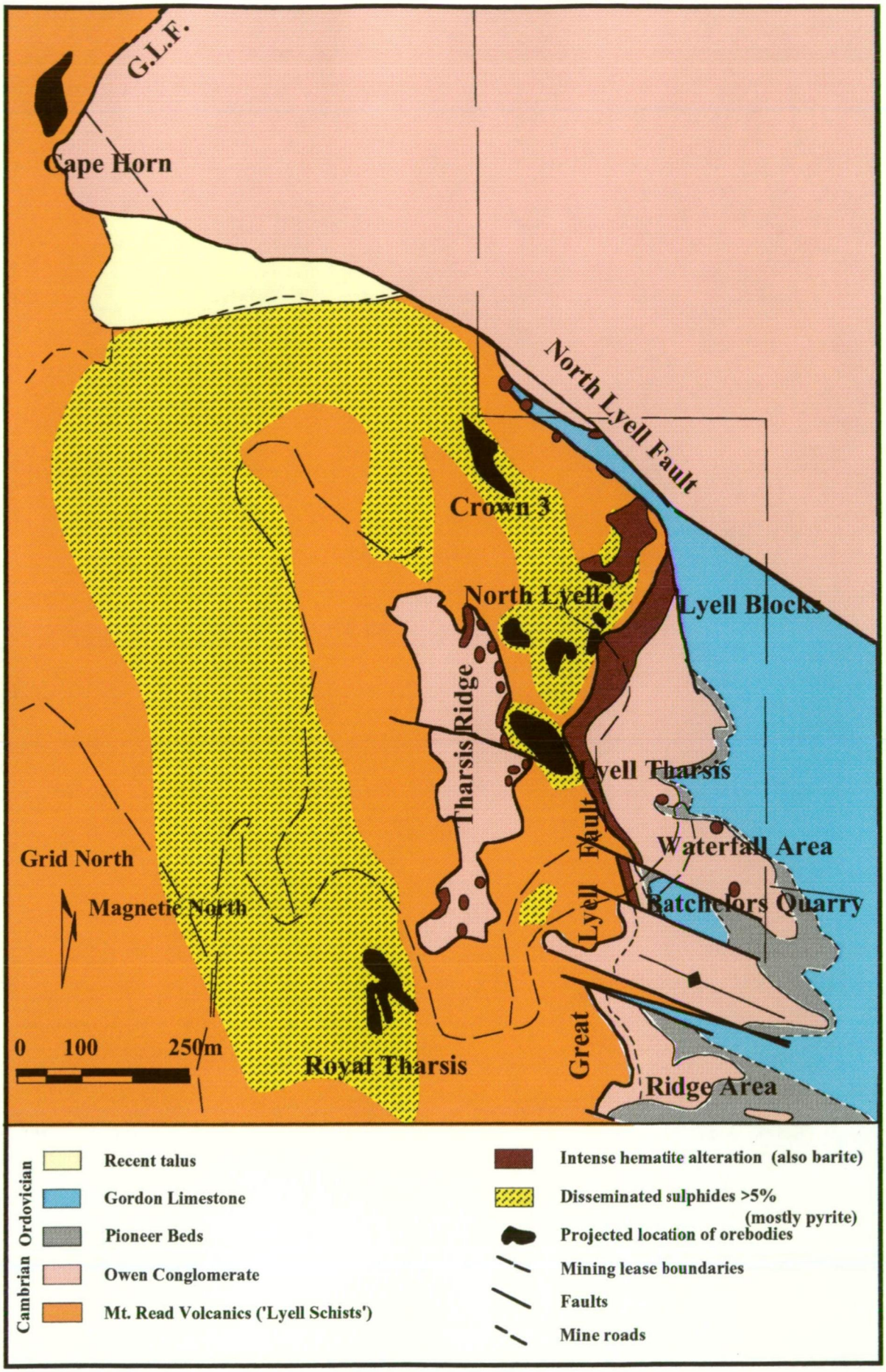

Figure 2 - Geology and alteration map of North Lyell mine area (modified after Hills, 1990)

The Cambrian volcanics are unconformably overlain by the sediments of the Late Cambrian to Ordovician Denison Group which include the siliciclastic Owen Conglomerate and the Pioneer beds. The Ordovician limestones and dark grey shales of the Gordon Group (upto 300m. thick) lie conformably on the Owen and contained some economic copper deposits.

The contact between the MRV and the Owen Conglomerate varies from an angular unconformity south of Queenstown (truncating the CVC, Tyndall Group and the Darwin Granite), to an apparently conformable contact between the west dipping Owen Conglomerate and the Tyndall volcaniclastics west of Lake Dora (Corbett and Turner, 1989). In the Mt. Lyell area the eastern margin of the CVC is faulted against the overlying Owen Conglomerate by the Great Lyell Fault (GLF), a longitudinal NNW-SSE structure with west side up movement. The HFZ and GLF are similar in style (steep westerly dipping faults), which are thought to shallow and join at depth and to have controlled the sedimentation of the Tyndall Group and Owen Conglomerate (Corbett and Solomon, 1989).

Cessation of volcanism and uplift of the Tyennan Block in the mid part of the Late Cambrian led to deposition of the Owen Conglomerate (Corbett and Turner, 1989). The GLF is thought to have been active during this period, forming the western scarp against which the Precambrian derived siliciclastic Owen Conglomerate was deposited. This western boundary was not breached until localised movement associated with the Haulage unconformity enabled transgression of marine sands of the Pioneer beds, onto the volcanics and other rocks on the western side of the Great Lyell Fault (Corbett et al, 1974; Reid, 1975).

The Owen Conglomerate is thought to be deposited as a series of continental alluvial fans formed as piedmont deposits around the margin of the uplifted Tyennan Block, in fault controlled graben structures, overlying Cambrian volcanic rocks (Corbett and Turner, 1989; Banks, 1962). A transgression to a marine environment towards the end of the Cambrian is suggested by the presence of marine fossils in the Upper Owen Conglomerate (Solomon, 1957; Banks, 1962). A period of marine sedimentation then followed which lasted from the Late Ordovician until the Middle Devonian when the Tabberabberan orogeny caused folding and faulting throughout most of Tasmania interrupting sedimentation.

Two main stages of Devonian folding and associated faulting have been recognised in the Mt. Lyell area with an earlier north-south fold generation being overprinted by folds with a NNW to WNW orientation. Numerous large postkinematic granitoid

plutons were emplaced in Western Tasmania in the later stages of the orogeny (Solomon et al, 1987), many of which are associated with mineralisation (eg. Renison Bell and Mt. Bischoff). Intrusive lamprophyre dykes appear to post date the cleavage and the mineralisation at Mt. Lyell and are thought to be Devonian or younger in age (Reid, 1975).

The Tabberabberan orogeny was followed by deposition of Permo-Triassic marine sediments which were intruded by Jurassic tholeiitic sills, with further faulting and sedimentation during the Mesozoic and Tertiary.

MINE SITE GEOLOGY

The major mineralisation at Mt Lyell occurs within the Cambrian rocks of the CVC which are composed of a series of acid lavas and pyroclastics of rhyolitic to dacitic composition with some andesitic lenses and minor shale (Corbett et al, 1974, and Reid, 1975). Cox, (1979, 1981) subdivided the CVC into six essentially conformable units (units A to F) varying from 0 to 800 metres in thickness. The felsic host rocks (unit D or 'the mine sequence' of Cox, 1979, 1981), range from 250 to 800 metres in thickness and are generally more intensely altered than the other rocks of the area. They consist of discontinuous, open framework volcanic breccia lenses, agglomerates, lapilli tuffs and lavas that are locally flow banded and were known as 'undifferentiated Lyell schists' by many earlier workers.

The main ore zone at North Lyell was closely associated with the intersection of the GLF and the WNW trending 12 West Fault which is thought to be a controlling factor in the mineralising event (Figure 2; Sillitoe, 1985). Mineralisation occurred primarily as coarse grained masses of bornite ± chalcopyrite ± covellite, within bodies of pyritic cherty quartz. Minor tennantite, galena, digenite, mawsonite, molybdenite, sphalerite, linnaeite, enargite, stromeyerite and rutile are associated with the mineralisation (Hills, 1990). Although the CVC is the principal host to mineralisation at North Lyell, bornite also occurs in the adjacent Owen Conglomerate (across the GLF), with some bornite masses showing relict pebble outlines on fresh faces (Wade and Solomon, 1958). Bornite rich ore was also mined from the eastern side of Lyell Tharsis adjacent to the hematite-barite alteration within the Owen Conglomerate (Arnold, 1985). Sillitoe (1985) notes that there is no fault displacement or truncation of the ore at the volcanics-conglomerate contact at North Lyell, suggesting the mineralisation was post deformation.

QUATERNARY

Moraine, alluvium

ELDON GROUP – SILURIAN

Crotty Quartzite

DENISON & GORDON GROUPS – ORDOVICIAN to UPPER CAMBRIAN

Ordovician limestone, shale (Gordon Group limestone)

Owen Conglomerate: Pioneer beds

Owen Conglomerate

MT READ VOLCANICS – UPPER CAMBRIAN

Tyndall Group

Felsic pyroclastics, post-mineralization

Siltstones, tuffs

Altered felsic volcanics (the "mine sequence")

Intermediate and felsic volcanics and intrusives, pre-mineralisation

Chert

Ore body

Siltstone, felsic and mafic volcanics (the western sequence)

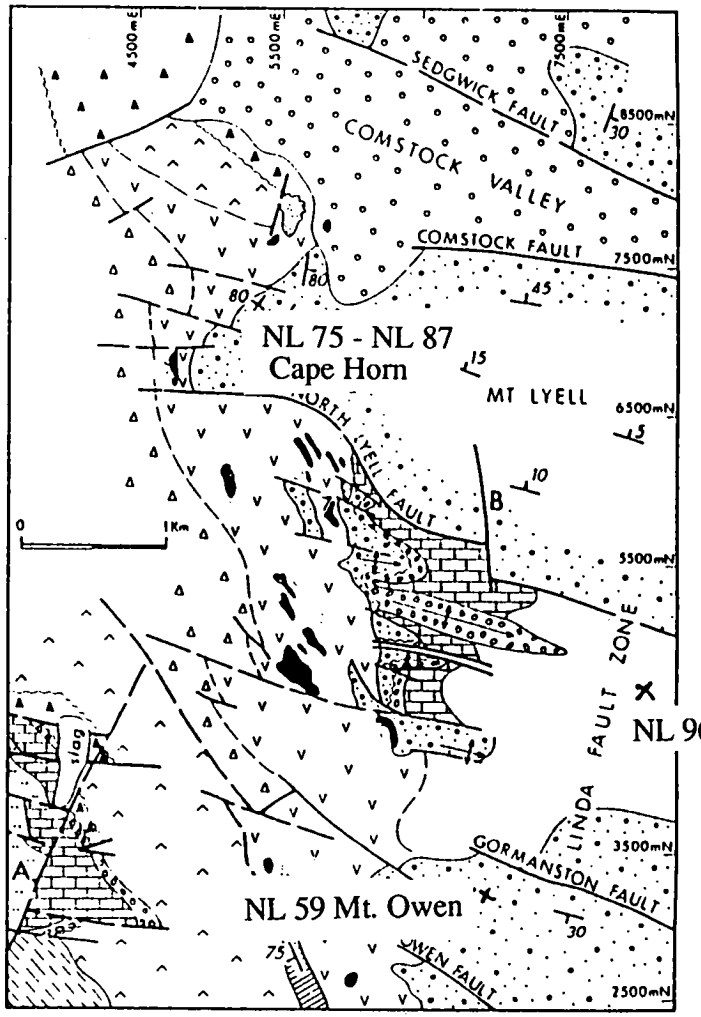

Figure 3 - Mt Lyell deposits and geology with locations of 'unaltered' samples of Owen Conglomerate and Pioneer Sandstone (after Solomon and Carswell, in Burrett et al. 1989)

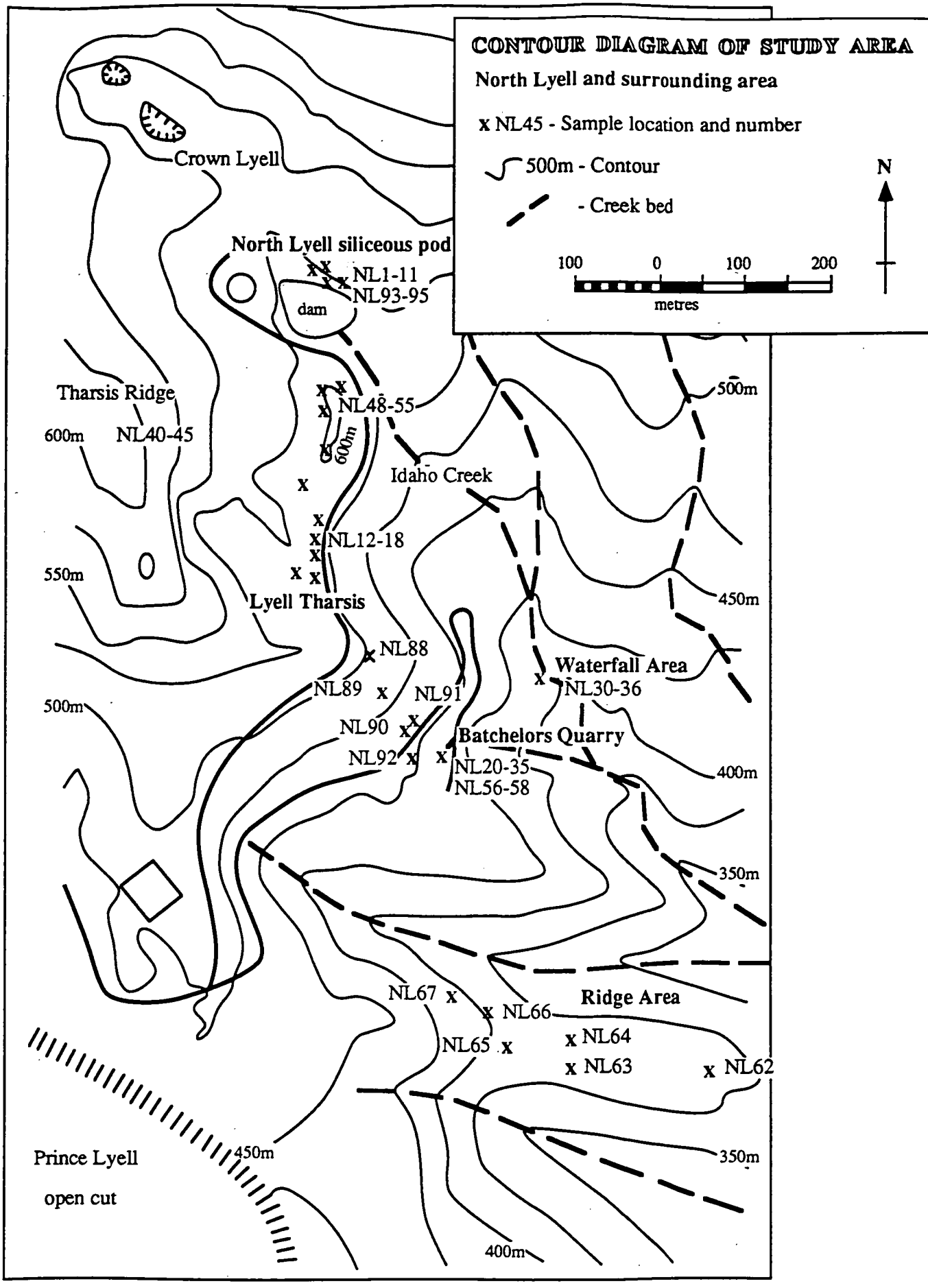

Figure 4 - Contour diagram of study area showing sample locations and different alteration areas

Alteration around North Lyell consists of an inner quartz-hematite-barite zone which grades outwards to a hematite-barite assemblage and then to a hematite zone. There is a strong host rock control on the secondary Fe-bearing minerals at North Lyell, with pyrite occurring mainly within the altered volcanics, and hematite in the conglomerate. Alteration/weathering within the Gordon Limestone is characterised by kaolinite + quartz with no carbonate preservation in any samples gathered from the North Lyell area. Native copper mineralisation has been exploited within the Gordon Limestone at Lyell Blocks, adjacent to the North Lyell area. Reid (1975) notes that river worn pebbles of native copper were intersected at the Pioneer Sandstone/Gordon Limestone interface suggesting either the copper was present when the Gordon Limestone was depositing or the contact forms a chemical boundary where copper has been enriched.

ALTERATION ASSOCIATED WITH THE NORTH LYELL MINERALISATION

As mentioned previously the Cu mineralisation at North Lyell occurs mainly within the sericite-pyrite-quartz altered volcanics but it has also been recognised replacing the adjacent Owen Conglomerate (Wade and Solomon, 1958; Sillitoe, 1985). Associated with this high grade Cu mineralisation is a halo of hydrothermal alteration which can be recognised within the adjacent Owen Conglomerate and Pioneer Beds (Markham, 1968; Sillitoe, 1985). The overlying Gordon Limestone appears as a dark grey-brown pug which contains very little or no carbonate adjacent to the alteration zone. This pug is not confined to the alteration areas however, similar examples of the Gordon can be found within areas unaffected by hydrothermal alteration. The types of alteration recognised within the Owen Conglomerate vary, depending upon a number of variables including;

- proximity to the hydrothermal system
- proximity to hydrothermal fluid conduits
- nature and the quantity of the fluids interacting with them.
- porosity of stratigraphy
- initial geochemical composition and mineralogy of stratigraphy
- degree of compaction of stratigraphy

Sixty samples of Owen Conglomerate, Pioneer sandstone and Gordon Limestone from locations within and around the Mt. Lyell lease were selected for detailed analysis (see Plates 1 to 5). This included thin section petrography, major and selected minor element X-ray fluorescence (XRF) analysis, selected X-ray diffraction (XRD) mineral identification, illite crystallinity of selected samples and electron microprobe analysis of some minerals. Samples were taken within the Owen Conglomerate from the North Lyell siliceous pod (Figure 5), along strike in the area between North Lyell and Lyell Tharsis (Figure 6), and across strike between Lyell Tharsis and Batchelors Quarry (Figures 2 and 3). Above the Haulage Unconformity, samples of the Pioneer Beds were obtained from Batchelors Quarry (Figure 7) and the Waterfall area (where the Owen Conglomerate-Pioneer Sandstone contact appears conformable), and adjacent to and along strike from the unconformity in the 'Ridge Area'. Samples of 'unaltered' Owen Conglomerate were obtained from Mt. Owen and Cape Horn Ridge adjacent to the mine lease (Figure 4). These areas were also utilised for observations of the stratigraphic variation in the clast composition within the Owen Conglomerate. Samples of the Gordon Limestone were obtained from the Waterfall area, Batchelors

Plate 1 North Lyell hematite-barite-silica alteration of Owen Conglomerate pod within volcanics.

Plate 2 Lyell Tharsis outcrop of hematite-barite altered Owen Conglomerate. Great Lyell Fault on left side of outcrop. North Lyell in background.

Plate 3 The Haulage unconformity at Batchelors Quarry with Owen Conglomerate beds on left, Pioneer Sandstone in middle and Gordon Limestone 'pug' on right.

Plate 4 A view down the 'Ridge Area' towards the east and Linda Valley. The Haulage Unconformity is in the bottom of the picture. See figure 3 for sample locations.

Plate 5 The Owen Conglomerate at Cape Horn. A traverse through the Owen Conglomerate was taken up this ridge to see if there was a host rock control on the North Lyell mineralisation.

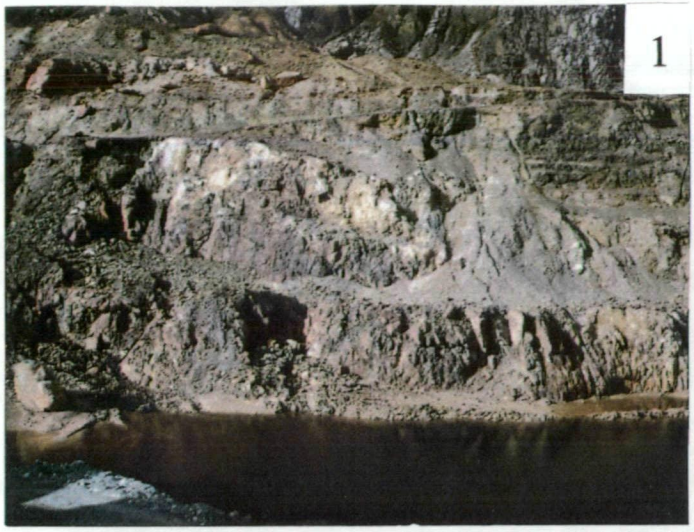
1

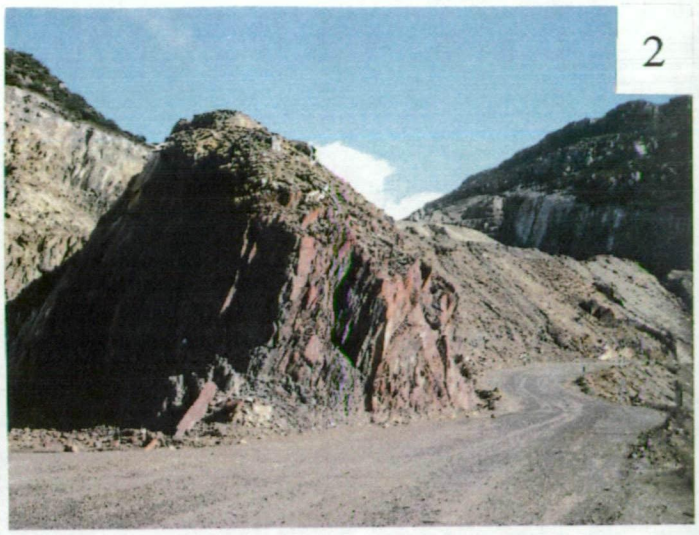
2


3


4


5

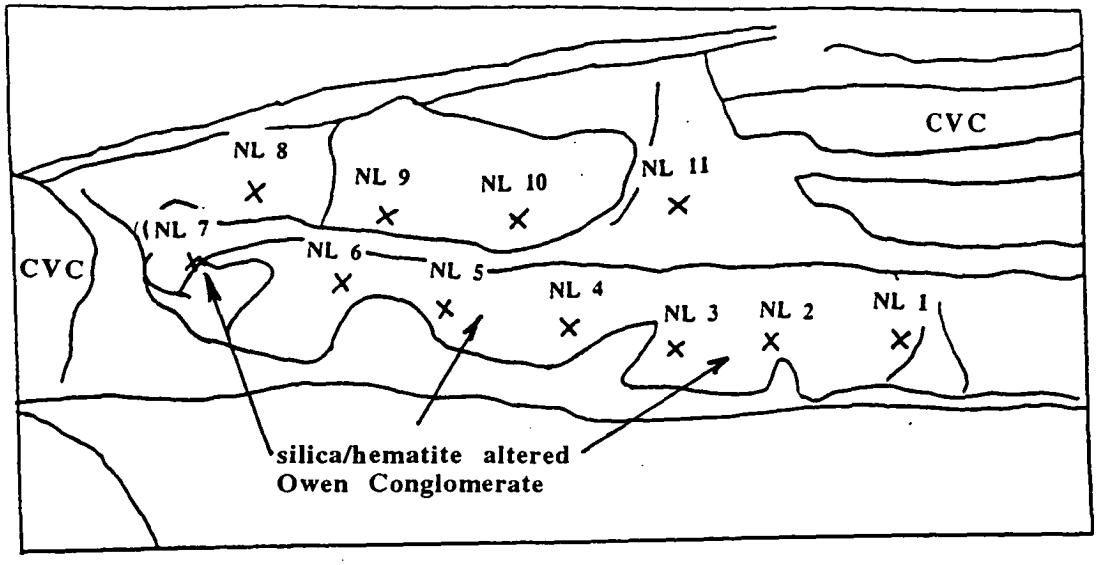

Figure 5 - Locations of samples obtained from North Lyell siliceous pod (see plate 1)

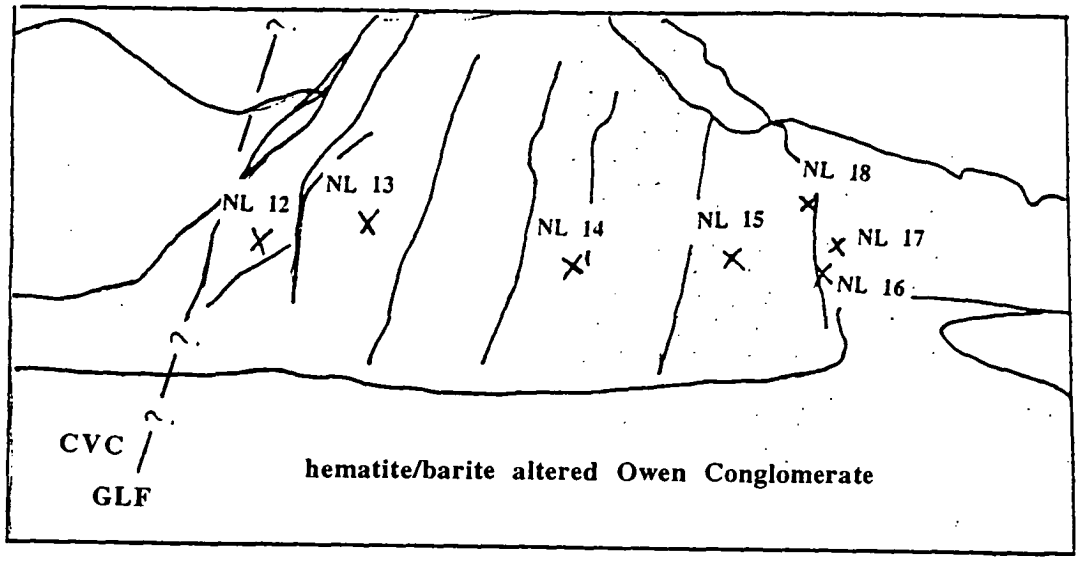

Figure 6 - Sample locations at Lyell Tharsis (see plate 2)

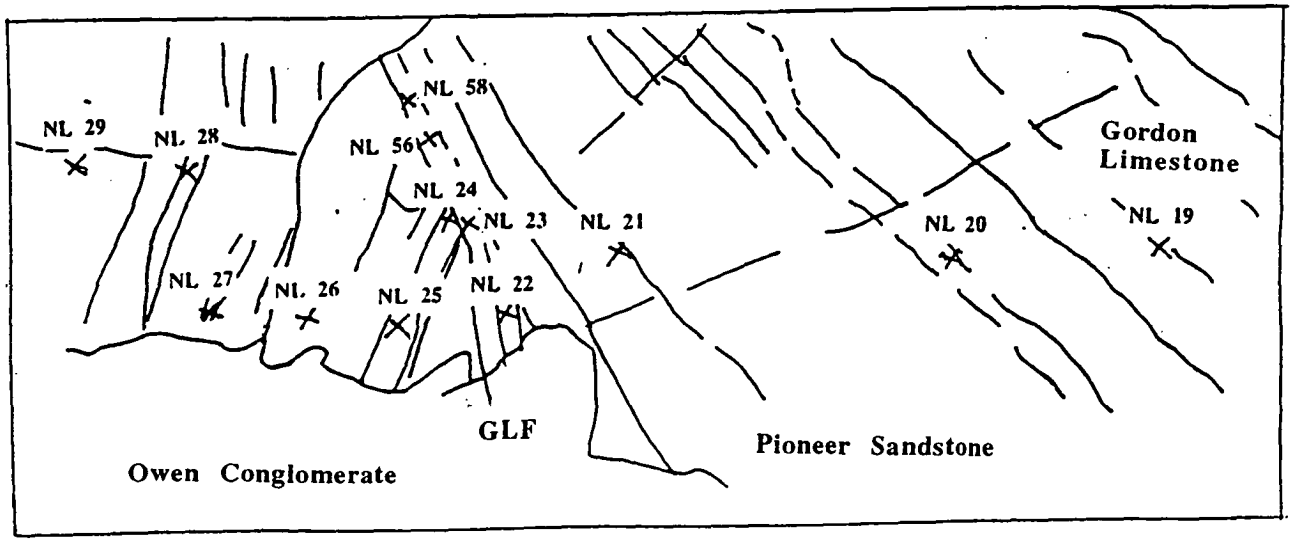

Figure 7 - Sample locations from Batchelors Quarry (see plate 3)

Quarry and Linda Valley for comparison of alteration/weathering within the mine area and surrounding it.

ALTERATION WITHIN THE OWEN CONGLOMERATE

The variations in alteration within the Owen Conglomerate are visible in both hand specimen and whole rock analyses. The most intensely altered samples were obtained from the highly silicified North Lyell pod which occurs as a large isolated outcrop within the volcanics adjacent to the old mine workings (Figure 5). Within these rocks all sedimentary textures, including clast outline, have been obscured by a process of quartz-hematite-barite flooding causing total recrystallisation of the major minerals. The samples obtained from Lyell Tharsis (Figure 6) have also undergone significant recrystallisation, however quartz is less dominant (more hematite-barite) and clast outlines can still be seen in thin section, and on outcrop scale within some of the totally hematised conglomerates. North Lyell and Lyell Tharsis are both closely associated with the N-S trending Great Lyell Fault and its intersection with NE-SW cross faults. Outcrop on Tharsis Ridge associated with cross faults display similar hematitic textures to Lyell Tharsis with excellent exposures of hematitic clasts within the conglomerate which were thought to have a sedimentary origin by some authors (Solomon, 1957, 1967), and a hydrothermal replacement origin by others (Arnold, 1985; Berry, 1991). The potential of these two theories are discussed from different perspectives in a later section.

These major fault intersections are thought to have been the major conduits for the mineralising fluids (Sillitoe, 1985; Berry, 1991), and show a strong correlation with small, Cu rich deposits and the more intense hematite/silica alteration. Preferential replacement of the more porous volcanic, conglomeratic and sandstone units appears to have occurred where they have been subject to this more intense hydrothermal activity. These inner zones of intense silicic and hematitic alteration grade out to a quartz-sericite dominated assemblage between North Lyell and Lyell Tharsis, a hematite-phosphate-barite assemblage at Lyell Tharsis and a chlorite dominated alteration assemblage around Batchelors' Quarry, with a variably hematitic matrix.

An intensely hematitic zone of Owen Conglomerate occurs directly under the Haulage Unconformity on the upper part of the Ridge Area. These Owen Conglomerate samples are more intensely hematitic than those found at Batchelors' Quarry, despite being in a similar stratigraphic position but further away from the highly altered North Lyell area. The proximity of this hematitic zone to fault intersections suggests it may have a

hydrothermal replacement origin, however there appears to be minimal transgression of any hydrothermal fluids into adjacent beds of Owen Conglomerate or across the Haulage Unconformity into the Pioneer Beds. The clasts within the hematitic Owen Conglomerate have different angularity and sorting characteristics to the 'standard' Owen Conglomerate, which suggests the hematite clasts had a detrital origin rather than a hydrothermal replacement origin (further discussion in section on the origin of the hematite clasts).

Samples obtained from Cape Horn and Mt. Owen (Figure 4) were similarly found to have beds enriched in hematite adjacent to those with very small amounts. It was considered unlikely that these more hematitic beds were directly associated with the hydrothermal alteration due to their distance from the mineralising system. In thin section the hematite appears to have an early diagenetic origin, however the occurrence of hematite as a coherent cement within some of the conglomerates and sandstones suggests the possibility of a hydrothermal component. If there was a significant hydrothermal component to the hematite, it would be expected that there would be consequential infiltration of fluids along and across, upper and lower stratigraphic contacts. It would also be expected that there would be lateral variation in the intensity and type of alteration within the stratigraphy as the fluids cooled (ie. particularly in the degree of hematisation). This is not readily apparent from field observations.

What appears to be a coherent hydrothermal hematite component occurs within some of the more porous sandstone and conglomerate layers on Mt. Owen and Cape Horn. Laminations of hematite and quartz rich layers within sandstones at Cape Horn occur on a variety of scales from millimetres to metres, with the hematite generally occurring as a contiguous cement. There is hematitic fluid infiltration along intersections between truncated cross bedding laminae and occasionally along lower stratigraphic contacts on Cape Horn (see Plates 6 and 7), however there is no indication of hematite infiltration of clasts within these areas (eg. hematitic selvedges). Whether these effects are of a hydrothermal, metamorphic or weathering character is not apparent in outcrop or hand specimen. The possibility of the first two has been raised, however Liesegang weathering and leaching of the iron oxides has produced some spectacular effects within the relatively unaltered, highly siliceous conglomerates and quartzites of Cape Horn (see Plates 7 to 9) and may have had some effect on the whole rock geochemistry. The whole rock trace element geochemistry of the hematitic and non hematitic rocks were utilised to give an indication for the origin of the hematite (ie. detrital or hydrothermal). Samples were chosen from the freshest material available to avoid the possibility of geochemical modification by weathering events.

Plate 6 Layered conglomerate and quartzite on Cape Horn. Note hematite infiltration downwards through quartzite and laminations at top of quartzite. Very little hematite occurs within the conglomerate.

Plate 7 Close up of hematite textures in quartzite in Plate 6. Note hematite infiltration along truncated bedding planes.

Plate 8 Close up of hematite textures in quartzite in Plate 6. Note enhanced weathering of hematitic portion.

Plate 9 Distorted hematite infiltrations within Owen Conglomerate - Cape Horn. Patterns are not thought to be hydrothermal, probably a weathering characteristic (Liesegang weathering?).

Plate 10 Hand specimen showing hematite banding and infiltration within quartzite from Cape Horn. In thin section the hematite appears diagenetic (see Plate 16).

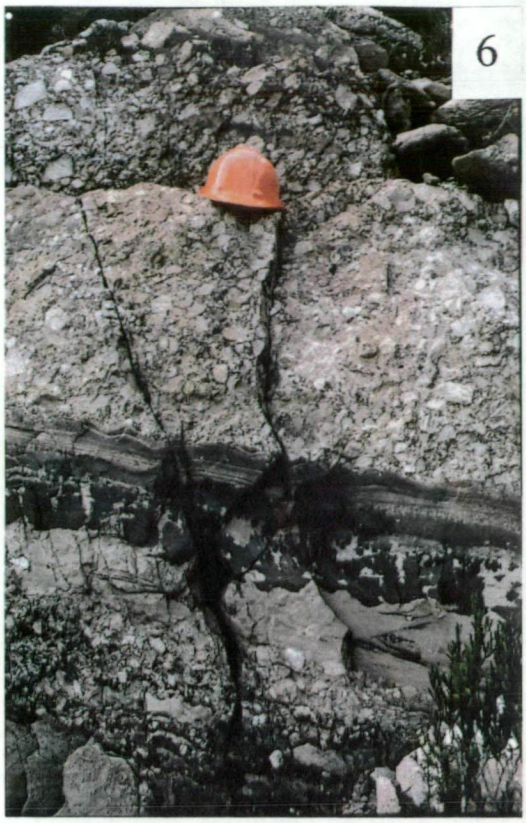
6


7


8

10


9

ALTERATION WITHIN THE PIONEER SANDSTONE

The most notable geochemical aspect of the Pioneer Beds is the large amount of chromium (eg. up to 1% in NL 58), which is a useful distinguishing feature for the transition from Owen Conglomerate to Pioneer Sandstone in areas where the unconformity is not obvious (eg. the Waterfall area). The chromium is present as detrital chromite, thought to be from the appearance of a more mafic source rock, and is not thought to be related to the hydrothermal fluid movement. The hydrothermal alteration associated with the North Lyell mineralising event extends across the Haulage Unconformity but appears distinctly less intense and quite variable above the unconformity in most locations. The hematite alteration above the Haulage Unconformity affects some of the sandstone beds more than others, which may be due to a number of reasons including;

- the barrier effect of the Haulage Unconformity
- waning of the hydrothermal system at the time of Pioneer deposition
- variable porosity of beds within the Pioneer

Variation in the alteration assemblage within the Pioneer Sandstone along strike, and across strike away from the Great Lyell Fault and Haulage Unconformity is well exposed in the Ridge Area. Hematitic conglomerate beds can be traced along strike and the variation in alteration, although not easily recognisable in hand specimen, is apparent in the geochemical analyses.

ALTERATION WITHIN THE GORDON LIMESTONE

In many ways this unit contains the answer to the timing of the mineralisation and associated hydrothermal alteration at North Lyell. Any scenario proposed for the age and origin of the main Mt. Lyell deposits must explain the occurrence of economic copper deposits within the overlying Ordovician Gordon Limestone. If it can be shown that the hydrothermal fluids have interacted with these Ordovician mudstones and carbonates, then the alteration must have occurred some time after the Ordovician, probably in the Devonian during the Tabberabberan Orogeny. If no evidence of hydrothermal alteration related to the mineralisation can be found, a Late Cambrian-Early Ordovician timing for mineralisation must be assumed. This is explored further in the section on modelling of the hydrothermal fluid geochemistry.

Due to pre glacial leaching (under very low pH conditions) and Pleistocene glaciation (Sillitoe, 1985; Arnold, 1985), outcrop of the Gordon Limestone around North Lyell and the majority of Linda Valley is quite poor. XRD analysis of the dark grey-brown Gordon Limestone pug from the North Lyell area shows the samples to be composed of quartz/muscovite/kaolinite ± goethite ± carbonaceous material (Table 1), with minor native copper visible in some hand specimens. These samples bear little resemblance to the 'precursor' Gordon Limestone samples found rarely in other, less affected areas, although similar brown-black pug may be found in Linda Valley well away from hydrothermally affected areas. Arnold (1985) mentions a quarry where the transition from 'pug' to normal limestone can be seen in outcrop, where he observed the schistosities to be obliterated, and bedding features retained in part, but commonly brecciated and disturbed. He also notes that the pug is more pyritic than the 'admittedly rare' fresh limestone.

The copper mineralised sediments that form the so called 'Copper Clay' deposits of Lyell Blocks, Balance Shaft, Lyell Consols and King Lyell, occur on the eastern side of the Mt. Lyell Cu field. They were mined for native copper by several companies around the turn of the century (Solomon, 1969), with Lyell Blocks being the only deposit to produce a significant quantity of native copper ore (Sillitoe,1985). Markham (1968) reports pyrite, chalcocite, digenite, covellite, bornite, chalcopyrite, sphalerite, galena, native copper and cuprite from heavy mineral concentrates of drill clay samples obtained at Lyell Blocks and Lyell Consols. He also notes the presence of a bornite 'cement' between 'framboidal aggregates' of spherical and oval shaped grains of chalcocite, and attributes the iron and copper sulphide mineralisation within the Gordon to a 'low temperature, sedimentary environment'.

Edwards (1958), Solomon (1969), and Walshe and Solomon, (1981) suggest the copper occurrences within the carbonates are of a supergene origin, however a Devonian hydrothermal origin is not discounted by all these authors. Sillitoe (1985) argues that the mineralisation is structurally controlled and emplaced at the same time as the other Mt. Lyell deposits, and by the same mechanism. He suggests that the sulphides present in the Gordon are hypogene in origin, Arnold (1985) suggests the pyrite present in the pug was introduced subsequent to the destruction of the carbonate texture by the acid leaching. Sillitoe (1985) also proposed that the native copper and cuprite within the Copper Clay deposits is due to deep Tertiary oxidation under karst conditions, which was restricted to the Gordon Limestone terrain.

In outcrop it can be seen that the Gordon Limestone has undergone a significant amount of fabric destructive weathering, having little or no mechanical integrity.

Whether or not this weathering has overprinted an earlier hydrothermal event (or vice versa) is a more complex geochemical question which is investigated in a later chapter. There is also very little competent carbonate found in drill core from the mine area, with most intersections of limestone being muddy grey material with very poor drillcore recovery. Samples of Gordon Limestone pug from Linda Valley (Cemetery Creek) (Figure 4) were collected to represent material unaffected by hydrothermal activity, but still influenced by the regional Devonian greenschist metamorphism. Samples of the pug obtained from the Waterfall area and Batchelors Quarry, adjacent to North Lyell are extremely unlikely to have escaped hydrothermal alteration at the time of mineralisation if they were present. Their proximity to the intensely altered hematite/barite pod at North Lyell and the similar alteration found within the Pioneer Beds, stratigraphically adjacent to the limestones, suggests there would definitely have been some interaction between the hydrothermal fluids and the overlying reactive limestones. To ascertain the extent, if any, of fluid penetration and gain an idea of the timing of the alteration, the samples collected were subjected to XRD and illite crystallinity tests, to compare their petrography and degree of metamorphism.

Sample no.	Composition - approx. wt. %				
	Quartz	Kaolinite	Mica	Goethite	Carbon-aceous material
NL 19	50	<5	50	-	-
NL 36	65	5	30	-	-
NL 69	85	-	10	5	-
NL 70	45	-	30	25	-
NL 96	90	-	5	-	5

Table 1 - Samples of brown-black Gordon Limestone pug from Batchelors Quarry (NL 19, NL 69 and NL 70), the Waterfall area (NL 36) and Cemetery Creek (NL 96), showing their mineralogy as determined by XRD analysis, (analysed by Tas. Dept. of Mines).

XRD Analyses of Gordon Limestone

From the data presented in Table 1 it is not clear whether or not there has been significant fluid infiltration into the samples from the Waterfall area and Batchelors Quarry. It would be expected that the samples from hydrothermally altered areas would contain significantly more mica and goethite than those from unaltered areas. This is evident in some samples (eg. NL 19 and NL 70), however the variable mineralogy of samples within these altered areas and the limited sampling undertaken from unaltered

areas leaves some scope for discussion. The lack of mica within the sample from Linda Valley (NL 96) would tend to support some hydrothermal interaction although there may be a parent rock control on the geochemistry confusing this variation. A more comprehensive discussion of alteration effects within the Gordon Limestone is included in the hydrothermal geochemistry section.

XRF analyses of the Gordon Limestone

Whole rock samples of fresh Gordon Limestone were obtained from areas within Queenstown and Linda Valley to compare with analyses of mineralised limestone taken by Solomon (1969). The whole rock XRF analyses of mineralised samples from Solomon (1969) have been normalised against the average of three fresh samples of Gordon Limestone obtained from unaltered sites around Queenstown and Linda Valley (NL97, NL98 and NL99; Figure 8). Some of the samples obtained by Solomon still contained a carbonate component ('slightly impure manganese-iron carbonates of variable composition') exhibiting a fine grainsize which was interpreted as being from a primary precipitate.

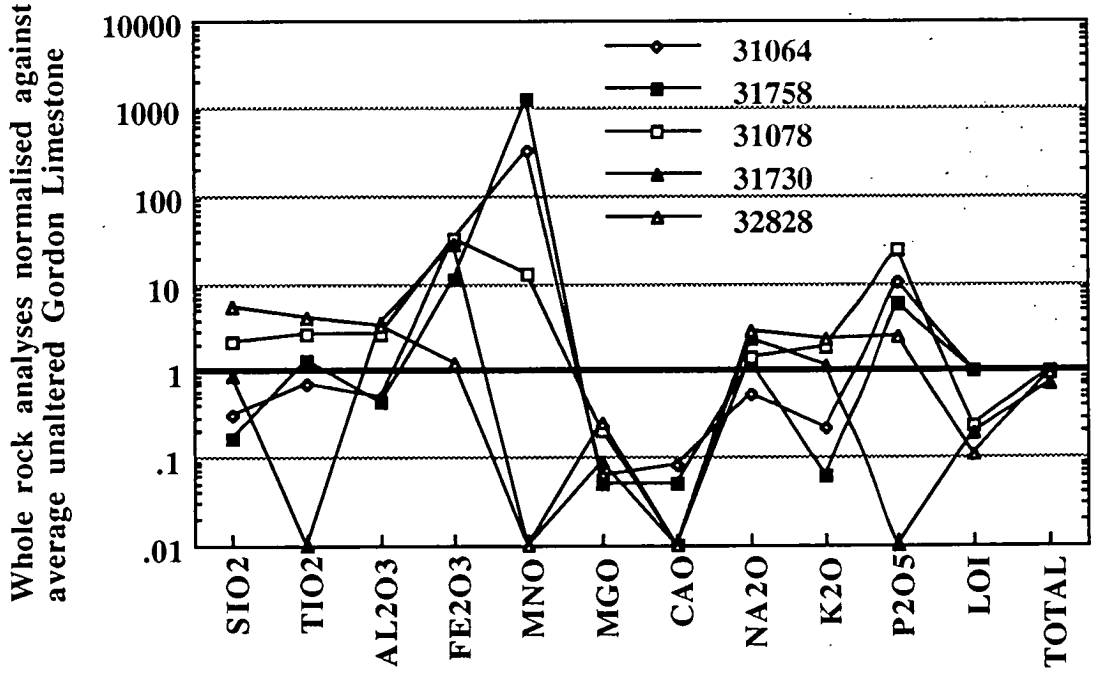

Figure 8 - XRF analyses of samples of Gordon Limestone and related materials obtained by Solomon (1969), normalised against an average unaltered Gordon Limestone composition (ie. from this study - average of NL97, NL98 and NL99). Description and location of Solomon samples; 31064 - Carbonate rock (mainly manganoan siderite), King Lyell; 31758 - Carbonate rock (mainly ferroan rhodochrosite), Lyell Consols; 31078 - Goethite matrix, King Lyell; 31730 - Goethite nodule Lyell Blocks; 32828 - Dark grey shale, King Lyell

The majority of these samples are from areas associated with copper mineralisation and would be expected to reflect any alteration fluid that may have interacted with them (subject to the mineralogy surviving mobilisation during weathering). There is substantial variation between the samples (compared with the unaltered analysis), with no clear alteration trend visible. All samples are enriched in Fe_2O_3 and most are enriched in P_2O_5 however this may be due to hypogene leaching of the underlying deposit, rather than hydrothermal activity. The presence of significant potassium and alumino silicates (such as muscovite-kaolinite) would suggest a hydrothermal origin, however K_2O and Al_2O_3 are only slightly enriched within a few samples. They are all depleted in CaO and MgO indicating a reduction in carbonate minerals during alteration/weathering. The results do not indicate the mechanism by which the geochemical variation was controlled.

STATISTICAL ANALYSIS OF WHOLE ROCK XRF RESULTS

1). Major and trace element associations

The initial rock chip sampling program analysed 38 whole rock samples from the alteration zone around North Lyell for the major elements and a range of trace elements including; Cr, Ni, V, Sb, Zn, Cu, Nb, Zr, Y, Sr, Rb, La, Ce, Nd, Ba, and Sc. The results from this were log normalised (to overcome the closure effect) then statistically evaluated, using the Macintosh computer program Data Desk® (v3.0 rl, 1985, Velleman and Pratt), which calculated the correlation coefficients between the elements (the Pearson Product-Moment Correlation). This established whether or not there is a valid association between the various elements within the alteration zone, or if they are exclusive of each other. From this information an idea of elemental associations and their relevance to the alteration assemblage can be established.

From this analysis it became apparent that there were three main associations which could be related to the alteration styles visible in hand specimen. The three associations and their related alteration styles are;

Association 1 - $Al_2O_3 + K_2O + Cr + Rb$ (sericite)
Association 2 - $Fe_2O_3 + P_2O_5 + La + Sb$ (hematite/magnetite/apatite)
Association 3 - Ba + Sr + Sb (barite)

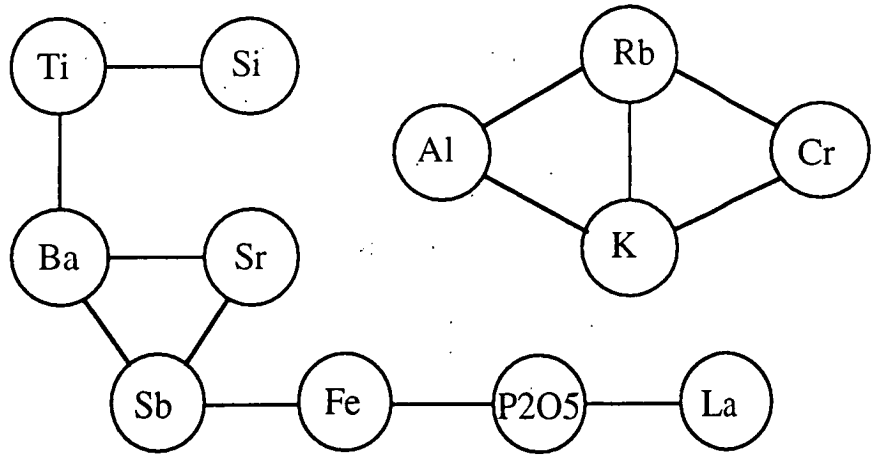

Figure 9 - Diagrammatic representation of Pearson Product-Moment Correlation for log normalised elements from all XRF whole rock analyses (at the 99% significance level, with 60 d.o.f.)

These results were used to pick the elements most useful for distinguishing the various types of alteration. The second round of rock chips (34 samples) were obtained from within the alteration zone and from areas thought to be unaffected by the hydrothermal

alteration. They were analysed for the major elements and Sb, Ba, Sr, Cr, La and Rb. The combined results from the first and second round of analyses produced associations almost identical to the initial observations when subjected to the same statistical tests. The correlation data is presented diagrammatically in Figure 9.

When the different alteration areas (ie. siliceous/hematitic/chloritic areas) are statistically analysed independantly of one another, the elemental associations established across the entire field are generally not retained. The associations between the elements becomes more varied and indistinct as the alteration becomes less apparent. Two strong elemental affinities are seen in most of the areas; Ba + Sr are closely correlated within the more altered areas but the relationship is not statistically significant in the relatively unaltered areas; K + Rb also show a strong elemental affinity in all areas sampled except the North Lyell siliceous pod. It can be seen that Ba and K are directly related to the alteration (ie. barite and mica alteration), and their close correlations with trace elements is controlled mainly by the capacity of these host minerals to retain the trace elements within the crystal lattice during alteration. The inability of the statistical analysis of the geochemistry to define distinct and coherent elemental associations within each sample area suggests that each area defines an alteration style. This possibility was investigated by testing the correlation between each rock chip sample.

2). Rock chip sample and sample area associations

After log normalising the whole rock XRF results, analysis of the correlation between the individual samples was performed to determine which whole rock analyses were significantly correlated with the others. The results from this analysis show a good correlation between samples within the more altered sampling areas (eg. the North Lyell siliceous pod). The samples obtained within the area between North Lyell and Lyell Tharsis showed some correlation with each other and a stronger geochemical association with the North Lyell samples rather than the more hematitic Lyell Tharsis rocks. Samples from Lyell Tharsis exhibited less significant correlation between each other and the surrounding specimens, which is probably due to the high geochemical variation within these variably hematite/barite/phosphate altered samples. There is some correlation between the highly ferruginous Lyell Tharsis samples and the similarly ferruginous samples obtained between Lyell Tharsis and Batchelors Quarry.

Batchelors Quarry is found to have statistically similar geochemistry to the Waterfall Area, the Ridge Area and the relatively unaltered Cape Horn area. All these localities show some geochemical correlation between samples adjacent to one another (ie. probably showing less effects from the alteration event). They commonly exhibit a negative correlation with the more altered samples at North Lyell and Lyell Tharsis,

although a less altered rock chip from Lyell Tharsis shows a significant correlation with the Batchelors Quarry samples. From these associations it was decided to divide the areas up into groups that can be treated as separate alteration zones. These sample areas and their alteration styles are;

Group 1 - North Lyell siliceous pod	- (silica/barite)
Group 2 - Area between North Lyell and Lyell Tharsis	- (silica/barite/mica)
Group 3 - Lyell Tharsis	- (hematite/barite/phosphate)
Group 4 - Batchelors Quarry	- (chlorite)
Group 5 - Ridge area, Cape Horn and Mt. Owen	- (hematite?)

These groups and their particular geochemistry and alteration styles shall be investigated further in the next section.

3). Hematitic sample associations

Analyses of hematite veins and clasts from this report, and Solomon, (1964 and 1969) were compared using the Pearson Product-Moment Correlation method. The analyses are difficult to compare however, as only limited trace elements were analysed by Solomon, and they were commonly different elements to those analysed in this study. Generally it can be seen that the hematised conglomerates from North Lyell and Lyell Tharsis have a good correlation with the hematite clasts from Tharsis Ridge and Razorback. A pebble of hematite from the Owen Conglomerate on Razorback Ridge (sample 31025 from Solomon, 1964) showed the best correlation with the North Lyell hematite pod (sample 31182 of Solomon 1969), with less significant correlations with samples obtained between Lyell Tharsis and Batchelors Quarry (a zone of intense hematisation). This suggests a relationship exists between these samples, however it does not define the origin of the pebble as being directly related to hydrothermal fluid replacement (as per the samples from North Lyell, etc.), or of detrital origin sourced from these rocks. The origin of these clasts is discussed in a later section.

The hematite veins from this study and Solomon (1964) showed a good correlation with each other and the clasts correlated with the hydrothermal, massive hematitic conglomerates and sandstones. The veins generally did not have a good correlation with the other hematitic samples except the chert breccia. The textures and geochemistry of these two hematitic rocks are very similar and they are thought to be genetic correlates. The main difference in geochemistry between the hematite veins and clasts within the various areas is the higher content of Al_2O_3, Na_2O, K_2O and P_2O_5 within the clasts. The geochemistry of the hematite veins, clasts and hematitic conglomerate

are statistically most closely associated with the Lyell Tharsis area, not the more siliceous North Lyell area.

MINERALOGY AND GEOCHEMISTRY OF NORTH LYELL AND THE SURROUNDING AREA

Mineralogical definition of alteration groups

The sample areas have been divided into groups using the observed geochemistry which supports the mineralogy seen in thin section. The highly altered quartz-hematite-barite replacement zone at North Lyell exhibits the most intense alteration both texturally and geochemically and occurs as an isolated outcrop within the volcanics at North Lyell. The intense hematite-barite-phosphate alteration within the Owen Conglomerate at Lyell Tharsis can be seen to grade along strike into a more sericitic-silicic zone of alteration between North Lyell and Lyell Tharsis. Across strike from Lyell Tharsis, within the Owen Conglomerate (away from the Great Lyell Fault), the hematite-barite-phosphate alteration diminishes to a zone of dominantly chloritic alteration around Batchelors Quarry with some evidence of hydrothermal hematite within most beds. The Ridge area exhibits a zone of intense hematite alteration within the Owen Conglomerate adjacent to the Haulage unconformity, something which is far less developed at Batchelors Quarry. The samples obtained further along the ridge are from the chromite rich Pioneer Sandstone (above the unconformity) and exhibit far less hematite alteration than the adjacent Owen Conglomerate.

'Average' samples of unaltered Owen Conglomerate and Pioneer Sandstone were chosen based upon their geochemistry, degree of sedimentary texture preservation, clast size and geographic separation from the alteration zones. It is difficult to ascribe a geochemical makeup for hydrothermally altered precursor rocks such as conglomerates (which may have great internal variation over a very small distance), however if a large enough sample fraction is utilised this internal variation may be minimised. For all whole rock analyses taken during this sampling program, a minimum sample size of approximately 3 kilograms was used. The majority of samples taken were quite homogeneous however some samples with larger clasts were utilised in the less altered material (a maximum clast size of approximately 1 centimetre was used in conjunction with the 3 kg. sample size)

The typical 'unaltered' Owen Conglomerate analysis was obtained by averaging three samples from relatively unaltered areas (NL30, NL79 and NL82). The geochemistry of two samples from Cape Horn and one from the Waterfall area were combined to

produce the composition shown in Table 2. A sample of Pioneer Sandstone from the Waterfall area (NL35) was chosen to represent the 'unaltered' Pioneer Sandstone based upon its trace element geochemistry, sedimentary texture preservation and distance from significant structural disruption. Comparison of these with the altered varieties will give an appreciation of the changes in geochemistry due to reaction with the hydrothermal fluids and possibly some indication of the composition of the fluids.

Mineralogy of Group 1 - North Lyell

These rocks are dominated by silica, with very high barium content (present as barite) and highly variable iron content (0.39% to 49.17% Fe_2O_3). The silica appears to postdate the hematite in most cases and is thought to represent a later overprinting effect within areas of higher fluid movement. The sample with the highest iron and barium content (ie. NL8, Figure 5), is located on the fringe of the siliceous pod, possibly reflecting its proximity to the more iron rich altered volcanics where the fluids are originating.

Recrystallised polycrystalline quartz with islands of barite-chlorite have obscured all sedimentary textures in most samples, however, relict conglomerate clast outline defined by hematite and mica may be seen in some examples. A example of siliceous-hematitic quartzite from the central pod (sample NL 4a and 4b) contains a hematitic phase adjacent to a clean white siliceous phase. In thin section it can be seen that the hematite is invading the more silicic portion of the sample. The two portions are almost identical mineralogically and geochemically except for a significant increase in iron at the expense of quartz in the hematitic section. Relict clast outlines are defined by the hematite which appears to be infiltrating along fractures and quartz grain boundaries. Barite and chlorite also occur interstitially to the relict clasts and within fractures along with a final quartz/mica overprint. The paragenesis of the alteration minerals from this area is characterised by a hematite-chlorite-barite-quartz-mica progression, with some local paragenetic variations.

Copper minerals such as covellite-chalcopyrite-bornite-tetrahedrite-idaite also occur within the siliceous pod in trace quantities. A sample from this area exhibits a copper mineral transition from pyrite-chalcopyrite-covellite, possibly representing an increase in Cu concentration within the hydrothermal fluids late in the paragenesis. The occurrence of chalcopyrite with intergrown chlorite and hematite lathes in some open space fill situations illustrates the close association of these minerals in the alteration/mineralising event. Disseminated and vein chalcopyrite also appears within highly silicified clasts which is postdated by further intense silicification and possible

Element	Average of Group 1 n=9	Average of Group 2 n=9	Average of Group 3 n=10	Average of Group 4 Pioneer Beds n=11	Average of Group 4 Owen Congl. n=4	Average of Group 5 Pioneer Beds n=2	Average of Group 5 Owen Congl. n=10	Unaltered Owen Congl.	Unaltered Pioneer Beds
SIO2	79.53	66.07	34.85	78.08	91.27	92.53	85.58	96.31	95.58
TIO2	0.70	0.34	0.22	0.43	0.23	0.17	0.17	0.11	0.12
AL2O3	1.23	0.94	3.66	5.41	3.16	1.79	1.65	1.07	1.64
FE2O3	8.98	29.21	55.86	12.13	3.50	3.01	10.68	1.57	0.26
MNO	0.01	0.01	0.03	0.01	0.01	0.01	0.01	0.00	0.00
MGO	0.10	0.03	0.11	0.53	0.10	0.11	0.09	0.04	0.02
CAO	0.01	0.01	0.44	0.05	0.02	0.01	0.02	0.02	0.01
NA2O	0.10	0.16	0.13	0.27	0.23	0.10	0.14	0.14	0.10
K2O	0.06	0.16	0.30	1.14	0.73	0.66	0.42	0.18	0.45
P2O5	0.16	0.02	0.56	0.23	0.09	0.03	0.05	0.03	0.01
LOI	1.42	0.95	1.52	1.44	0.67	0.57	0.74	0.40	1.80
TOTAL	99.64	97.90	99.89	99.72	99.98	99.06	99.52	99.87	99.99
SB	23	43	40	3	2	2	4	2	2
BA	44208	13814	15676	1604	509	79	135	120	79
SR	1678	308	911	222	81	8	44	35	8
CR	51	106	51	2895	172	3944	132	60	3944
LA	29	5	38	61	16	21	17	7	21
RB	2	5	11	39	25	25	15	5	25

Table 2 - A comparison of the average whole rock geochemistry of the Owen Conglomerate from each sample area, with Pioneer Sandstone samples listed separately. The last two columns show selected 'unaltered' Owen Conglomerate and Pioneer Sandstone analyses. The unaltered Owen Conglomerate is an average of three samples (NL 30, NL 79 and NL 82), and the unaltered Pioneer Sandstone is an analysis of NL 35.

hydrothermal brecciation. Microprobe analyses of unknown sulphides revealed Ag tellurides and Pb sellenides in trace quantities as late stage vein minerals within samples from this area.

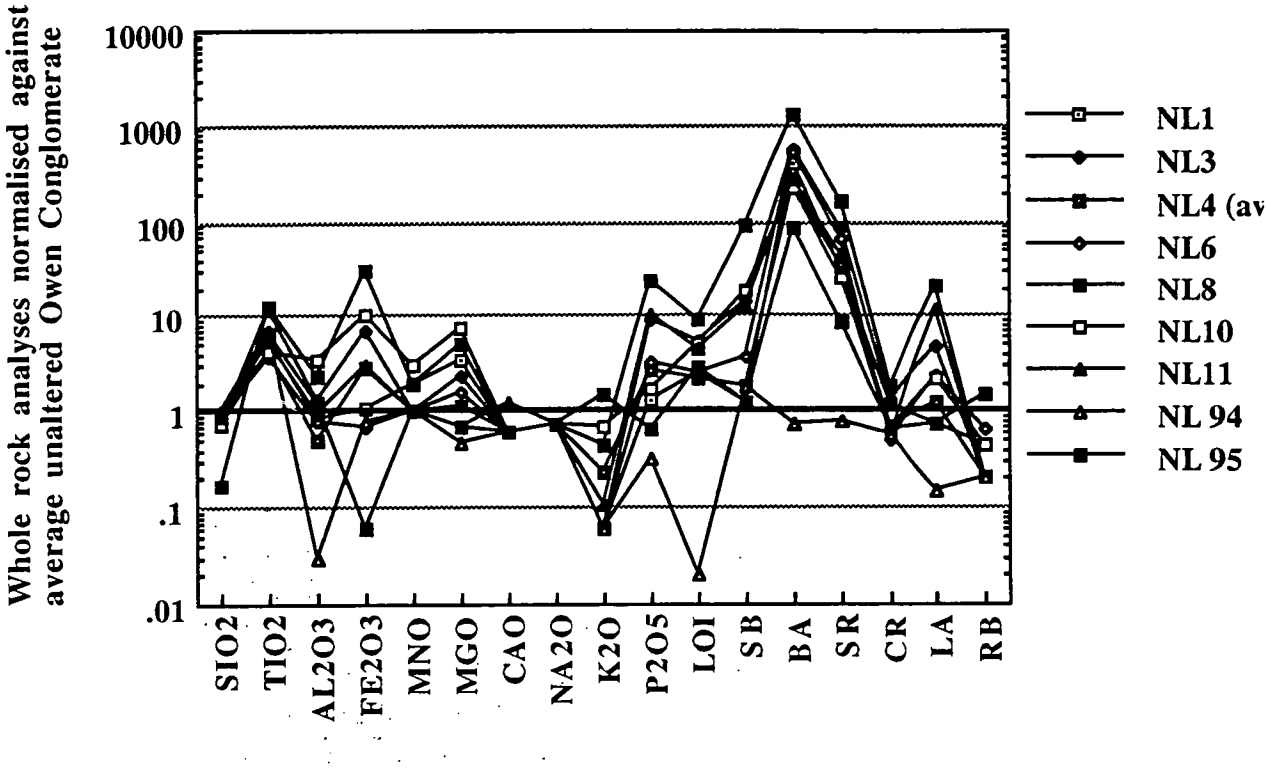

Figure 10 - Whole rock XRF analyses of Owen Conglomerate samples from the North Lyell siliceous pod (Group 1) normalised against average unaltered Owen Conglomerate (shown as dark line at 1.0). For description of samples see Appendix I

Geochemistry of Group 1 - North Lyell

All samples obtained from this area contain only minor Cr (30-108 ppm as chromite), indicating that the pod is not composed of altered and mineralised Pioneer Sandstone as suggested by Sillitoe (1985), but more probably the recrystallised Middle Owen Conglomerate. The geochemistry of the rocks from this area has been highly modified by the hydrothermal fluids as can be seen in the spider diagram in Figure 10. Compared with the average unaltered Owen Conglomerate, the samples from this area have been enriched in most elements. Depletion in CaO, Na_2O, K_2O and Rb possibly reflects a related style of geochemical alteration within the associated volcanics. Solomon (1964), Green (1971) and Walshe (1971), Walshe and Solomon (1981) established the major variations of the Mt. Lyell host rock geochemistry due to alteration involved the loss of CaO, Na_2O, Rb and Sr and addition of H_2O and Ba. Loss of Al_2O_3 and addition of P_2O_5 were listed as minor changes.

Elements enriched compared to unaltered Owen Conglomerate	Elements depleted compared to unaltered Owen Conglomerate
TiO_2, Fe_2O_3, MnO, MgO, P_2O_5, Sb, Ba, Sr, La	CaO, Na_2O, K_2O, Rb

Significant enrichment of TiO_2, which is generally considered to be an immobile element, suggests the rutile visible in thin section has a hydrothermal rather than detrital origin. It also suggests the alteration event had the intensity to move relatively immobile elements. The intensely silicified samples obtained from below a bornite-chalcopyrite-pyrite mineralised section (NL94 and NL95 from drillcore), are notably depleted in most elements compared to the unaltered Owen Conglomerate (except TiO_2) and may represent a silicic 'bleached zone'. These samples have been totally recrystallised, silicified and brecciated, with variable barite-quartz and sulphide veining producing a rock which appears to have little in common with its precursor.

Mineralogy of group 2- between North Lyell and Lyell Tharsis

The samples were obtained from a strongly folded area with clearly defined stratigraphic layering, between the North Lyell siliceous pod and Lyell Tharsis. The majority of samples from this area appear to be totally recrystallised quartzites with variable amounts of hematite/goethite present as veins, disseminations within the quartz and bordering some weakly developed relict clasts. The majority of quartz grains have been recrystallised into polycrystalline aggregates with more coarsely crystalline quartz-barite-hematite-mica islands and veins interspersed throughout the polycrystalline quartz fabric.

Samples of a hematite vein from this area exhibit classic botryoidal and colloform textures from growth in a tension gash. There are no textures to indicate the hematite has replaced a pre-existing rock and field occurrence suggests a structural origin. Aluminous mica (mainly pyrophyllite), quartz and barite aggregates fill gaps in the hematite layers and botryoids within the vein. Infiltration of the hematite into the surrounding country rock appears limited as can be seen by the lack of hematite within adjacent samples.

Geochemistry of group 2

There is significant geochemical variation between adjacent samples within this area (see Figure 11), especially within the alteration minerals such as Ba and Fe_2O_3. This variable alteration intensity between neighbouring beds, possibly reflects an original stratigraphic or diagenetic feature (ie. variable porosity or mineralogical composition). Generally the rocks are quite enriched in barium and some are enriched in iron oxide,

although not to the extent of the adjacent North Lyell samples. There appears to be less hydrothermal rutile within this area, the majority of the TiO_2 present is probably associated with the hematite as ilmenite and rutile intergrowths (Deer et al, 1982).

Elements enriched compared to unaltered Owen Conglomerate	Elements depleted compared to unaltered Owen Conglomerate
TiO_2, Fe_2O_3, Sb, Ba, Sr	Al_2O_3, MgO, CaO, K_2O, P_2O_5, Cr, La, Rb

The depletion of the above elements (many to below detection limits) and the prevalent silicification suggests a similar type of 'silicic bleaching' to that found at North Lyell. The alteration style is geochemically quite similar to the North Lyell alteration, although in thin section it is apparent that it has been far less intense.

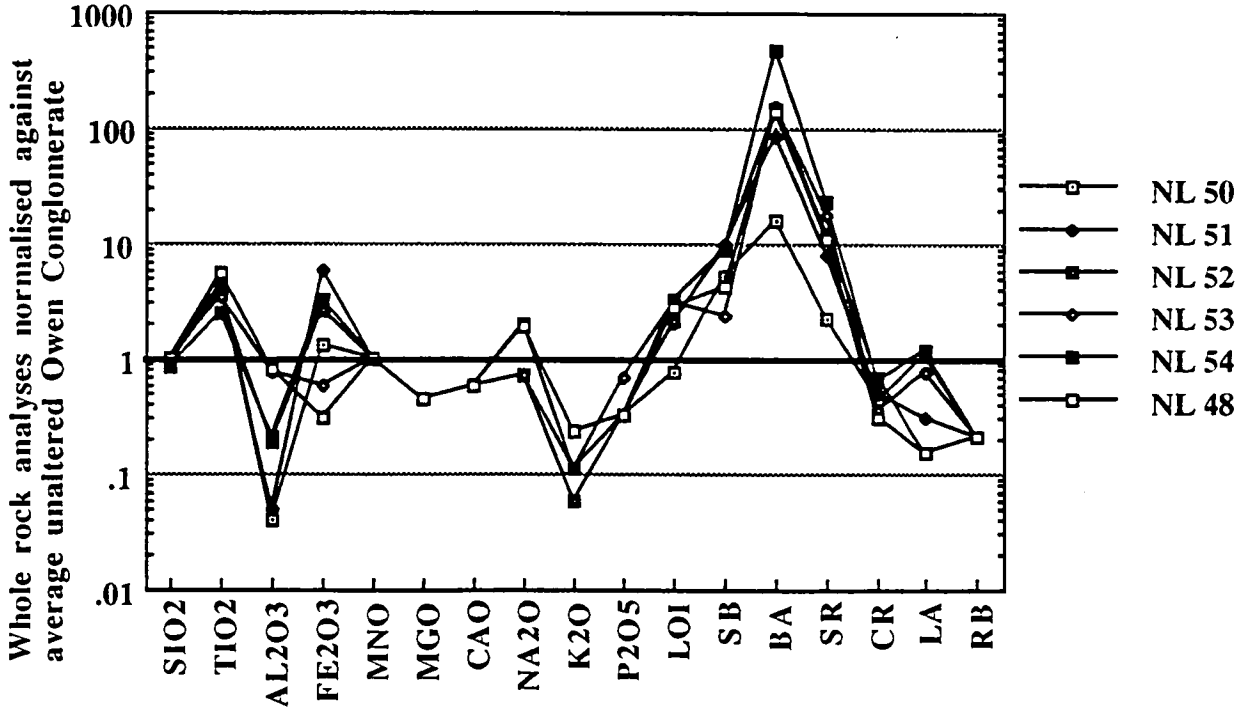

Figure 11 - Whole rock XRF analyses of Owen Conglomerate samples from the area between the North Lyell siliceous pod and the Lyell Tharsis mine area (Group 2). Intensely hematitic samples excluded (>68% Fe_2O_3). Sample descriptions in Appendix I

Mineralogy of Group 3 - Lyell Tharsis

The Lyell Tharsis orebody occurred within the volcanics directly abbutting the GLF and closely associated with an unnamed NW trending crossfault. The host rocks were dark green massive hematitic and chloritic siliceous rocks with disseminated chalcopyrite, minor pyrite, some bornite, sphalerite and galena (Reid, 1975). This area exhibited the strongest hematite-barite-pyrophyllite alteration of all areas, and the strongest foliation

within samples closest to the GLF. There is no intense silicification such as that seen at North Lyell or the area between North Lyell and Lyell Tharsis. There has only been localised remobilisation of silica within some specimens, mostly associated with the GLF.

Mineralogically this was the most diverse area with intense hematite-barite-muscovite-pyrophyllite-chlorite-phosphate alteration producing a variety of textures and alteration minerals. Samples obtained directly adjacent to the GLF exhibit a foliation defined by hematite and mica which occur between the polycrystalline quartz clasts. Pyrophyllite, muscovite and hematite also appear within the clasts as disseminations amongst the microcrystalline quartz. Green-light brown chlorite and minor barite occur within veins and open spaces associated with veins. Phosphates associated with this area include Gorceixite (a hydrous barium phosphate), apatite and some iron phosphates (with a percent analysis average of four analyses of $FeO_{(57.1)}Al_2O_{3(2.7)}P_2O_{5(40.2)}$). The iron phosphates appear to be genetically related to the oxidation of pyrite cubes (see Plates 11 and 12), possibly occurring at the same time as the mineralisation and related hydrothermal alteration, suggesting the fluids were reasonably oxidised.

Zones of barite enrichment occur within the intensely hematised samples from Lyell Tharsis with the barite appearing as coarsely crystalline infills of open spaces. The crystals exhibit undulose extinction and fill spaces between framboidal and botryoidal hematite which appear as overgrowths of previously deposited barite. Crystal boundaries of the coarse barite are defined by fine grained hematite and smaller crystals of barite (see Plates 13 and 14). The barite crystallisation appears to be synchronous with and postdate the hematite and is associated with minor chlorite.

Further away from the GLF (across strike) within the Owen Conglomerate, clasts of quartz and hematite are more prominent. The quartz clasts are coarsely crystalline and polycrystalline with examples showing variable degrees of hematite infiltration up to complete hematite replacement. This can be seen in hand specimen and outcrop with some examples of completely hematised conglomerate retaining their conglomeratic textures (see Plate 15). This hematisation appears most intense adjacent to the NW trending crossfault and extends onto Tharsis Ridge to the west. A comparison of the hematite rich samples from this area and surrounding areas is presented in a later section.

Plate 11 Iron phosphate replacement of pyrite cubes within hematitic rock from Lyell Tharsis, plane polarised light and reflected light. X10.

Plate 12 Same grain as Plate 11 under crossed polars.

Plate 13 Hematite bands coating barite crystals with barite forming cement between hematite. Plane polarised and reflected light. X20.

Plate 14 Botryoidal hematite with chlorite/barite cement. Plane polarised light X20

Plate 15 Totally hematised conglomerate (note clastic textures bottom right) from area between Lyell Tharsis and Batchelors Quarry.

Plate 16 Diagenetic hematite dusting of quartz grains in sample from Mt Owen. Plane polarised light. X5

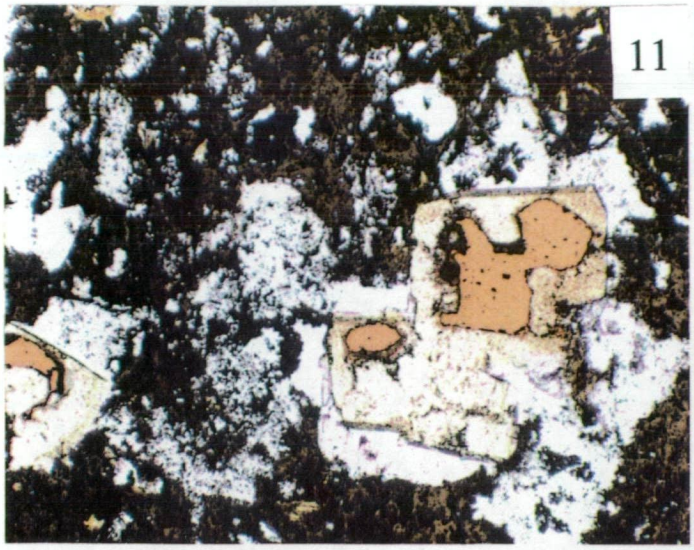
11

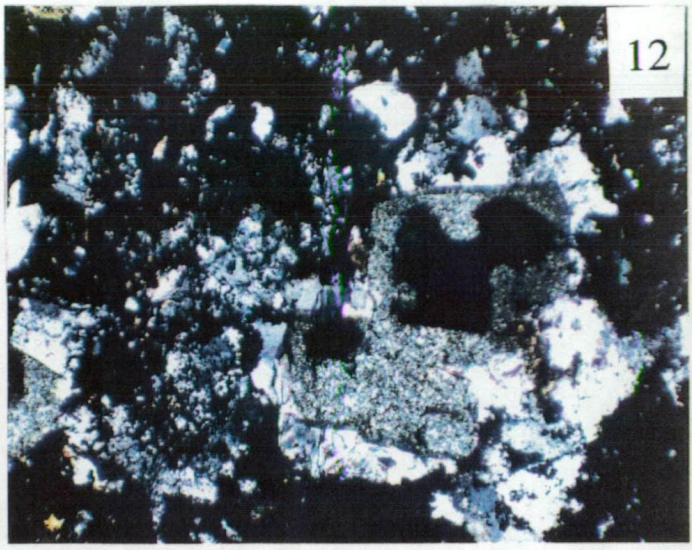
12

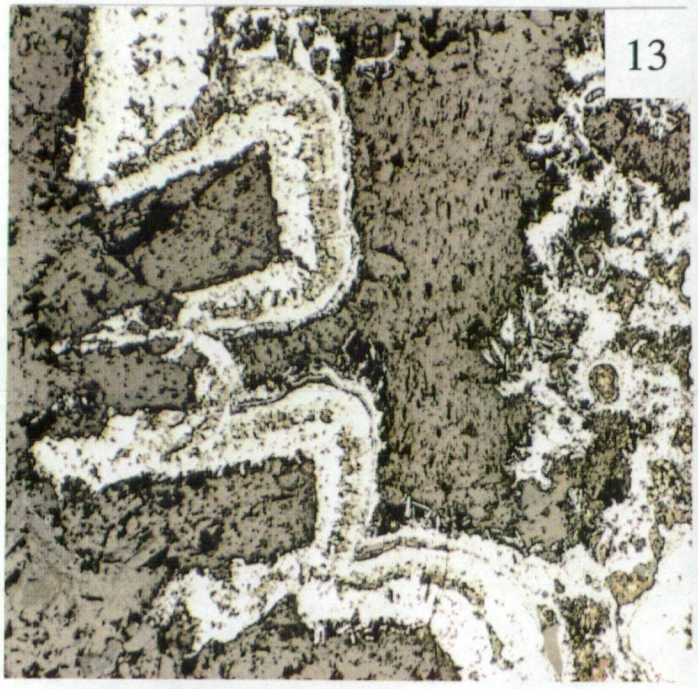
13

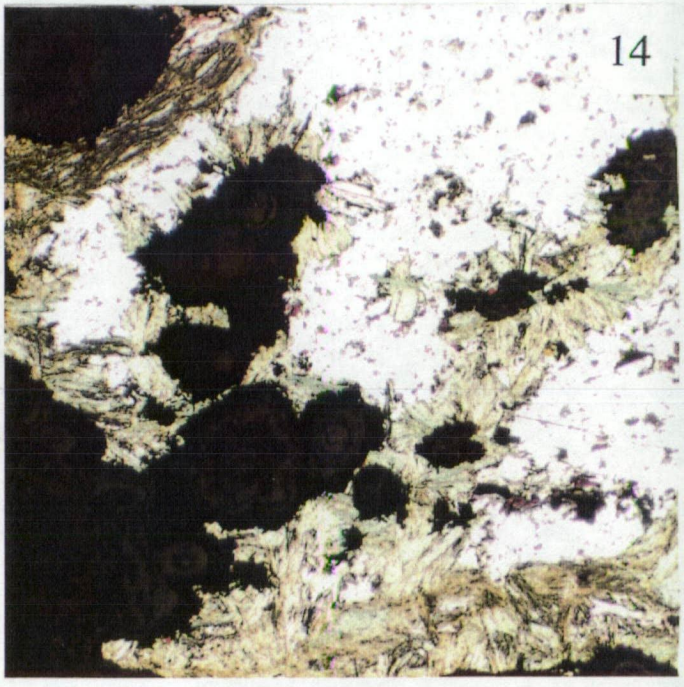
14


15

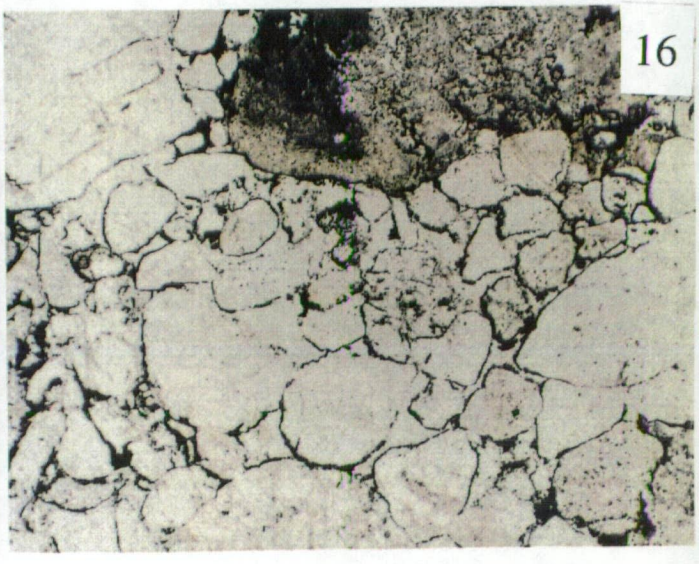
16

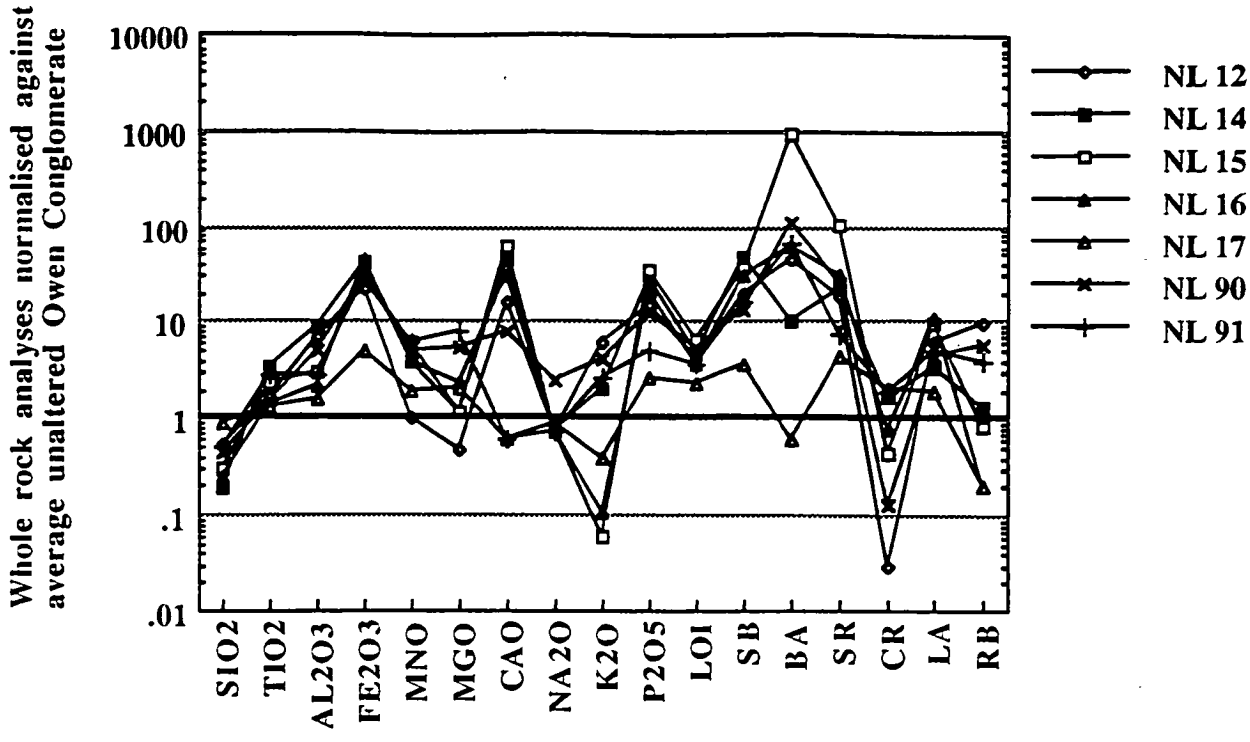

Figure 12 - Whole rock XRF analyses of Owen Conglomerate samples from the Lyell Tharsis mine area (Group 3). Intensely hematitic (>68% Fe_2O_3) samples excluded. Sample descriptions in Appendix I

Geochemistry of Group 3 - Lyell Tharsis

In general the samples from this area are enriched in most elements except SiO_2, K_2O and Rb (compared to the average unaltered Owen Conglomerate, Figure 12) and these vary between samples. Carbonate alteration related to granite emplacement has been found in areas surrounding Mt Lyell (Payne, 1991), and iron-calcium carbonate has been described within the alteration assemblages of Lyell Tharsis and other deposits in the Mt Lyell field (Reid, 1975; Eastoe et al, 1987). There was no carbonate alteration recognised from thin section work in this study, however, significant enrichment of CaO within samples from the Lyell Tharsis area suggests there may be a carbonate component present within the alteration. The principle occurrence of CaO observed within this area was as apatite.

Enriched compared to unaltered Owen Conglomerate	Depleted compared to unaltered Owen Conglomerate
TiO_2, Al_2O_3, Fe_2O_3, MnO, MgO, CaO, P_2O_5, Sb, Ba, Sr, La	SiO_2, Na_2O

Aluminium is present in anomalous amounts within the geochemistry of many samples from this area and reflects the relative abundance of pyrophyllite associated with the

alteration. There is no significant corresponding increase within the other mica minerals (eg. K_2O and Na_2O). The significant increase in Al_2O_3 with respect to the unaltered Owen Conglomerate indicates it is probably not of sedimentary origin but is acting as a relatively mobile element derived from the hydrothermal alteration of feldspars within the adjacent volcanics. The mica alteration within all areas will be discussed further in a later section.

Antimony is significantly enriched within samples from this area compared with the unaltered Owen Conglomerate and also when compared with samples from the adjacent highly altered North Lyell area, and the less altered Batchelors Quarry area. This sets the Lyell Tharsis alteration apart from the alteration within the surrounding areas, both along strike (ie. the area between the North Lyell siliceous pod and Lyell Tharsis), and across strike (ie. the area around Batchelors Quarry). The correlation between the hematite alteration and Sb is best defined within this alteration at Lyell Tharsis. This alteration zone may well characterise the later phase of alteration described by Hendry (1972), with an assemblage dominated by chalcopyrite, hematite, barite, apatite and a rare earth phase.

Mineralogy of the Owen Conglomerate in Group 4 - Batchelors Quarry

The Owen Conglomerate within this area is composed predominantly of grain supported equigranular sandstones and quartzites with variable amounts of intergranular hematite, chlorite and mica. Minor amounts of angular-rounded, quartz-hematite-mica lithic fragments and hematite grains occur in some samples, and are generally of similar size to the surrounding quartz grains. The quartz grains are rarely polycrystalline, range from angular to rounded and exhibit triple junctions and quartz overgrowths within the less hematitic-micaceous samples. Most grains exhibit varying degrees of undulose extinction, however some show good uniformity of extinction, including the quartz overgrowths. The coarser grained sandstones contain more interstitial chlorite and mica, and laminations within the sandstones are defined by the relative grainsize and abundances of hematite, quartz and mica. The rocks of the Owen Conglomerate from this area generally appear to have undergone minimal hydrothermal alteration and structural disruption despite being within a zone of intense folding and hydrothermal fluid movement.

Geochemistry of the Owen Conglomerate in Group 4 - Batchelors Quarry

The geochemistry of the Owen Conglomerate samples shows very little significant difference compared with the unaltered Owen Conglomerate (see figure 13). There is a slight increase in the proportion of mica minerals K_2O and Al_2O_3 and some of the other

alteration minerals (Ba and Fe_2O_3) consistent with some infiltration of hydrothermal fluids. Significantly these alteration minerals tend to decrease in abundance away from the Haulage unconformity, which suggests it may have acted as a conduit for the alteration fluids.

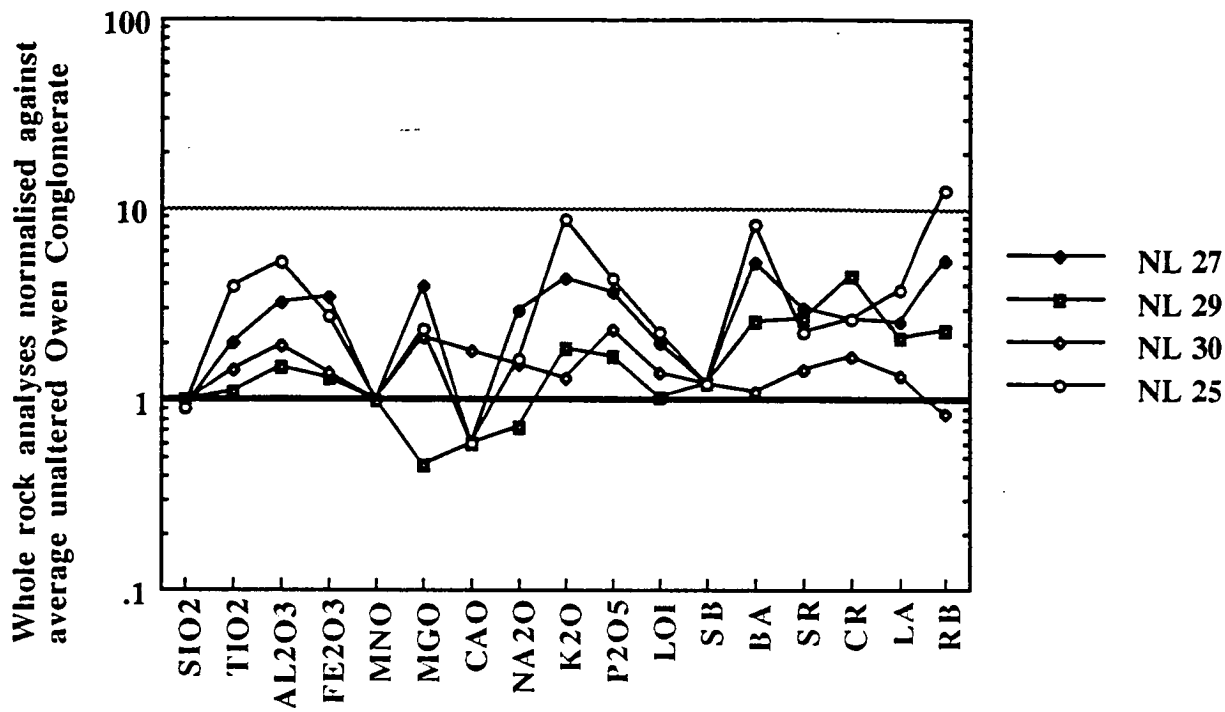

Figure 13 - Whole rock XRF analyses of Owen Conglomerate samples from the Batchelors Quarry and Waterfall area (Group 4) normalised against unaltered Owen Conglomerate value. Pioneer Sandstone samples not included within this graph. Sample descriptions in Appendix I

Mineralogy of the Pioneer Sandstone in Group 4 - Batchelors Quarry and Waterfall area

The mineralogy and stratigraphy of the chromite rich Pioneer Beds is quite variable within this area despite the unit being only 5 metres thick at Batchelors Quarry, thickening to10 metres in the Waterfall area. The Pioneer Beds unconformably overlie the Owen Conglomerate units at Batchelors Quarry (see Plate 3), but the contact appears conformable or disconformable in the Waterfall area (150 metres to the NE). Individual beds range in thickness from a few centimetres to almost two metres and vary from fine grained chloritic sandstones to white chromite rich quartzites, to hematite-chromite rich pebble conglomerates. A minor amount of native copper is present within the more hematitic beds of both the Owen Conglomerate and Pioneer Sandstone at Batchelors Quarry, however none was found within the units at the Waterfall.

A cross bedded, white chromite rich sandstone and the underlying hematitic pebble conglomerate can be recognised both at Batchelors Quarry and the Waterfall area and are thought to be stratigraphic equivalents. These two units occur near the base of the Pioneer Beds at Batchelors Quarry, and near the top of the succession in the Waterfall area. This progressive thickening of the Pioneer Sandstone unit to the NE can be seen at Batchelors Quarry and is thought to continue across to the Waterfall area. The sedimentary features visible in the two units at Batchelors Quarry can also be recognised in the equivalent units in the Waterfall area.

Mineralogically there are slight differences between the units in the two areas. The chromite sandstones exhibit mica infiltration along fractures in both areas, however the sample from Batchelors Quarry contains less mica than the equivalent unit at the Waterfall. The sandstones from both areas also exhibit no hematite infiltration. The hematitic conglomerate unit at Batchelors Quarry contains more interstitial hydrothermal hematite but less mica than the equivalent at the Waterfall.

The basal layers of the Pioneer Beds at Batchelors Quarry are relatively poorly sorted and polymict with variable amounts of hematite (both sedimentary and hydrothermal), chlorite and mica. These minerals occur mainly interstitially to the quartz rich clasts and grains, but they also appear within some of the more irregular, polycrystalline clasts. The quartzose source rocks for these beds appear to be essentially the same as those for the underlying Owen Conglomerate (except for additional detrital chromite), however there is a marked variation in grain and clast size and sorting. The Pioneer Beds are significantly more unsorted and contain a proportion of larger grains and clasts, whereas the underlying Owen Conglomerate (dominated by sandstones at Batchelors Quarry) is essentially monomict with very little variation in grainsize.

Geochemistry of the Pioneer Sandstone in Group 4 - Batchelors Quarry and Waterfall area

The Pioneer Beds were normalised against the unaltered Owen Conglomerate to establish if there was significant hydrothermal fluid movement across the Haulage unconformity. The geochemical differences between the unaltered Pioneer Sandstone and unaltered Owen Conglomerate are relatively minor. The main differences being a slightly higher level of hematite and lower level of chromium within the Owen Conglomerate compared with the Pioneer Sandstone (Figure 14). Due to the similarity of the two units it was considered realistic to compare the two from a geochemical standpoint.

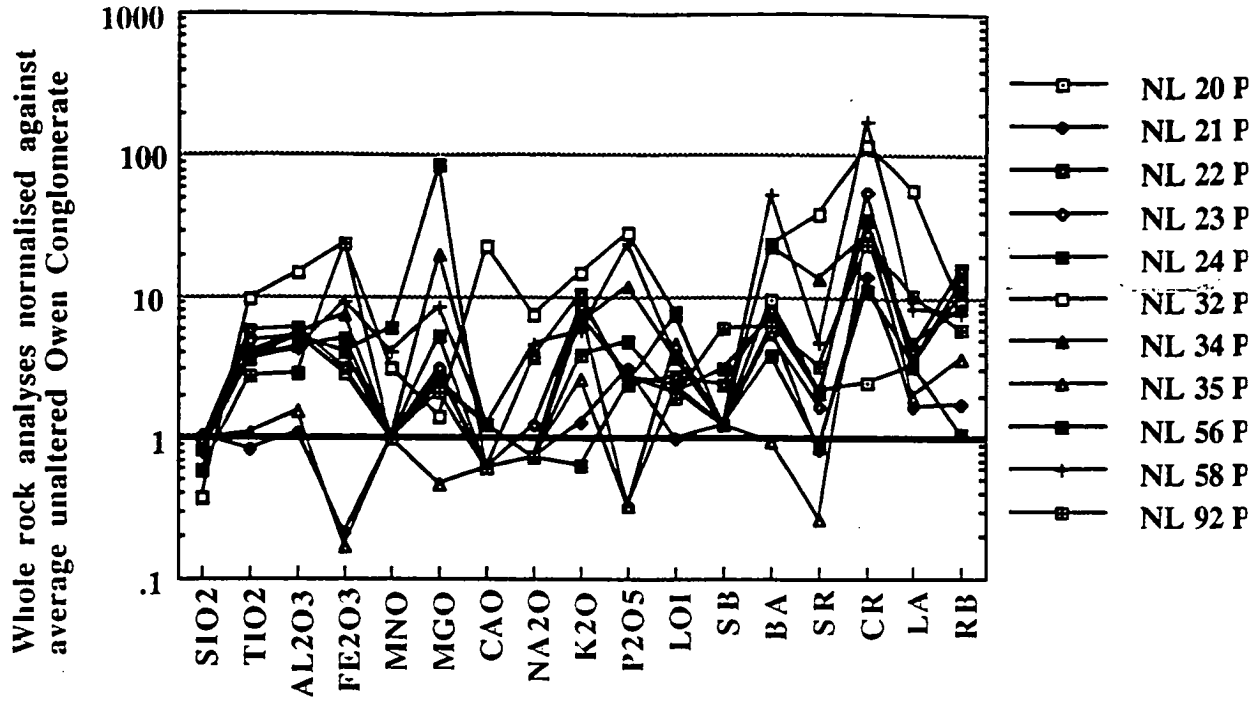

Figure 14 - Whole rock XRF analyses of Pioneer Sandstone samples from the Batchelors Quarry and Waterfall area (Group 4) normalised against unaltered Owen Conglomerate value. Owen Conglomerate samples not included within this graph. Sample descriptions in Appendix I

In general there is an increase in the alteration minerals within the Pioneer Sandstone relative to the unaltered Owen Conglomerate, suggesting there has been hydrothermal fluid movement across the unconformity. It is also notable that the Pioneer Beds are more enriched in the alteration elements than the underlying Owen Conglomerate within this area. The type of sediments being affected by the alteration fluids must also be considered to accurately interpret this information. The porosty of the units being affected by the hydrothermal fluids has been postulated to have a marked effect upon the ultimate degree of alteration within the rocks. The textural differences between the units above and below the Haulage Unconformity tends to suggest otherwise.

Enriched compared to unaltered Owen Conglomerate	Depleted compared to unaltered Owen Conglomerate
TiO_2, Al_2O_3, Fe_2O_3, MgO, K_2O, P_2O_5, Sb, Ba, Sr, La, Rb	CaO, Na_2O

As mentioned previously, the sandstones representing the Owen Conglomerate at Batchelors Quarry have a much more polymict clast and grain make-up and are less well sorted. This variation in size fraction tends to create a less porous unit which has a lower susceptibility to infiltration by hydrothermal fluids yet this unit exhibits a greater

degree of alteration than the more porous sandstones above the unconformity. The lack of alteration within the essentially monomict, well sorted, white chromite sandstones of the Pioneer Beds suggests there are other factors controlling the alteration distribution apart from the primary porosity. The obvious explanation is that the hydrothermal fluids did not affect the Pioneer Beds at Batchelors Quarry, however there are several beds above the Haulage Unconformity which contain the geochemical signature of the alteration fluids. Conglomeratic samples from the Pioneer Sandstone in the Waterfall Area contain a high proportion of alteration minerals and anomalous amounts of elements such as vanadium, zinc, titanium and aluminium. The presence of these elements cannot be attributed solely to hydrothermal alteration. The recognition of detrital hematite clasts within the beds suggests these elements may have been derived from a pre-existing alteration phase. This would also suggest there was a major alteration event prior to deposition of the Pioneer Sandstone (ie. a Late Cambrian-Early Ordovician event).

The geochemical variation along strike within the chromite sandstone and hematitic pebble conglomerate between Batchelors Quarry and the Waterfall Area basically mirrors the mineralogical differences defined earlier. Moving from Batchelors Quarry to the Waterfall, within the chromite sandstone there is a significant decrease in barium and strontium (barite), a significant increase in chromium, a slight increase in Al_2O_3, K_2O and Rb (mica) and a slight decrease in Cu. Within the hematitic conglomerate there is significant decrease in Fe_2O_3, P_2O_5 (hematite), Ba (barite) and a slight increase in Al_2O_3 and K_2O (mica) towards the Waterfall Area.

Mineralogy of group 5 - The Ridge Area, Cape Horn and Mount Owen

All the sediments obtained from these areas are composed almost entirely of quartzose grains and clasts (including Precambrian schistose quartzite clasts), with only a very few examples of the more hematitic lithic fragments. Many grains and clasts have a fine coating of primary or early diagenetic hematite crystals where the hematite defines the clast and grain boundaries and a silica cement fills the voids between the grains (see Plate 16). The hematite may be abundant enough to coalesce and form a coherent cement in some instances. These hematite crystals are thought to have deposited on the quartz grains from pore water trapped during diagenesis. Quartz overgrowths related to pressure solutions between adjacent quartz grains can be seen in some examples of these 'dust rings' of hematite which have been overgrown by quartz.

The zones of hematite enrichment where a coherent cement is formed occur as bands within the sandstones, which essentially define the bedding layers or as lobate pendants seeping down through the stratigraphy (see Plates 6 to 8). The narrow sandstone bands

and lobes exhibiting this phenomenon appear identical to the adjacent non-hematitic varieties from a sedimentary perspective (ie. grain size, sorting, grain supported, etc.), except the non-hematitic variety has a cement composed purely of silica. These spectacular hematite patterns within the sandstones of Cape Horn are thought to be due to weathering effects (Liesegang weathering and hematite crystallisation) rather than hydrothermal fluids. The post-depositional redistribution of the hematite within the sandstones is thought to be strongly controlled by topography and the ability of the connate waters to effect dissolution of the existing cement.

The major occurrence of mica in the Cape Horn and Mt. Owen samples is within the schistose quartzite clasts and other mica bearing clasts, there was also a very minor amount of detrital mica grains within the cement. Clays of unknown origin also form part of the cement between the quartz grains in some samples, possibly due to recent weathering The limited extent of the mica and its principal mode of occurrence as isolated crystals within the hematite-silica cement, suggests the majority of this is detrital and not of hydrothermal origin. There was no hydrothermal hematite recognised and no chlorite found within any of the samples from these areas.

Samples obtained from the Owen Conglomerate in the Ridge Area (ie. closer to the mineralisation), contained a larger amount of interstitial mica which is more likely to have a hydrothermal origin. It occurs as infiltrations along fractures and grain boudaries, frequently associated with hematite. One rock specimen obtained from directly below the Haulage Unconformity contained an abundance of hematite clasts and in thin section hydrothermal hematite disseminations were observed. Chlorite can be seen within voids in the hematite clasts but there was none present between grains. A sample obtained from further along the ridge (further away from the mineralisation) contained a small amount of chlorite within the matrix, closely associated with some clay minerals.

Geochemistry of group 5 - The Ridge Area, Cape Horn And Mount Owen

The geochemistry of this area is not very anomalous with respect to the unaltered Owen Conglomerate (Figure 15). The main elements consistently enriched within the Owen Conglomerate in this area are Fe_2O_3, slight Al_2O_3, slight K_2O and Rb. This corresponds to the hematite enrichment directly below the Haulage Unconformity on the ridge and the sample containing significant amounts of diagenetic hematite.

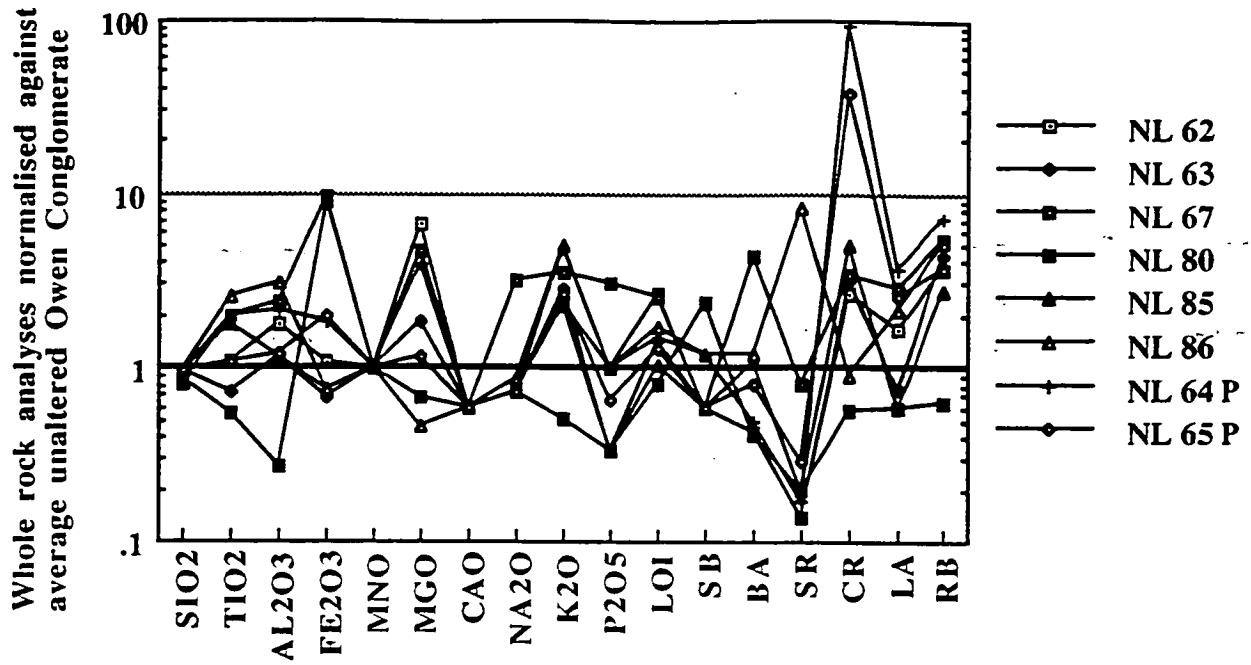

Figure 15 - Whole rock XRF analyses of Owen Conglomerate and Pioneer Sandstone samples from the Ridge Area, Cape Horn and Mt. Owen normalised against unaltered Owen Conglomerate. Sample descriptions in Appendix I

The Pioneer Sandstone samples contain slightly more Fe_2O_3 and Al_2O_3, and significantly more MgO, K_2O and Rb than the unaltered Owen Conglomerate, suggesting there has been hydrothermal fluid activity within these units. Two laterally equivalent examples of Pioneer sandstone from the same bed on the ridge were sampled 100 metres apart and analysed to determine their variation along strike. The samples are geochemically very similar, however the western end of the ridge (ie. closest to the Haulage Unconformity and alteration), contains slightly more Fe_2O_3 and Ba and slightly less Al_2O_3, MgO, K_2O and Rb. This gradation along strike away from the mineralisation of hematite+barite (very weak in this case), to the chlorite and the mica alteration, confirms the observations from Batchelors Quarry. The quantities of these elements within the Ridge Area are significantly lower than the other areas and the alteration minerals are barely visible in hand specimen. However the comparative lateral variation of these alteration elements within the same stratigraphic unit does indicate there are consistent zonation patterns within areas that have been affected by hydrothermal fluid activity.

Mineralogy of Hematitic samples

Eight samples of hematitic conglomerate and vein material (with >68% Fe_2O_3) were considered separately due to their unusual mineralogy and geochemistry. The samples

were obtained from around the North Lyell, Lyell Tharsis and Ridge areas and typify the alteration around the hydrothermally enriched Cu deposits at Mt. Lyell. These samples contain significant information about the geochemistry of the hydrothermal fluid and its interaction with the conglomeratic country rock. The sample descriptions, locations and hematite content are listed below;

NL 16 - hematitic conglomerate - Lyell Tharsis -	69.38% Fe_2O_3
NL 18 - hematitic sandstone - Lyell Tharsis -	84.11% Fe_2O_3
NL 40 - hematite clast - Tharsis Ridge -	78.27% Fe_2O_3
NL 49 - hematite vein - North Lyell -	94.28% Fe_2O_3
NL 55 - hematitic chert breccia - between North Lyell and Lyell Tharsis	69.68% Fe_2O_3
NL 66 - hematitic conglomerate - Ridge area -	69.68% Fe_2O_3
NL 88 - hematitic conglomerate - Lyell Tharsis -	88.23% Fe_2O_3
NL 89 - hematitic conglomerate - Lyell Tharsis -	69.78% Fe_2O_3

The statistical correlation of these samples and others from Solomon (1964), are covered in the statistics section.

The mineralogy of these samples is essentially the same; they are dominated by hematite which occurs as botryoidal, colloform and laminated growths with inclusions of chlorite, barite, muscovite, hematite crystals, quartz and minor zircon and tourmaline. Quartz occurs both as a void filling cement and as fine sand grains from the relict sediment. Partial and total hematite replacement of quartz clasts is visible within thin section of some samples. Conglomeratic textures are visible in some outcrop indicating replacement, however the majority of the hematitic samples exhibit few sedimentary textures. The chert breccia contains chert pebbles with partially hematised selvedges surrounded by a hematite matrix. Botryoidal, colloform and laminated textures may be seen in hand specimen surrounding the chert clasts.

The origin of the botryoidal hematite is poorly understood, however Solomon (1969) suggests it was at least partly precipitated from solution and the botryoids indicate precipitation from colloidal solutions. He also notes the rarity of colloform hematite and suggests it may originate from the dehydration of colloform iron hydroxides during metamorphism. The hematite textures observed at Lyell Tharsis are suggestive of deposition from solution within open space, rather than simple host rock replacement.

Geochemistry of Hematitic samples

The hematitic rocks are generally enriched in most elements associated with the alteration except K_2O and Rb (ie. muscovite) (Figure 16). Most of the enrichment occurs at the expense of quartz which is severely depleted in all these samples. The enrichment of Ca and P_2O_5 (apatite), Al_2O_3 (pyrophyllite), Fe_2O_3 (hematite) and Ba and Sr (barite) relative to the unaltered Owen Conglomerate is noticeable in thin section in most samples although the overwhelming abundance of hematite is thought to obscure some interstitial mineralogy.

Enriched compared to unaltered Owen Conglomerate	Depleted compared to unaltered Owen Conglomerate
TiO_2, Al_2O_2, Fe_2O_2, CaO, P_2O_2, Sb, Ba, Sr, La	SiO_2, K_2O, Rb

If the origin of the hematite within the hematitic conglomerates was directly related to the vein hematite, it would be expected that there would be some similarities in geochemistry. The only true 'vein hematite' analysed (NL 49) displays a geochemical composition very rich in Ba and very depleted in K_2O and Sr relative to the other hematite samples. Assuming the conglomerates were being hematised by the vein material, a geochemical composition somewhere between the hematite vein and the unaltered Owen Conglomerate would be expected for the hematitic conglomerates. This is not readily apparent with most elements, indeed the vein appears more depleted in many elements than the hematitic conglomerates. The hematitic chert breccia is the most geochemically similar to the vein (see statistics section also) suggesting there may be a relationship between the two. The hematitic textures within the two rocks are very similar, the only visible difference in hand specimen is the chert clasts within the breccia. The origin of the hematite in both cases is hydrothermal and the similarities in geochemistry suggests a genetic link between the two.

The geochemical differences between the hematitic conglomerates and the adjacent hematite veins may be due to a number of reasons including; original geochemistry of the unaltered conglomerate; variable thermodynamic conditions affecting element solubility; more than one episode of alteration (ie. another geochemical episode overprinting the hematite) or the conglomerate porosity and its relative exposure to the vein material. The conglomerates exhibit a more phosphate rich alteration style, similar to the later alteration style suggested by Hendry (1972). Analyses for copper showed very little associated with the hematitic veins and conglomerates, however the fluids would have crossed a major redox front at the GLF where most Cu minerals and much of the barite would have been deposited.

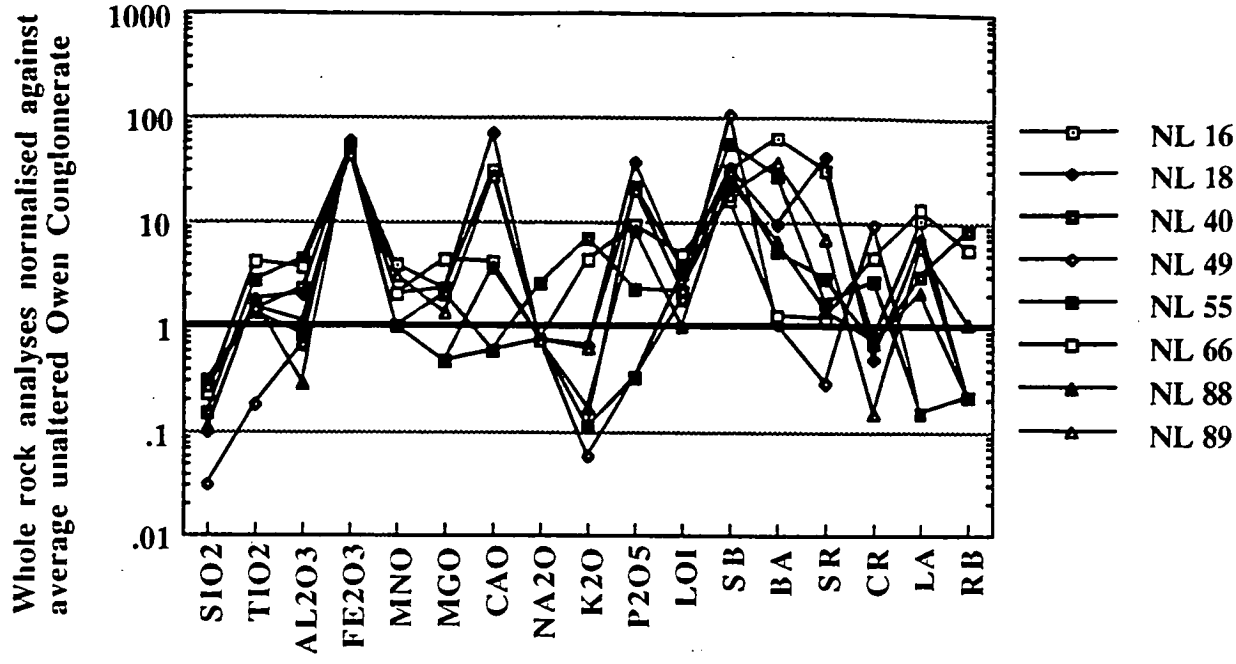

Figure 16 - Whole rock XRF analyses of hematitic Owen Conglomerate samples from North Lyell, Lyell Tharsis and the Ridge Area, normalised against unaltered Owen Conglomerate. Sample descriptions in Appendix I

CHLORITE AND MICA ANALYSIS

Analytical methods

Quantitative geochemical analyses of chlorites and micas from the North Lyell area were obtained using a Cameca SX50 electron microprobe to test for geochemical zonation within these minerals associated with the alteration. The minerals were analysed in polished thin sections using a beam width of 20 μ, an acceleration voltage of 15 kV and a sample current of 10 nA.

Chlorite

A regional Devonian lower greenschist metamorphic event related to the Tabberrabberan Orogeny has had significant effect upon the Mt. Lyell area (Cox,1981; Walshe and Solomon,1981), producing chlorite as the main greenschist facies metamorphic mineral. Markham (1968), suggested many of the mineral phases at Mt. Lyell had undergone recrystallisation and localised remobilisation due to this metamorphic event. Walshe (1977) and Hendry (1981) determined that the composition of many phases (notably chlorite and associated sulphides) was due to a hydrothermal

influence as opposed to a metamorphic one. Walshe and Solomon (1981) suggested a temperature of 260-290 °C reflected metamorphic re-equilibration within chlorites. There were no distinctive optical properties recognised within the samples collected in this study to suggest they were metamorphic rather than hydrothermal. Many of chlorites seen in this study occurred within hydrothermally remobilised assemblages. However if the peak metamorphism associated with the Devonian orogeny attained or surpassed the temperatures and pressures of the hydrothermal event, the chlorite analyses may give misleading results and should be treated with suspicion when the chlorite paragenesis is unknown.

The average of the microprobe analyses of chlorites from the different areas investigated within this study are listed in Table 3, and the classification of these samples according to the system suggested by Foster (1962), can be found in Figure 17. The analyses fall predominantly within the Thuringite-Ripidolite fields with variation in the Fe/(Fe+Mg+Mn) ranging from a low of 42.29 in a sample of Pioneer Sandstone from Batchelors Quarry, to a high of 91.21 from a hematite-barite rich sample from Lyell Tharsis. The silicon-aluminium occupancy of the tetrahedral site within the chlorites varies from $Si_{2.62}Al_{1.38}$ within the North Lyell siliceous pod, to $Si_{2.01}Al_{1.99}$ from a hematitic sandstone at Lyell Tharsis. The high Al content of these samples suggests a substitution of Al^{IV} for Si formed under oxidising conditions during chlorite formation. The formation of 'oxidised chlorites' via the reaction $Fe^{+2} \Rightarrow Fe^{+3}$ with corresponding loss of hydrogen results in a lower H_2O^+ figure, which results in a low total of octahedral ions, whereas the occurrence of primary Fe^{+3} in the chlorite structure is compensated by the replacement of Al for Si (Deer et al, 1982). Thus if Fe^{+3} is the major iron species incorporated within the chlorite structure at the time of crystallisation the substitution of Al^{IV} for Si will result in a high Al content. If the Fe^{+2} is the dominant iron species within the formative chlorite and undergoes oxidation to Fe^{+3} after crystallisation, the resultant loss of H_2O^+ will be reflected in the analysis as a low total of octahedral ions and total H_2O^+.

The analyses obtained from the study area do not have a low total for H_2O^+ or for the total of octahedral ions, but they do have a high Al content, suggesting they were formed under conditions where the more oxidised Fe^{+3} was the dominant iron species and was incorporated within the chlorite structure. This suggests there was a significant amount of hematite present during deposition rather than just magnetite.

	Average NL1 n=11	Average NL3 n=18	Average NL4 n=17	Average NL6 n=10	Average NL8 n=9	Average NL1(n=14	Average NL11 n=14	Average NL12 n=7	Average NL1! n=13	Average NL1! n=10	Average NL2! n=5	Average NL25 n=3	Average NL27 n=6	Average NL29 n=11
SiO2	22.7286	22.7506	22.9566	22.0313	21.8796	22.2127	21.5704	21.5864	19.8150	20.2742	24.8486	24.4947	22.1055	21.7374
Al2O3	24.7184	24.1126	23.9262	24.0742	23.9341	24.1404	24.2324	24.0680	26.4990	25.5311	22.7797	22.6931	23.2639	23.7456
Cr2O3	0.0316	0.0211	0.0312	0.0254	0.0194	0.0110	0.0174	0.0135	0.0155	0.0149	0.0081	0.0660	0.0213	0.1621
MgO	6.2486	6.0956	8.6016	5.0925	4.8430	5.5405	3.2148	4.4557	2.5414	2.7864	16.0307	13.1876	6.4079	4.3484
MnO	0.2375	0.1434	0.2377	0.1408	0.1879	0.1598	0.1304	0.5160	0.5181	0.5366	0.1834	0.1088	0.1350	0.1080
FeO	35.0357	34.8782	31.1088	37.1617	37.0650	36.6032	39.7996	37.2167	38.4563	38.4822	23.0113	27.2457	33.8214	38.4456
H2O	10.9695	10.8468	10.9070	10.7496	10.6583	10.8086	10.6421	10.6215	10.5290	10.4960	11.4216	11.2854	10.5696	10.6574
Total*	100.0019	98.9289	97.7941	99.3069	98.6276	99.5100	99.6375	98.5136	98.3936	98.1456	98.3195	99.0941	96.3714	99.2317
Fe ratio	76.0191	76.3400	67.1718	80.4260	81.1822	78.8407	87.4450	82.6186	89.6377	88.7440	44.8060	53.7933	74.8617	83.2764
* excluding TiO2 and CaO														
Cations on 36 (O,OH) basis														
Si	4.9699	5.0295	5.0487	4.9160	4.9202	4.9295	4.8615	4.8750	4.5150	4.6332	5.2184	5.2062	5.0167	4.8918
Al	6.3703	6.2853	6.2004	6.3314	6.3438	6.3071	6.4376	6.4055	7.1116	6.8768	5.6382	5.6845	6.2234	6.2989
Cr	0.0055	0.0037	0.0055	0.0045	0.0034	0.0019	0.0031	0.0024	0.0028	0.0027	0.0013	0.0000	0.0038	0.0000
Mg	2.0360	2.0077	2.8157	1.6938	1.6235	1.8320	1.0800	1.4995	0.8640	0.9489	5.0177	4.1777	2.1671	1.4591
Mn	0.0440	0.0269	0.0443	0.0266	0.0358	0.0300	0.0249	0.0987	0.1000	0.1039	0.0326	0.0000	0.0259	0.0000
Fe	6.4076	6.4618	5.7255	6.9345	6.9704	6.7943	7.5018	7.0291	7.3288	7.3544	4.0402	4.8430	6.4190	7.2372
Total**	19.8393	19.8215	19.8454	19.9127	19.9037	19.9086	19.9148	19.9174	19.9258	19.9249	19.9563	19.9444	19.8637	19.9417
** excluding Ti and Ca														
Aluminium sites calculated on the basis of 14 oxygens														
Al (iv)	1.5151	1.4852	1.4757	1.5420	1.5399	1.5352	1.5693	1.5625	1.7425	1.6834	1.3908	1.3969	1.4917	1.5541
Al (vi)	1.6701	1.6574	1.6246	1.6237	1.6320	1.6183	1.6496	1.6403	1.8133	1.7550	1.4283	1.4453	1.6201	1.5953
Fe2+/totR2+	0.7549	0.7605	0.6669	0.8012	0.8077	0.7849	0.8716	0.8148	0.8838	0.8748	0.4444	0.5369	0.7454	0.8322
Temperatures (deg. celcius) calculated using the chlorite solid solution geothermometer of Cathelineau and Nieva (1985)														
	339.15	332.82	330.78	344.86	344.42	343.43	350.65	349.22	387.43	374.88	312.77	314.07	334.18	347.43

Table 3 - Average chlorite microprobe analyses and geothermometer calculations

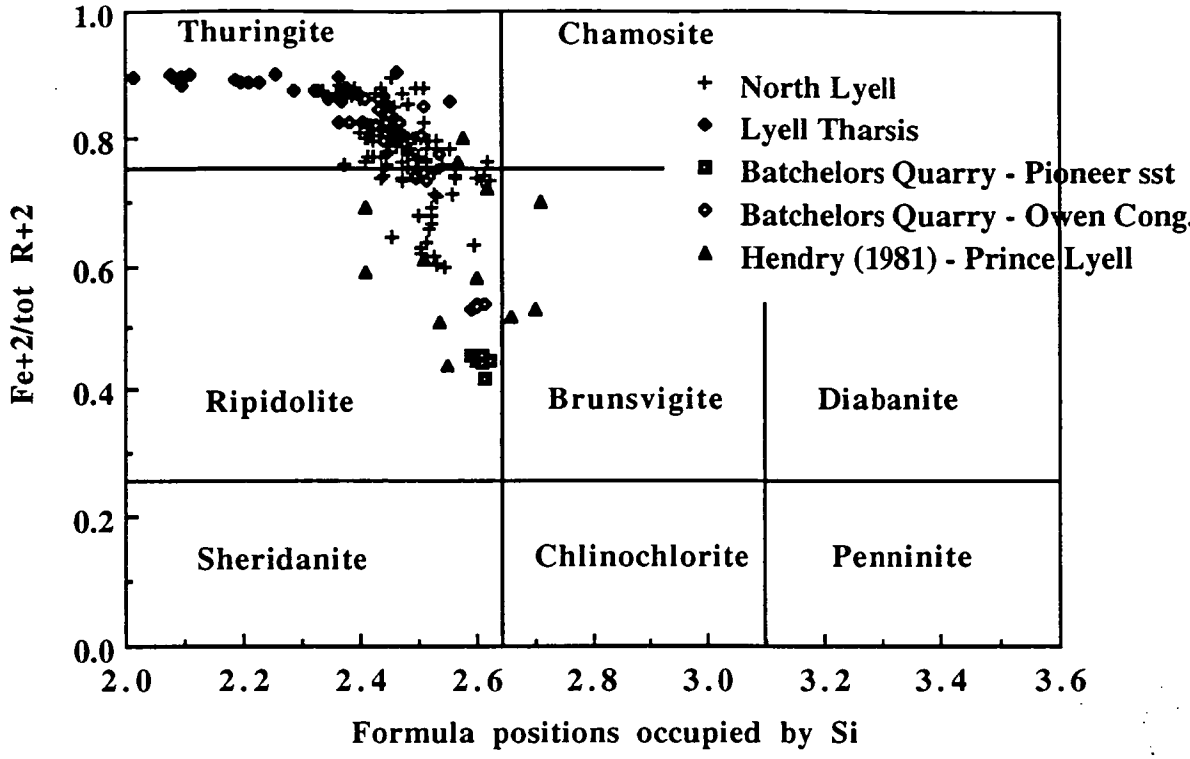

Figure 17 ; Comparison of chlorite analyses from North Lyell, Lyell Tharsis, Batchelors Quarry and Prince Lyell (Hendry, 1981). Classification using the method of Foster, (1962). (tot R+2 = Fe^{+2}, Mg^{+2}).

The study by Hendry (1981) of the chlorites, phengites and siderites from Prince Lyell notes the association between the presence of magnetite and the deficiency of Al^{VI} compared to Al^{IV}. Within the samples obtained for this study there were no samples where Al^{IV} exceeded Al^{VI}, which also suggests a dominance of Fe^{+3}. Some of the analyses obtained from the Prince Lyell orebody by Hendry (1981) are plotted on Figure 17 for comparison with the chlorites from this study.

Chlorite Geothermometry

Cathelineau and Nieva (1985) proposed a solid solution geothermometer utilising the Al^{IV} occupancy in the chlorite structure. A sample from Mt. Lyell was included in their data to show that it fitted their model, which was based on chlorite analyses from the Los Azufres geothermal system in Mexico. Utilising this technique for temperature estimation at Mt. Lyell generated a range of temperatures from 309°C within the siliceous pod at North Lyell, to 439°C within a hematitic sandstone at Lyell Tharsis. The average temperature for the entire sampled area was 345°C with a standard deviation of 23°C, although a better appreciation of the temperatures and their reliability can only be gained by considering each area separately (Table 4).

	North Lyell	Lyell Tharsis	Batchelors Quarry	
			Owen Conglomerate	Pioneer sst
Fe ratio average	77.63	87.64	75.59	44.81
Standard dev	6.61	3.26	11.02	1.31
Temperature average	339.96	373.98	337.60	312.77
Standard dev	12.42	30.26	13.74	2.31

Table 4 - Table of averages for each area calculated on 14 oxygens, temperature from Cathelineau and Nieva (1985)

The average temperature calculations obtained for the different areas are slightly higher than the six component chlorite solid solution calculations of Walshe and Solomon (1981), of 270-310°C in the Prince Lyell deposit. They also list homogenisation temperatures from fluid inclusions within recrystallised fluorite from a quartz-chlorite-chalcopyrite vein at Western Tharsis with a range from 200-225°C. The temperatures obtained for the North Lyell pod and Batchelors Quarry are very similar, however the degree of hydrothermal alteration experienced by the two is vastly different. North Lyell has been completely recrystallised while Batchelors Quarry has only undergone relatively mild alteration. The temperature calculations for North Lyell are not thought to accurately reflect the temperature of hydrothermal alteration experienced within that area. This may be due to the Devonian metamorphic overprint or inaccuracies inherent within the chlorite geothermometer model when applied to a situation where the conditions of mineralisation are different to the model conditions. The temperatures calculated for Lyell Tharsis and Batchelors Quarry are thought to be more realistic interpretations.

The variation in the Fe ratio is of more interest, showing a strong zonation between the Owen Conglomerate at Lyell Tharsis and Batchelors Quarry, and a sudden drop across the Haulage Unconformity. This is consistent with the degree of hematite alteration found within these areas and the increasing chlorite concentration towards the less altered areas such as Batchelors Quarry. It is also interesting to note the decrease in the Fe ratio within the Owen Conglomerate towards the Haulage Unconformity which does

not parallel the iron content of the respective rocks. Overall it can be seen that there is a steady increase in the Fe ratio towards the more intense hematite alteration areas.

Mica Analyses

Thin section investigation of the micas obtained from the study area revealed a variety of occurrences and types of mica. Within the Owen Conglomerate it occurs as grains in the Precambrian quartzite clasts, detrital grains within the less altered conglomerates and sandstones and as a hydrothermal product within veins and in the matrix of some hydrothermally altered rocks. Microprobe analyses of these various micas were tabulated and the activities of Na, K and Al calculated using the technique of Bird and Norton (1981). The calculated activities from the different alteration areas are shown plotted on a ternary diagram (Figure 18).

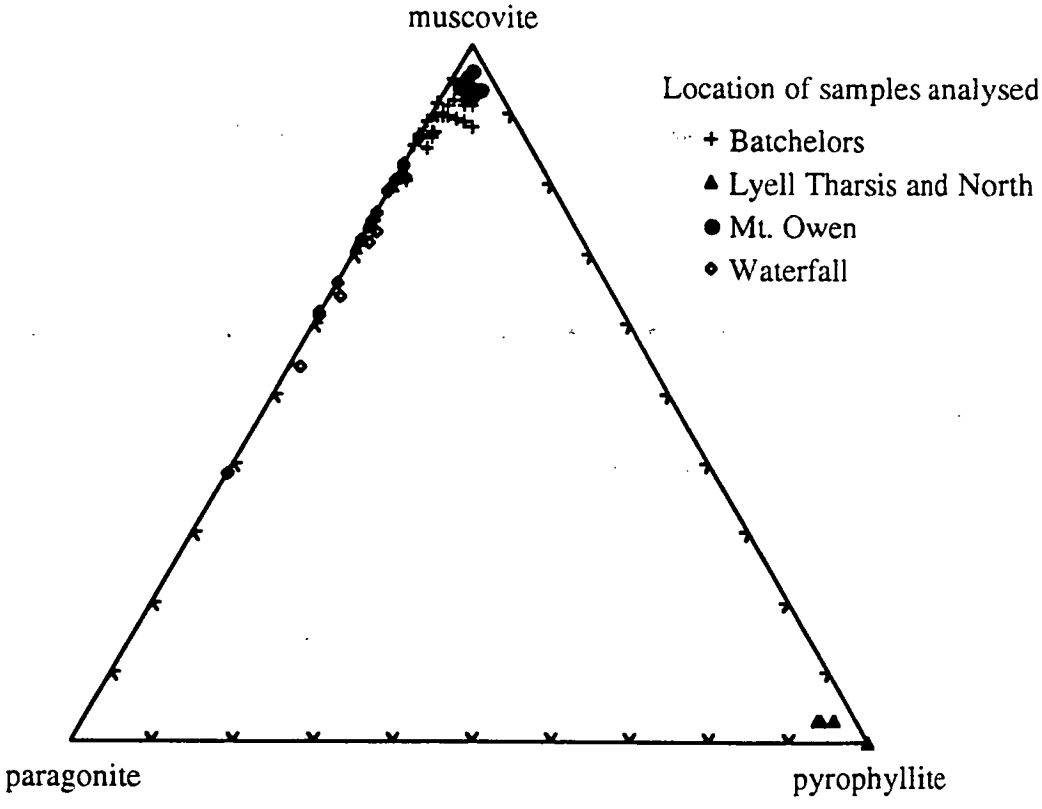

Figure 18 - Ternary plot of muscovite-pyrophyllite-paragonite activities calculated from microprobe analyses of samples from Lyell Tharsis (including North Lyell), Batchelors Quarry, the Waterfall Area and Mt. Owen.

There was a broad zonation in mica chemistry recognised between the most intensely altered North Lyell-Lyell Tharsis areas to the unaltered sample obtained from Mt. Owen. The intensely silica/hematite altered samples are dominated by hydrothermal pyrophyllite with minor Na rich phengite. Mica analyses from Batchelors Quarry (above and below the Haulage Unconformity) generally had consistent geochemistry, with minor Na enrichment in some analyses. The analyses from the lower parts of the

Pioneer Beds (close to the Haulage Unconformity) and the Owen Conglomerate at Batchelors Quarry contain slightly more Na than the micas from the upper parts of the Pioneer Beds and the Mt. Owen samples. The sample of Pioneer Sandstone from the Waterfall Area contained significantly more Na within the micas than those from Batchelors Quarry which is also reflected in the whole rock geochemistry (ie. there is a good correlation between high sodium in micas and the corresponding whole rock analysis).

Parry et al (1984) found the composition of hydrothermal muscovite to be largely dependant upon the activities of Na^+ and K^+ in solution. If the unaltered sample obtained from Mt. Owen is taken as a standard for mica composition (ie. mica composition unrelated to hydrothermal alteration), it can be seen that there is an overall increase in the Na content of the micas towards the more intensely altered specimens at North Lyell (see Figure 19). The high quantities of Na within the mica analyses from the Waterfall area would suggest this sample has been in contact with a more sodic hydrothermal fluid (ie. higher Na activity than Batchelors Quarry). The equivalent whole rock analysis of this specimen shows anomalous levels for most alteration minerals including K_2O, Fe_2O_3 and Ba. There does appear to be a general correlation between the quantity of alteration minerals within a specimen and the sodium content of the corresponding micas (ie. the more higher temperature alteration minerals in whole rock the higher the Na content of micas). However sodium was not generally found to be a significant alteration element within whole rock analyses, with levels frequently below detection limits particularly within the intensely silicified North Lyell area. The most enriched Na levels within the phengites occurred around Lyell Tharsis (with intense hematite alteration) and the Waterfall Area (within a very hematitic sample), suggesting the Na within the alteration fluid is being recorded within the micas by a higher Na content. This is unusual because the alteration at Mt. Lyell was pervasively albite destructive with corresponding removal of Na, so the Na saturation with respect to muscovite is puzzling.

The phengite geochemistry appears to define a halo of alteration around the more intensely silicified and hematised areas. An inner zone of aluminium enrichment at Lyell Tharsis is recognised by the dominance of the sheet silicate pyrophyllite with an average composition of $Al_{2.12}[Si_{3.88}O_{10}](OH)_2$, with little deviation from this composition. Minor Na rich phengite was associated with the pyrophyllite at Lyell Tharsis with an average composition of $K_{0.64}Na_{0.24}(Al_{1.90}(Mg_{0.02}Fe_{0.17}))(Si_{3.02}Al_{0.98})O_{10}(OH)_2$. The other altered sample from the Waterfall Area had an average phengite composition very similar to this, ie. $K_{0.64}Na_{0.25}(Al_{1.91}(Mg_{0.02}Fe_{0.13}))\ (Si_{3.04}Al_{0.96})O_{10}(OH)_2$. This grades out to areas

with less intense alteration containing phengites of lower sodic composition. The average of the phengite analyses from Batchelors Quarry contain significantly less Na but more K and Mg (ie. $K_{0.83}Na_{0.07}(Al_{1.76}(Mg_{0.12}Fe_{0.16}))\ (Si_{3.14}Al_{0.86})O_{10}(OH)_2$. The unaltered sample from Mt. Owen had values very similar to this with an average composition of $K_{0.86}Na_{0.03}(Al_{1.78}(Mg_{0.12}Fe_{0.15}))\ (Si_{3.19}Al_{0.81})O_{10}(OH)_2$. Figure 19 defines the variation in alteration, from most altered (pyrophyllites) on the left to the least altered phengites from Mt. Owen and Batchelors Quarry.

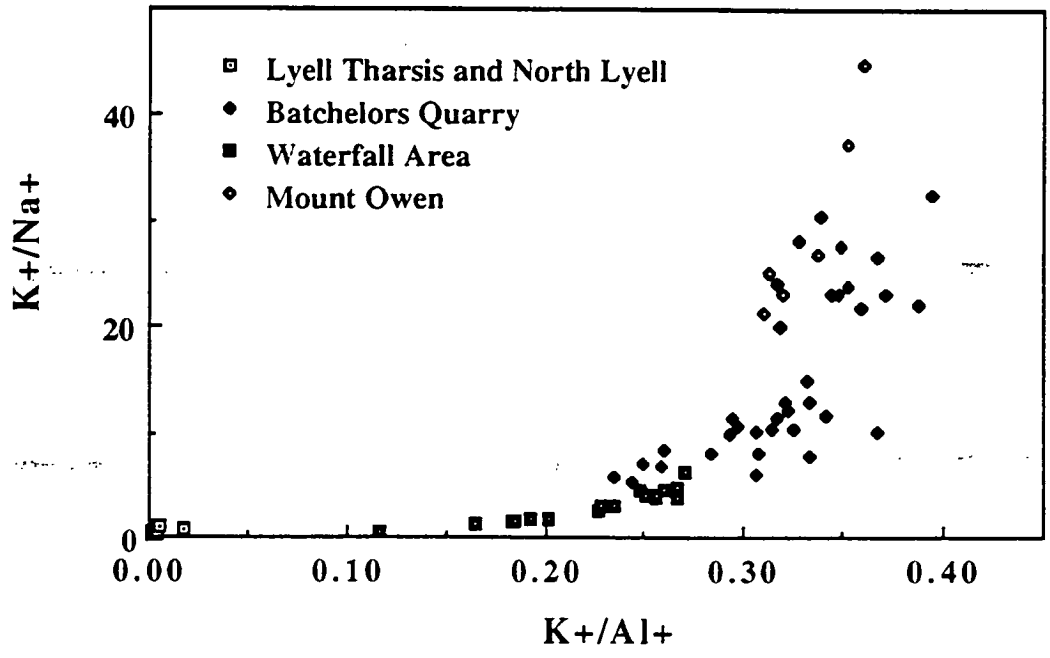

Figure 19 - A plot of ionic ratios of potassium, aluminium and sodium from different areas within the study area. Data obtained from microprobe analyses of phengites and pyrophyllites.

There was no apparent zonation of volatiles within the micas, indeed most of the analyses contained F and Cl levels below detection limits. The effect of 'Fe-F avoidance' (Munoz, 1984) may be occurring within these micas affected by high Fe fluids. This has been observed within micas from numerous other deposits (eg. Jacobs and Parry, 1979; Ekström, 1972) and suggests the octahedral Mg controls the (F, OH) exchange (Parry et al., 1984; Gunow et al., 1980). The micas within the ferruginous rocks from the study area generally contain less Mg and have correspondingly lower fluorine values. Chlorine was not present within the micas in sufficient quantities to warrant observation.

HYDROTHERMAL FLUID GEOCHEMISTRY

Computer Modelling of North Lyell Hydrothermal Fluids

Mineralisation at Mt. Lyell is believed to be primarily of Cambrian, syngenetic, volcanic stockwork origin, with minor volcanogenic exhalative mineralisation. A later episode of epigenetic hydrothermal enrichment is recognised at North Lyell and several other deposits (Solomon et al, 1987; Arnold, 1985). The timing of this secondary Cu enrichment event has been debated for some time. The presence of ore within the Late Cambrian - Early Ordovician Owen Conglomerate (Wade and Solomon, 1958; Sillitoe, 1985) suggests that remobilisation must have occurred syn or post-conglomerate deposition. A Devonian age associated with the regional Tabberabberan Orogeny is favoured by many authors (eg. Solomon et al., 1987; Arnold, 1985; Solomon and Walshe,1981), although some argue for a Late Cambrian - Early Ordovician event associated with a late stage of volcanism (Reid, 1975).

The aims of this section are twofold; to determine a likely process for the formation of the North Lyell deposit, and to investigate the extent and mode of alteration within the surrounding sediments to ascertain the timing of the mineralisation. Recognition of the various styles of alteration and the extent, both along and across strike within the country rocks around the North Lyell area are major factors to be considered when defining a mineralisation age for North Lyell. By modelling the hydrothermal alteration within the sediments surrounding North Lyell, an appreciation of the styles of alteration expected may be gained and utilised in conjunction with the whole rock analyses for testing of potential anomalism. To investigate possible origins of alteration associated with the secondary hydrothermal event at North Lyell, numerical simulations have been undertaken using the computer programs GEOCAL, SOLVEQ and CHILLER (Reed, 1982; Reed and Spycher, 1984, 1985). These programs utilise the thermodynamic database SOLTHERM (Reed and Spycher, 1991). Additional thermodynamic data was derived using SUPCRT92 (Johnson et al., 1991).

A hypothetical high temperature fluid (based on the data of Walshe and Solomon, 1981) has been developed using forced mineral equilibrium techniques. This fluid has then been used in simulations that test a variety of potential depositional mechanisms including; boiling, cooling and fluid rock interactions with the volcanics and the surrounding sediments.

Physico-Chemical Conditions Of North Lyell Fluids

Most of the initial conditions used in the modelling of the North Lyell fluids are those formulated by Walshe and Solomon, (1981). Initial parameters of ΣS (0.0015m), pH

(4.65, ie. 1 unit acid), $\log fO_2$ (-30.474, ie. $\log \Sigma SO_4/H_2S = -1$), and temperature (300° C) were selected as representative of the hydrothermal mineralising fluid. Initial estimates for other component species obtained from Walshe and Solomon (1981) include Ca (mCa^{+2}=0.001), Na (mNa^{+2}=0.9), Cl (mCl^{-}=1.0), K (mK^{+}=0.1) and Mg (mMg^{+2}=0.025). These values were progressively modified to maintain charge balance (using Cl^{-}), pH (using H^{+}) etc. as the fluid was updated from the basic composition listed above. The concentrations of unknown component species (eg. SiO_2, Al, Fe, etc.) were determined by forcing equilibrium between the initial fluid and the appropriate sulphide, oxide, silicate, sulphate or phosphate minerals. The following minerals were used in forced mineral equilibrium calculations; $SiO_{2(aq)}$ - quartz; Al^{+3} - muscovite; Fe^{+2} - pyrite; Zn^{+2} - sphalerite; Cu^{+} - chalcopyrite; Pb^{+2} - galena; Ag^{+} - acanthite; $AuCl^{-}$ - gold; Ba^{+2} - barite; HPO_4^{-2} - apatite. This resulted in the theoretical fluid being saturated with each of these species, which in reality was obviously not the case for some metals.

Several potential mineralising fluid compositions were tested using CHILLER. If metal concentrations were found to be too high or low for realistic mineral assemblages to be reproduced component species concentrations were modified until a realistic starting fluid was produced. The base metal, gold and silver values were modified to approximate potential ore forming fluids adapted from Skinner (1979) (after Muffler and White, 1969), White (1974) and Large et al. (1991). The updated values for the metals within the fluid were; Cu=10 ppm, Au=1 ppb, Ag=100 ppb, Zn=1 ppm and Pb=1 ppm. At this level Cu was supersaturated within the fluid and precipitated prior to initiation of the simulations. The amount of Cu needed for saturation of the fluid was approximately 6.11 ppm. This 'dumping' of Cu at the start of each simulation has been adjusted by subtracting the amount of Cu precipitated before initiation of the simulation from the total amount of Cu deposited during the simulation. The concentrations of all component species of the initial hypothetical fluid are listed in Table 5 along with some modified compositions.

Depositional Processes at North Lyell

The hypothetical hydrothermal Fluid 1 (Table 5) has been subjected to simulations of boiling, cooling and water-rock interactions (Figure 20), using average compositions of the average Cambrian altered volcanics (both mafic and felsic varieties), Owen Conglomerate and Gordon Limestone. In the following sections the mineral assemblages precipitated during these simulations are compared with the actual known mineralogy to gain a greater understanding of the likely depositional processes that operated at North Lyell.

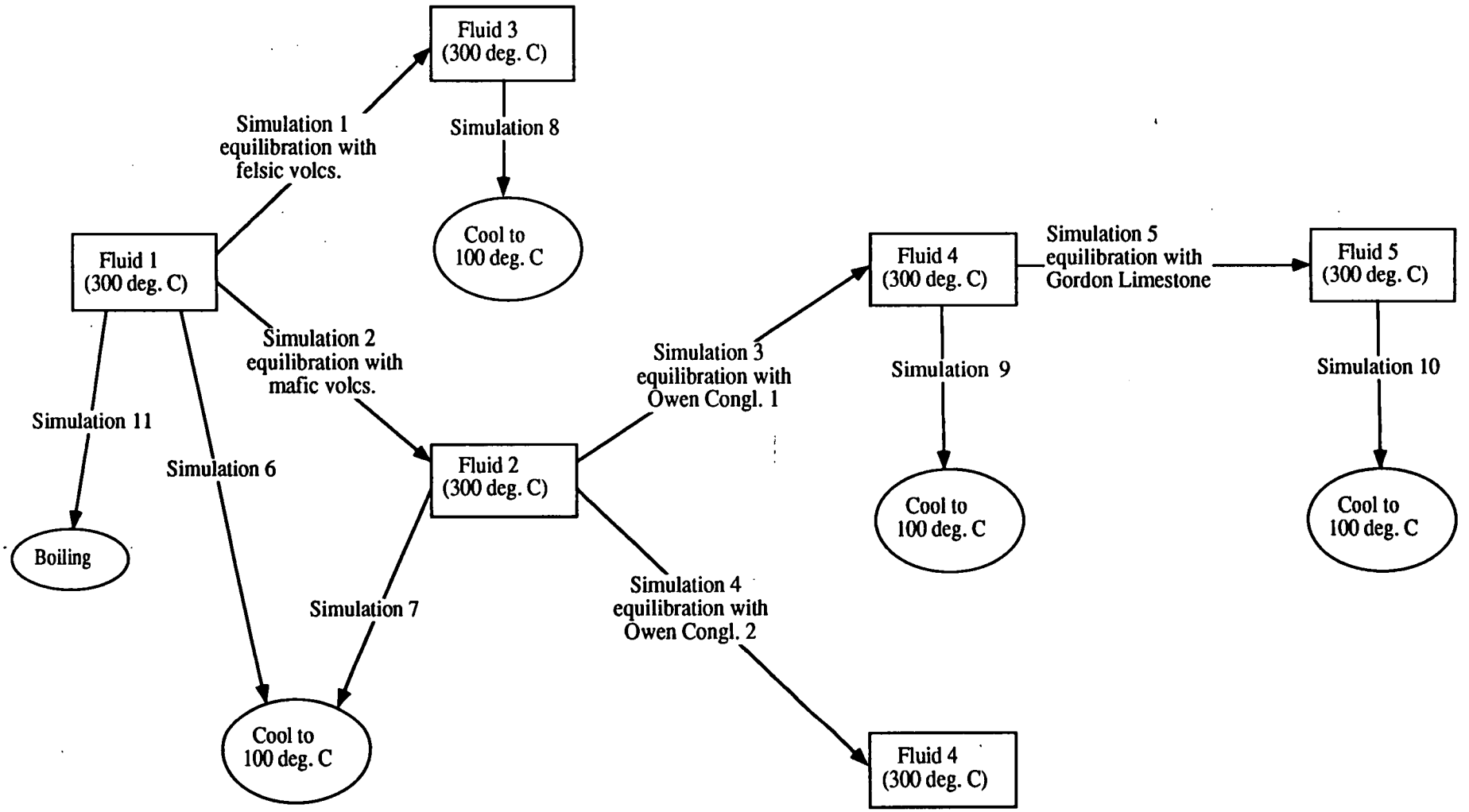

Figure 20 - Flow diagram showing manipulation of fluids with titrations, cooling and boiling simulations numbered for reference in text . Owen Conglomerate 1 = 85% quartz, 10% hematite and 5% kaolinite. Owen Conglomerate 2 = 50% quartz, 50% hematite

	Mineral for equilibration	Fluid 1	Fluid 2 (fveq)	Fluid 3 (mveq)
pH		4.65	4.73	4.72
log $f(O_2)$		-30.474	-30.52	-30.54
ΣS		0.0015	0.0015	0.0015
H^+		2.45 E-01	2.44 E-01	2.44 E-01
H_2O		1.00 kg	1.00 kg	1.00 kg
Cl^-		1.03 E+00	1.03 E+00	1.03 E+00
SO_4^{-2}		7.72 E-05	7.61 E-05	8.06 E-05
HCO_3^-		2.44 E-01	2.44 E-01	2.44 E-01
HS^-		1.52 E-03	1.40 E-03	1.45 E-03
$SiO_{2(aq)}$	quartz	9.73 E-03	1.03 E-02	1.02 E-02
Al^{+3}	muscovite	5.58 E-06	1.54 E-04	1.33 E-04
Ca^{+2}		1.01 E-03	1.01 E-03	1.01 E-03
Mg^{+2}		4.41 E-03	4.69 E-03	5.23 E-03
Fe^{+2}	pyrite	2.48 E-04	2.13 E-04	2.37 E-04
K^+		1.01 E-01	1.01 E-01	1.00 E-01
Na^+		9.11 E-01	9.11 E-01	9.11 E-01
Mn^{+2}	chlorite	6.82 E-07	6.82 E-07	6.82 E-07
Zn^{+2}	sphalerite	1.60 E-05	1.60 E-05	1.60 E-05
Cu^+	chalcopyrite	2.00 E-04	1.24 E-05	1.24 E-05
Pb^{+2}	galena	5.10 E-06	5.10 E-06	5.10 E-06
Ag^+	acanthite	1.00 E-06	1.00 E-06	1.00 E-06
$AuCl_2^-$	gold	4.61 E-09	4.61 E-09	4.61 E-09
Ba^{+2}	barite	1.42 E-03	1.41 E-03	1.41 E-03
HPO_4^{-2}	apatite	1.16 E-04	1.16 E-04	1.16 E-04

Table 5 - Potential ore forming fluid compositions for North Lyell, modelled at 300°C. Component species values in molal units unless otherwise stated. Fluid 1 is the initial hypothetical mineralising fluid composition, based on estimates of by Walshe and Solomon (1981). Fluid 2 (fveq) is modified Fluid 1 by equilibration with average felsic volcanic from Mt. Lyell (specimen no. 31634 from Solomon, 1964). Fluid 3 (mveq) is modified Fluid 1 by equilibration with average mafic volcanic from Mt. Lyell (specimen no. 31699 from Solomon, 1964).

Rock titrations

If the composition of the hydrothermal fluids responsible for mineralisation and alteration at North Lyell were controlled primarily by the altered Cambrian volcanics, fluids entering the Owen Conglomerate would have a composition largely buffered by the widespread quartz-sericite-chlorite-pyrite alteration within the CVC. For this reason simulated titrations of Fluid 1 into the volcanics was undertaken to see if a quartz-sericite-chlorite-pyrite alteration assemblage could be produced. This allowed potentially more realistic fluid compositions to be calculated, which could then be reacted with the Owen Conglomerate and Gordon Limestone and also subjected to cooling simulations. For these purposes, an average rock composition for each of the

units around North Lyell was defined. This enabled a comparison to be made between the simulated and observed alteration assemblages within the various lithologies.

The average composition of an altered felsic and altered mafic volcanic rock from the Mt. Lyell area were obtained by doing 200 point counts on two thin sections (sample nos. 31699 and 31634; Solomon, 1964). The average mineral compositions of the Owen Conglomerate and Gordon Limestone used in this simulation were determined from thin sections and whole rock analyses obtained for this study (NL 37 for the conglomerate; NL 97 for the carbonate). The mineral compositions used for the titration exercises are listed below (Table 6). Mineral fractionation was allowed during all simulations and pressures were maintained at a level sufficient to suppress boiling of the fluid.

Minerals	Mafic volcanic (31699)	Felsic volcanic (31634)	Owen Conglomerate (NL 37)	Gordon Limestone (NL 97)
Quartz	35%	55%	85%	10%
Chlorite	50%	9%	-	-
Muscovite	12%	35%	-	5%
Pyrite	3%	1%	-	-
Hematite	-	-	10%	-
Kaolinite	-	-	5%	-
Calcite	-	-	-	85%

Table 6 - Average mineral compositions for various units within the study area used in titration simulations. Compositions of volcanics from Solomon (1964), mafic volcanics from specimen 31699, felsic volcanics from specimen 31634 (Tasmania Geology Dept. numbers).

Titration into felsic volcanic (simulation 1)

Progressive titration of the fluid into the felsic volcanics until equilibrium was attained produced the mineral assemblage shown in Figure 21. This simulation caused 53% of the available Cu to be deposited as chalcopyrite in progressively smaller increments.

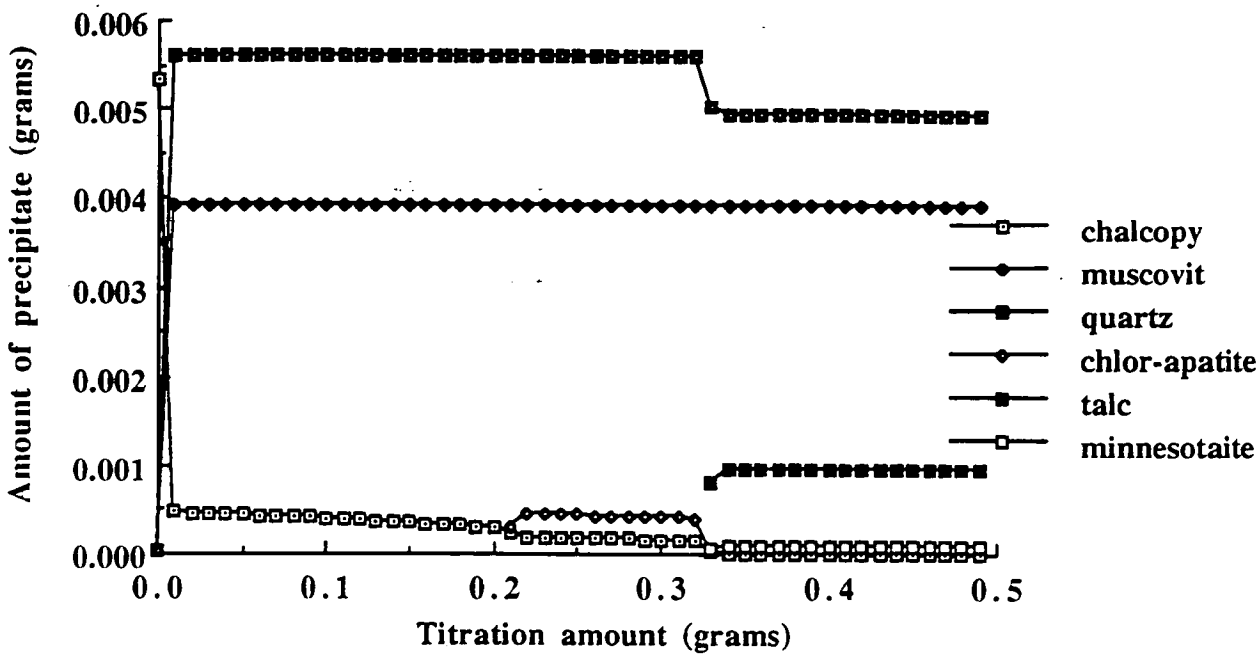

Figure 21 - Plot of titration amount into felsic volcanic showing precipitation cycles of minerals up until equilibrium is attained

The appearance of minnesotaite and talc in the assemblage corresponded with a decrease in the rate of quartz precipitation and the disappearance of chlor-apatite from the precipitating assemblage. These events occurred directly after the pH and log fO_2 reached stable levels after some initial variation. The pH rose steadily from an initial low of 4.48 to stabilise at 4.73, the log fO_2 decreased steadily from -30.32 to -30.52 at final equilibrium. Quartz and muscovite were precipitated continuously and dominated the final assemblage (Figure 22). There was no gold deposited during this simulation possibly due to the high a_{H_2S} (ie. very little pyrite deposition). The lack of pyrite precipitation is thought to reflect the initial wallrock concentrations of pyrite.

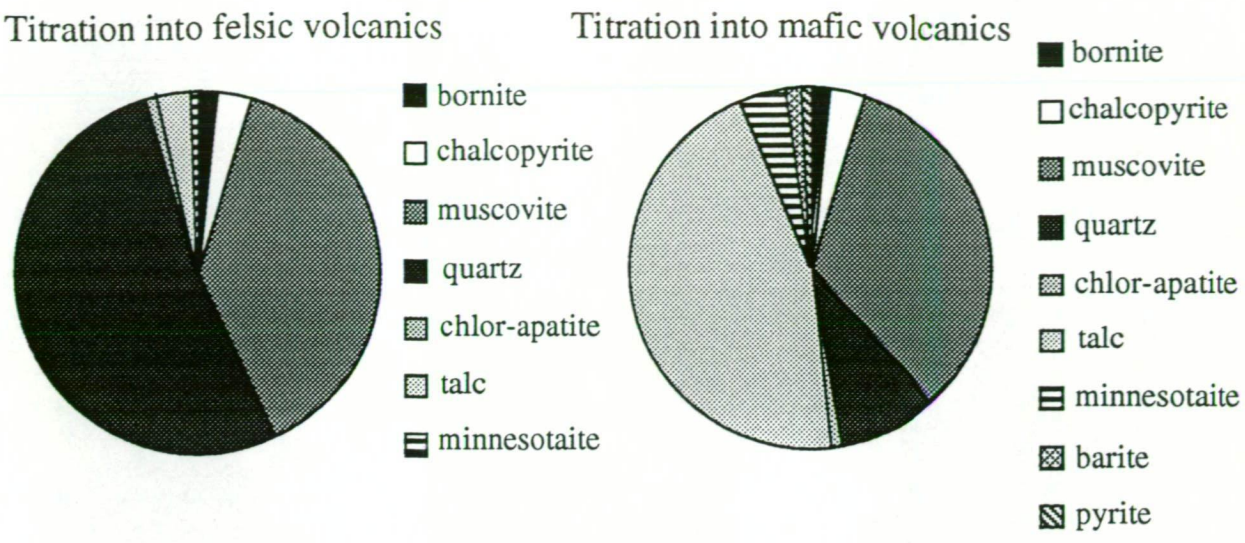

Figure 22 - Relative proportion of minerals precipitated during titration of Fluid 1 into felsic volcanics (left) and mafic volcanics (right) showing all mineral phases. Composition of volcanic rocks used in this simulation are listed in Table 6

Titration into mafic volcanic (simulation 2)

Titration of Fluid 1 into the mafic volcanics produced a more varied assemblage than the equivalent felsic volcanics titration, but Cu was deposited in similar quantities. Most of the available Cu (58%) was deposited as chalcopyrite, initially in large increments which decreased steadily to the point where pyrite became the dominant sulphide (Figure 23). Talc is the dominant alteration mineral during this simulation and is considered to represent chlorite as explained previously.

Changes in pH and log fO_2 were similar to the felsic volcanic titration, with a steady rise in pH from an initial low of 4.48 to a plateau of 4.72, and a consistent decrease in log fO_2 from -30.32 to an equilibrium of -30.54. Gold was not deposited during this simulation.

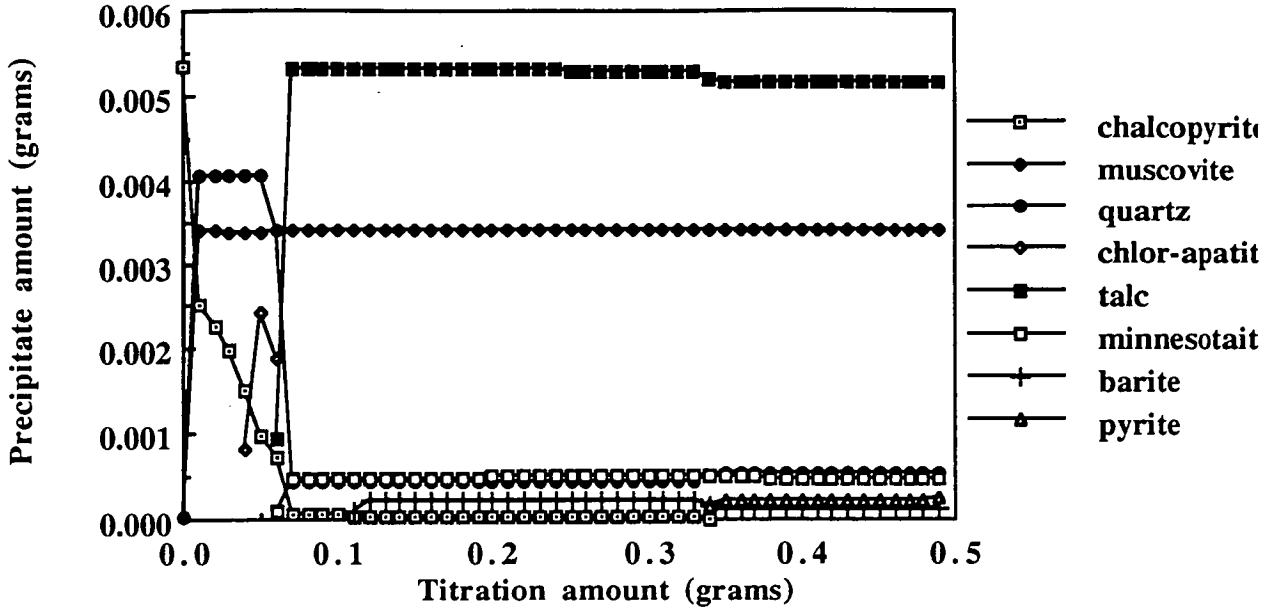

Figure 23 - Plot of titration amount into mafic volcanic showing precipitation cycles of minerals up until equilibrium is attained

Titration into Owen Conglomerate 1 (simulation 3)

Titration of Fluid 1 into a rock composed of 85% quartz, 10% hematite, 5% kaolinite at 300°C was simulated to see if the North Lyell assemblages could be reproduced. 58% of the available Cu was deposited as chalcopyrite, and the initially high precipitation rates decreased quickly as Cu was rapidly depleted from the fluid. Chalcopyrite ceased to precipitate and pyrite deposition was reduced to insignificant amounts upon the commencement of hematite deposition. The co-precipitation of hematite and pyrite indicates that log $fO2$ was buffered by these minerals. The pH of the fluid remained moderately acidic (muscovite-stable), but oxygen fugacities eventually evolved to more oxidised (hematite-stable) conditions. Bornite replaced chalcopyrite as the stable Cu mineral in the hematite field, however the rapid depletion of Cu in the early part of this simulation prevented bornite deposition.

Of the total Fe introduced into the system, 1% was precipitated as pyrite, and 5% as hematite. Barite had two small windows of deposition during the simulation, depositing a total of 1% of the available Ba at the beginning and the end of the titration. This is consistent with field observations at North Lyell which recognise more than one stage of barite crystallisation within the Owen Conglomerate. Muscovite and quartz were deposited continuously through the titration and dominate the final assemblage (Figure

24). During the simulation the pH initially rose quickly from a low of 4.48 to a high of 4.75 then dropped slowly to 4.71. The log fO_2 fluctuated in an opposing manner starting at -30.32, dropping rapidly to a low of -30.47, and then rising slowly to -30.40. Pyrophyllite did not precipitate during this simulation. Pyrophyllite is a constituent of alteration within the Owen Conglomerate at North Lyell, however the pH in Fluid 1 was not low enough to allow pyrophyllite to form.

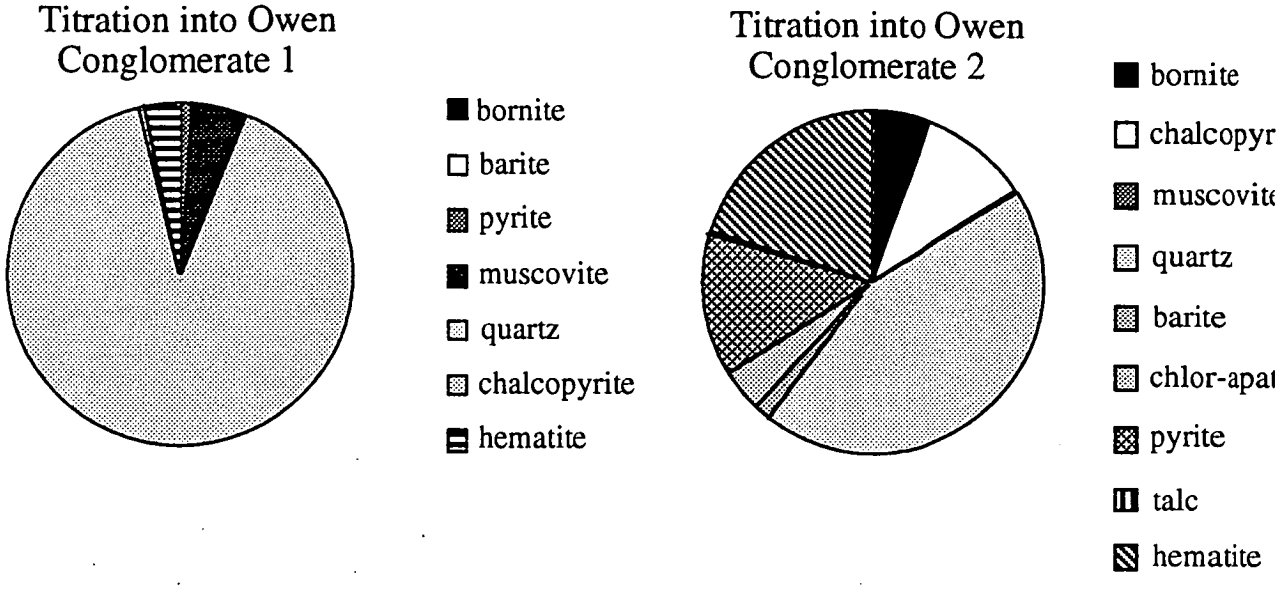

Figure 24 - Relative proportions of minerals precipitated during titration of Fluid 1 into Owen Conglomerate 1 (quartz-hematite-kaolinite rock 85/10/5%) and Owen Conglomerate 2 (quartz-hematite rock 50/50%) showing all mineral phases. Composition of the fluid (Fluid 1) used in this simulation is listed in Table 5

Titration into Owen Conglomerate 2

This titration was intended to simulate a sharp redox front where the reduced hydrothermal fluids intersect a highly oxidised environment. The sharp transformation in Fe-bearing minerals visible across the Great Lyell Fault at North Lyell and Lyell Tharsis and their rich copper grades suggest that it was an effective trap mechanism for metal deposition. The simulation proved to be equally effective at precipitating metals as the previous titration. However, as Figure 24 shows, the quantity of other minerals (notably quartz and muscovite) associated with the bornite and chalcopyrite are vastly reduced, thereby increasing the relative proportion of Cu minerals. Although the simulation precipitated the same amount of metal (58% of available Cu) in the same period as the less oxidised system, it reached equilibrium much faster and was not swamped by quartz. This increased the metal content of the final precipitated body however, the efficiency of metal deposition was not improved.

The pH and log fO_2 values were slightly different to the previous titration without the slow decline of pH or slow rise of fO_2. The fluid was most likely buffered by the oxidation of pyrite in the following reaction;

$$4FeS_2 + 8H_2O + 15O_2 = 2Fe_2O_3 + 8SO_4^{-2} + 16H^+$$

Minor talc (chlorite substitute) and chlor-apatite are precipitated during this simulation. Chlor-apatite follows the trend of pyrite with a sharp decrease in precipitation rate when hematite becomes the dominant Fe mineral. A small amount of talc is deposited just before pyrite deposition ceases (Figure 25) and hematite appears within the assemblage.

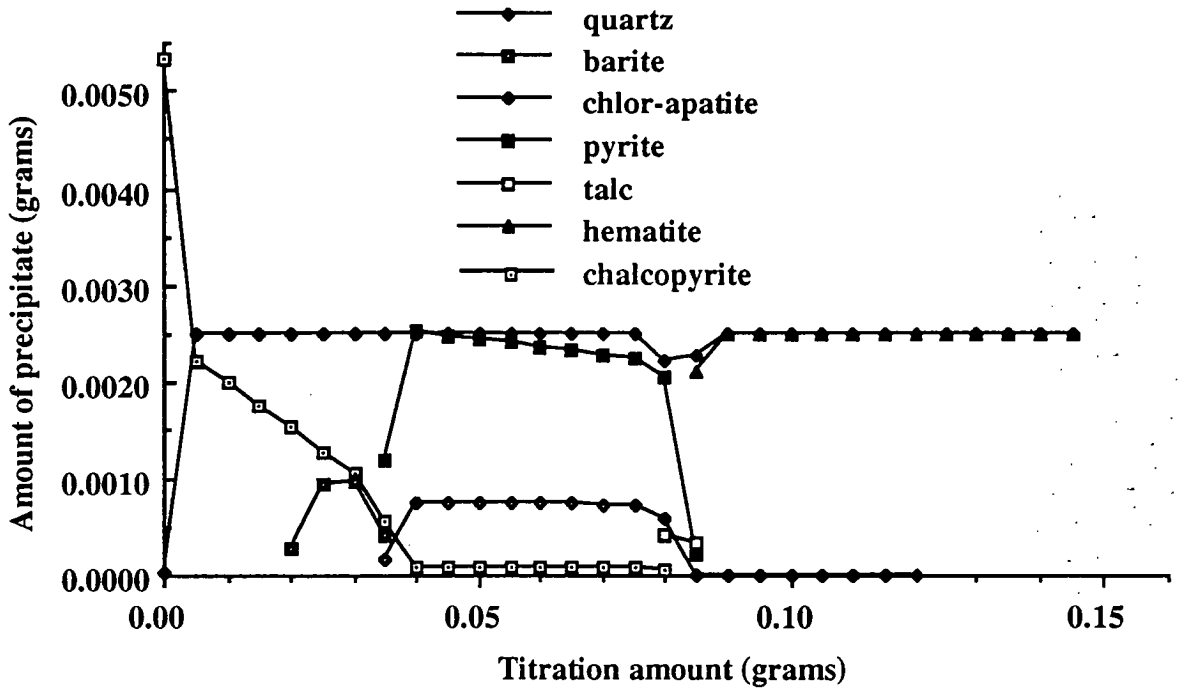

Figure 25 - Plot of titration into Owen Conglomerate 2 showing precipitation cycles of minerals up until equilibrium is attained

Simulations using a fluid in partial equilibrium with the volcanics

Two titrations into the Owen Conglomerate were carried out using fluids which were partially equilibrated with the altered volcanics. This was intended to simulate a fluid dominated system where the rocks had little effect upon the fluid chemistry during their passage through the volcanics. 1.08 kilograms of fluid was interacted with 0.1 and 0.05 grams of the mafic volcanic (water/rock ratios of 10800 and 21600 respectively).The resultant fluids were then titrated into the Owen Conglomerate until they were in equilibrium. The results were similar to those obtained from the rock buffered fluid titration using the same examples (simulation 3).

Titration into the Owen Conglomerate produced a quartz-muscovite dominated alteration assemblage. More chalcopyrite, muscovite and barite were precipitated during this simulation than for the equivalent titration with the rock buffered fluid (simulation 3). pH increased slightly (as it did in simulation 3), but oxygen fugacities decreased slightly during the initial increments prior to increasing, in contrast to simulation 3.

Cooling of the initial fluid (simulation 6)

The Cu-rich 'Fluid 1' was cooled from 300-100°C with pressures kept above liquid-vapor saturation to prevent boiling to simulate hot hydrothermal fluids ascending along open conduits to a cooler environment (such as the Owen Basin). The major minerals deposited were quartz, pyrite and bornite (see Figure 26). Minor phases include kaolinite, muscovite, barite, galena, sphalerite and acanthite. Figure ? illustrates that cooling was a relatively successful mechanism for Cu deposition (69% total metal available precipitated) with the majority of Cu being deposited in the interval 300-200°C (67% of total available Cu). It was a successful mechanism for removal of Pb (96%), Ag (93%) and Zn (71%) which were precipitated at lower temperature ranges (ie. 180-100°C) when the continued reduction in temperature had finally lowered the solubility of metal chloride complexes to saturation levels. Bornite was the dominant copper mineral, precipitating 56% of the available Cu. Chalcopyrite was precipitated between 270 and 255°C, fixing Cu out of solution. Most of the copper precipitation occurred between 300 to 260°C, with only minor precipitation thereafter.

The precipitation of muscovite followed by kaolinite from a fluid saturated in aluminium suggests that the pH was too high to allow pyrophyllite precipitation. It is significant that the Au in solution did not precipitate during cooling because North Lyell contains significant Au values. Another mechanism is most likely required for gold deposition. Only minor precipitation of iron and barium occurred (between 1-2%). There was a steady decrease in pH (from 4.48 to 3.31) and log fO_2 (from -30.32 to -51.93) during cooling.

The cooling simulation produced a mineral assemblage that would most likely be represented in the field as quartz veins with minor sulphides (bornite + pyrite + chalcopyrite ± galena ± sphalerite ± acanthite ± covellite) and minor gangue minerals (muscovite ± barite ± kaolinite). The sulphides would be deposited in order of decreasing solubility, ie.bornite-chalcopyrite-acanthite-galena-sphalerite, creating a mineral zonation within the veins, closely associated with the temperature variations.

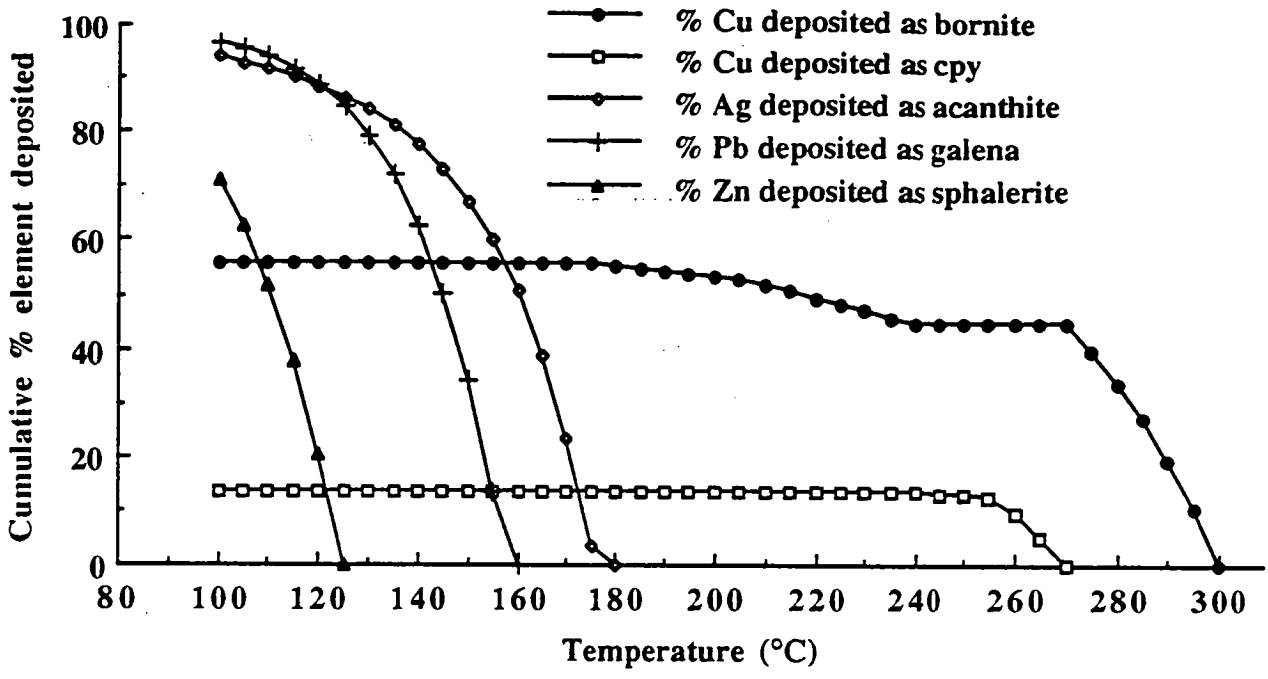

Figure 26 - Diagram illustrating the proportion of metallic elements to precipitate from solution per increment of cooling for Fluid 1 (after removal of metals deposited due to Cu supersaturation). The fluid was cooled in increments of 5°C. Total metals available for deposition within the fluid were; Cu, 6.60×10^{-3} g; Ag, 1.0×10^{-4} g; Pb, 1.1×10^{-3} g; Zn, 1.1×10^{-3} g

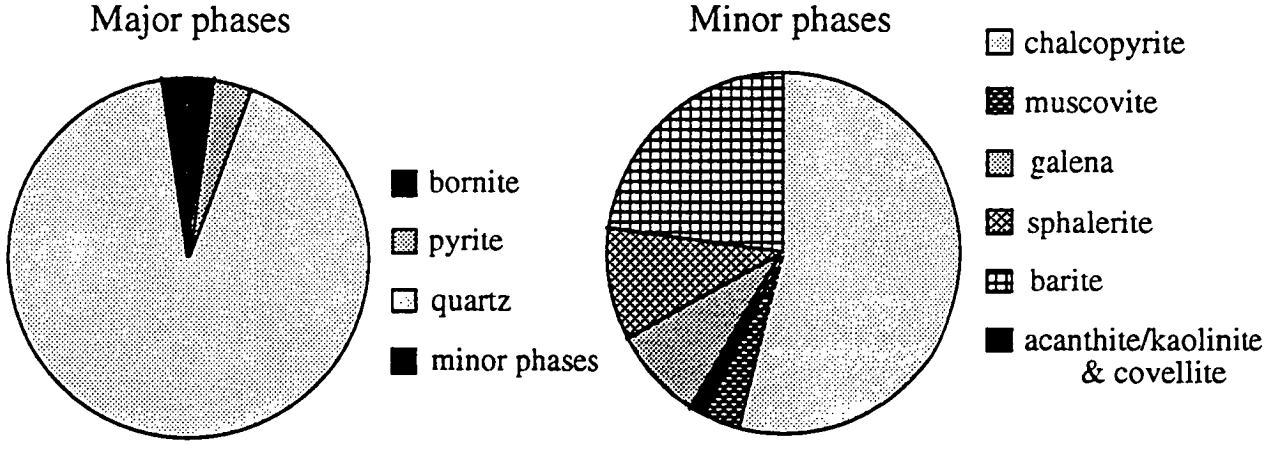

Figure 27 - Relative proportion of minerals precipitated during cooling of Fluid 1 showing major minerals on the left (including minor mineral phases) and minor phases on the right.

Cooling of fluids in equilibrium with the Cambrian volcanics (simulations 7 and 8)

The initial fluid (Fluid 1) was equilibrated with both the felsic (Fluid 2) and mafic volcanics (Fluid 3). Both new fluids were then cooled from 300-100°C without boiling. These scenarios are equivalent to the mineralising fluid migrating through the volcanic pile where they are buffered by either the mafic or felsic units. In this simulation cooling occurs entirely within the volcanics prior to their entry into the Owen Basin. A comparison of fluid compositions before and after equilibration with the mafic and felsic volcanics is presented in Table 5 Note that most of the copper in the initial fluid was deposited during equilibration with the volcanics because Cu was supersaturated in the initial fluid (discussed previously). These two cooling simulations should be considered as likely end members within the volcanic terrain. It is highly unlikely that the fluids would be buffered by only one volcanic facies (ie. mafic or felsic). It is more likely that the fluid would be modified by interaction with both volcanic rock types, resulting in a composition somewhere between Fluids 2 and 3 (Table 5).

Cooling of fluids 2 and 3 produced very similar precipitates, with only slight variations in quantities of most minerals. The fluid from the felsic-buffered volcanics produced more muscovite (approx. 13% more), quartz, chalcopyrite, and sphalerite, while the mafic buffered fluid produced more barite, pyrite, bornite, covellite and abundantly more talc (ie. 4% of total minerals as opposed to 0.8% for felsic buffered volcanic fluid). These differences are largely reflections of the original variation in fluid composition (Table 5). The felsic-buffered fluid contained more SiO_2, Al_2O_3 and K, as shown by the higher proportion of muscovite and quartz precipitated. Similarly Fluid 2 contained more SO_4, Mg and Fe, which is reflected in the precipitation of more pyrite, talc and barite. Despite the difference in the type of Cu minerals deposited (chalcopyrite vs. bornite), the same amount of copper was present within the two systems (Table 5) and both deposited approximately 98% of the available copper. Barite was only deposited at the start of each simulation with the variation in the amount deposited reflecting an initial variation in log fO_2.

Metal precipitation during these two simulations is similar to what occurred during the cooling of Fluid 1. Gold was not deposited in this cooling simulation, however metal precipitation was generally very efficient, with most metals (except zinc and gold) showing greater than 90% metal deposition within narrow temperature ranges. More iron (as pyrite) was deposited during these simulations and there was a greater variety of copper minerals (bornite, chalcopyrite and covellite), reflecting variations in the oxygen fugacity. Within both fluids, 93% of the available Fe was deposited as pyrite

from 300-200°C, 52% of the available Cu was deposited as chalcopyrite from 300-230°C and a further 44% of the Cu was deposited from 230-165°C. The pH and fO_2 both decreased steadily with temperature (4.74 to 3.46 and -30.54 to -52.07 respectively).

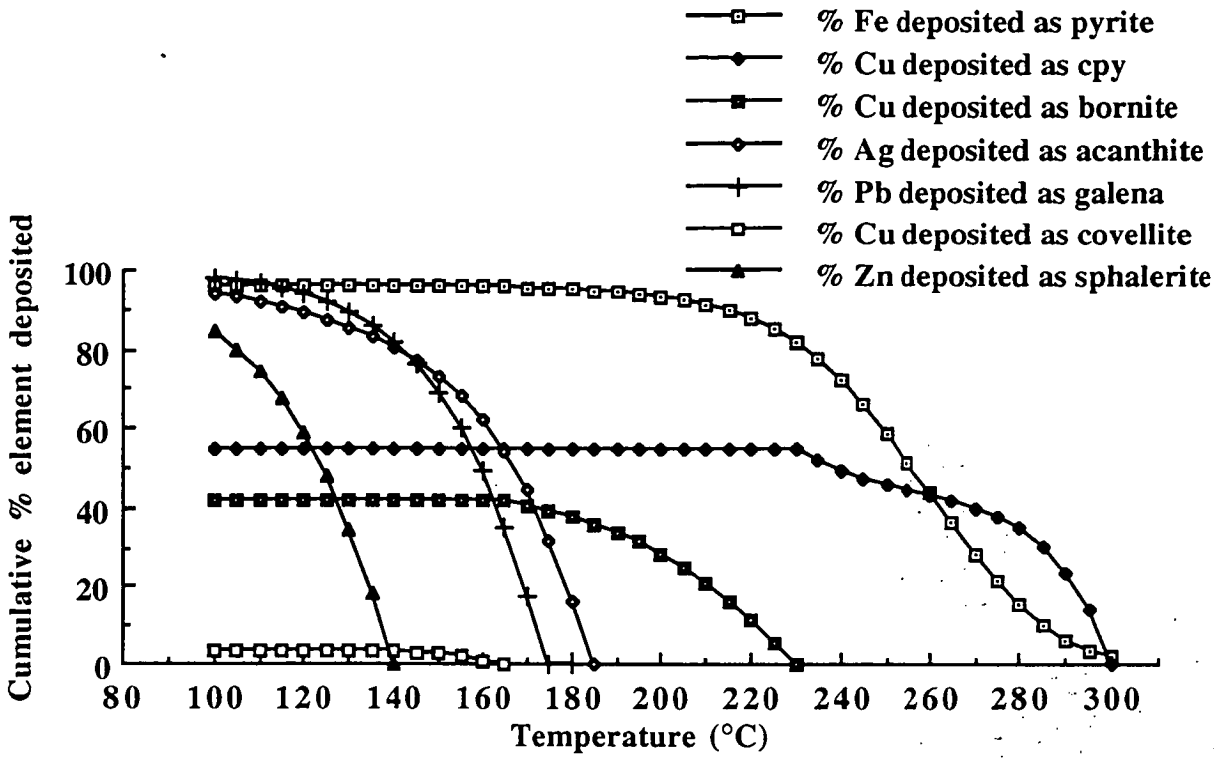

Figure 28 - Diagram illustrating the cumulative percentage of metallic elements to precipitate from solution per increment of cooling for a fluid in equilibrium with the felsic volcanics. Metal precipitation within the mafic volcanics is virtually identical. The fluid was cooled in increments of 5°C while maintaining pressures above liquid-vapor saturation to prevent boiling.

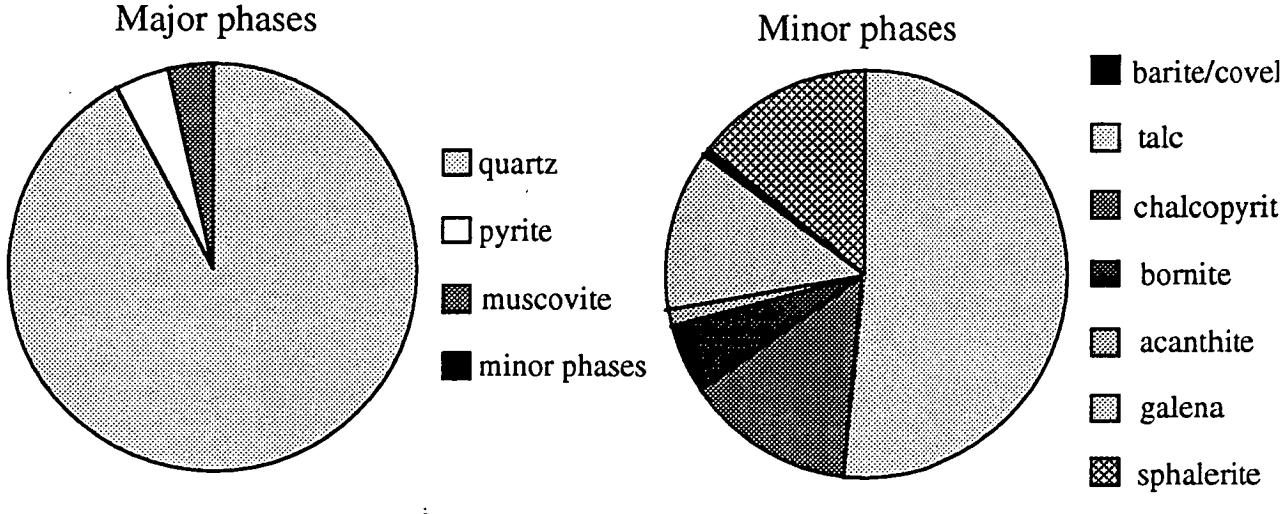

Figure 29 - Relative proportion of minerals precipitated during cooling of fluid buffered by felsic volcanics showing relative proportions of all major minerals on the left (including the sum of all minor mineral phases), and the relative proportions of all the minor phases precipitated on the right.

The thermodynamic data for chlorite in the SOLTHERM database is poor. Consequently, talc precipitated during the cooling simulations (Figure 29) where chlorite would be expected to form. This problem occurred within many of the simulations and cannot be resolved with the current available data for chlorite. For the purposes of this exercise, talc is considered to be a 'substitute' for chlorite within the results of all simulations.

Cooling of a fluid equilibrated with the Owen Conglomerate (simulation 9)

This simulation represents hot hydrothermal fluids first equilibrating with the mafic volcanics, and then within the overlying Owen Conglomerate, within which the fluids cooled. The assemblage formed from this simulation produced the best approximation of the mineralisation within the North Lyell mine and the siliceous hematite pod. The highly siliceous nature of the North Lyell rocks mineralised by chalcopyrite-bornite-gold and containing accessory pyrite-hematite-muscovite is very similar to the assemblages found within the volcanics and the Owen Conglomerate at North Lyell.

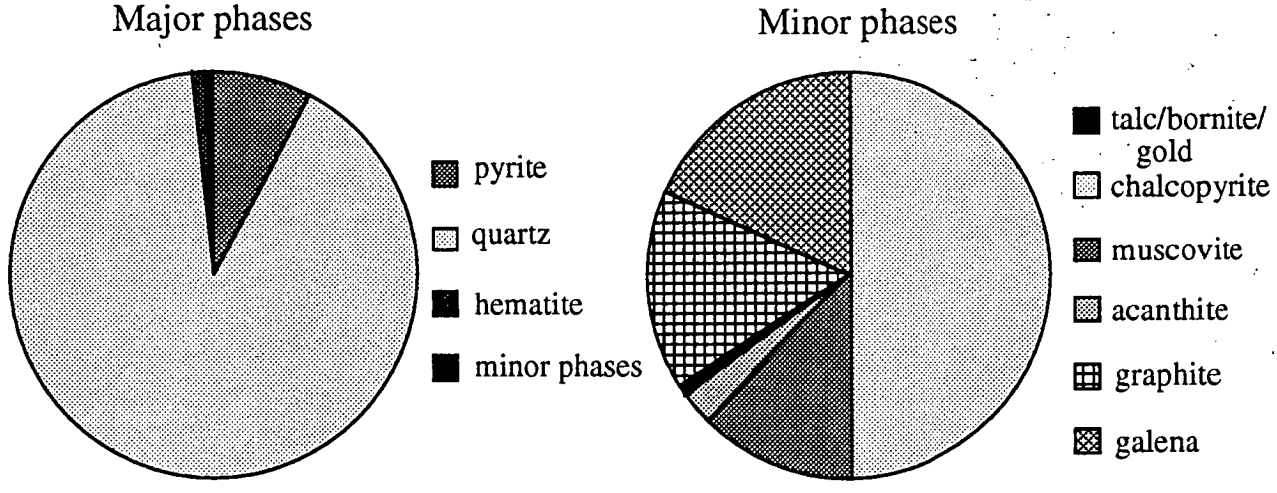

Figure 30 - Relative proportion of minerals precipitated during cooling of a fluid in equilibrium with the Owen Conglomerate (and the mafic volcanics) showing major minerals on the left (including minor mineral phases) and the proportions of all the minor phases in the diagram on the right.

The precipitate in this simulation is dominated by quartz and pyrite (Figure 30). The minor phases are dominated by chalcopyrite, with accessory galena, muscovite, graphite, talc, bornite and gold. The paragenesis of the mineral assemblage is shown in Figure 31. The simulated assemblage has similarities with the paragenetic sequence found at North Lyell which also displays late stage deposition of metallic elements such

as Ag (present as hessite, Ag_2Te, within the North Lyell assemblage, not acanthite), galena (with variable amounts of selenium) and some Cu-rich sulphides (bornite and idaite). These are found in late stage veins within highly silicified and occasionally brecciated samples from the North Lyell pod. The initial precipitation of hematite and barite, then stabilisation of pyrite as the dominant Fe mineral within the assemblage suggests the simulation is representative of a fluid dominated system that is initially buffered by the Owen Conglomerate. The precipitation of pyrite and graphite (Figure 31) indicate reduction occurred during cooling and the fluid has diverged away from the buffered assemblage. This scenario may be expected within the Owen Conglomerate adjacent to the Great Lyell Fault.

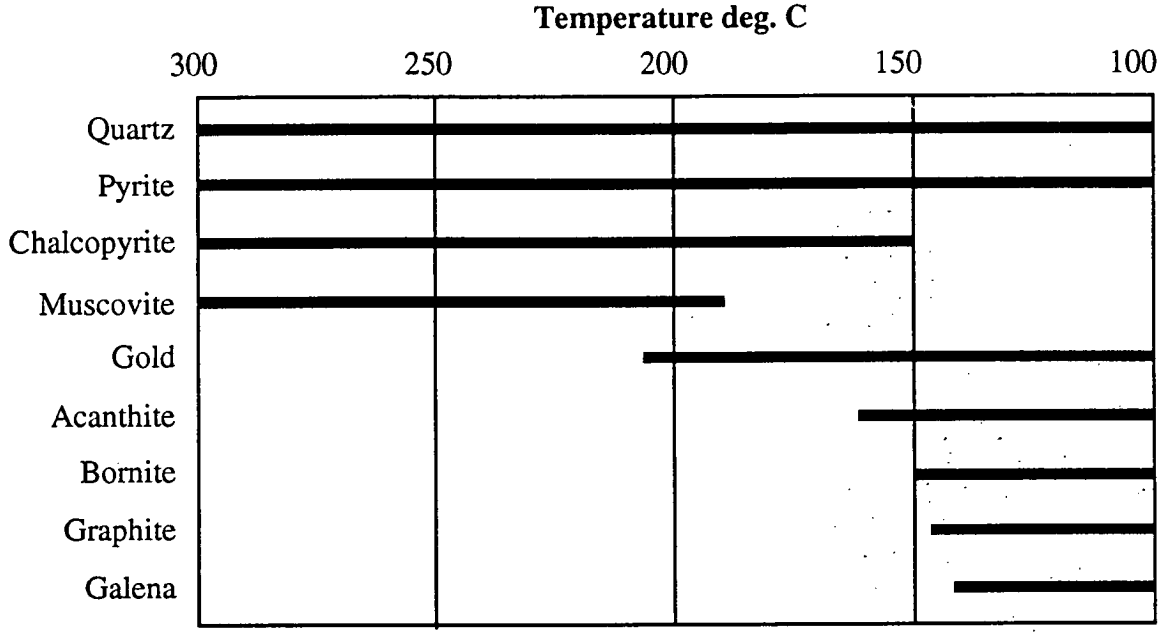

Figure 31 - Temperature ranges for minerals precipitated during the cooling simulation of a fluid initially in equilibrium with the Owen Conglomerate (after equilibrating with the mafic volcanics).

Cooling of this fluid was an efficient mechanism for Cu and Au metal deposition in the lower temperatures (between 220-100°C), with 75% of the available gold being deposited.(Figure 32). Chalcopyrite precipitation removed 97% of the available Cu and bornite removed another 2% , leaving only 1% in the fluid at the end of the simulation. A similar result was obtained for Ag with 96% of available Ag being deposited as acanthite. Iron was also virtually all precipitated, with 86% deposited as pyrite and 13% as hematite. The total hematite and talc products were precipitated prior to the initiation of cooling, suggesting Fe and Mg were slightly oversaturated within the initial fluid. Oxygen fugacity decreased steadily with temperature from -30.43 to -53.78, the pH decreased similarly from 4.74 to 3.32.

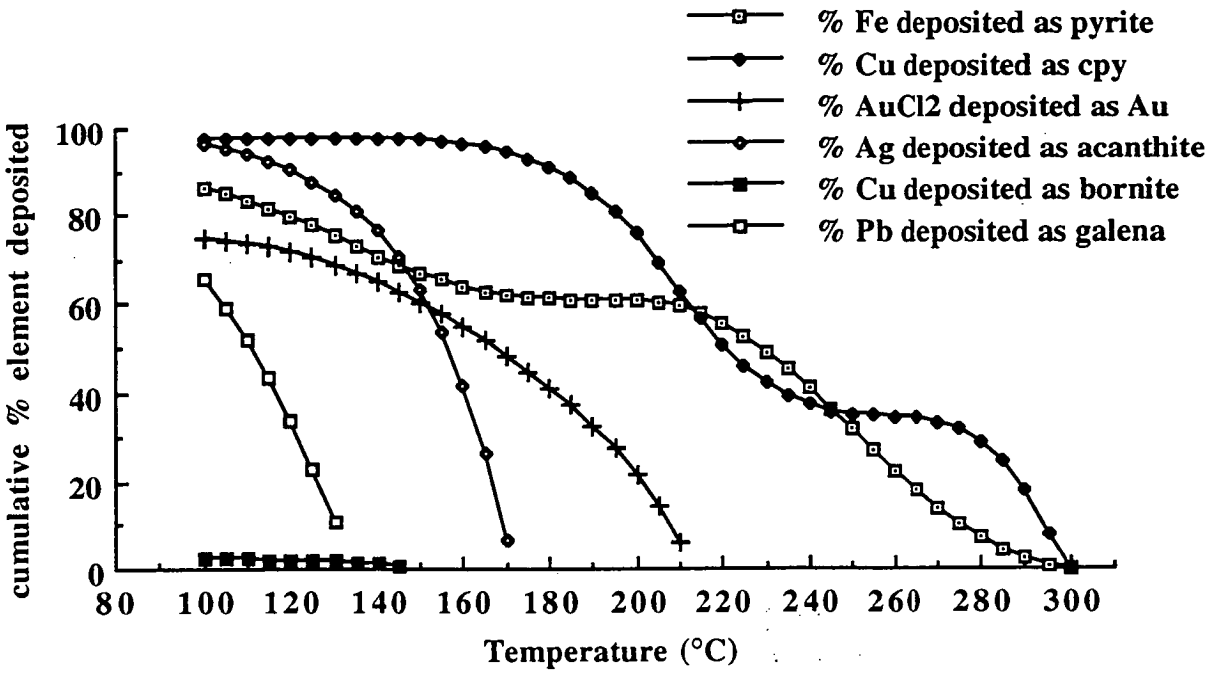

Figure 32 - Diagram illustrating the cumulative percentage of metallic elements to precipitate from solution per increment of cooling for a fluid initially equilibrated with the mafic volcanics and then the Owen Conglomerate. The fluid was cooled in increments of 5°C while maintaining pressures above liquid-vapor saturation to prevent boiling. Total metals available for deposition within the fluid were; Fe, 0.027 g; Cu, 7.91×10^{-4} g; Ag, 1.08×10^{-4} g; Pb, 1.06×10^{-3} g; Au, 8.73×10^{-7} g.

The precipitation of Au began at 210°C and continued steadily to 100°C.Graphite began precipitating at 140°C and continued to 100°C (Figure 32). Huston and Large (1989) suggest transport of gold as $AuCl_2^-$ is favoured in solutions with low pH (<4.5), high temperature (300°C) and high salinity ($aCl^- > 10^0$). However, the low salinity and low temperatures that gold was deposited within the modelled system enabled transport as a bisulphide complex. Deposition of gold in this system may be a result of pyrite precipitation reducing H_2S and resulting in Au deposition by the following reaction;

$$4Au(HS)_2^- + 2H_2O + 4H^+ = 4Au^0 + 8H_2S + O_2$$

Huston and Large (1989) noted that the solubility of gold will decrease by two orders of magnitude for each order of magnitude decrease in the activity of reduced sulphur. The abundant pyrite precipitated during this simulation suggests this may be an effective mechanism for gold deposition in this system.

The deposition of Pb and Ag began fairly late in the simulation, but the minerals were deposited rapidly with most of these metals precipitated by the end of the simulation. Figure 32 shows a slight peculiarity in the deposition of pyrite and chalcopyrite precipitation patterns which appear antithetic. When chalcopyrite precipitation is high, pyrite precipitation is low and vica versa, indicating the dominance of iron within this simulation (ie. when pyrite precipitation is high there is less Fe available for chalcopyrite).

Cooling of a fluid equilibrated with the Gordon Limestone (simulation 10)

Cooling after equilibration with the mafic volcanics, the Owen Conglomerate and then the Gordon Limestone at 300°C was completed, with saturation pressures maintained to prevent boiling. This is a potential scenario for the main stage of hydrothermal mineralisation when pulses of hot mineralised fluid equilibrated with the volcanics and the conglomerate and then cooled within the overlying carbonates. This produced the assemblage shown in Figure 33.

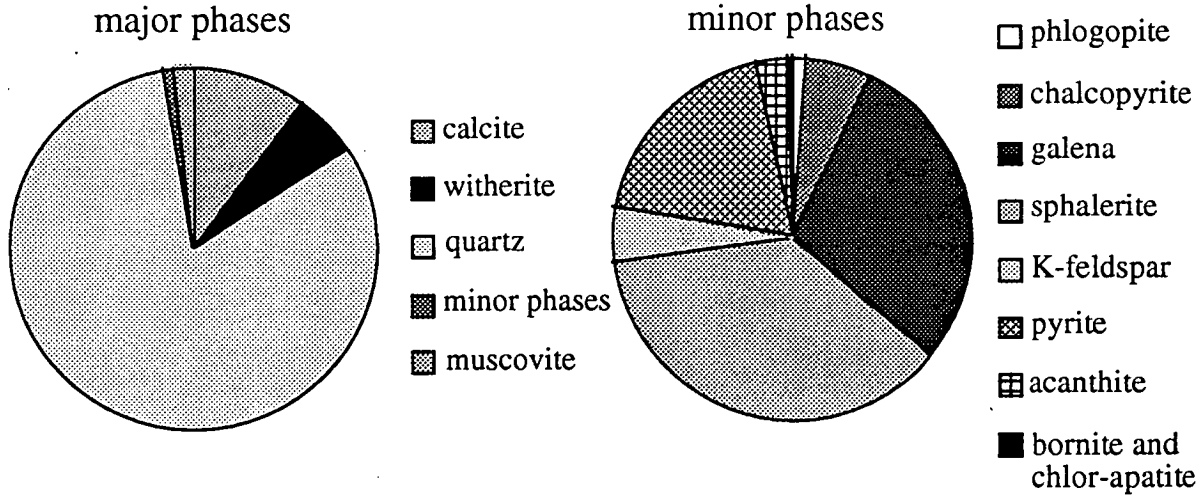

Figure 33 - Relative proportion of minerals precipitated during cooling of a fluid in equilibrium with the Gordon Limestone (after equilibrating with the Owen Conglomerate and the mafic volcanics) showing major minerals on the left (including the sum of all minor mineral phases) and the proportions of all the minor phases on the right.

The occurrence of K-feldspar in place of muscovite in the precipitating mineral assemblage at 255°C (Figure 34) suggests the fluid pH was close to the boundary between the two minerals and possibly buffered by the reaction -

$$KAl_3Si_3O_{10}(OH)_2 + 2K^+ + 6SiO_2 \Leftrightarrow 3KAlSi_3O_8 + 2H^+$$

muscovite K-feldspar

The temperature and the activities of K^+ and $SiO_{2(aq)}$ also affect this reaction. For the fluid composition to move to the right and then back to the left again suggests that more than one parameter is controlling this reaction, because the pH of the fluid decreased steadily throughout the simulation (5.74 to 4.16) as did the log fO_2 (-31.58 to -52.79).

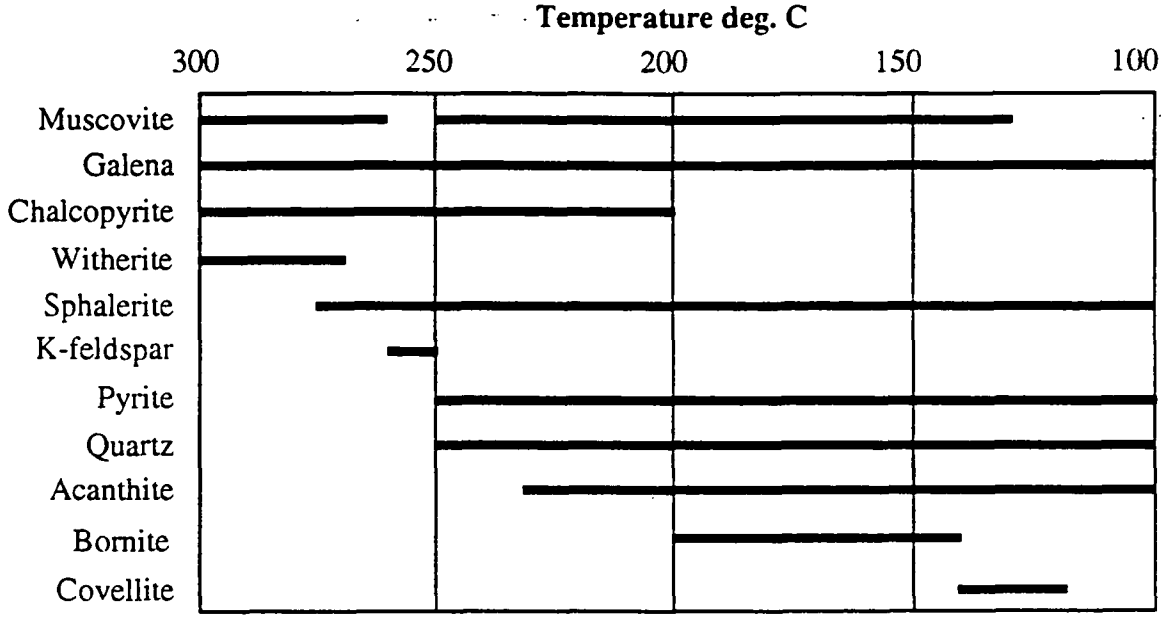

Figure 34 - Temperature ranges for minerals precipitated during the cooling simulation of a fluid in equilibrium with the Gordon Limestone (after equilibrating with the Owen Conglomerate and the mafic volcanics).

The precipitation of minerals such as witherite ($BaCO_3$) and galena during the simulation (which are not present in altered samples of the Gordon Limestone), suggests that Ba and Pb concentrations have been overestimated within the initial fluid, or that hydrothermal alteration did not affect the limestone. The prominence of barite within the alteration around North Lyell suggests the fluids circulating during the mineralising event could contain a significant amount of Ba and if the fluids had intercepted the Gordon Limestone, some indication of this might be expected (unless all the Ba was deposited within the Owen Conglomerate). There were no barium minerals observed within the Gordon Limestone, although the intense weathering within the area may have mobilised and dispersed these minerals. The abundance of kaolinite, sericite, copper and goethite (Solomon, 1969; this study) within samples of the Gordon Limestone obtained from the alteration area do support the hypothesis that Fe- and K-rich alteration fluids have been in contact with the carbonate.

Boiling (simulation 11)

To investigate what would happen if confining pressures were insufficient to prevent boiling during the ascent of the fluids through the subsurface, a single stage isoenthalpic boiling simulation was conducted for Fluid 1 from 300°C to 100°C. Boiling is considered an unlikely mechanism for metal deposition within the North Lyell area due to the lack of diagnostic vein textures. However, boiling of Fluid 1 produced a mineral assemblage similar to that found in the main body of the volcanics within the North Lyell deposit. Despite the lack of recognised boiling textures within the deposit, this remains a possible mechanism for metal deposition in the Mt. Lyell system. Boiling simulations for the fluids equilibrated with the volcanics and the Owen Conglomerate (Fluids 2 and 3) were not successful due to charge and chemical imbalances caused by the loss of volatiles.

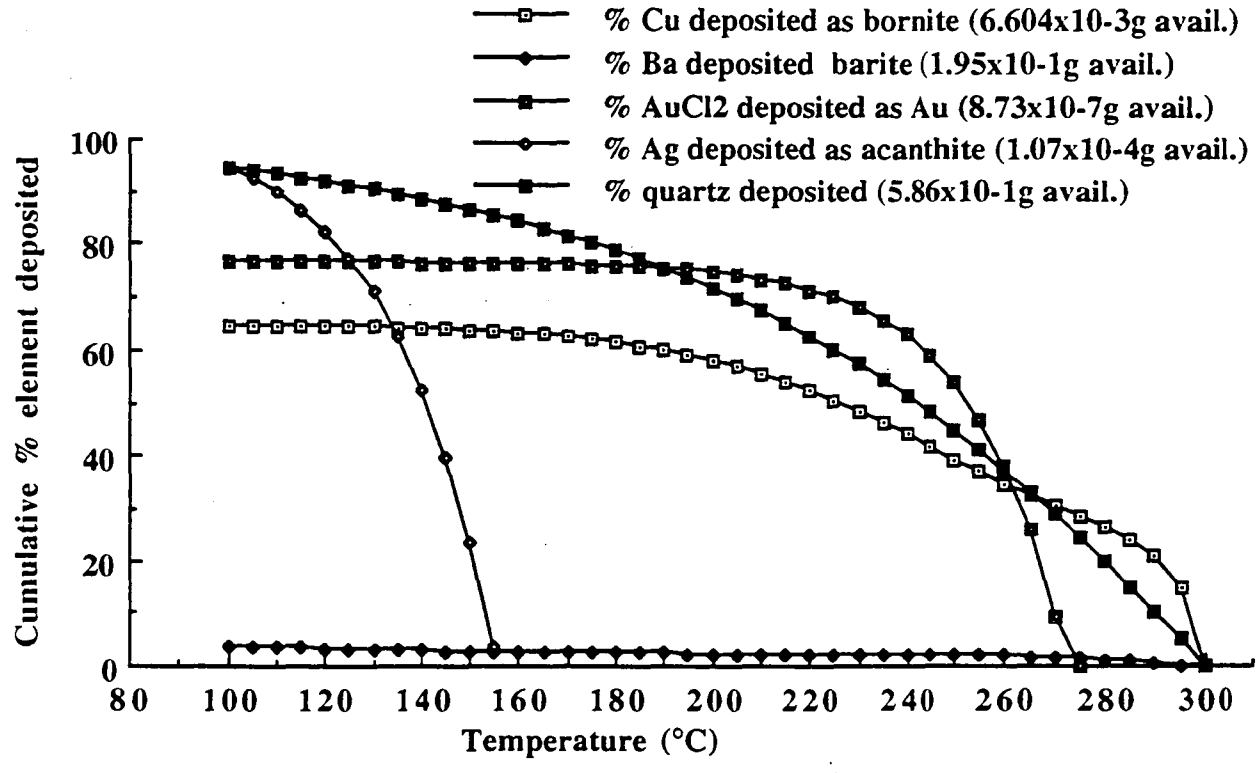

Figure 35 - Diagram illustrating the proportion of metallic elements to precipitate from solution per increment of boiling for Fluid 1. The fluid was cooled in increments of 5°C while maintaining liquid-vapor saturation conditions suitable for boiling.

Both chalcopyrite and bornite were deposited upon initiation of boiling due to the supersaturation of Cu within the initial fluid. Bornite was the only copper mineral produced during the boiling process. Figure 35 shows that boiling was most effective for precipitating copper and gold from the fluid although no pyrite was produced. The efficiency of the boiling process in precipitating gold is shown graphically in Figure 35, with 71% of the available gold depositing in the temperature range 270-220°C. Cu

deposition was not as effective but still deposited 60% of the available Cu as bornite from 300-190°C. Ag deposition was rapid in the lower temperature ranges, with 94% precipitating from 155-100°C. Neither Pb or Zn were deposited during this simulation, but both were deposited in the simulated cooling without boiling. Quartz precipitated steadily throughout the simulation and dominated the final assemblage (Figure 36) The pH initially increased during this simulation, and then decreased steadily (4.48 to 4.58 to 3.99) while the log fO_2 dropped steadily throughout the process (-30.32 to -51.16).

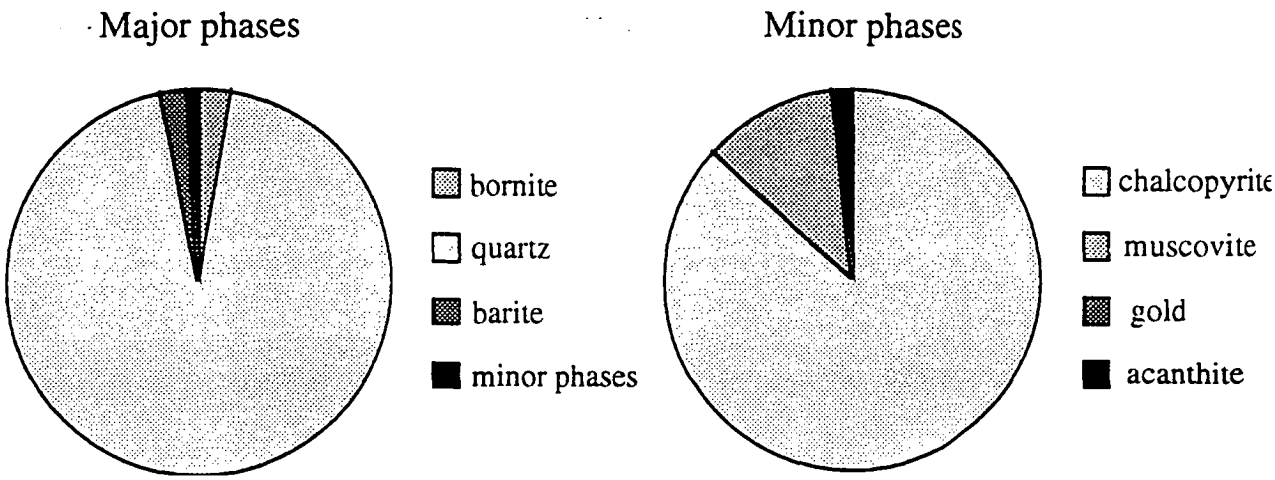

Figure 36 - Relative proportion of minerals precipitated during boiling of Fluid 1 showing major minerals on the left (including minor mineral phases) and the proportions of all the minor phases in the diagram on the right.

Transport of Au was determined to be as $Au(HS)_2^-$ (as determined from data output) within the H_2S field, with the deposition of Au from the bisulphide complex occurring during boiling ie.;

$$4Au(HS)_2^- + 2H_2O + 4H^+ = 4Au^0 + 8H_2S + O_2$$

According to Huston and Large (1989), the most effective way to precipitate gold transported as a bisulphide is to reduce the activity of the reduced sulphur. Boiling of the fluid with corresponding evolution of H_2S gas according to the above reaction is seen as an effective mechanism for accomplishing this (Seward, 1984). This is basically the same mechanism which caused precipitation of gold in the cooling simulation (simulation) except the reduced sulphur is being removed by gas evolution, not metal precipitation.

Simulations using a fluid with an initial pH of 3.0

The presence of pyrophyllite surrounding and within some of the deposits at Mt. Lyell has been used to provide an estimate of fluid temperatures (eg. Walshe and Solomon,

1981; Hendry, 1972) and thermodynamic parameters within the hydrothermal fluid. At 300°C the muscovite-pyrophyllite boundary occurs at a pH of around 3.0. To attempt a simulation which could precipitate pyrophyllite, Fluid 1 was modified so that it had an initial pH of 3.0 The resultant fluid was then reacted with various lithologies. None of the titrations produced a pyrophyllite bearing assemblage, and large quantities of magnetite and muscovite deposited. This, combined with a lack of any significant metal precipitation indicate that these simulations were not a reasonable approximation of the North Lyell hydrothermal system.

SEDIMENTARY VERSUS ALTERATION ORIGIN FOR THE HEMATITE CLASTS

The presence of hematite clasts on Tharsis Ridge has been noted by many authors including Solomon (1967), who advocated a detrital origin for the clasts and Arnold (1985), who suggested the clasts were of hydrothermal replacement origin. The lack of regional extent of the hematitic clasts suggests they were locally derived and their lack of mechanical competency suggests they would be unlikely to survive transportation in a high energy environment like the Owen Basin for great distances. The hematite clasts tend to be larger and more angular than the associated quartzite clasts (see Plates 17 and 18) and are obviously not derived from the same source rock in many cases. These observations suggest a detrital origin, however the hematite clasts are always found within a hematitic matrix, suggestive of pervasive hydrothermal alteration. For hydrothermal fluids to selectively replace some clasts but not others within a conglomerate requires a variety of clasts, some more susceptible to replacement than others. Within the Owen Conglomerate the clasts most likely to be replaced are the more reactive volcanic clasts (as opposed to the quartzite clasts). These are generally restricted to the Lower Owen Conglomerate (Solomon, 1959) and would not be expected within the North Lyell area (although the western side of Tharsis Ridge is classified as Lower Owen Conglomerate).

To establish whether there was a host rock control on the hematisation of clasts around Tharsis Ridge, North Lyell and Lyell Tharsis, a clast count from the Middle Owen Conglomerate was undertaken. This was to establish if there was a significant component of volcanic or other clasts which may have been more susceptible to replacement by the hematitic fluids. Samples from a traverse up Cape Horn and Mt. Owen were selected to approximate a section through the 'unaltered' Middle Owen Conglomerate. The size, sorting, sphericity, angularity and composition of their clasts were recorded and compared with those observed on Tharsis Ridge and the Lyell Tharsis area. Very few of the clasts examined were established as being volcanic in origin, the vast majority were found to be quartzitic, presumably from the Precambrian Tyennan Block. There were very few clasts containing significant hematite located during the traverse through the unaltered Owen Conglomerate and there were no beds recognised with substantial numbers of volcanic clasts or other clasts of similar composition. The survey generally supported the contention that there was no host rock control on the hematite alteration. However Solomon (1964) suggested the volcanic clasts were very restricted and only found near the volcanics, and subsequently replaced by circulating hematitic fluids.

Plate 17 Hematite clast from Tharsis Ridge. Note irregular size and shape compared to other clasts in conglomerate. Matrix of conglomerate contains limited hematite.

Plate 18 Hematite clasts from Tharsis Ridge. Note variation in size and angularity between quartzite clasts and hematite clasts. The clast was considerably more hematite rich than the matrix.

Plate 19 Totally hematised conglomerate between Lyell Tharsis and Batchelors Quarry.

Plate 20 Hematite band passing through zone of intense barite alteration. Lyell Tharsis.

Plate 21 Hematite clasts in Pioneer Beds (adjacent to Great Lyell Fault).

Plate 22 Hematite conglomerate with clasts displaying textures suggestive of a detrital origin rather than hydrothermal.

17

18

19

20

21

22

Despite the sedimentary evidence for the hematite clasts having a detrital origin, there were a few clasts observed with hematite infiltrating the edges and along fractures. Examples of Owen Conglomerate showing complete hydrothermal replacement by hematite and to a lesser extent barite, can be found in the Lyell Tharsis area (see Plates 21 and 22), with examples showing partial replacement of clasts less common. The conglomerate textures may still be seen in some hematitic outcrops. The evidence for a hydrothermal component to the hematite alteration/replacement is very strong within these cases of total replacement with retention of a conglomeratic texture. Many of the hematite clasts observed within the Owen Conglomerate adjacent to the Haulage Unconformity and within the Pioneer Sandstone are interpreted here to be of detrital origin. The clast makeup within the hematitic conglomerates appears quite different to the unaltered conglomerates. The hematitic conglomerates contain clasts of unusual size and sphericity (Plates 17 and 18) which have not been found within unaltered Owen Conglomerate elsewhere. The clasts are commonly more hematitic than the matrix, suggesting they actively assimilated hematite from the surrounding matrix. Textures within the clasts of the conglomerate pictured in Plate 22 are more suggestive of hematised source rocks which have undergone very little mechanical reworking rather than selective hydrothermal replacement. However, the totally hematised conglomerate beds between Lyell Tharsis and Batchelors Quarry are thought to be from hydrothermal replacement of sediments located near the fluid conduits, and may have provided suitable source rocks for the detrital hematitic conglomerates.

All of the hematite clasts observed were contained within a hematitic matrix, although frequently the clast was substantially more hematitic than the matrix (see Plates 20 and 21). It is unlikely that the clasts could be selectively enriched or totally replaced by hematite while the matrix remained relatively unaffected. Textures observed in some hematite clasts (see Plate 21) are more closely related to the totally hematised conglomerates and sandstones stratigraphically below them than hematised quartzite clasts. The variety of hematite clast shapes and sizes are not reminiscent of the normal siliciclastic Owen Conglomerate which generally shows good sorting and rounding of clasts. The sample in Plate 21 is more suggestive of a locally derived conglomerate of pre-existing hematitic rock. The close association of this sample with the Haulage Unconformity also raises the possibility that the structural disruption associated with the Haulage event mobilised these clasts from a pre-existing hematitic conglomerate.

These observations lead to the implication that the main stage of hematite emplacement occurred during the Late Cambrian or Early Ordovician, prior to deposition of the Pioneer Sandstone. The paucity of hematite alteration within the Pioneer Sandstone also suggests that the hydrothermal event was declining during sedimentation. The presence

of a hydrothermal hematite matrix within examples of the Pioneer Sandstone suggests there was still some hydrothermal activity occurring during its deposition but not of the intensity that caused total replacement of the Owen Conglomerate.

DISCUSSION

Most authors are in agreement that there have been two stages of mineralisation within the Mt. Lyell Cu fields; an initial Cambrian event producing a large stockwork system dominated by chalcopyrite with minor exhalative sulphide mineralisation; and a later hydrothermal event which locally enriched the Cu mineralisation along the Great Lyell Fault. The timing of this secondary hydrothermal event has been a topic of spirited discussion for many years with numerous authors favouring a Devonian event associated with the Tabberabberan Orogeny. Much of the evidence found during this survey suggests that the hydrothermal fluids were circulating during the deposition of the Late Cambrian-Early Ordovician sediments, precluding a Devonian event.

There is significant geophysical evidence for a N-S trending Cambrian granite ridge beneath Mt Lyell, however there is virtually no evidence for a Devonian granite (Payne, 1991; Leaman and Richardson, 1989). There are also several lines of evidence suggesting that the Cambrian mineralisation may be related to this ridge. These include -

- The alteration associated with the Mt Lyell deposit is consistant with propylitic and phyllic alteration zones commonly associated with porphyry copper deposits (Henley and McNab, 1978).
- Sulphur and oxygen isotope studies suggest a magmatic origin with a seawater influence (Solomon et al, 1988; Manning, 1990).
- Trace element (Se, Ni and Cd) studies of pyrite suggest the mineralisation had a significant magmatic input (Huston, in prep.).
- Anomalous Mo within the Western Tharsis deposit, similar to a climax type Molybdenum deposit (Manning, 1990).

However there is also evidence suggesting the Cambrian mineralisation is part of a sub sea floor massive sulphide stringer system, with a minor exhalative component. The combination of these observations suggests that the Mt Lyell system is composed of a late stage porphyry Cu deposit overprinting a massive sulphide deposit (as shown in Figure 37), similar to that proposed for mineralisation at the Jukes Proprietary Prospect, south of Mt Lyell (Doyle, 1990). The alteration, mineralisation, timing and structural setting of the Late Cambrian - Early Ordovician hydothermal event at North Lyell suggests it may be related to a late stage granite intrusion or porphyry. This intrusive event may be related to structural disruption associated with the Haulage unconformity.

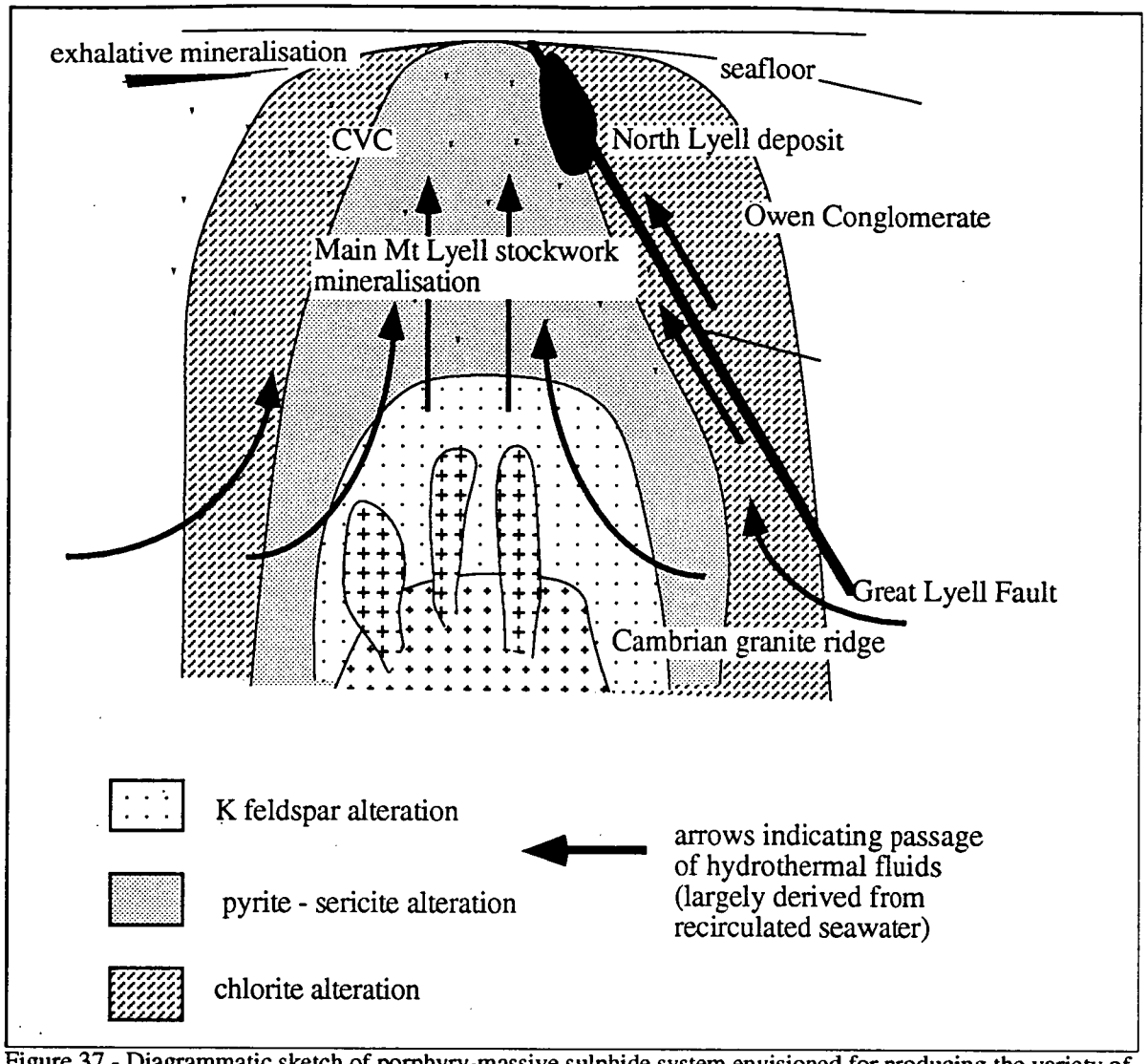

Figure 37 - Diagrammatic sketch of porphyry-massive sulphide system envisioned for producing the variety of deposits observed. These include; exhalative mineralisation (eg. Tasman and Crown Lyell Extended), stockwork mineralisation (eg. West Lyell) and hydrothermal mineralisation (eg. North Lyell). It involves a sub sea floor porphyry with mineralisation genetically related to granite emplacement during the Cambrian and a further episode of mineralisation in the Late Cambrian - Early Ordovician.

Thermodynamic simulations suggest a fluid in equilibrium with the volcanics would not deposit gold. When this fluid is equilibrated with the Owen Conglomerate and then cooled (eg. in the Owen Basin) gold was deposited. This suggests that an input from Owen Conglomerate connate fluids is also required to obtain an assemblage representative of North Lyell. A thermal gradient was similarly necessary to stimulate gold deposition, titrations at constant temperature did not achieve this during simulations. It could also be argued that the overburden above North Lyell during the Devonian may have prevented a suitable thermal gradient being established for deposition of the observed assemblage.

CONCLUSIONS

Alteration within the Owen Conglomerate around North Lyell grades from a central pod of intense silica-barite-hematite alteration to a more hematite-barite-phosphate rich alteration assemblage around Lyell Tharsis, to a hematite-chlorite dominated assemblage at Batchelors Quarry. This alteration assemblage is continued above the Haulage Unconformity, indicating it did not act as a barrier to the hydrothermal fluids. The alteration is poorly developed above the unconformity suggesting the hydrothermal system was on the decline during the deposition of the Pioneer Sandstone.

As hydrothermal fluids progressed through the North Lyell system, their compositions were modified by interaction with the various host lithologies, producing distinct alteration assemblages within the surrounding units. Statistical analysis of the altered Owen Conglomerate delineated three main elemental associations which can be related to the alteration observed around North Lyell. Sericitic (Al2O3-K2O-Rb), hematite-apatite (Fe2O3-P2O5-La-Sb) and barite (Ba-Sr-Sb) alteration zones were delineated. Statistical comparison of altered whole rock analyses with an average unaltered Owen Conglomerate analysis delineated five distinct zones displaying combinations of these alteration styles. The variation in alteration between these groups broadly defines the passage of the hydrothermal fluids from the most intense alteration at North Lyell and Lyell Tharsis, to the weak alteration found above the Haulage Unconformity.

The change in alteration styles from the volcanics through to the Owen Conglomerate reflects the transition from a weakly acidic, reduced, sulphide-rich environment, to acidic, highly oxidised conditions within the conglomerate. Oxidation of the fluid occurred primarily at the contact of the CVC with the Owen Conglomerate, as demonstrated by intense hematisation in the Owen Conglomerate adjacent to the GLF. The presence of minor aluminium and iron phosphates replacing euhedral pyrite within the highly altered Owen Conglomerate, together with the abundance of pyrophyllite and hematite, provides evidence for the passage of acidic, oxidised fluids in the vicinity of the GLF. Away from the GLF, the transition to sericite-hematite alteration within the Owen Conglomerate indicates progressive neutralisation and oxidation of acidic alteration fluids by reaction with the conglomerate.

Structural disruption prior to and during the Haulage movement, possibly related to intrusive activity, mobilised clasts of hematite which are found both above and below the Haulage unconformity within the sediments. This suggests the main alteration and mineralisation at North Lyell occurred prior to the Haulage event, during deposition of the Owen Conglomerate in the Late Cambrian-Early Ordovician. Hydrothermal fluid

activity was reduced, but still active during deposition of the Pioneer Sandstone and possibly also during Gordon Limestone deposition. The copper minerals found within the Gordon Limestone ('copper clays') may have occurred through a number of mechanisms including; detrital, hydrothermal, supergene or hypogene processes.

Computer modelling of hydrothermal fluid geochemistry and metal deposition processes showed that temperature changes were the most successful mechanisms for obtaining significant metal deposition (particularly gold). Modelling was done in an environment representative of North Lyell, by cooling a fluid after equilibrating it with the volcanics and the Owen Conglomerate.

ACKNOWLEDGEMENTS

The author is indebted to Ron Berry for suggesting the topic and sharing his abundant local knowledge and David Cooke for persisting through the thermodynamic trials and providing those useful computer hints. This project would not have been possible without the logistic and technical support of the Mt. Lyell Mining and Railway Company Ltd.,including access to drill core, company reports and maps. Chief Geologist Murray Flitcroft is thanked for his ready assistance with invaluable discussions on local geology and interpretation. The staff and fellow students at the Codes Key Centre are thanked for their encouragement and advice. This thesis would not have been possible without the assistance and support of my very special Sandra.

REFERENCES

Adams, C.J., Black, L.P., Corbett, K.D. and Green, G.R., 1985. Reconnaissance studies bearing on the tectonothermal history of early Palaeozoic and late Proterozoic sequences in western Tasmania ; Australian Jour. Earth Sci., 32 :7-36.

Arnold, G.O., 1985. Mount Lyell 1985: an exploration perspective. Unpublished report to Goldfields Exploration Pty. Ltd.

Banks, M.R., 1962. Ordovician system. J. Geol. Soc. Aust., 9(2); 146-176.

Berry, R.F., 1991. An excursion guide for the Mt. Lyell mining lease with emphasis on the Great Lyell Fault, Haulage Unconformity and North Lyell alteration. Unpublished AMIRA report 2 for P291; 1-22.

Bird, D.K. and Norton, D.L., 1981. Theoretical prediction of phase relations among aqueous solutions and minerals; Salton Sea geothermal system. Geochim. et Cosmo. Acta, 45; 1479-1493

Black, L.P. and Adams, C.J., 1980. Radiometric dating studies bearing on the late Proterozoic-early Paleozoic evolution of western Tasmania. 4th Australian Geological Convention abstacts, Hobart, Jan. 1980, p. 24.

Blainey, G., 1954. The peaks of Lyell. Melbourne University Press, Melbourne.

Bradley, J., 1954. The geology of the West Coast Range of Tasmania, Part 1. Pap. Proc. R. Soc. Tasm., 88: 193-243.

Bradley, J., 1856. The geology of the West Coast Range of Tasmania, Part 2. Pap. R. Soc. Tasm., 90: 65-130.

Bradley, 1957. Geology of the West Coast of Tasmania, Part 3, porphyroid metasomatism. Pap. R. Soc. Tasm., 91: 163-190.

Bryant, C.J., 1975. The geology and mineralisation of the corridor area, Mount Lyell, Tasmania - Crown Lyell, North Lyell, Lyell Tharsis, B.Sc. (Hons) thesis (Unpublished), University of Tasmania.

Campana, B. and King, D., 1963. Palaeozoic Tectonism, Sedimentation and Mineralisation in West Tasmania. J. Geol. Soc. Aust., 10(1):. 1-54.

Carey, S. W., 1953, Geological structure of Tasmania in relation to mineralization, in Geology of Australian Ore Deposits (Ed. A.B. Edwards), pp. 1108-1128 (5th Empire Mining and Metallurgical Congress: Melbourne).

Cathelineau, M. and Nieva, D., 1985. A chlorite solid solution geothermometer, the Los Azufres (Mexico) geothermal system. Contrib. Mineral. Petrol. 91: 235-244

Collins, P.L.F. and Williams, E., 1986. Metallogeny and tectonic development of the Tasman fold belt system in Tasmania. Ore Geology Reviews, 1: 153-201.

Conolly, H.J.C., 1947, Geology in exploration, Mt Lyell example. Proc. Australas. Inst. Min. Metall., 146-7: 1-22.

Corbett, K.D., 1979. Stratigraphy, correlation and evolution of the Mt Read Volcanics in the Queenstown, Jukes-Darwin and Mt Sedgwick areas. Dep. Mines Tasmania Geol. Surv. Bull. 58.

Corbett, K.D., 1981. Stratigraphy and mineralization in the Mt. Read Volcanics, western Tasmania. Econ. Geol., 76: 209-230.

Corbett, K.D., 1992. Stratigraphic-volcanic setting of massive sulphide deposits in the Cambrian Mt. Read Volcanics. Tasmania. Econ. Geol., 87: 564-586.

Corbett, K.D., Calver, C.R., Everard, J.L. and Seymour, D.B., 1989. Queenstown, 1:25,000 geological series, Department of Resources and Energy, Tasmania.

Corbett, K.D., and Lees, T.C., 1987. Stratigraphic and structural relationships and evidence for Cambrian deformation at the western margin of the Mt Read Volcanics, Tasmania. Aust. J. Earth Sci., 34: 45-67.

Corbett, K.D., Reid, K.O., Corbett, E.B., Green, G.R., Wells, K., Sheppard, N.W., 1974. The Mt. Read Volcanics and Cambrian - Ordovician relationships at Queenstown, Tasmania. J. Geol. Soc. Aust., 21(2): 173-186.

Corbett, K.D. and Solomon, M., 1989. Cambrian Mt. Read Volcanics and associated mineral deposits (in Geology and Mineral resources of Tasmania) Eds. C.F. Burrett and E.L. Martin. Geol. Soc. Aust. Spec. Publ., 15: 84-86.

Cox, S.F., 1979. Deformation of the Mount Read Volcanics and associated sulphide deposits, Mount Lyell. Ph.D. thesis (unpublished), Monash University.

Cox, S.F., 1981. The stratigraphic and structural setting of the Mt. Lyell volcanic hosted sulphide deposits. Tasmania. Econ. Geol., 76: 231-245.

Crawford,A.J., Corbett, K.D. and Everard, J.L., 1992. Geochemistry of the Cambrian volcanic-hosted massive sulfide-rich Mount Read Volcanics, Tasmania, and some tectonic implications. Econ. Geol., 87: 597-619.

Deer, W.A., Howie, R.A. and Zussman, J., 1982. An introduction to the rock forming minerals, Longman.

Eastoe, C.J., Solomon, M. and Walshe, J.L., 1987. District scale alteration associated with massive sulphide deposits in the Mt. Read Volcanics, western Tasmania. Econ. Geol. 82: 1239-1258.

Edwards, A.B., 1939. Some observations on the mineral composition of the Mt. Lyell copper ores, Tasmania, and their modes of occurence. Proc. Australas. Inst. Min. Metall., 114: 67-109.

Edwards, A.B., 1958. Cuprite and native copper in the Mount Lyell copper clay deposits. CSIRO Mineragraphic Report No. 752.

Ekstrom, T.K., 1972. The distribution of fluorine among some coexisting minerals. Contrib. Mineral. Petrol. 34: 192-200.

Foster, M.D., 1962. Interpretation of the composition and classification of the chlorites. USGS Prof. Paper: 414-448.

Green, G.R., 1971. Geology and mineralization of the Cape Horn-Lyell Comstock area, Mt. Lyell, Unpub. Honours Thesis, Univ. of Tasmania.

Gregory, J.W., 1905. The Mt. Lyell mining field, Tasmania. Trans. Australas. Inst. Min. Eng., 10: 26-196.

Gulson, B.L. and Porritt, P.M., 1987. Base metal exploration of the Mt. Read volcanics, Western Tasmania: Pt.II. Pb Isotope signatures and genetic implications. Econ. Geol., 82: 291-307.

Gulson, B.L. and Vaasjoki, M., 1987. Lead isotope data from the Thalanga, Dry River and Mt. Chalmers base metal deposits and their bearing on exploration and ore genesis in Eastern Australia. Aus. Jour. Earth Sci. 34: 159 - 173.

Hall, G. and Solomon, M., 1962. Metallic mineral deposits in Geology of Tasmania, J. geol. Soc. Aust., 9: 285-309.

Hendry, D.A.F., 1972. The geochemistry of the Mt. Lyell copper ores, Tasmania. Unpubl. PhD. Thesis, Univ. of Cambridge.

Hendry, D.A.F., 1981. Chlorites, Phengites and Siderites from the Prince Lyell ore deposit, Tasmania, and the origin of the deposit. Econ. Geol., 76: 285-303.

Henley, R.W. and McNab, A., 1978. Magmatic vapor plumes and ground water interaction in porphyry copper emplacement. Econ. Geol. v. 73:20

Hills, P.B., 1990. Mt Lyell copper-gold-silver deposits. In Geology of the Mineral Deposits of Australia and Papua New Guinea (Ed. F.E. Hughes), pp. 1257-1266.

Huston, D.L. and Large, R.R., 1989. A chemical model for the concentration of gold in volcanogenic massive sulphide deposits. Ore Geol. Rev., 4: 171-200.

Jacobs, D.C. and Parry, W.T., 1979. Geochemistry of biotite in the Santa Rita porphyry copper deposit, New Mexico. Econ. Geol., 74: 860-887.

Jago, J.B., Reid, K.O., Quilty, P.G., Green, G.R. and Daly, B., 1972. Fossiliferous Cambrian limestone from within the Mt. Read Volcanics, Mt. Lyell mine area, Tasmania. J. Geol. Soc. Aust., 19(3): 379 - 382.

Johnson, J.W., Oelkers, E.H. and Helgeson, H.C.. 1991. *SUPCRT92* ; A software package for calculating the standard molal thermodynamic properties of minerals, gases, aqueous species and reactions from 1 to 5000 bars and 0° to 1000°C. Laboratory of theoretical geochemistry, University of California, Berkeley.

Leaman, D.E. and Richardson, R.G. 1989. The granites of west and northwest Tasmania - a geophysical interpretation. Bull. Geol. Surv. Tas., 66.

Loftus - Hills, C.L., 1927. A synopsis of the geology of the Lyell district of Tasmania. Proc. Australas. Inst. Min. Metall., 66: 129-148.

Loftus-Hills, G.D., 1967. Cobalt and nickel in Tasmanian pyrites, in The Geology of Western Tasmania - a Symposium (Geology Department, University of Tasmania: Hobart).

Loftus - Hills, G. and Solomon, M., 1967. Cobalt, nickel and seleniumin sulphides as indicators of ore genesis. Mineralium Deposita, 2: 228-242.

Loftus - Hills, G., 1968. Cobalt, nickel and selenium in Tasmanian ore minerals. Unpubl. PhD thesis, Univ. of Tasmania.

Loftus-Hills, G., Groves, D.I., and Solomon, M., 1969. The selenium content of some Tasmanian sulphides. Proc. Australas. Inst. Min. Metall., 232: 55-65.

McPhie, J., and Allen, R., 1992. Facies architecture of mineralized submarine volcanic sequences: Cambrian Mount Read Volcanics, western Tasmania. Econ. Geol., 87: 587-596.

Markham, N.L., 1963. An interpretation of the Mount Lyell (Tasmania) copper ore paragenesis. Proc. Australas. Inst. Min. Metall., 206: 123-141.

Markham, N.L., 1968. Some genetic aspects of the Mt. Lyell mineralisation. Mineral. Deposita, 3: 199-221.

Markham, N.L. and Lawrence, L.J., 1965. Mawsonite, a new copper-iron-tin sulphide from Mt. Lyell, Tasmania and Tingha, New South Wales. Am. Mineral., 50: 900-908.

Markham, N.L. and Otterman, J., 1968. Betechtinite from Mt. Lyell, Tasmania. Mineral. Deposita, 3: 171-173.

McDougall, I. and Leggo, P.J., 1965. Isotopic age determinations on granite rocks from Tasmania. Geol. Soc. Aust. Journ., 12: 295-332.

Muffler, L.J.P. and White, D.E., 1965. Recent metamorphism of Pliocene and Quaternary sediments of the Salton Sea geothermal field, California, USA. Abstracts of the international symposium on volcanology, New Zealand. 119-120.

Munoz, J.L., 1984. F-OH and Cl-OH exchange in micas with applications to hydrothermal ore deposits. In Reviews in Mineralogy 13, Micas. S.W. Bailey ed.. Miner. Soc. Am., 469-494.

Nye, P.B.,Blake, F. and Henderson, Q.J., 1934. Report on the geology of the Mt. Lyell mining field. Unpublished Report to Dept. Mines, Tasmania.

Parry, W.T., Ballantyne, W.T. and Jacobs, D.C., 1984. Geochemistry of hydrothermal sericite from Roosevelt hot springs and the Tintic and Santa Rita porphyry copper systems. Econ. Geol. 79: 72-86.

Payne, B., 1991. Geophysics and geology of the Sedgwick-Red Hills area, Tasmania. Unpublished PhD Thesis, University of Tasmania.

Reed, M.H. and Spycher, N.F., 1991. *SOLTHERM* ; Database of equilibrium constants for aqueous-mineral-gas equilibria. Dept. of Geological Sciences, University of Oregon.

Reid, K.O., 1975. Economic geology of Aust. and PNG. ed. Knight, C.L. AusIMM Monogr. 5: 604-619.

Seward, T.M., 1984. The transport and deposition of gold in hydrothermal systems. In Foster, R.P., Gold '82 : The geology, geochemistry and genesis of gold deposits. Geol. Soc. of Zimbabwe special Publ. 1: 165-181.

Sillitoe, R.H., 1985. Further comments on geology and exploration at Mount Lyell, Tasmania. Unpublished report to Goldfields Exploration Pty. Ltd.

Skinner, B.J., 1979. The many origins of hydrothermal mineral deposits. in Barnes, H.L. (ed.), Geochemistry of Hydrothermal Ore Deposits.

Solomon, M., 1957. Palaeozoic sedimentation, tectonics, and mineralization in the Mt. Lyell area (Tasmania), with special reference to the origin and economic significance of the Lyell schists, Unpublished Master of Science thesis, University of Tasmania, 122.

Solomon, M., 1964. The spilite - keratophyre association of West Tasmania and the ore deposits at Mt. Lyell, Rosebery and Hercules, Unpubl. PhD. Thesis, Univ. of Tasmania.

Solomon, M., 1959. Discussion of the mineralised rift valleys of Tasmania. Proc. Aust. Inst. Min. Met., 192: 33-39.

Solomon, M., 1967. Fossil gossans (?) at Mt. Lyell, Tasmania. Econ. Geol. 62: 757-772.

Solomon, M., 1969. The copper clay deposits at Mount Lyell, Tasmania. Proc. Aust. Inst. Min. Met., 230: 39-47.

Solomon, M., 1981. An introduction to the geology and metallic ore deposits of Tasmania. Econ. Geol., 76: 194-208.

Solomon, M. and Elms, R.G., 1965. Copper ore deposits of Mt. Lyell, Proc. 8th Commonw. Min. Met. Cong., 1: 478 - 484.

Solomon, M. and Carswell, J.T., 1989. Mt. Lyell, (in Geology and Mineral resources of Tasmania) Eds. C.F. Burrett and E.L. Martin. Geol. Soc. Aust. Spec. Publ., 15: 125-132.

Solomon, M., Rafter, T.A. and Jensen, M.L., 1969. Isotope studies on the Rosebery, Mount Farrell and Mount Lyell ores, Tasmania. Mineral. Deposita 4: 172-199.

Solomon, M., Vokes, F.M. and Walshe, J.L., 1987. Chemical remobilization of volcanic-hosted sulphide deposits at Rosebery and Mt. Lyell, Tasmania. Ore Geology Reviews, 2: 173-190.

Solomon, M. and Walshe, J.L., 1981. An investigation into the environment of formation of the volcanic hosted Mt. Lyell copper deposits using geology, mineralogy, stable isotopes and a six - component chlorite solid solution model. Econ. Geol. 76: 246 - 284.

Steiner, A., and Rafter, T.A., 1966. Sulphur isotopes in pyrite, pyrrhotite, alunite and anhydrite from steam wells in the Taupo volcanic zone, New Zealand. Econ. Geol. 61: 1115-1129.

Wade, M.L. and Solomon, M., 1958. Geology of the Mt. Lyell mines, Tasmania. Econ. Geol., 53: 367-416.

Walshe, J.L., 1971. Geology of the southern Mt. Lyell field and trace element studies of the pyrite mineralisation, Unpubl. Honours Thesis, Univ. of Tasmania.

Walshe, J.L., 1977. The geochemistry of the Mt. Lyell copper deposits, Unpubl. PhD. Thesis, Univ. of Tasmania.

Walshe, J.L., and Solomon, M., 1981. An investigation into the environment of formation of the volcanic-hosted Mt. Lyell copper deposits using geology, mineraology, stable isotopes and a six component chlorite solid solution model. Econ. Geol., 76: 246-284.

White, D.E., 1974. Diverse origins of hydrothermal ore fluids. Econ. Geol., 69; 954-973.

Whitford, D.J., and Wallace, D.B., 1984. The Mt. Read Volcanics at Que River: Primary geochemical affinities and REE geochemistry (abs). Australian Geol. Conv., 8th, Sydney, August, 1984, Abstracts, 547-548.

Williams, E., Solomon, M. and Green, G.R., 1975. The geological setting of metalliferous ore deposits in Tasmania, in Economic Geology of Australia and Papua New Guinea, Vol. 1 Metals (Ed. C.L. Knight), pp. 567-581 AusIMM: Melbourne).

APPENDIX I

Rock Sample Descriptions

Guide to code for preparation of samples;

R - Rock chip handspecimen

PT - Polished thin section

T - Thin section

PD - Powdered specimen

P - X-ray pill

XRD - X-ray diffraction analysis

M - Modal analysis

	A	B	C	D	E	F	G
1	CATALOG #	FIELD #	DESCRIPTION	FORMATION	LOCALITY	CO-ORDS	PREPS
2	78186	NL 1	silicified conglomerate	Owen Congl.	North Lyell	5343300N 383190E	R,PT,PD,
3	78187	NL 3	silicified conglomerate	Owen Congl.	North Lyell	5343300N 383190E	R,PT,PD,
4	78188	NL 4	Hematitic quartzite	Owen Congl.	North Lyell	5343300N 383190E	R,PT,PD,
5	78189	NL 6	Hematitic quartzite	Owen Congl.	North Lyell	5343300N 383190E	R,PT,PD,
6	78190	NL 8	Schistose hematitic qtzite	Owen Congl.	North Lyell	5343300N 383190E	R,PT,PD,
7	78191	NL 10	Conglomerate	Owen Congl.	North Lyell	5343300N 383190E	R,PT,PD,
8	78192	NL 11	Conglomerate	Owen Congl.	North Lyell	5343300N 383190E	R,PT,PD,
9	78193	NL 12	Schistose hematitc congl.	Owen Congl.	Lyell Tharsis	5343000N 383190E	R,PT,PD,XRD
10	78194	NL 14	Schistose hematitc congl.	Owen Congl.	Lyell Tharsis	5343000N 383190E	R,PD,
11	78195	NL 15	Mass. hematite/chlorite	Owen Congl.	Lyell Tharsis	5343000N 383190E	R,PT,PD,
12	78196	NL 16	Hematitic/sericitic congl.	Owen Congl.	Lyell Tharsis	5343000N 383190E	R,PT,PD,
13	78197	NL 17	Hematite/chloritic sst.	Owen Congl.	Lyell Tharsis	5343000N 383190E	R,PD,
14	78198	NL 18	Hematitic sandstone	Owen Congl.	Lyell Tharsis	5343000N 383190E	R,PT,PD,
15	78199	NL 19	Brown limestone pug	Gordon Lst.	Batchelors' Quarry	5342800N 383360E	R,T,PD,XRD
16	78200	NL 20	Hematitic sandstone	Pioneer Sst.	Batchelors' Quarry	5342800N 383360E	R,PT,PD,
17	78201	NL 21	Sandstone	Pioneer Sst.	Batchelors' Quarry	5342800N 383360E	R,PT,PD,
18	78202	NL 22	Sandstone/quartzite	Pioneer Sst.	Batchelors' Quarry	5342800N 383360E	R,PT,PD,
19	78203	NL 23	Hematitic sst/qtzite	Pioneer Sst.	Batchelors' Quarry	5342800N 383360E	R,PT,PD,
20	78204	NL 24	Hem/ser/ chl sandstone	Pioneer Sst.	Batchelors' Quarry	5342800N 383360E	R,PT,PD,
21	78205	NL 25	Hem/ser/ chl sandstone	Owen Congl.	Batchelors' Quarry	5342800N 383360E	R,PT,PD,
22	78206	NL 27	Hematitic sericitic sst.	Owen Congl.	Batchelors' Quarry	5342800N 383360E	R,PT,PD,
23	78207	NL 29	Hematitic sandstone	Owen Congl.	Batchelors' Quarry	5342800N 383360E	R,PT,PD,
24	78208	NL 30	Hematitic sandstone	Owen Congl.	Waterfall Area	5342880N 383420E	R,PT,PD,
25	78209	NL 32	Schistose/hematitic congl	Pioneer Sst.	Waterfall Area	5342880N 383420E	R,PT,PD,
26	78210	NL 34	Schistose conglomerate	Pioneer Sst.	Waterfall Area	5342880N 383420E	R,PT,PD,
27	78211	NL 35	Sandstone	Pioneer Sst.	Waterfall Area	5342880N 383420E	R,PT,PD,
28	78212	NL 36	Brown limestone pug	Gordon Lst.	Waterfall Area	5342880N 383420E	R,P,PD,XRD
29	78213	NL 40	Hematitic clast	Owen Congl.	Tharsis Ridge	5342880N 383050E	R,
30	78214	NL 41	Hematitic matrix	Owen Congl.	Tharsis Ridge	5342880N 383050E	R,PD
31	78215	NL 42	Conglomerate	Owen Congl.	Tharsis Ridge	5342880N 383050E	R,PT
32	78216	NL 45	Hematitic quartzite	Owen Congl.	Tharsis Ridge	5342880N 383050E	R,PT
33	78217	NL 48	Sericitic quartzite	Owen Congl.	North Lyell	5343100N 383160E	R,PD,PT
34	78218	NL 49	Hematite	Owen Congl.	North Lyell	5343100N 383160E	R,PD,PT
35	78219	NL 50	Silicified conglomerate	Owen Congl.	North Lyell	5343100N 383160E	R,PD,PT
36	78220	NL 51	Silicified conglomerate	Owen Congl.	North Lyell	5343100N 383160E	R,PD,PT
37	78221	NL 52	Silicified conglomerate	Owen Congl.	North Lyell	5343100N 383160E	R,PD,PT
38	78222	NL 53	Silicified conglomerate	Owen Congl.	North Lyell	5343100N 383160E	R,PD,PT

	A	B	C	D	E	F	G
39	78223	NL 54	Silicified conglomerate	Owen Congl.	North Lyell	5343100N 383160E	R,PD,PT
40	78224	NL 55	Hematite conglomerate	Owen Congl.	North Lyell	5343100N 383160E	R,PD
41	78225	NL 56	Copper clays'	Pioneer Sst.	Batchelor's Quarry	5342800N 383360E	R,PD,PT
42	78226	NL 57	Conglomerate	Pioneer Sst.	Batchelor's Quarry	5342800N 383360E	R,
43	78227	NL 58	Conglomerate	Pioneer Sst.	Batchelor's Quarry	5342800N 383360E	R,PD
44	78228	NL 59	Hematitic conglomerate	Owen Congl.	Mt Owen	5340200N 383750E	R,
45	78229	NL 62	Conglomerate	Owen Congl.	Ridge Near Gormanston	5342170N 383860E	R,PD,PT
46	78230	NL 63	Conglomerate	Owen Congl.	Ridge Near Gormanston	5342250N 383620E	R,PD,PT
47	78231	NL 64	Hematitic conglomerate	Pioneer Sst.	Ridge Near Gormanston	5342290N 383560E	R,PD,PT
48	78232	NL 65	Hematitic conglomerate	Pioneer Sst.	Ridge Near Gormanston	5342320N 383400E	R,PD
49	78233	NL 66	Hematitic conglomerate	Owen Congl.	Ridge Near Gormanston	5342380N 383370E	R,PD,PT
50	78234	NL 67	Hematitic conglomerate	Owen Congl.	Ridge Near Gormanston	5342380N 383370E	R,PD,PT
51	78235	NL 69	Gordon Limestone	Gordon Lst.	Batchelors' Quarry	5342800N 383360E	R,
52	78236	NL 70	Goeth nodule in Gord. lst.	Gordon Lst.	Batchelors' Quarry	5342800N 383360E	R,
53	78237	NL 71	Silicified/pyritic qtzite.	Owen Congl.	DDH NL1101 44m	5343100N 383160E	R,PT,
54	78238	NL 72	Hematite veined congl.	Owen Congl.	DDH NL1102 14m	5343100N 383160E	R,PT
55	78239	NL 75	Conglomerate	Owen Congl.	Cape Horn	5344000N 382220E	R,M
56	78240	NL 76	Conglomerate	Owen Congl.	Cape Horn	5344000N 382400E	R,M
57	78241	NL 77	Conglomerate	Owen Congl.	Cape Horn	5344000N 382520E	R,M
58	78242	NL 78	Conglomerate	Owen Congl.	Cape Horn	5344000N 382660E	R,PT,M
59	78243	NL 79	Sandstone	Owen Congl.	Cape Horn	5344000N 382520E	R,PD,PT
60	78244	NL 80	Sandstone	Owen Congl.	Cape Horn	5344000N 382660E	R,PD,PT
61	78245	NL 81	Conglomerate	Owen Congl.	Cape Horn	5344000N 382850E	R,M
62	78246	NL 82	Sandstone	Owen Congl.	Cape Horn	5344000N 382850E	R,PD
63	78247	NL 83	Conglomerate	Owen Congl.	Cape Horn	5344000N 383120E	R,M
64	78248	NL 84	Conglomerate	Owen Congl.	Cape Horn	5344000N 383220E	R,M
65	78249	NL 85	Sandstone	Owen Congl.	Cape Horn	5344000N 383220E	R,PD
66	78250	NL 86	Sandstone	Owen Congl.	Cape Horn	5340200N 383750E	R,PD
67	78251	NL 87	Conglomerate	Owen Congl.	Mt Owen	5340200N 383750E	R,PT,M
68	78252	NL 88	Hem/barite schistose sst.	Owen Congl.	btw LT and BQ	5342850N 383240E	R,PD,PT
69	78253	NL 89	Hem/barite schistose sst.	Owen Congl.	btw LT and BQ	5342850N 383240E	R,PD,PT
70	78254	NL 90	Hem/barite schistose sst.	Owen Congl.	btw LT and BQ	5342850N 383240E	R,PD,PT
71	78255	NL 91	Chloritic hematite sst.	Owen Congl.	btw LT and BQ	5342850N 383240E	R,PD,PT
72	78256	NL 92	Hematite Sandstone	Pioneer Sst.	btw LT and BQ	5342850N 383240E	R,PD,PT
73	78257	NL 93	Bornite/cpy/pyrite congl?	Owen Congl.	DDH NL1100 8.2m	5343100N 383160E	R,PD
74	78258	NL 94	Siliceous breccia & cpy	Owen Congl.	DDH NL1100 15 m	5343100N 383160E	R,PD
75	78259	NL 95	Silicified white congl.	Owen Congl.	DDH NL1100 21.7m	5343100N 383160E	R,PD
76	78260	NL 96	Brown Lst pug	Gordon Lst.	Cemetery Ck. Linda Vall	5341500N 384930E	R,PD,XRD

	A	B	C	D	E	F	G
77	78261	NL 97	Calcarcous siltstone	Gordon Lst.	Queenstown quarry	5340800N 380400E	R,PD
78	78262	NL 98	Limestone	Gordon Lst.	Queenstown quarry	5340800N 380400E	R,PD
79	78263	NL 99	Limestone	Gordon Lst.	Linda Ck.	5341350N 386400E	R,PD

APPENDIX II

XRF Results

	A	B	C	D	E	F	G	H	I	J	K	L
1		NL 1	NL 3	NL 4a	NL 4b	NL 4 (avge)	NL 6	*NL 8	NL 10	NL 11	*NL 12	*NL 14
2												
3	SiO2	87.31	71.91	83.76	92.93	88.37	85.52	16.81	72.22	85.83	51.87	18.70
4	TiO2	0.65	1.32	0.46	0.49	0.47	0.40	1.35	0.46	0.60	0.19	0.38
5	Al2O3	0.88	1.46	0.62	0.47	0.54	0.85	2.48	3.79	1.05	7.53	9.47
6	Fe2O3	1.66	11.41	8.47	0.39	4.41	1.10	49.17	16.12	4.76	35.86	67.22
7	MnO	0.02	0.01	0.01	0.00	0.00	0.00	0.02	0.03	0.00	0.01	0.04
8	MgO	0.15	0.10	0.02	0.05	0.03	0.07	0.22	0.33	0.03	0.02	0.05
9	CaO	0.00	0.00	0.02	0.00	0.01	0.00	0.01	0.00	0.02	0.27	0.75
10	Na2O	0.10	0.10	0.10	0.10	0.10	0.10	0.20	0.10	0.10	0.10	0.20
11	K2O	0.00	0.00	0.05	0.03	0.04	0.01	0.08	0.12	0.02	1.08	0.36
12	P2O5	0.04	0.27	0.08	0.08	0.08	0.10	0.71	0.05	0.30	0.46	0.87
13	BaSO4	8.15	11.19	5.28	4.79	5.03	10.85	25.33	4.74	5.48	0.92	0.00
14	Loss	1.04	2.23	1.13	0.68	0.91	1.01	3.62	2.04	1.81	1.70	1.95
15												
16	Total	100.00	100.00	100.00	100.00	100.00	100.00	100.00	100.00	100.00	100.00	100.00
17												
18	Cr	69	83	55	30	42.5	30	108	39	34	2	101
19	Ni	11	21	1	8	4.5	16	0	19	13	0	0
20	V	28	121	72	0	0	0	0	0	0	0	145
21	Sb	2	24	0	7	3	6	150	30	21	33	81
22	Zn	42	48	18	14	16	26	60	69	29	47	25
23	Cu	343	231	94	64	79	49	270	65	131	85	85
24	Nb	16	36	16	19	18	15	25	13	14	8	0
25	Zr	207	518	118	132	125	125	434	134	230	163	37
26	Y	8	30	4	5	4	17	24	3	12	25	9
27	Sr	1173	2890	1215	1158	1186	2339	5763	874	1533	651	780
28	Rb	2	1	0	2	0	3	0	2	0	46	6
29	La	5	32	12	4	8	16	140	15	76	40	23
30	Ce	7	53	18	8	13	22	0	13	120	91	49
31	Nd	1	17	3	1	2	7	0	1	32	43	23
32	Ba	47971	65864	31078	28194	29606	63863	149092	27899	32255	5415	1254
33	Sc											24

	M	N	O	P	Q	R	S	T	U	V	W	X
1		*NL 15	*NL 16	NL 17	*NL18	NL 20	NL 21	NL 22	NL 23	NL 24	NL 25	NL 27
2												
3	SiO2	29.57	23.84	88.82	9.36	86.73	97.47	84.63	84.97	84.64	86.74	88.63
4	TiO2	0.26	0.16	0.15	0.20	0.41	0.09	0.61	0.53	0.40	0.43	0.22
5	Al2O3	3.17	2.38	1.76	2.23	5.68	1.17	6.27	5.44	4.68	5.60	3.42
6	Fe2O3	42.36	69.38	7.90	84.11	4.33	0.33	4.77	6.33	7.83	4.27	5.45
7	MnO	0.06	0.04	0.02	0.02	0.00	0.00	0.01	0.01	0.00	0.01	0.01
8	MgO	0.05	0.10	0.09	0.10	0.12	0.10	0.22	0.13	0.11	0.10	0.17
9	CaO	1.01	0.52	0.01	1.20	0.01	0.02	0.01	0.01	0.02	0.01	0.01
10	Na2O	0.20	0.20	0.12	0.20	0.10	0.10	0.50	0.17	0.10	0.22	0.40
11	K2O	0.01	0.02	0.07	0.12	1.59	0.22	1.85	1.51	1.31	1.57	0.77
12	P2O5	1.05	0.63	0.08	1.10	0.08	0.09	0.07	0.01	0.08	0.13	0.11
13	BaSO4	19.53	1.29	0.00	0.00	0.00	0.00	0.00	0.00	0.00	0.00	0.00
14	Loss	2.73	1.45	0.98	1.36	0.95	0.40	1.06	0.88	0.84	0.92	0.79
15												
16	Total	100.00	100.00	100.00	100.00	100.00	100.00	100.00	100.00	100.00	100.00	100.00
17												
18	Cr	27	48			147	870	2200	3301	2182	160	160
19	Ni	0	0	8	0	7	10	16	7	9	5	10
20	V	0	143	49	81	37	8	60	59	57	35	25
21	Sb	61	50	6	53	2	2	4	2	5	2	2
22	Zn	141	130	27	57	20	45	142	213	133	20	29
23	Cu	79	76	27	85	322	46	77	65	370	252	97
24	Nb	0	3.3	3.3	7	8	3	12	10	8	9	4
25	Zr	80	79.5	74.1	111	195	54	371	385	241	214	174
26	Y	11.4	14.5	6	13	17	17	30	21	17	18	9
27	Sr	3567	1083	153	1429	76	28	71	58	72	77	103
28	Rb	4.2	0	0	0	60	8	77	61	51	59	25
29	La	64	72	13	46	22	11	28	22	21	25	17
30	Ce	0	180	36	98	56	29	55	46	47	63	44
31	Nd	0	101	18	47	27	14	24	20	18	27	16
32	Ba	114953	7593	76	1134	1148	751	954	663	837	980	619
33	Sc			2	19	12	1	11	13	9	11	4

	Y	Z	AA	AB	AC	AD
1		NL 29	NL 30	NL 32	NL 34	NL 35
2						
3	SiO2	95.32	94.40	36.27	78.24	95.58
4	TiO2	0.12	0.16	1.04	0.43	0.12
5	Al2O3	1.59	2.03	15.92	5.72	1.64
6	Fe2O3	2.06	2.20	38.63	11.65	0.26
7	MnO	0.00	0.01	0.03	0.01	0.00
8	MgO	0.01	0.09	0.06	0.88	0.02
9	CaO	0.00	0.03	0.38	0.02	0.01
10	Na2O	0.10	0.21	0.99	0.10	0.10
11	K2O	0.33	0.23	2.66	1.12	0.45
12	P2O5	0.05	0.07	0.87	0.35	0.01
13	BaSO4	0.00	0.00	0.00	0.00	0.00
14	Loss	0.41	0.56	3.15	1.48	1.80
15						
16	Total	100.00	100.00	100.00	100.00	100.00
17						
18	Cr	266	100	7040	1730	1787
19	Ni	2	6	0	53	1
20	V	18	18	350	77	18
21	Sb	2	2	2	2	2
22	Zn	23	8	283	41	22
23	Cu	54	7	84	23	13
24	Nb	3.1	4	12	9	4
25	Zr	69	185	181	188	76
26	Y	13	7	27	46	10
27	Sr	93	50	1355	469	9
28	Rb	11	4	43	40	17
29	La	14	9	380	31	13
30	Ce	32	16	704	60	26
31	Nd	12	6	269	25	10
32	Ba	304	134	2902	2816	111
33	Sc	2	3	25	8	1

sample no	NL 40	NL 48	NL 49	NL 50	NL 51	NL 52	NL 53	NL 54	NL 55
SIO2	14.09	94.39	2.61	96.37	88.09	92.10	94.24	84.20	28.53
TIO2	0.30	0.60	0.02	0.50	0.48	0.39	0.38	0.27	0.15
AL2O3	4.63	0.85	0.71	0.04	0.05	0.20	0.84	0.23	0.90
FE2O3	78.27	0.49	94.28	2.11	9.20	4.08	0.94	5.02	68.52
MNO	0.01	0.00	0.00	0.00	0.00	0.01	0.00	0.01	0.00
MGO	0.09	0.00	0.00	0.00	0.00	0.00	0.00	0.00	0.00
CAO	0.00	0.00	0.00	0.00	0.00	0.00	0.00	0.00	0.00
NA2O	0.35	0.26	0.01	0.07	0.00	0.04	0.07	0.27	0.04
K2O	1.27	0.04	0.01	0.01	0.00	0.00	0.02	0.02	0.02
P2O5	0.07	0.00	0.01	0.01	0.00	0.00	0.02	0.00	0.00
SO3	0.01	0.86	0.18	0.12	0.61	1.09	0.93	3.25	0.35
BAO	0.10	1.91	0.02	0.19	1.13	2.00	2.07	6.12	0.41
LOI	0.88	1.14	0.72	0.31	0.80	0.84	1.24	1.30	1.35
TOTAL	100.07	100.54	98.57	99.73	100.36	100.75	100.75	100.69	100.27
	NL40	NL48	NL49	NL50	NL51	NL52	NL53	NL54	NL55
SB	48	7	178	9	17	15	4	15	94
BA	636	16925	125	1977	10155	17491	18542	55224	3252
SR	98	386	10	78	283	425	614	823	59
CR	43	19	558	28	31	42	22	39	169
LA	20	0	0	7	2	1	5	8	0
RB	39	0	0	0	0	0	0	0	0

sample no	NL 56	NL 58	NL 62	NL 63	NL 64	NL 65	NL 66	NL 67	NL 79
SIO2	80.22	74.14	93.64	94.48	91.45	93.61	21.96	80.39	96.00
TIO2	0.39	0.39	0.12	0.08	0.22	0.12	0.46	0.22	0.10
AL2O3	5.50	4.41	1.90	1.27	2.27	1.31	3.94	2.59	0.76
FE2O3	6.39	14.39	1.71	1.09	2.90	3.11	69.68	15.16	2.35
MNO	0.06	0.04	0.00	0.00	0.01	0.01	0.02	0.01	0.00
MGO	3.76	0.36	0.29	0.08	0.17	0.05	0.19	0.20	0.00
CAO	0.01	0.02	0.00	0.00	0.00	0.00	0.07	0.01	0.00
NA2O	0.03	0.63	0.07	0.06	0.02	0.00	0.03	0.43	0.08
K2O	0.11	0.99	0.42	0.50	0.85	0.46	0.79	0.63	0.18
P2O5	0.07	0.72	0.03	0.00	0.03	0.02	0.28	0.09	0.01
SO3	0.00	0.09	0.03	0.00	0.00	0.02	0.13	0.00	0.00
BAO	0.05	0.69	0.00	0.00	0.02	0.01	0.05	0.07	0.02
LOI	2.96	1.52	1.05	0.58	0.61	0.52	1.94	1.03	0.37
TOTAL	99.55	98.39	99.26	98.14	98.55	99.24	99.54	100.83	99.87
	NL56	NL58	NL62	NL63	NL64	NL65	NL66	NL67	NL79
SB	2	2	1	1	2	1	26	1	2
BA	448	6280	52	52	59	98	149	516	188
SR	30	162	5	5	6	10	41	28	19
CR	674	10441	157	190	5684	2204	276	205	22
LA	22	55	11	5	24	17	91	19	6
RB	5	36	17	20	33	17	26	25	6

sample no	NL 79B	NL 80	NL 82	NL 85	NL 86	NL 88	NL 89	NL 90	NL 91
SIO2	97.37	84.20	98.54	95.63	93.58	10.30	26.30	41.69	48.05
TIO2	0.06	0.06	0.07	0.20	0.28	0.19	0.17	0.17	0.32
AL2O3	0.81	0.29	0.43	1.23	3.28	0.31	1.21	5.41	3.16
FE2O3	0.11	14.07	0.17	1.20	1.21	88.23	69.78	47.68	46.10
MNO	0.00	0.00	0.00	0.00	0.00	0.01	0.03	0.05	0.06
MGO	0.00	0.03	0.00	0.01	0.00	0.02	0.06	0.24	0.35
CAO	0.00	0.00	0.00	0.00	0.00	0.06	0.45	0.13	0.00
NA2O	0.03	0.00	0.00	0.08	0.12	0.02	0.02	0.34	0.07
K2O	0.22	0.09	0.12	0.40	0.89	0.03	0.11	0.72	0.46
P2O5	0.00	0.00	0.00	0.01	0.03	0.25	0.60	0.38	0.15
SO3	0.00	0.00	0.00	0.00	0.02	0.01	0.23	0.73	0.43
BAO	0.00	0.00	0.00	0.01	0.01	0.08	0.52	1.51	0.89
LOI	0.66	0.33	0.28	0.42	0.70	0.41	0.91	2.13	1.53
TOTAL	99.26	99.07	99.61	99.19	100.12	99.92	100.39	101.18	101.57
	NL79B	NL80	NL82	NL85	NL86	NL88	NL89	NL90	NL91
SB	1	4	1	1	2	40	30	22	27
BA	29	50	38	132	143	781	4331	13386	7836
SR	14	7	35	7	283	50	245	897	252
CR	12	35	59	306	54	45	9	8	116
LA	6	4	5	4	14	14	40	29	34
RB	7	3	4	13	24	0	5	27	18

sample no	NL 92	NL 93	NL 94	NL 95	NL 97	NL 98	NL 99
SIO2	55.99	74.24	95.68	94.46	14.90	2.84	23.70
TIO2	0.30	0.92	0.78	0.71	0.17	0.04	0.26
AL2O3	3.03	1.42	0.03	1.32	3.76	0.66	4.66
FE2O3	38.47	13.85	1.21	0.10	1.92	0.36	2.00
MNO	0.01	0.01	0.00	0.00	0.05	0.01	0.04
MGO	0.09	0.03	0.00	0.05	12.29	1.48	6.16
CAO	0.00	0.01	0.00	0.00	28.72	51.96	29.68
NA2O	0.08	0.06	0.01	0.06	0.08	0.00	0.18
K2O	0.68	0.03	0.01	0.27	1.52	0.30	2.00
P2O5	0.14	0.02	0.01	0.02	0.03	0.00	0.04
SO3	0.02	0.00	2.32	0.65	0.20	0.18	0.70
BAO	0.08	0.00	0.00	1.15	0.03	0.00	0.00
LOI	0.78	7.85	0.00	1.13	36.15	39.99	29.09
TOTAL	99.67	98.44	100.05	99.92	99.82	97.82	98.51
	NL92	NL93	NL94	NL95	NL97	NL98	NL99
SB	10	3	3	2	1	0	0
BA	733	15355	91	10373	162	24	202
SR	110	358	28	302	596	1217	357
CR	1475	65	34	40	40	14	46
LA	70	1	1	5	12	5	19
RB	27	0	0	7	57	8	70

APPENDIX III

Microprobe analyses

Guide to the code for numbering of all microprobe sample analyses -

The sample analyses numbers (in the slide/ring/micano column) contain the polished thin section number (the first one or two numbers), the ring number, and the analysis number (of the same grain) is always the last digit.

For example number 1061 indicates slide number 10, ring number 6, analysis number 1. Number18121, indicates slide number 18, ring number 12, analysis number 1, or 2732 indicates slide number 27, ring number 3, analysis number 2.

probemicaE clipped

	A	B	C	D	E	F	G	H
1	slide/ring/micano	SiO2	TiO2	Al2O3	MgO	CaO	MnO	FeO
2								
3	1031	66.6692	0.0168	29.6616	0.0251	0.0425	0.0000	0.2500
4	1032	65.5757	0.0000	29.2724	0.0187	0.0184	0.0000	0.3443
5	1033	65.1703	0.0084	29.8503	0.0368	0.0322	0.0000	0.3081
6	1051	51.1986	0.0674	29.6378	1.1127	0.0045	0.1884	11.3823
7	1061	64.6048	0.0000	29.6992	0.0235	0.0102	0.0354	0.4520
8	1062	67.3817	0.0000	29.4663	0.0303	0.0316	0.0519	0.2951
9								
10	1211	46.7984	0.0696	35.8652	0.1354	0.0275	0.0000	2.2221
11	1221	43.5547	0.0192	35.2925	0.1713	0.0295	0.0000	7.0419
12	1222	46.3711	0.0000	37.6702	0.1577	0.0378	0.0000	1.8310
13	1232	47.0860	0.0445	37.7406	0.1281	0.0343	0.0439	1.3461
14	1241	45.7851	0.0000	36.8643	0.2557	0.0595	0.0000	3.1113
15	1242	45.8645	0.0084	37.1114	0.1128	0.0345	0.0000	1.7375
16	1271	60.7753	0.0334	32.6014	0.0504	0.0503	0.0000	0.6908
17	1272	63.6064	0.0028	31.4195	0.0712	0.0729	0.0000	0.6729
18	12121	57.6440	0.0000	32.7631	0.1448	0.1364	0.0000	0.7480
19								
20	15151	64.3680	0.0475	28.5608	0.0376	0.0000	0.0000	0.8232
21	15152	66.4789	0.0111	29.7030	0.0013	0.0582	0.0000	0.4900
22								
23	1611	66.0658	0.0000	29.0283	0.0026	0.0239	0.1117	0.8731
24	1651	61.6817	0.0000	32.5581	0.0212	0.0638	0.0693	0.4823
25	1671	60.6437	0.0196	31.9510	0.0155	0.0000	0.0376	0.3868
26	1681	65.1358	0.0306	29.8039	0.0193	0.0103	0.0186	0.4267
27	16101	66.2308	0.0389	29.3474	0.0128	0.0536	0.0000	0.5473
28								
29	1831	62.9042	0.0000	31.4572	0.0293	0.0057	0.0000	0.5083
30	1841	66.2370	0.0378	29.9565	0.0045	0.0391	0.0000	0.7094
31	1882	64.9722	0.0407	30.1132	0.0325	0.0208	0.0000	0.8977
32	18121	65.7543	0.0000	30.0655	0.0019	0.0254	0.0000	0.4815
33								
34	2141	46.4892	0.7510	34.3581	1.0314	0.0314	0.0000	3.3176
35								
36	2351	45.9696	0.0934	33.9861	0.7737	0.0173	0.0559	2.7449
37	2352	46.5712	0.0586	34.3016	0.6797	0.0173	0.0002	2.6069
38	2371	46.6776	0.1922	34.8362	0.8345	0.0104	0.0777	2.1398
39	2381	46.5144	0.0515	34.7054	0.7569	0.0023	0.0355	2.7317
40	23101	52.7001	0.0458	31.6945	0.7905	0.0207	0.0000	2.3358
41	23131	46.9795	0.1276	34.7725	0.7918	0.0138	0.0286	2.8378
42	23132	46.9410	0.6261	32.3804	2.3255	0.0000	0.0000	2.4034
43	23133	46.7632	0.6015	32.3110	2.2389	0.0035	0.0152	1.9322
44	23134	47.1410	0.1254	34.1147	0.7278	0.0438	0.0002	2.6633
45								
46	2721	47.9028	0.0227	37.8190	0.3085	0.1146	0.0000	1.8607
47	2731	49.5347	0.0988	31.5736	1.1485	0.0000	0.0154	3.4870
48	2732	45.3762	0.3012	35.5971	0.4181	0.0199	0.0000	3.3252
49	27101	48.0641	0.3340	32.6773	1.7904	0.0070	0.0155	2.3369
50	27131	49.7139	0.2537	30.1117	2.9900	0.0000	0.0000	1.8199
51								
52	3221	46.8360	0.0309	36.9057	0.1743	0.0000	0.0000	1.4895
53	3231	45.5510	0.0351	37.0186	0.1640	0.0000	0.0000	1.9672
54	3261	46.9288	0.0686	37.3591	0.0930	0.0646	0.0000	2.3547
55	3262	48.1883	0.0434	35.1816	0.1349	0.0185	0.0528	2.9768
56	3281	46.1780	0.0447	35.6541	0.3993	0.0623	0.0000	3.7626
57	3282	45.9887	0.1121	36.7074	0.3320	0.0520	0.0068	2.7428
58	3291	45.6874	0.0266	37.0331	0.0806	0.0381	0.0136	3.5836
59	32111	46.3053	0.0000	38.9346	0.1124	0.0694	0.0359	0.8897
60	32131	45.1195	0.0577	36.7978	0.1931	0.0743	0.0888	1.9838
61	32141	46.1011	0.0463	34.7525	0.7576	0.0000	0.0324	2.8678
62	32142	46.7854	0.0266	37.5728	0.0982	0.0393	0.1024	2.0361
63	32161	45.9610	0.0436	37.1551	0.1360	0.0000	0.0000	1.7279
64	32181	45.5617	0.6752	36.3989	0.5550	0.0046	0.1108	1.4436
65								
66	3711	39.4077	0.3046	20.5012	0.3763	0.0356	0.0000	30.1987
67	3712	51.1734	0.1340	31.7642	0.1964	0.0350	0.0000	3.0360
68	3721	48.1641	0.0523	34.7715	0.4907	0.0374	0.0515	2.2091
69	3741	34.2794	0.4335	25.4949	0.3004	0.0345	0.0000	29.2044
70	3771	49.0079	0.2018	32.5695	1.9841	0.0258	0.0069	0.9932
71	3791	47.4939	0.0469	34.2463	1.2602	0.0305	0.0620	1.3319
72	37131	48.8754	0.1977	30.6752	1.7615	0.0140	0.0000	3.7465

	I	J	K	L	M	N	O	P
1	slide/ring/micano	Na2O	K2O	H2O	F	Cl	Total	Fe ratio
2								
3	1031	0.1709		5.0675	0.0000	0.0448	102.0645	84.8500
4	1032	0.2036	0.0530	4.9963	0.0000	0.0179	100.5004	91.1600
5	1033	0.2182	0.1313	4.8800	0.2423	0.0556	100.9335	82.4500
6	1051	0.8879	0.2910	4.5122	0.0842	0.0294	99.3965	85.3700
7	1061	0.0809	0.0543	4.9741	0.0000	0.0424	100.2767	92.0800
8	1062	0.0648	0.0478	5.0955	0.0000	0.0406	102.5057	86.5500
9								
10	1211	2.1547	6.9682	4.4924	0.0525	0.0000	98.7861	90.2000
11	1221	2.1193	7.0533	4.2300	0.3991	0.0138	99.9246	95.8500
12	1222	1.9671	7.7891	4.4931	0.1827	0.0000	100.5000	86.6900
13	1232	2.9041	6.0566	4.5515	0.1175	0.0000	100.0533	85.9000
14	1241	1.9140	7.1615	4.3973	0.2715	0.0174	99.8377	87.2200
15	1242	1.7349	7.9563	4.4724	0.0921	0.0087	99.1333	89.6300
16	1271	0.8648	0.7441	4.9342	0.0133	0.0000	100.7580	88.5000
17	1272	0.7372	1.1976	5.0046	0.0794	0.0000	102.8644	84.1300
18	12121	1.2713	2.3809	4.8177	0.0000	0.0212	99.9275	74.3500
19								
20	15151	0.0685	0.1162	4.9091	0.0000	0.0089	98.9398	92.4800
21	15152	0.0950	0.1303	5.0026	0.1334	0.0303	102.1339	99.5400
22								
23	1611	0.2075	0.0944	5.0267	0.0900	0.0160	101.4500	99.5400
24	1651	0.8750	0.8988	4.8498	0.2777	0.0160	101.7937	93.6000
25	1671	0.3792	0.1436	4.8665	0.0000	0.0107	98.4541	93.8900
26	1681	0.3920	0.4749	5.0054	0.0268	0.0000	101.3443	92.8500
27	16101	0.1344	0.1051	5.0462	0.0000	0.0000	101.5166	95.9900
28								
29	1831	1.3456	0.3386	4.9361	0.1201	0.0251	101.6702	90.6900
30	1841	0.0920	0.0551	5.0750	0.0000	0.0072	102.2138	98.8800
31	1882	0.2445	0.2632	5.0089	0.0404	0.0000	101.6340	93.9400
32	18121	0.1338	0.0574	4.9396	0.2156	0.0306	101.7057	99.2900
33								
34	2141	0.7363	9.0474	4.3712	0.3052	0.0000	100.4389	64.3500
35								
36	2351	0.6257	9.8899	4.2870	0.3036	0.0035	98.7505	67.0100
37	2352	0.6500	10.3185	4.3804	0.1980	0.0156	99.7977	68.2800
38	2371	0.8036	9.9180	4.4657	0.0926	0.0000	100.0481	59.8600
39	2381	0.5949	9.5530	4.3475	0.2891	0.0052	99.5873	67.2300
40	23101	0.5884	8.6438	4.5328	0.2498	0.0104	101.6126	62.3800
41	23131	0.6470	9.8784	4.4475	0.1702	0.0017	100.6965	67.0100
42	23132	0.2400	11.1475	4.3756	0.2504	0.0000	100.6901	36.7000
43	23133	0.1677	11.2951	4.2969	0.3582	0.0017	99.9850	32.8000
44	23134	0.6443	9.9299	4.3824	0.2389	0.0172	100.0290	67.2500
45								
46	2721	0.6805	5.8565	4.5746	0.0672	0.0249	99.2320	77.0900
47	2731	0.4246	9.6991	4.5250	0.0133	0.0035	100.5237	63.1100
48	2732	1.1892	8.2291	4.3442	0.2390	0.0459	99.0851	81.6900
49	27101	0.5273	9.7684	4.3465	0.3611	0.0035	100.2324	42.4400
50	27131	0.2548	10.2657	4.2652	0.5245	0.0229	100.2223	25.4600
51								
52	3221	1.3084	8.9014	4.4184	0.3054	0.0000	100.3700	82.7400
53	3231	1.3767	8.5788	4.3735	0.2784	0.0000	99.3434	87.0600
54	3261	2.3895	6.6382	4.5340	0.1309	0.0123	100.5738	93.4200
55	3262	2.0509	6.8284	4.5698	0.0000	0.0088	100.0543	92.6500
56	3281	1.7373	7.7326	4.3389	0.3765	0.0140	100.2914	84.0900
57	3282	2.3715	6.8420	4.5188	0.0262	0.0334	99.7339	82.2900
58	3291	2.6592	6.3078	4.5372	0.0000	0.0211	99.9882	96.1600
59	32111	4.4094	4.1942	4.4624	0.3272	0.0000	99.7405	82.2100
60	32131	0.9429	9.2188	4.3765	0.2135	0.0000	99.0665	85.7700
61	32141	1.3956	8.8600	4.3774	0.2112	0.0000	99.4019	68.2400
62	32142	3.1454	5.7057	4.5797	0.0394	0.0000	100.1309	92.4400
63	32161	1.5208	8.7836	4.5355	0.0000	0.0000	99.8636	87.6900
64	32181	1.5655	9.0022	4.4005	0.2401	0.0280	99.9863	61.1300
65								
66	3711	0.2397	5.6926	3.9578	0.0000	0.0034	100.7177	97.8300
67	3712	0.2795	9.9170	4.4117	0.3602	0.0053	101.3129	89.6600
68	3721	0.3066	9.9888	4.5577	0.0000	0.0000	100.6298	72.1100
69	3741	0.2417	6.1570	3.8766	0.0649	0.0000	100.0875	98.2000
70	3771	0.2498	10.1654	4.4678	0.1362	0.0176	99.8260	22.0500
71	3791	0.2882	10.1553	4.4576	0.1089	0.0001	99.4819	38.3100
72	37131	0.1771	10.0212	4.3694	0.2262	0.0404	100.1046	54.4100

	Q	R	S	T	U	V	W	X
1	slide/ring/micano	Cations =	Si	Ti	Al	Mg	Ca	Mn
2								
3	1031		7.8715	0.0015	4.1275	0.0044	0.0054	0.0000
4	1032		7.8633	0.0000	4.1369	0.0033	0.0024	0.0000
5	1033		7.8020	0.0008	4.2117	0.0066	0.0041	0.0000
6	1051		6.7334	0.0067	4.5938	0.2181	0.0006	0.0210
7	1061		7.8079	0.0000	4.2107	0.0042	0.0013	0.0036
8	1062		7.9138	0.0000	4.0787	0.0053	0.0040	0.0052
9								
10	1211		6.2124	0.0069	5.6112	0.0268	0.0039	0.0000
11	1221		5.9054	0.0020	5.6396	0.0346	0.0043	0.0000
12	1222		6.0717	0.0000	5.8132	0.0308	0.0053	0.0000
13	1232		6.1285	0.0044	5.7893	0.0249	0.0048	0.0048
14	1241		6.0602	0.0000	5.7507	0.0504	0.0084	0.0000
15	1242		6.0871	0.0008	5.8049	0.0223	0.0049	0.0000
16	1271		7.3767	0.0031	4.6636	0.0091	0.0065	0.0000
17	1272		7.5645	0.0002	4.4039	0.0126	0.0093	0.0000
18	12121		7.1669	0.0000	4.8009	0.0268	0.0182	0.0000
19								
20	15151		7.8592	0.0044	4.1099	0.0068	0.0000	0.0000
21	15152		7.8574	0.0010	4.1376	0.0002	0.0074	0.0000
22								
23	1611		7.8750	0.0000	4.0780	0.0005	0.0031	0.0113
24	1651		7.4191	0.0000	4.6154	0.0038	0.0082	0.0071
25	1671		7.4685	0.0018	4.6375	0.0028	0.0000	0.0039
26	1681		7.7837	0.0027	4.1975	0.0034	0.0013	0.0019
27	16101		7.8704	0.0035	4.1102	0.0023	0.0068	0.0000
28								
29	1831		7.5451	0.0000	4.4469	0.0052	0.0007	0.0000
30	1841		7.8237	0.0034	4.1702	0.0008	0.0050	0.0000
31	1882		7.7487	0.0037	4.2327	0.0058	0.0027	0.0000
32	18121		7.8085	0.0000	4.2079	0.0003	0.0032	0.0000
33								
34	2141		6.1732	0.0750	5.3770	0.2041	0.0045	0.0000
35								
36	2351		6.2201	0.0095	5.4198	0.1560	0.0025	0.0064
37	2352		6.2362	0.0059	5.4134	0.1356	0.0025	0.0000
38	2371		6.2070	0.0192	5.4595	0.1654	0.0015	0.0088
39	2381		6.2179	0.0052	5.4678	0.1508	0.0003	0.0040
40	23101		6.7905	0.0044	4.8132	0.1518	0.0029	0.0000
41	23131		6.2208	0.0127	5.4266	0.1563	0.0020	0.0032
42	23132		6.2631	0.0628	5.0918	0.4625	0.0000	0.0000
43	23133		6.2774	0.0607	5.1119	0.4480	0.0005	0.0017
44	23134		6.2818	0.0126	5.3577	0.1446	0.0062	0.0000
45								
46	2721		6.2273	0.0022	5.7944	0.0598	0.0160	0.0000
47	2731		6.5540	0.0098	4.9235	0.2265	0.0000	0.0017
48	2732		6.0884	0.0304	5.6292	0.0836	0.0029	0.0000
49	27101		6.3782	0.0333	5.1107	0.3541	0.0010	0.0017
50	27131		6.5959	0.0253	4.7086	0.5913	0.0000	0.0000
51								
52	3221		6.1548	0.0031	5.7158	0.0341	0.0000	0.0000
53	3231		6.0627	0.0035	5.8068	0.0325	0.0000	0.0000
54	3261		6.1187	0.0067	5.7408	0.0181	0.0090	0.0000
55	3262		6.3203	0.0043	5.4383	0.0264	0.0026	0.0059
56	3281		6.1250	0.0045	5.5722	0.0790	0.0089	0.0000
57	3282		6.0747	0.0111	5.7145	0.0654	0.0074	0.0008
58	3291		6.0312	0.0026	5.7617	0.0159	0.0054	0.0015
59	32111		6.0134	0.0000	5.9591	0.0218	0.0097	0.0040
60	32131		6.0425	0.0058	5.8080	0.0385	0.0107	0.0101
61	32141		6.1742	0.0047	5.4854	0.1512	0.0000	0.0037
62	32142		6.1012	0.0026	5.7748	0.0191	0.0055	0.0113
63	32161		6.0767	0.0043	5.7896	0.0268	0.0000	0.0000
64	32181		6.0427	0.0673	5.6895	0.1097	0.0007	0.0124
65								
66	3711		5.9695	0.0347	3.6601	0.0850	0.0058	0.0000
67	3712		6.6946	0.0132	4.8975	0.0383	0.0049	0.0000
68	3721		6.3370	0.0052	5.3919	0.0962	0.0053	0.0057
69	3741		5.2608	0.0500	4.6114	0.0687	0.0057	0.0000
70	3771		6.4777	0.0201	5.0736	0.3909	0.0037	0.0008
71	3791		6.3159	0.0047	5.3674	0.2498	0.0043	0.0070
72	37131		6.5320	0.0199	4.8317	0.3509	0.0020	0.0000

	Y	Z	AA	AB	AC	AD
1	slide/ring/micano	Fe	Na	K	Total	Si/Al
2						
3	1031	0.0247	0.0391	0.0175	12.0916	1.9071
4	1032	0.0345	0.0473	0.0081	12.0959	1.9008
5	1033	0.0308	0.0506	0.0201	12.1267	1.8525
6	1051	1.2519	0.2264	0.0488	13.1007	1.4658
7	1061	0.0455	0.0189	0.0083	12.1004	1.8543
8	1062	0.0290	0.0148	0.0072	12.0578	1.9403
9						#DIV/0!
10	1211	0.2467	0.5546	1.1800	13.8424	1.1071
11	1221	0.7985	0.5571	1.2199	14.1614	1.0471
12	1222	0.2005	0.4994	1.3010	13.9219	1.0445
13	1232	0.1465	0.7328	1.0056	13.8417	1.0586
14	1241	0.3444	0.4912	1.2092	13.9146	1.0538
15	1242	0.1929	0.4464	1.3470	13.9063	1.0486
16	1271	0.0701	0.2035	0.1152	12.4478	1.5818
17	1272	0.0669	0.1700	0.1817	12.4091	1.7177
18	12121	0.0778	0.3065	0.3776	12.7747	1.4928
19						#DIV/0!
20	15151	0.0841	0.0162	0.0181	12.0987	1.9123
21	15152	0.0484	0.0218	0.0196	12.0935	1.8990
22						#DIV/0!
23	1611	0.0870	0.0480	0.0144	12.1172	1.9311
24	1651	0.0485	0.2041	0.1379	12.4441	1.6075
25	1671	0.0398	0.0905	0.0266	12.2675	1.6105
26	1681	0.0426	0.0908	0.0724	12.1964	1.8544
27	16101	0.0544	0.0310	0.0159	12.0945	1.9148
28						#DIV/0!
29	1831	0.0510	0.3129	0.0518	12.4138	1.6967
30	1841	0.0701	0.0211	0.0083	12.1025	1.8761
31	1882	0.0895	0.0565	0.0400	12.1796	1.8307
32	18121	0.0478	0.0308	0.0087	12.1073	1.8557
33						#DIV/0!
34	2141	0.3684	0.1896	1.5325	13.9243	1.1481
35						#DIV/0!
36	2351	0.3106	0.1641	1.7070	13.9961	1.1477
37	2352	0.2919	0.1688	1.7626	14.0169	1.1520
38	2371	0.2380	0.2072	1.6824	13.9888	1.1369
39	2381	0.3054	0.1542	1.6290	13.9346	1.1372
40	23101	0.2517	0.1470	1.4208	13.5823	1.4108
41	23131	0.3143	0.1661	1.6686	13.9705	1.1464
42	23132	0.2682	0.0621	1.8973	14.1079	1.2300
43	23133	0.2169	0.0436	1.9341	14.0948	1.2280
44	23134	0.2968	0.1665	1.6879	13.9540	1.1725
45						#DIV/0!
46	2721	0.2023	0.1715	0.9712	13.4446	1.0747
47	2731	0.3858	0.1089	1.6370	13.8474	1.3312
48	2732	0.3731	0.3094	1.4085	13.9255	1.0816
49	27101	0.2593	0.1357	1.6536	13.9277	1.2480
50	27131	0.2019	0.0655	1.7374	13.9260	1.4008
51						#DIV/0!
52	3221	0.1637	0.3334	1.4921	13.8970	1.0768
53	3231	0.2190	0.3552	1.4565	13.9363	1.0441
54	3261	0.2568	0.6041	1.1041	13.8582	1.0658
55	3262	0.3265	0.5215	1.1425	13.7882	1.1622
56	3281	0.4174	0.4468	1.3083	13.9620	1.0992
57	3282	0.3030	0.6073	1.1529	13.9370	1.0630
58	3291	0.3956	0.6806	1.0622	13.9567	1.0468
59	32111	0.0966	1.1102	0.6948	13.9095	1.0091
60	32131	0.2222	0.2448	1.5749	13.9575	1.0404
61	32141	0.3212	0.3624	1.5137	14.0164	1.1256
62	32142	0.2221	0.7953	0.9492	13.8810	1.0565
63	32161	0.1910	0.3898	1.4814	13.9598	1.0496
64	32181	0.1601	0.4026	1.5230	14.0080	1.0621
65						#DIV/0!
66	3711	3.8256	0.0704	1.1000	14.7510	1.6310
67	3712	0.3322	0.0709	1.6549	13.7064	1.3669
68	3721	0.2431	0.0782	1.6765	13.8392	1.1753
69	3741	3.7482	0.0719	1.2054	15.0221	1.1408
70	3771	0.1098	0.0640	1.7140	13.8545	1.2767
71	3791	0.1481	0.0743	1.7227	13.8942	1.1767
72	37131	0.4187	0.0459	1.7084	13.9095	1.3519

	A	B	C	D	E	F	G	H	I	J	K	L	M	N	O	P	Q
1		111	112	122	131	132	141	142	151	152	162	171	AVERAGE	311	312	313	314
2	SiO2	22.8980	22.9173	22.8278	22.3440	22.7920	21.4887	22.4154	22.7723	23.1263	23.0779	23.3551	22.7286	25.0838	24.2003	25.3361	23.3521
3	Al2O3	24.4598	24.3635	24.9366	24.7079	24.6565	24.9385	24.9952	24.6418	25.1497	24.8976	24.1548	24.7184	26.8779	23.8905	25.203	24.0289
4	Cr2O3	0.0177	0.0491	0.1187	0.0340	0.0000	0.0041	0.0109	0.0068	0.0002	0.0399	0.0665	0.0316	0.018	0	0	0.0123
5	MgO	5.9520	5.2042	6.8297	6.7367	6.8628	6.2856	6.8164	5.8130	6.5147	6.2837	5.4358	6.2486	4.9549	6.6853	6.4395	6.6013
6	MnO	0.2553	0.1747	0.2820	0.2619	0.2448	0.2117	0.2940	0.1514	0.2232	0.2301	0.2834	0.2375	0.144	0.1573	0.1399	0.1321
7	FeO	34.9011	36.3784	34.3129	35.0632	34.9781	35.8678	35.0292	35.3067	34.1470	33.2917	36.1171	35.0357	30.9474	34.4541	31.6962	33.8904
8	H2O	10.9145	10.9066	11.0564	10.9707	11.0442	10.8465	11.0318	10.9202	11.0688	10.9356	10.9692	10.9695	11.2324	11.1016	11.2639	10.9222
9	Total*	99.4560	100.0160	100.4103	100.1646	100.6285	99.6429	100.6327	99.6421	100.2560	98.7821	100.3896	100.0019	99.2772	100.5261	100.1026	98.9449
10	Fe ratio	76.8200	79.7600	73.9700	74.6300	74.2300	76.3100	74.4100	77.3900	74.7500	74.9600	78.9800	76.0191	77.88	74.39	73.5	74.31
11																	
12	* excluding	TiO2 and CaO															
13																	
14	Cations on 36 (O,OH) basis																
15	Si	5.0322	5.0401	4.9524	4.8853	4.9501	4.7521	4.8738	5.0019	5.0115	5.0619	5.1071	4.9699	5.3565	5.2288	5.3953	5.1284
16	Al	6.3353	6.3150	6.3759	6.3668	6.3113	6.4998	6.4052	6.3791	6.4232	6.4363	6.2252	6.3703	6.7646	6.0836	6.3253	6.2193
17	Cr	0.0031	0.0085	0.0204	0.0059	0.0000	0.0007	0.0019	0.0012	0.0000	0.0069	0.0115	0.0055	0.003	0	0	0.0021
18	Mg	1.9497	1.7059	2.2085	2.1954	2.2216	2.0719	2.2091	1.9031	2.1042	2.0544	1.7717	2.0360	1.5771	2.153	2.0439	2.1608
19	Mn	0.0475	0.0325	0.0518	0.0485	0.0450	0.0397	0.0541	0.0282	0.0410	0.0427	0.0525	0.0440	0.026	0.0288	0.0252	0.0246
20	Fe	6.4144	6.6908	6.2254	6.4112	6.3531	6.6334	6.3695	6.4855	6.1883	6.1068	6.6048	6.4076	5.5268	6.2256	5.6447	6.2243
21	Total**	19.7938	19.7981	19.8419	19.9207	19.8917	19.9976	19.9227	19.8048	19.7726	19.7141	19.7746	19.8393	19.2575	19.7275	19.4385	19.7609
22	Al iv	1.4839	1.4800	1.5238	1.5574	1.5250	1.6240	1.5631	1.4991	1.4943	1.4691	1.4465	1.5151	1.3218	1.3856	1.3024	1.4358
23	** excluding	332.5320	331.6934	341.0027	348.1254	341.2469	362.2646	349.3461	335.7483	334.7293	329.3793	324.5813	339.1499	298.1075	311.6629	293.9889	322.3203
24	cations on 14 O,OH																
25	Si	2.5161	2.52005	2.4762	2.44265	2.47505	2.37605	2.4369	2.50095	2.50575	2.53095	2.55355	2.48492727	2.67825	2.6144	2.69765	2.5642
26	Al	3.16765	3.1575	3.18795	3.1834	3.15565	3.2499	3.2026	3.18955	3.2116	3.21815	3.1126	3.18514091	3.3823	3.0418	3.16265	3.10965
27	Cr	0.00155	0.00425	0.0102	0.00295	0	0.00035	0.00095	0.0006	0	0.00345	0.00575	0.00273182	0.0015	0	0	0.00105
28	Mg	0.97485	0.85295	1.10425	1.0977	1.1108	1.03595	1.10455	0.95155	1.0521	1.0272	0.88585	1.01797727	0.78855	1.0765	1.02195	1.0804
29	Mn	0.02375	0.01625	0.0259	0.02425	0.0225	0.01985	0.02705	0.0141	0.0205	0.02135	0.02625	0.02197727	0.013	0.0144	0.0126	0.0123
30	Fe	3.2072	3.3454	3.1127	3.2056	3.17655	3.3167	3.18475	3.24275	3.09415	3.0534	3.3024	3.20378182	2.7634	3.1128	2.82235	3.11215
31																	
32	Al vi	1.6838	1.6776	1.6642	1.6261	1.6307	1.6260	1.6395	1.6905	1.7174	1.7491	1.6662	1.6701	2.0606	1.6562	1.8603	1.6739
33	6-tot vi	0.1105	0.1079	0.0930	0.0464	0.0595	0.0015	0.0442	0.1011	0.1159	0.1490	0.1194	0.0862	0.3745	0.1401	0.2828	0.1213
34	Fe2+/totR2+	0.76256598	0.79376453	0.73363423	0.74074245	0.73704421	0.75853631	0.73783405	0.77054225	0.74258115	0.74437767	0.7835805	0.75494365	0.77515814	0.74049052	0.73176644	0.74013342

	R	S	T	U	V	W	X	Y	Z	AA	AB	AC	AD	AE	AF	AG	AH
1		315	321	322	331	332	341	342	343	351	352	361	362	363	371	372	373
2	SiO2	22.3117	22.8746	23.679	23.5426	24.4298	21.4171	21.1371	22.2534	21.9306	23.6994	22.6122	21.6622	22.1251	21.5434	23.1824	23.9248
3	Al2O3	23.7506	24.9192	23.3299	24.0559	24.4989	23.412	23.8331	24.432	24.6432	23.9563	24.6434	24.2836	24.2837	24.4111	23.671	24.4026
4	Cr2O3	0.0435	0.0505	0	0	0	0	0.0354	0.0231	0.0353	0.0441	0.0123	0.0002	0.0002	0.0749	0.0476	0.0083
5	MgO	5.7563	5.9732	6.8386	6.8237	6.7689	5.6055	5.0854	5.4917	5.9144	5.7873	6.0998	5.8526	5.9291	5.835	6.1954	6.1826
6	MnO	0.1887	0.1467	0.1276	0.1459	0.1617	0.1362	0.1892	0.1172	0.2125	0.1451	0.171	0.0842	0.0751	0.1521	0.1117	0.1481
7	FeO	36.3839	34.9981	33.5072	34.2452	33.1605	35.7136	36.5117	36.2512	36.0464	33.6104	35.4838	35.1849	36.423	35.3232	34.6124	31.7874
8	H2O	10.7799	10.9802	10.8738	11.0157	11.16	10.5009	10.5148	10.8265	10.8545	10.8559	10.9541	10.6632	10.8408	10.6902	10.8467	10.8796
9	Total*	99.2211	99.958	98.362	99.8585	100.2799	96.8033	97.3233	99.4317	99.7063	98.1439	100.0789	97.7313	99.6821	98.0924	98.7211	97.3869
10	Fe ratio	78.09	76.75	73.4	73.88	73.42	78.21	80.2	78.79	77.48	76.6	76.63	77.18	77.55	77.33	75.87	74.35
11																	
12	* excluding																
13																	
14	Cations on 36.																
15	Si	4.9646	4.997	5.2233	5.1264	5.2507	4.8922	4.8218	4.9303	4.8463	5.2365	4.9515	4.8748	4.8954	4.8338	5.1266	5.2747
16	Al	6.2284	6.4157	6.0653	6.1735	6.2059	6.3028	6.4077	6.3796	6.4181	6.2384	6.3598	6.4379	6.3324	6.4554	6.1694	6.3408
17	Cr	0.0076	0.0087	0	0	0	0	0.0064	0.004	0.0062	0.0077	0.0021	0	0	0.0133	0.0083	0.0015
18	Mg	1.9091	1.9449	2.2485	2.2147	2.1685	1.9085	1.7291	1.8135	1.948	1.9059	1.9909	1.9623	1.9554	1.9514	2.0421	2.0317
19	Mn	0.0356	0.0272	0.0238	0.0269	0.0294	0.0264	0.0366	0.022	0.0398	0.0272	0.0317	0.016	0.0141	0.0289	0.0209	0.0277
20	Fe	6.7704	6.3937	6.1813	6.2361	5.9604	6.8223	6.9655	6.7167	6.6615	6.2106	6.498	6.619	6.7396	6.6282	6.4011	5.8609
21	Total**	19.9174	19.7908	19.7431	19.7826	19.6318	19.9564	19.9712	19.8724	19.9325	19.6344	19.8509	19.9082	19.9379	19.9218	19.7786	19.5466
22	Al iv	1.5177	1.5015	1.3884	1.4368	1.3747	1.5539	1.5891	1.5349	1.5769	1.3818	1.5243	1.5626	1.5523	1.5831	1.4367	1.3627
23	** excluding	339.7077	336.2685	312.2467	322.5326	309.3382	347.3930	354.8659	343.3487	352.2653	310.8455	341.0983	349.2400	347.0533	353.5921	322.5114	306.7906
24	cations on 14 O,OH																
25	Si	2.4823	2.4985	2.61165	2.5632	2.62535	2.4461	2.4109	2.46515	2.42315	2.61825	2.47575	2.4374	2.4477	2.4169	2.5633	2.63735
26	Al	3.1142	3.20785	3.03265	3.08675	3.10295	3.1514	3.20385	3.1898	3.20905	3.1192	3.1799	3.21895	3.1662	3.2277	3.0847	3.1704
27	Cr	0.0038	0.00435	0	0	0	0	0.0032	0.002	0.0031	0.00385	0.00105	0	0	0.00665	0.00415	0.00075
28	Mg	0.95455	0.97245	1.12425	1.10735	1.08425	0.95425	0.86455	0.90675	0.974	0.95295	0.99545	0.98115	0.9777	0.9757	1.02105	1.01585
29	Mn	0.0178	0.0136	0.0119	0.01345	0.0147	0.0132	0.0183	0.011	0.0199	0.0136	0.01585	0.008	0.00705	0.01445	0.01045	0.01385
30	Fe	3.3852	3.19685	3.09065	3.11805	2.9802	3.41115	3.48275	3.35835	3.33075	3.1053	3.249	3.3095	3.3698	3.3141	3.20055	2.93045
31																	
32	Al vi	1.5965	1.7064	1.6443	1.6500	1.7283	1.5975	1.6148	1.6550	1.6322	1.7375	1.6557	1.6564	1.6139	1.6446	1.6480	1.8078
33	6-tot vi	0.0459	0.1107	0.1289	0.1112	0.1926	0.0239	0.0196	0.0690	0.0431	0.1907	0.0840	0.0450	0.0315	0.0511	0.1200	0.2321
34	Fe2+/totR2+	0.77685856	0.76426642	0.73120327	0.73558866	0.73059338	0.77905038	0.79777121	0.78537686	0.77017793	0.76262632	0.76262235	0.76989287	0.77385723	0.76995992	0.75626469	0.7399846

	AI	AJ	AK	AL	AM	AN	AO	AP	AQ	AR	AS	AT	AU	AV	AW	AX	AY
1		374	355	AVERAGE	411	412	421	422	423	424	432	441	442	452	461	471	472
2	SiO2	24.8308	23.5575	23.1221	22.4937	22.9543	22.5355	23.2721	22.9785	22.5852	22.6855	23.2931	23.4115	23.5411	22.9826	23.4259	22.792
3	Al2O3	24.5061	23.9828	24.3189	23.1348	23.8239	23.2551	23.2458	24.3354	24.6581	23.6028	24.2182	24.4745	23.4591	24.3612	24.6757	24.0928
4	Cr2O3	0.0236	0.0002	0.0195	0.0963	0	0.0287	0	0.0294	0.0112	0	0	0	0.0791	0.0197	0	0.0959
5	MgO	6.7236	6.4769	6.0919	7.8782	7.4086	5.9837	7.4926	8.7883	9.3208	7.3725	10.2232	10.3154	9.3716	9.9066	9.9288	8.3381
6	MnO	0.1231	0.1268	0.1426	0.2662	0.2276	0.2233	0.2003	0.2146	0.2846	0.2612	0.2643	0.2283	0.1527	0.2589	0.2518	0.2027
7	FeO	32.4862	32.008	34.3057	31.8474	33.1627	35.9409	33.7218	30.2181	30.7144	32.2804	27.6164	28.2444	28.7353	29.0662	28.8069	31.8774
8	H2O	11.1636	10.8606	10.8991	10.6778	10.8876	10.7419	10.896	10.9327	11.0178	10.7342	10.9616	11.0781	10.8622	11.0011	11.1061	10.9265
9	Total*	99.865	97.8557	98.9706	96.4271	98.5342	98.7196	98.842	97.534	98.609	96.9365	96.5767	97.7838	96.2147	97.6484	98.245	98.3254
10	Fe ratio	73.13	74.04	76.0445	69.58	71.66	77.23	71.75	66.02	65.11	71.24	60.48	60.77	63.36	62.42	62.15	68.34
11																	
12	* excluding																
13																	
14	Cations on 36.																
15	Si	5.3352	5.2028	5.0860	5.0529	5.0571	5.0321	5.1231	5.0415	4.9169	5.0693	5.0971	5.0691	5.1985	5.011	5.0594	5.0034
16	Al	6.2057	6.2426	6.3078	6.1249	6.1859	6.1201	6.0311	6.2926	6.3268	6.216	6.2458	6.2455	6.1054	6.2601	6.281	6.2234
17	Cr	0.004	0	0.0034	0.0171	0	0.0051	0	0.0051	0.0019	0	0	0	0.0138	0.0034	0	0.0166
18	Mg	2.1533	2.1321	1.9975	2.6378	2.4328	1.9915	2.4585	2.8739	3.0246	2.4555	3.3344	3.3291	3.0846	3.2195	3.1962	2.7283
19	Mn	0.0224	0.0237	0.0266	0.0507	0.0425	0.0422	0.0373	0.0399	0.0525	0.0494	0.049	0.0419	0.0286	0.0478	0.0461	0.0377
20	Fe	5.8374	6.0583	6.3265	5.9829	6.11	6.7116	6.2082	5.5445	5.592	6.0324	5.0538	5.1144	5.3066	5.3	5.2031	5.8522
21	Total**	19.5599	19.6683	19.7541	19.8728	19.8405	19.9051	19.8614	19.8036	19.9187	19.8227	19.78	19.8067	19.7397	19.8516	19.7953	19.8716
22	Al iv	1.3324	1.3986	1.4570	1.4736	1.4715	1.4840	1.4385	1.4793	1.5416	1.4654	1.4515	1.4655	1.4008	1.4945	1.4703	1.4983
23	** excluding	300.3685	314.4228	326.8168	330.3347	329.8888	332.5426	322.8829	331.5448	344.7711	328.5938	325.6428	328.6150	314.8792	334.7824	329.6447	335.5891
24	cations on 14 O,OH																
25	Si	2.6676	2.6014	2.54302045	2.52645	2.52855	2.51605	2.56155	2.52075	2.45845	2.53465	2.54855	2.53455	2.59925	2.5055	2.5297	2.5017
26	Al	3.10285	3.1213	3.15391364	3.06245	3.09295	3.06005	3.01555	3.1463	3.1634	3.108	3.1229	3.12275	3.0527	3.13005	3.1405	3.1117
27	Cr	0.002	0	0.00170227	0.00855	0	0.00255	0	0.00255	0.00095	0	0	0	0.0069	0.0017	0	0.0083
28	Mg	1.07665	1.06605	0.99874318	1.3189	1.2164	0.99575	1.22925	1.43695	1.5123	1.22775	1.6672	1.66455	1.5423	1.60975	1.5981	1.36415
29	Mn	0.0112	0.01185	0.01329318	0.02535	0.02125	0.0211	0.01865	0.01995	0.02625	0.0247	0.0245	0.02095	0.0143	0.0239	0.02305	0.01885
30	Fe	2.9187	3.02915	3.16323636	2.99145	3.055	3.3558	3.1041	2.77225	2.796	3.0162	2.5269	2.5572	2.6533	2.65	2.60155	2.9261
31																	
32	Al vi	1.7705	1.7227	1.6969	1.5889	1.6215	1.5761	1.5771	1.6671	1.6219	1.6427	1.6715	1.6573	1.6520	1.6356	1.6702	1.6134
33	6-tot vi	0.2230	0.1703	0.1278	0.0754	0.0858	0.0513	0.0709	0.1038	0.0436	0.0887	0.1100	0.1000	0.1381	0.0808	0.1071	0.0775
34	Fe2+/totR2+	0.72848211	0.73754885	0.75761191	0.68995779	0.7116816	0.76745223	0.71325827	0.65550997	0.64504966	0.70659342	0.59899019	0.60272939	0.6302525	0.61863131	0.61608686	0.67905131

	AZ	BA	BB	BC	BD	BE	BF	BG	BH	BI	BJ	BK	BL	BM	BN	BO	BP
1		481	482	491	492	AVERAGE	611	612	621	622	631	641	651	661	671	672	681
2	SiO2	22.7339	22.3969	23.0889	23.0923	22.9566	21.55	21.8636	21.7543	21.5966	21.7643	23.5674	22.4758	22.5675	22.9219	25.5932	21.6604
3	Al2O3	23.5121	23.743	24.1737	23.9792	23.9262	24.5015	23.8359	25.0299	24.4435	23.8246	24.1721	23.4094	24.2941	23.2186	26.0998	24.254
4	Cr2O3	0.0209	0.1499	0	0	0.0312	0.0041	0.0002	0.0041	0.0081	0.0378	0.0302	0.0365	0.0878	0	0	0.0041
5	MgO	8.2364	6.1958	9.847	9.6201	8.6016	4.608	4.7469	5.111	5.0629	5.2502	4.9561	5.2449	4.9647	5.7164	5.0451	5.2802
6	MnO	0.2676	0.2355	0.2362	0.2644	0.2377	0.1454	0.2153	0.1313	0.1512	0.0968	0.1478	0.1122	0.12	0.1635	0.0731	0.1427
7	FeO	31.6054	34.6605	30.0338	30.3176	31.1088	37.6094	38.6246	36.7631	38.1252	36.3623	34.2449	37.4603	34.7013	37.1571	30.2756	37.0991
8	H2O	10.8013	10.7404	11.0441	11.009	10.9070	10.7012	10.7545	10.8145	10.7957	10.6245	10.7555	10.7637	10.691	10.8496	11.1561	10.7273
9	Total*	97.2446	98.1308	98.4326	98.2945	97.7941	99.161	100.118	99.6117	100.2165	97.9739	97.5394	99.5265	97.488	100.0444	98.2429	99.17
10	Fe ratio	68.47	75.96	63.3	64.08	67.1718	82.13	82.11	80.2	80.92	79.58	80.76	80.06	79.74	78.56	77.14	79.83
11																	
12	* excluding																
13																	
14	Cations on 36.																
15	Si	5.0485	5.0019	5.0146	5.0314	5.0487	4.8304	4.8764	4.8251	4.7984	4.9136	5.2559	5.0087	5.0633	5.0676	5.5027	4.8433
16	Al	6.1537	6.2493	6.1878	6.1575	6.2004	6.4727	6.2656	6.5429	6.4008	6.3392	6.3533	6.1482	6.424	6.0499	6.6137	6.3917
17	Cr	0.0037	0.0265	0	0	0.0055	0.0007	0	0.0007	0.0014	0.0068	0.0053	0.0064	0.0156	0	0	0.0007
18	Mg	2.7262	2.0624	3.1877	3.1242	2.8157	1.5395	1.5781	1.6897	1.6767	1.7667	1.5278	1.7438	1.6603	1.8837	1.6168	1.7598
19	Mn	0.0503	0.0446	0.0434	0.0488	0.0443	0.0276	0.0407	0.0247	0.0285	0.0185	0.0279	0.0212	0.0228	0.0306	0.0133	0.027
20	Fe	5.8696	6.4734	5.4551	5.5242	5.7255	7.05	7.2044	6.8191	7.0841	6.8654	6.3868	6.9812	6.511	6.8699	5.4438	6.9374
21	Total**	19.8644	19.8602	19.89	19.8879	19.8454	19.9293	19.9782	19.9031	19.9957	19.9134	19.5619	19.914	19.7079	19.9046	19.1904	19.9605
22	Al iv	1.4758	1.4991	1.4927	1.4843	1.4757	1.5848	1.5618	1.5875	1.6008	1.5432	1.3721	1.4957	1.4684	1.4662	1.2487	1.5784
23	** excluding	330.8017	335.7483	334.4002	332.6169	330.7811	353.9530	349.0701	354.5156	357.3498	345.1214	308.7862	335.0265	329.2307	328.7743	282.5884	352.5837
24	cations on 14 O,OH																
25	Si	2.52425	2.50095	2.5073	2.5157	2.52434706	2.4152	2.4382	2.41255	2.3992	2.4568	2.62795	2.50435	2.53165	2.5338	2.75135	2.42165
26	Al	3.07685	3.12465	3.0939	3.07875	3.10020294	3.23635	3.1328	3.27145	3.2004	3.1696	3.17665	3.0741	3.212	3.02495	3.30685	3.19585
27	Cr	0.00185	0.01325	0	0	0.00274118	0.00035	0	0.00035	0.0007	0.0034	0.00265	0.0032	0.0078	0	0	0.00035
28	Mg	1.3631	1.0312	1.59385	1.5621	1.40785882	0.76975	0.78905	0.84485	0.83835	0.88335	0.7639	0.8719	0.83015	0.94185	0.8084	0.8799
29	Mn	0.02515	0.0223	0.0217	0.0244	0.02213824	0.0138	0.02035	0.01235	0.01425	0.00925	0.01395	0.0106	0.0114	0.0153	0.00665	0.0135
30	Fe	2.9348	3.2367	2.72755	2.7621	2.86276471	3.525	3.6022	3.40955	3.54205	3.4327	3.1934	3.4906	3.2555	3.43495	2.7219	3.4687
31																	
32	Al vi	1.6011	1.6256	1.6012	1.5945	1.6246	1.6516	1.5710	1.6840	1.5996	1.6264	1.8046	1.5785	1.7437	1.5588	2.0582	1.6175
33	6-tot vi	0.0759	0.0842	0.0557	0.0569	0.0827	0.0399	0.0174	0.0492	0.0057	0.0483	0.2242	0.0484	0.1593	0.0492	0.4049	0.0204
34	Fe2+/totR2+	0.67887256	0.75444035	0.62801916	0.63516994	0.6668818	0.81814067	0.81652915	0.79909767	0.80599138	0.79363281	0.80412968	0.79819807	0.79459611	0.78207463	0.76956135	0.79519039

	BQ	BR	BS	BT	BU	BV	BW	BX	BY	BZ	CA	CB	CC	CD	CE	CF	CG
1		682	AVERAGE	811	812	813	814	821	822	831	832	833	AVERAGE	1011	1012	1031	1032
2	SiO2	22.1588	22.4562	21.5547	21.8837	21.5259	21.84	21.2038	22.1819	22.0282	22.3093	22.389	21.8796	21.819	22.1839	21.9304	22.1322
3	Al2O3	23.9303	24.2511	24.1498	23.8196	24.7983	23.7829	24.2681	24.1217	23.7037	23.3692	23.3936	23.9341	24.5624	24.305	23.9474	24.5007
4	Cr2O3	0.0715	0.0237	0.0269	0.0609	0.0002	0.0298	0.0352	0.0217	0	0	0	0.0194	0	0	0.0231	0.0095
5	MgO "	4.94	5.0772	4.5524	5.1286	4.5485	5.0623	4.9547	4.9792	4.4388	4.4365	5.4858	4.8430	6.2223	6.3818	5.2477	4.8889
6	MnO	0.1291	0.1357	0.1854	0.1515	0.2001	0.2284	0.1551	0.1839	0.2094	0.179	0.1981	0.1879	0.117	0.1657	0.1066	0.204
7	FeO	37.7146	36.3448	38.3003	36.8987	36.6648	36.6577	36.1338	36.384	38.6968	37.9248	35.9239	37.0650	36.1052	35.6949	37.0116	36.1182
8	H2O	10.7737	10.7839	10.6197	10.677	10.667	10.6406	10.5517	10.7123	10.7235	10.6606	10.6719	10.6583	10.8489	10.8763	10.7188	10.736
9	Total*	99.7587	99.0709	99.4612	98.6621	98.4194	98.2795	97.3678	98.5904	99.8586	98.9092	98.1001	98.6276	99.6858	99.6982	99.0145	98.6449
10	Fe ratio	81.13	80.1800	82.59	80.21	81.97	80.35	80.43	80.47	83.1	82.82	78.7	81.1822	76.56	75.92	79.87	80.65
11																	
12	* excluding																
13																	
14	Cations on 36.																
15	Si	4.9334	4.9932	4.8357	4.9163	4.8404	4.9232	4.8201	4.9668	4.9273	5.0196	5.0322	4.9202	4.8241	4.8924	4.9076	4.9448
16	Al	6.2792	6.3568	6.3854	6.3068	6.572	6.3186	6.5018	6.3671	6.2488	6.197	6.1969	6.3438	6.4004	6.2173	6.3158	6.4515
17	Cr	0.0126	0.0042	0.0048	0.0108	0	0.0053	0.0063	0.0038	0	0	0	0.0034	0	0	0.0041	0.0017
18	Mg	1.6393	1.6735	1.5223	1.7173	1.5245	1.7009	1.6788	1.6618	1.4799	1.4879	1.8378	1.6235	2.0505	2.0978	1.7503	1.6281
19	Mn	0.0244	0.0256	0.0352	0.0288	0.0381	0.0436	0.0299	0.0349	0.0397	0.0341	0.0377	0.0358	0.0219	0.031	0.0202	0.0386
20	Fe	7.0221	6.7646	7.1858	6.9324	6.8949	6.9107	6.8693	6.8132	7.2387	7.1361	6.7525	6.9704	6.6758	6.5833	6.9265	6.7485
21	Total**	19.9207	19.8233	19.9692	19.9208	19.8735	19.909	19.9192	19.8477	19.9483	19.8819	19.8637	19.9037	19.975	19.9391	19.9308	19.8247
22	Al iv	1.5333	1.5034	1.5822	1.5419	1.5798	1.5384	1.5900	1.5166	1.5364	1.4902	1.4839	1.5399	1.5880	1.5538	1.5462	1.5276
23	** excluding	343.0196	336.6683	353.3904	344.8348	352.8915	344.1023	355.0464	339.4742	343.6671	333.8695	332.5320	344.4231	354.6218	347.3717	345.7583	341.8095
24	cations on 14 O,OH																
25	Si	2.4667	2.49661667	2.41785	2.45815	2.4202	2.4616	2.41005	2.4834	2.46365	2.5098	2.5161	2.46008889	2.41205	2.4462	2.4538	2.4724
26	Al	3.1396	3.17838333	3.1927	3.1534	3.286	3.1593	3.2509	3.18355	3.1244	3.0985	3.09845	3.17191111	3.2002	3.10865	3.1579	3.22575
27	Cr	0.0063	0.00209167	0.0024	0.0054	0	0.00265	0.00315	0.0019	0	0	0	0.00172222	0	0	0.00205	0.00085
28	Mg	0.81965	0.83675833	0.76115	0.85865	0.76225	0.85045	0.8394	0.8309	0.73995	0.74395	0.9189	0.81173333	1.02525	1.0489	0.87515	0.81405
29	Mn	0.0122	0.0128	0.0176	0.0144	0.01905	0.0218	0.01495	0.01745	0.01985	0.01705	0.01885	0.01788889	0.01095	0.0155	0.0101	0.0193
30	Fe	3.51105	3.3823	3.5929	3.4662	3.44745	3.45535	3.43465	3.4066	3.61935	3.56805	3.37625	3.4852	3.3379	3.29165	3.46325	3.37425
31																	
32	Al vi	1.6063	1.6750	1.6106	1.6116	1.7062	1.6209	1.6610	1.6670	1.5881	1.6083	1.6146	1.6320	1.6123	1.5549	1.6117	1.6982
33	6-tot vi	0.0508	0.0931	0.0178	0.0492	0.0651	0.0515	0.0500	0.0781	0.0328	0.0627	0.0715	0.0532	0.0137	0.0891	0.0398	0.0942
34	Fe2+/totR2+	0.80845748	0.79924698	0.8218636	0.79880164	0.81524091	0.79844487	0.80080438	0.80062045	0.82649601	0.82421085	0.78262633	0.80772737	0.76310555	0.75565019	0.79642405	0.80194172

	CH	CI	CJ	CK	CL	CM	CN	CO	CP	CQ	CR	CS	CT	CU	CV	CW	CX
1		1041	1042	1051	1052	1053	1054	1061	1062	1071	1072	AVERAGE	1111	1112	1113	1121	1122
2	SiO2	22.3302	22.2108	22.3536	22.2553	22.8232	22.5718	22.2928	22.4746	21.2719	22.3275	22.2127	21.0944	21.7642	21.7344	20.4195	21.7977
3	Al2O3	24.1016	24.0762	23.7465	24.1754	23.7578	24.4977	24.5358	24.3656	23.6186	23.7746	24.1404	24.1581	23.4872	24.2181	24.9704	24.1505
4	Cr2O3	0.0095	0	0.0558	0	0.0403	0	0.0053	0.004	0.0067	0	0.0110	0	0.004	0.0226	0	0.0309
5	MgO	5.467	5.314	5.7695	5.3786	6.4366	5.5291	5.7418	5.094	4.955	5.1406	5.5405	3.086	3.2566	3.0967	3.0791	3.7711
6	MnO	0.1469	0.1771	0.2332	0.2028	0.2103	0.1203	0.194	0.0727	0.1464	0.1407	0.1598	0.1251	0.1704	0.1182	0.1365	0.1386
7	FeO	36.8549	37.3233	36.3563	37.8584	35.3951	36.1198	36.5338	37.3129	36.912	36.8486	36.6032	40.5582	39.5281	40.3644	38.7317	38.2991
8	H2O	10.8259	10.8213	10.7907	10.8935	10.8903	10.881	10.9011	10.8792	10.5172	10.7396	10.8086	10.5817	10.5517	10.6917	10.4701	10.6327
9	Total*	99.7359	99.9574	99.3133	100.8075	99.6076	99.7297	100.2121	100.2201	97.4851	99.028	99.5100	99.6057	98.8036	100.2632	97.9022	98.8436
10	Fe ratio	79.16	79.84	78.06	79.88	75.63	78.62	78.21	80.46	80.76	80.15	78.8407	88.09	87.25	88	87.63	85.12
11																	
12	* excluding																
13																	
14	Cations on 36.																
15	Si	4.9476	4.9232	4.9689	4.9004	5.0269	4.9758	4.9052	4.9581	4.8514	4.9867	4.9295	4.7816	4.9475	4.876	4.678	4.9174
16	Al	6.2936	6.2896	6.2211	6.2738	6.1672	6.3647	6.3629	6.3351	6.3485	6.2582	6.3071	6.454	6.2926	6.4034	6.7421	6.421
17	Cr	0.0017	0	0.0098	0	0.007	0	0.0009	0.0007	0.0012	0	0.0019	0	0.0007	0.004	0	0.0055
18	Mg	1.8054	1.7557	1.9115	1.7652	2.1131	1.8167	1.8831	1.675	1.6844	1.7113	1.8320	1.0427	1.1034	1.0355	1.0514	1.268
19	Mn	0.0276	0.0333	0.0439	0.0378	0.0392	0.0225	0.0361	0.0136	0.0283	0.0266	0.0300	0.024	0.0328	0.0225	0.0265	0.0265
20	Fe	6.8289	6.9186	6.7585	6.9714	6.5197	6.6589	6.7228	6.8839	7.0402	6.8826	6.7943	7.6886	7.5146	7.5731	7.4206	7.2255
21	Total**	19.9048	19.9262	19.9156	19.956	19.8857	19.8402	19.9129	19.8705	19.9639	19.8751	19.9086	19.9914	19.8987	19.9174	19.9353	19.8694
22	Al iv	1.5262	1.5384	1.5156	1.5498	1.4866	1.5121	1.5474	1.5210	1.5743	1.5067	1.5352	1.6092	1.5263	1.5620	1.6610	1.5413
23	** excluding	341.5123	344.1023	339.2513	346.5225	333.0946	338.5188	346.0130	340.3977	351.7239	337.3618	343.4328	359.1332	341.5229	349.1126	370.1303	344.7180
24	cations on 14 O,OH																
25	Si	2.4738	2.4616	2.48445	2.4502	2.51345	2.4879	2.4526	2.47905	2.4257	2.49335	2.46475357	2.3908	2.47375	2.438	2.339	2.4587
26	Al	3.1468	3.1448	3.11055	3.1369	3.0836	3.18235	3.18145	3.16755	3.17425	3.1291	3.15356071	3.227	3.1463	3.2017	3.37105	3.2105
27	Cr	0.00085	0	0.0049	0	0.0035	0	0.00045	0.00035	0.0006	0	0.00096786	0	0.00035	0.002	0	0.00275
28	Mg	0.9027	0.87785	0.95575	0.8826	1.05655	0.90835	0.94155	0.8375	0.8422	0.85565	0.91600357	0.52135	0.5517	0.51775	0.5257	0.634
29	Mn	0.0138	0.01665	0.02195	0.0189	0.0196	0.01125	0.01805	0.0068	0.01415	0.0133	0.01502143	0.012	0.0164	0.01125	0.01325	0.01325
30	Fe	3.41445	3.4593	3.37925	3.4857	3.25985	3.32945	3.3614	3.44195	3.5201	3.4413	3.39712857	3.8443	3.7573	3.78655	3.7103	3.61275
31																	
32	Al vi	1.6206	1.6064	1.5950	1.5871	1.5971	1.6703	1.6341	1.6466	1.6000	1.6225	1.6183	1.6178	1.6201	1.6397	1.7101	1.6692
33	6-tot vi	0.0484	0.0398	0.0480	0.0257	0.0669	0.0807	0.0450	0.0671	0.0236	0.0673	0.0535	0.0046	0.0545	0.0447	0.0407	0.0708
34	Fe2+/totR2+	0.78838361	0.79454729	0.7755999	0.79451586	0.75181042	0.78357515	0.77792178	0.80302129	0.80432771	0.79839916	0.78489095	0.87816523	0.86865955	0.87742003	0.87316585	0.84806338

	CY	CZ	DA	DB	DC	DD	DE	DF	DG	DH	DI	DJ	DK	DL	DM	DN	DO
1		1131	1141	1151	1152	1162	1171	1172	1173	1174	AVERAGE	1271	1272	1281	12102	12111	12112
2	SiO2	22.083	20.913	22.3145	21.3741	21.8877	20.8691	21.4107	22.3801	21.9433	21.5704	21.6764	21.1766	21.422	21.0558	21.9381	22.0029
3	Al2O3	23.9688	25.0024	23.6054	24.5763	24.0214	24.6419	24.6269	23.73	24.0961	24.2324	24.2045	23.0935	24.4453	24.5189	23.7017	24.3946
4	Cr2O3	0.044	0	0	0	0.0901	0	0.0066	0.045	0	0.0174	0.0285	0	0	0.0121	0	0.0298
5	MgO	3.2563	3.1728	3.135	3.5026	2.6361	2.9226	3.4229	3.0811	3.5884	3.2148	4.1129	4.3588	4.1522	4.2656	5.0191	4.947
6	MnO	0.0865	0.1795	0.1098	0.1196	0.172	0.1174	0.1498	0.0725	0.1299	0.1304	0.5491	0.46	0.6009	0.5104	0.5282	0.4437
7	FeO	40.0004	39.7163	40.6461	39.3627	41.1604	40.4536	40.5448	39.7426	38.086	39.7996	36.2471	36.7384	37.9867	38.6422	37.026	36.3615
8	H2O	10.7092	10.6372	10.7194	10.6666	10.6953	10.5873	10.7543	10.6841	10.6079	10.6421	10.5462	10.3564	10.6741	10.6721	10.6835	10.7407
9	Total*	100.1753	99.663	100.5421	99.6583	100.6659	99.5919	100.9494	99.7827	98.4779	99.6375	97.3868	96.2659	99.3364	99.6772	98.9255	98.9563
10	Fe ratio	87.35	87.59	87.94	86.35	89.79	88.62	86.96	87.88	85.66	87.4450	83.39	82.73	83.91	83.74	80.76	80.68
11																	
12	* excluding																
13																	
14	Cations on 36.																
15	Si	4.9462	4.7158	4.9832	4.8065	4.9088	4.7281	4.7755	5.0244	4.9618	4.8615	4.9301	4.9047	4.8139	4.7325	4.9255	4.9137
16	Al	6.3272	6.6447	6.2253	6.5135	6.3493	6.5798	6.4736	6.2788	6.4215	6.4376	6.4881	6.3038	6.4742	6.4949	6.2717	6.4207
17	Cr	0.0078	0	0	0	0.016	0	0.0012	0.008	0	0.0031	0.0051	0	0	0.0021	0	0.0053
18	Mg	1.0871	1.0664	1.0456	1.174	0.8812	0.9869	1.1379	1.031	1.2094	1.0800	1.3943	1.5047	1.3907	1.429	1.6796	1.6467
19	Mn	0.0164	0.0343	0.0208	0.0228	0.0327	0.0225	0.0283	0.0138	0.0249	0.0249	0.1058	0.0902	0.1144	0.0972	0.1004	0.0839
20	Fe	7.4926	7.4897	7.6063	7.4025	7.7198	7.6647	7.5627	7.4617	7.2021	7.5018	6.8944	7.116	7.1388	7.2633	6.9521	6.7909
21	Total**	19.8818	19.9602	19.8941	19.93	19.9081	19.982	19.9872	19.8269	19.825	19.9148	19.8233	19.9373	19.9425	20.019	19.9345	19.8673
22	Al iv	1.5269	1.6421	1.5034	1.5968	1.5456	1.6360	1.6123	1.4878	1.5191	1.5693	1.5350	1.5477	1.5931	1.6338	1.5373	1.5432
23	** excluding	341.6609	366.1178	336.6718	356.4900	345.6309	364.8122	359.7807	333.3599	340.0049	350.6533	343.3699	346.0661	355.7045	364.3451	343.8582	345.1107
24	cations on 14 O,OH																
25	Si	2.4731	2.3579	2.4966	2.40325	2.4544	2.36405	2.38775	2.5122	2.4809	2.43074286	2.46505	2.45235	2.40695	2.36625	2.46275	2.45685
26	Al	3.1636	3.32235	3.11265	3.25675	3.17465	3.2899	3.2368	3.1394	3.21075	3.21881429	3.24405	3.1519	3.2371	3.24745	3.13585	3.21035
27	Cr	0.0039	0	0	0	0.008	0	0.0006	0.004	0	0.00154286	0.00255	0	0	0.00105	0	0.00265
28	Mg	0.54355	0.5332	0.5228	0.587	0.4406	0.49345	0.56895	0.5155	0.6047	0.54001786	0.69715	0.75235	0.69535	0.7145	0.8398	0.82335
29	Mn	0.0082	0.01715	0.0104	0.0114	0.01635	0.01125	0.01415	0.0069	0.01245	0.01245714	0.0529	0.0451	0.0572	0.0486	0.0502	0.04195
30	Fe	3.7463	3.74485	3.80315	3.70125	3.8599	3.83235	3.78135	3.73085	3.60105	3.750875	3.4472	3.558	3.5694	3.63165	3.47605	3.39545
31																	
32	Al vi	1.6367	1.6803	1.6093	1.6600	1.6291	1.6540	1.6246	1.6516	1.6917	1.6496	1.7091	1.6043	1.6441	1.6137	1.5986	1.6672
33	6-tot vi	0.0652	0.0245	0.0544	0.0404	0.0541	0.0090	0.0110	0.0951	0.0901	0.0471	0.0937	0.0403	0.0340	-0.0085	0.0353	0.0721
34	Fe2+/totR2+	0.87162783	0.8718686	0.87703945	0.86082588	0.89414735	0.88363058	0.86639783	0.87717628	0.85369352	0.87161746	0.82129966	0.81690755	0.82587721	0.826361	0.79615442	0.79691369

	DP	DQ	DR	DS	DT	DU	DV	DW	DX	DY	DZ	EA	EB	EC	ED	EE	EF
1		12141	AVERAGE	1511	1521	1522	1541	1542	1551	1552	1553	1571	1572	1581	1582	1591	15101
2	SiO2	21.8327	21.5864	20.8465	20.8965	18.6888	18.1604	17.8949	19.635	20.6093	21.1587	20.252	20.7345	20.4129	18.8376	19.0895	18.1154
3	Al2O3	24.1175	24.0680	24.5644	24.013	27.193	28.3631	28.73	26.6168	24.1349	28.8711	24.6218	24.318	24.8917	27.1935	26.9101	28.5414
4	Cr2O3	0.0243	0.0135	0	0	0	0.0336	0	0	0	0.0192	0	0.0362	0	0	0	0.0255
5	MgO **	4.3346	4.4557	2.8112	3.0739	2.442	2.2076	2.2671	2.1032	3.3143	1.9694	2.8895	3.0166	2.9208	2.4884	2.3443	2.3355
6	MnO	0.5196	0.5160	0.4376	0.4823	0.4776	0.5528	0.5821	0.535	0.489	0.5016	0.5254	0.4725	0.474	0.5533	0.5608	0.584
7	FeO	37.5151	37.2167	39.343	39.0103	39.6136	38.3941	38.6781	38.2559	38.9833	34.1098	39.3988	39.1133	39.8232	39.0263	38.899	38.6058
8	H2O	10.6774	10.6215	10.5057	10.4415	10.5059	10.4829	10.5197	10.4436	10.4422	10.7325	10.4285	10.4615	10.5307	10.501	10.4739	10.5382
9	Total*	99.0473	98.5136	98.5493	97.9361	98.934	98.1946	98.6731	97.595	98.0099	97.3754	98.1173	98.1624	99.087	98.6117	98.2864	98.7729
10	Fe ratio	83.12	82.6186	88.82	87.82	90.21	90.83	90.67	91.19	86.98	90.79	88.58	88.04	88.56	89.93	90.43	90.4
11																	
12	* excluding																
13																	
14	Cations on 36.																
15	Si	4.9046	4.8750	4.7596	4.8004	4.2669	4.1554	4.0803	4.5097	4.7341	4.7288	4.6581	4.7541	4.6496	4.3029	4.3717	4.1233
16	Al	6.3854	6.4055	6.61	6.5013	7.3172	7.6488	7.7206	7.2048	6.5339	7.6047	6.6745	6.5714	6.6822	7.3207	7.2632	7.6564
17	Cr	0.0043	0.0024	0	0	0	0.0061	0	0	0	0.0034	0	0.0066	0	0	0	0.0046
18	Mg	1.4514	1.4995	0.9567	1.0525	0.831	0.7529	0.7705	0.72	1.1347	0.656	0.9906	1.0309	0.9916	0.8472	0.8002	0.7924
19	Mn	0.0989	0.0987	0.0846	0.0938	0.0924	0.1071	0.1124	0.1041	0.0951	0.095	0.1024	0.0918	0.0914	0.1071	0.1088	0.1126
20	Fe	7.0479	7.0291	7.5121	7.4944	7.5637	7.3469	7.3753	7.348	7.4888	6.3753	7.5785	7.4999	7.5858	7.455	7.4499	7.3486
21	Total**	19.8976	19.9174	19.9312	19.9457	20.0745	20.0172	20.0594	19.8879	19.9935	19.4657	20.0044	19.957	20.0086	20.0348	19.9952	20.0432
22	Al iv	1.5477	1.5625	1.6202	1.5998	1.8666	1.9223	1.9599	1.7452	1.6330	1.6356	1.6710	1.6230	1.6752	1.8486	1.8142	1.9384
23	** excluding	346.0767	349.2188	361.4685	357.1375	413.7686	425.6043	433.5762	387.9953	364.1753	364.7379	372.2427	362.0523	373.1450	409.9472	402.6440	429.0117
24	cations on 14 O,OH																
25	Si	2.4523	2.4375	2.3798	2.4002	2.13345	2.0777	2.04015	2.25485	2.36705	2.3644	2.32905	2.37705	2.3248	2.15145	2.18585	2.06165
26	Al	3.1927	3.20277143	3.305	3.25065	3.6586	3.8244	3.8603	3.6024	3.26695	3.80235	3.33725	3.2857	3.3411	3.66035	3.6316	3.8282
27	Cr	0.00215	0.0012	0	0	0	0.00305	0	0	0	0.0017	0	0.0033	0	0	0	0.0023
28	Mg	0.7257	0.74974286	0.47835	0.52625	0.4155	0.37645	0.38525	0.36	0.56735	0.328	0.4953	0.51545	0.4958	0.4236	0.4001	0.3962
29	Mn	0.04945	0.04934286	0.0423	0.0469	0.0462	0.05355	0.0562	0.05205	0.04755	0.0475	0.0512	0.0459	0.0457	0.05355	0.0544	0.0563
30	Fe	3.52395	3.51452857	3.75605	3.7472	3.78185	3.67345	3.68765	3.674	3.7444	3.18765	3.78925	3.74995	3.7929	3.7275	3.72495	3.6743
31																	
32	Al vi	1.6450	1.6403	1.6848	1.6509	1.7921	1.9021	1.9005	1.8573	1.6340	2.1668	1.6663	1.6628	1.6659	1.8118	1.8175	1.8899
33	6-tot vi	0.0559	0.0461	0.0385	0.0288	-0.0356	-0.0056	-0.0296	0.0567	0.0067	0.2701	-0.0021	0.0259	-0.0003	-0.0165	0.0031	-0.0167
34	Fe2+/totR2+	0.81969482	0.81475263	0.87825894	0.86733714	0.89119959	0.89521013	0.89308808	0.89915689	0.85894524	0.89461572	0.87395491	0.86979565	0.87506921	0.8865185	0.89125363	0.89035088

	EG	EH	EI	EJ	EK	EL	EM	EN	EO	EP	EQ	ER	ES	ET	EU	EV	EW
1		15111	15112	15121	15131	AVERAGE	1811	1812	1821	1822	1871	1881	1891	18121	18131	18141	18142
2	SiO2	18.3529	18.1596	18.8303	18.6167	19.4051	17.5576	21.5434	19.5624	21.4536	21.487	20.47	19.3644	18.2812	17.401	22.243	20.7793
3	Al2O3	28.8356	28.3625	29.1859	29.1607	26.9171	29.3627	23.7613	26.9832	23.6201	23.809	24.5226	27.1336	28.3253	28.8221	23.3114	24.4818
4	Cr2O3	0.0429	0.0389	0.0107	0.0536	0.0145	0	0.0108	0.0054	0.035	0	0.0515	0	0.0341	0	0	0.0122
5	MgO **	2.1076	2.1938	2.1073	2.1863	2.4877	2.0759	3.5142	2.3528	2.2141	3.1883	3.1597	2.4998	2.4381	2.3316	3.1749	3.2464
6	MnO	0.5629	0.5311	0.6095	0.5533	0.5269	0.6043	0.5983	0.5732	0.3409	0.4776	0.6274	0.5612	0.5969	0.5685	0.5261	0.4605
7	FeO	37.48	37.9829	38.3761	39.1567	38.5695	37.4645	38.5714	38.2308	40.1717	39.5363	38.9489	38.8597	37.2922	38.0146	36.8172	38.9297
8	H2O	10.5122	10.4505	10.7141	10.7403	10.5236	10.4489	10.5474	10.5244	10.4418	10.5633	10.4666	10.5724	10.4556	10.4198	10.4272	10.5124
9	Total*	97.9043	97.7196	99.8718	100.5021	98.4613	97.5212	98.5571	98.2758	98.2772	99.0825	98.2553	99.0078	97.4599	97.6559	96.5434	98.4757
10	Fe ratio	91.01	90.79	91.21	91.07	89.8517	91.14	86.22	90.25	91.12	87.57	87.55	89.85	89.71	90.28	86.84	87.19
11																	
12	* excluding																
13																	
14	Cations on 36.																
15	Si	4.1877	4.1681	4.2157	4.1577	4.4236	4.0305	4.8993	4.4589	4.9282	4.8791	4.6911	4.3934	4.1939	4.0057	5.1167	4.7412
16	Al	7.7546	7.6742	7.7008	7.6754	7.2286	7.9442	6.3686	7.248	6.3948	6.3718	6.6234	7.2553	7.6585	7.8196	6.32	6.5835
17	Cr	0.0077	0.0071	0.0019	0.0095	0.0026	0	0.0019	0.001	0.0064	0	0.0093	0	0.0062	0	0	0.0022
18	Mg	0.7168	0.7505	0.7032	0.7278	0.8459	0.7103	1.1912	0.7993	0.7581	1.0791	1.0793	0.8453	0.8337	0.8	1.0886	1.1041
19	Mn	0.1088	0.1033	0.1156	0.1047	0.1017	0.1175	0.1152	0.1106	0.0663	0.0919	0.1218	0.1078	0.116	0.1109	0.1025	0.089
20	Fe	7.152	7.2908	7.185	7.3133	7.3535	7.1924	7.3357	7.2868	7.7173	7.5079	7.4647	7.3731	7.1547	7.3183	7.0828	7.4285
21	Total**	19.9294	19.9922	19.9301	19.9941	19.9591	19.9961	19.9137	19.9136	19.8712	19.935	19.991	19.979	19.9707	20.0744	19.72	19.9584
22	Al iv	1.9062	1.9160	1.8922	1.9212	1.7882	1.9848	1.5504	1.7706	1.5359	1.5605	1.6545	1.8033	1.9031	1.9972	1.4417	1.6294
23	** excluding	422.1756	424.2562	419.2034	425.3601	397.1390	438.8624	346.6393	393.3878	343.5716	348.7835	368.7397	400.3406	421.5175	441.4949	323.5623	363.4216
24	cations on 14 O,OH																
25	Si	2.09385	2.08405	2.10785	2.07885	2.21178056	2.01525	2.44965	2.22945	2.4641	2.43955	2.34555	2.1967	2.09685	2.00285	2.55835	2.3706
26	Al	3.8773	3.8371	3.8504	3.8377	3.61429722	3.9721	3.1843	3.624	3.1974	3.1859	3.3117	3.62765	3.82925	3.9098	3.16	3.29175
27	Cr	0.00385	0.00355	0.00095	0.00475	0.00130278	0	0.00095	0.0005	0.0032	0	0.00465	0	0.0031	0	0	0.0011
28	Mg	0.3584	0.37525	0.3516	0.3639	0.42293056	0.35515	0.5956	0.39965	0.37905	0.53955	0.53965	0.42265	0.41685	0.4	0.5443	0.55205
29	Mn	0.0544	0.05165	0.0578	0.05235	0.05086111	0.05875	0.0576	0.0553	0.03315	0.04595	0.0609	0.0539	0.058	0.05545	0.05125	0.0445
30	Fe	3.576	3.6454	3.5925	3.65665	3.67675833	3.5962	3.66785	3.6434	3.85865	3.75395	3.73235	3.68655	3.57735	3.65915	3.5414	3.71425
31																	
32	Al vi	1.9712	1.9212	1.9583	1.9166	1.8261	1.9874	1.6340	1.8535	1.6615	1.6255	1.6573	1.8244	1.9262	1.9127	1.7184	1.6624
33	6-tot vi	0.0400	0.0065	0.0398	0.0106	0.0234	0.0025	0.0450	0.0482	0.0676	0.0351	0.0099	0.0126	0.0216	-0.0273	0.1447	0.0268
34	Fe2+/totR2+	0.89651023	0.89516981	0.89769859	0.89780009	0.88584846	0.89678562	0.84883304	0.88899191	0.90348525	0.86507507	0.86139768	0.88553001	0.88281674	0.8893088	0.85604129	0.86161501

	EX	EY	EZ	FA	FB	FC	FD	FE	FF	FG	FH	FI	FJ	FK	FL	FM	FN
1		AVERAGE	21101	2311	2312	2313	2332	2351	AVERAGE	2751	2761	2771	2781	2791	27161	AVERAGE	25141
2	SiO2	20.0130	26.54	24.5051	25.0331	25.037	24.7366	24.9312	24.8486	22.176	22.0675	22.059	22.0227	22.0921	22.2154	22.1055	24.5001
3	Al2O3	25.8303	24.3129	22.5984	22.7428	22.9301	22.6966	22.9304	22.7797	23.4503	23.269	23.0577	23.4368	23.2829	23.0868	23.2639	22.8354
4	Cr2O3	0.0135	0.8493	0	0.0403	0	0.0002	0	0.0081	0.0126	0.0742	0	0.0002	0	0.0406	0.0213	0.0617
5	MgO	2.7451	21.1547	15.7299	16.8958	15.8033	15.9918	15.7328	16.0307	6.7184	6.622	6.6925	6.4842	6.397	5.5332	6.4079	13.4788
6	MnO	0.5395	0.0483	0.2055	0.1314	0.1996	0.1732	0.2071	0.1834	0.1371	0.117	0.1172	0.1555	0.1373	0.1456	0.1350	0.0388
7	FeO	38.4397	12.4104	23.5272	21.9296	22.8508	23.2188	23.5301	23.0113	33.934	33.8618	33.2508	33.5743	33.8812	34.4263	33.8214	27.2242
8	H2O	10.4891	11.9126	11.3361	11.4795	11.44	11.3957	11.4567	11.4216	10.655	10.6048	10.5167	10.5674	10.5756	10.498	10.5696	11.3374
9	Total*	98.1011	97.2573	97.9577	98.2855	98.3125	98.2312	98.8107	98.3195	97.115	96.7111	95.6962	96.2447	96.4542	96.0069	96.3714	99.4851
10	Fe ratio	88.8836	24.84	45.85	42.29	44.96	45.08	45.85	44.8060	74	74.22	73.76	74.48	74.9	77.81	74.8617	53.1600
11																	
12	* excluding																
13																	
14	Cations on 36.																
15	Si	4.5762	5.3457	5.1851	5.2306	5.2496	5.2067	5.2198	5.2184	4.9923	4.9913	5.0312	4.9988	5.0107	5.0759	5.0167	5.1835
16	Al	6.9625	5.7697	5.6355	5.6007	5.6663	5.6304	5.6581	5.6382	6.2218	6.2101	6.1981	6.2697	6.2238	6.217	6.2234	5.6940
17	Cr	0.0025	0.1352	0	0.0067	0	0	0	0.0013	0.0022	0.0133	0	0	0	0.0073	0.0038	0.0000
18	Mg	0.9354	6.3489	4.9609	5.262	4.9388	5.0171	4.9096	5.0177	2.2543	2.2325	2.2751	2.1937	2.1626	1.8844	2.1671	4.2505
19	Mn	0.1045	0.0082	0.0368	0.0233	0.0355	0.0309	0.0367	0.0326	0.0261	0.0224	0.0226	0.0299	0.0264	0.0282	0.0259	0.0000
20	Fe	7.3511	2.0898	4.1632	3.832	3.9989	4.0871	4.1199	4.0402	6.3886	6.4051	6.3422	6.3732	6.4265	6.5782	6.4190	4.8169
21	Total**	19.9385	19.7019	19.9919	19.9605	19.906	19.9752	19.9477	19.9563	19.8909	19.8867	19.8698	19.8663	19.867	19.8015	19.8637	19.9639
22	Al iv	1.7119	1.3272	1.4075	1.3847	1.3752	1.3967	1.3901	1.3908	1.5039	1.5044	1.4844	1.5006	1.4947	1.4621	1.4917	1.4083
23	** excluding	380.9383	299.2539	316.3016	311.4718	309.4550	314.0088	312.6182	312.7711	336.7674	336.8735	332.6381	336.0774	334.8142	327.8932	334.1773	316.4715
24	cations on 14 O,OH																
25	Si	2.28809091	2.67285	2.59255	2.6153	2.6248	2.60335	2.6099	2.60918	2.49615	2.49565	2.5156	2.4994	2.50535	2.53795	2.50835	2.59175
26	Al	3.48125909	2.88485	2.81775	2.80035	2.83315	2.8152	2.82905	2.8191	3.1109	3.10505	3.09905	3.13485	3.1119	3.1085	3.11170833	2.847
27	Cr	0.00122727	0.0676	0	0.00335	0	0	0	0.00067	0.0011	0.00665	0	0	0	0.00365	0.0019	0
28	Mg	0.46768182	3.17445	2.48045	2.631	2.4694	2.50855	2.4548	2.50884	1.12715	1.11625	1.13755	1.09685	1.0813	0.9422	1.08355	2.12525
29	Mn	0.05225	0.0041	0.0184	0.01165	0.01775	0.01545	0.01835	0.01632	0.01305	0.0112	0.0113	0.01495	0.0132	0.0141	0.01296667	0
30	Fe	3.67555455	1.0449	2.0816	1.916	1.99945	2.04355	2.05995	2.02011	3.1943	3.20255	3.1711	3.1866	3.21325	3.2891	3.20948333	2.40845
31																	
32	Al vi	1.7694	1.5577	1.4103	1.4157	1.4580	1.4186	1.4390	1.4283	1.6071	1.6007	1.6147	1.6343	1.6173	1.6465	1.6201	1.4388
33	6-tot vi	0.0352	0.2189	0.0092	0.0257	0.0554	0.0139	0.0279	0.0265	0.0584	0.0693	0.0654	0.0674	0.0750	0.1082	0.0739	0.0275
34	Fe2+/totR2+	0.87607353	0.24740437	0.45445317	0.42029987	0.44564927	0.44740616	0.45442412	0.44444224	0.73694774	0.73961894	0.73405942	0.74134562	0.74592305	0.77474443	0.74535145	0.53123277

	FO	FP	FQ	FR	FS	FT	FU	FV	FW	FX	FY	FZ	GA	GB	GC	GD	GE
1		25151	25152	AVERAGE	2911	2931	2951	2981	2982	2991	2992	29101	29112	29131	29132	29141	29142
2	SiO2	24.7659	24.2181	24.4947	22.2678	22.0300	21.0362	21.8455	22.6303	21.3178	21.5307	21.7285	22.3403	21.5864	20.7776	21.3040	21.5646
3	Al2O3	22.8160	22.4278	22.6931	23.5610	24.3766	23.5291	23.7760	24.2868	22.1059	22.9672	23.6957	24.0395	24.0410	23.7036	23.2358	22.9568
4	Cr2O3	0.0588	0.0775	0.0660	0.0425	0.0691	0.0637	0.0996	0.2608	0.1606	0.0863	0.0896	0.4018	0.3583	0.2316	0.0477	0.1185
5	MgO	13.1253	12.9588	13.1876	4.9893	4.2930	3.5784	4.1602	3.8403	5.6836	5.7638	4.2238	4.5848	3.5209	4.4417	4.6971	5.5025
6	MnO	0.1449	0.1426	0.1088	0.1083	0.0854	0.0851	0.1503	0.0836	0.1240	0.0932	0.1168	0.0749	0.0776	0.1119	0.1337	0.1604
7	FeO	27.3621	27.1508	27.2457	36.6780	38.9385	39.5334	40.0579	38.1994	36.9390	36.9565	38.5259	38.2725	39.1645	37.6419	38.2279	37.6619
8	H2O	11.3520	11.1669	11.2854	10.6608	10.8198	10.4766	10.7689	10.8159	10.4061	10.5675	10.6289	10.8535	10.6381	10.4463	10.5243	10.5979
9	Total*	99.6311	98.1662	99.0941	98.3132	100.6342	98.3661	100.8844	100.1243	96.8029	97.9786	99.0160	100.6689	99.4014	97.3671	98.1944	98.5788
10	Fe ratio	54.0500	54.1700	53.7933	80.5300	83.6100	86.1300	84.4300	84.8300	78.5400	78.2900	83.7000	82.4300	86.2100	82.6700	82.0900	79.4100
11																	
12	* excluding																
13																	
14	Cations on 36.																
15	Si	5.2330	5.2020	5.2062	5.0102	4.8839	4.8163	4.8658	5.0187	4.9138	4.8871	4.9035	4.9372	4.8672	4.7709	4.8555	4.8808
16	Al	5.6818	5.6777	5.6845	6.2478	6.3691	6.3490	6.2415	6.3479	6.0054	6.1441	6.3023	6.2614	6.3887	6.4146	6.2414	6.1237
17	Cr	0.0000	0.0000	0.0000	0.0000	0.0000	0.0000	0.0000	0.0000	0.0000	0.0000	0.0000	0.0000	0.0000	0.0000	0.0000	0.0000
18	Mg	4.1337	4.1489	4.1777	1.6732	1.4186	1.2212	1.3811	1.2694	1.9527	1.9500	1.4207	1.5103	1.1833	1.5202	1.5956	1.8563
19	Mn	0.0000	0.0000	0.0000	0.0000	0.0000	0.0000	0.0000	0.0000	0.0000	0.0000	0.0000	0.0000	0.0000	0.0000	0.0000	0.0000
20	Fe	4.8350	4.8772	4.8430	6.9014	7.2191	7.5695	7.4617	7.0846	7.1206	7.0152	7.2708	7.0735	7.3850	7.2282	7.2863	7.1286
21	Total**	19.9203	19.9489	19.9444	19.8621	19.9227	19.9967	20.0003	19.7833	20.0574	20.0331	19.9373	19.8861	19.9065	20.0007	20.0190	20.0441
22	Al iv	1.3835	1.3990	1.3969	1.4949	1.5581	1.5919	1.5671	1.4907	1.5431	1.5565	1.5483	1.5314	1.5664	1.6146	1.5723	1.5596
23	** excluding	311.2171	314.5077	314.0654	334.8673	348.2740	355.4498	350.1953	333.9650	345.1001	347.9343	346.1935	342.6162	350.0467	360.2690	351.2887	348.6031
24	cations on 14 O,OH																
25	Si	2.6165	2.601	2.60308333	2.5051	2.44195	2.40815	2.4329	2.50935	2.4569	2.44355	2.45175	2.4686	2.4336	2.38545	2.42775	2.4404
26	Al	2.8409	2.83885	2.84225	3.1239	3.18455	3.1745	3.12075	3.17395	3.0027	3.07205	3.15115	3.1307	3.19435	3.2073	3.1207	3.06185
27	Cr	0	0	0	0	0	0	0	0	0	0	0	0	0	0	0	0
28	Mg	2.06685	2.07445	2.08885	0.8366	0.7093	0.6106	0.69055	0.6347	0.97635	0.975	0.71035	0.75515	0.59165	0.7601	0.7878	0.92815
29	Mn	0	0	0	0	0	0	0	0	0	0	0	0	0	0	0	0
30	Fe	2.4175	2.4386	2.42151667	3.4507	3.60955	3.78475	3.73085	3.5423	3.5603	3.5076	3.6354	3.53675	3.6925	3.6141	3.64315	3.5643
31																	
32	Al vi	1.4574	1.4399	1.4453	1.6290	1.6265	1.5827	1.5537	1.6833	1.4596	1.5156	1.6029	1.5993	1.6280	1.5928	1.5485	1.5023
33	6-tot vi	0.0583	0.0471	0.0443	0.0837	0.0546	0.0220	0.0249	0.1397	0.0038	0.0018	0.0513	0.1088	0.0879	0.0330	0.0106	0.0053
34	Fe2+/totR2+	0.53909708	0.54034411	0.53687801	0.80486553	0.83576647	0.86108046	0.84381644	0.84804884	0.78478613	0.7824923	0.83654145	0.82405228	0.86189793	0.82623108	0.82035375	0.79339781

	GF	GG	GH	GI	GJ	GK	GL	GM
1		AVERAGE		Hendry 1981 chlorite results		1	2	3
2	SiO2	21.6892				25.33	23.43	
3	Al2O3	23.5596				22.3	22.57	
4	Cr2O3	0.1562						
5	MgO	4.5600				13.55	11.06	
6	MnO	0.1081				0	0.16	
7	FeO	38.2152				26.57	31.64	
8	H2O	10.6311						
9	Total*	98.9485				87.75	88.86	
10	Fe ratio	82.5285				66.226321	74.0983607	
11						27.57		
12	* excluding							
13								
14	Cations on 36.							
15	Si	4.8931						
16	Al	6.2644						
17	Cr	0.0000						
18	Mg	1.5348						
19	Mn	0.0000						
20	Fe	7.2111						
21	Total**	19.9576						
22	Al iv	1.5534						
23	** excluding	347.2925						
24	cations on 14 O,OH							
25	Si	2.44657308						
26	Al	3.13218846						
27	Cr	0						
28	Mg	0.76740769						
29	Mn	0						
30	Fe	3.60555769						
31								
32	Al vi	1.5788						
33	6-tot_vi	0.0483						
34	Fe2+/totR2+	0.82451092						

Miscellaneous mineral analyses

	A	B	C	D	E	F	G	H	I	J	K	L	M	N	O	P	Q
1	slide/ring/no.	SO3	P2O5	SiO2	TiO2	Al2O3	Cr2O3	MgO	CaO	MnO	FeO	NiO	Na2O	K2O	Cl	Total	O = Cl
2																	
3	1211	0.0209	0.0118	47.1064	0.003	34.3048	0.0111	0.1453	0.0599	0	2.3634	0	1.8097	6.692		92.5282	
4	12121	0.0425	0.0111	61.8362	0	27.9429	0	0.1335	0.1363	0	0.6236	0.0411	0.8726	1.3578	0.0524	93.0501	-0.0118
5																	
6	1561	0.4676	32.615	0.0108	0	13.4669	0.0178	0	28.5613	0.3042	1.2251	0	0.0762	0.0237		76.7687	
7																	
8	1631	3.9691	9.5226	9.2541	0.1034	24.1451	0	0.5043	0.8264	0.0921	25.2359	0.0091	0.0602	0.178	0.0828	73.9832	-0.0187
9	1641	0.2729	30.5604	0.2025	0	1.3689	0	0	0.0236	0.0004	44.0668	0.0391	0.0142	0.0145	0.0402	76.6036	-0.0091
10	1642	0.2921	31.1534	0.1856	0	1.4184	0	0.0276	0.04	0	44.84	0.0213	0.0106	0.0245	0.0563	78.0698	-0.0127
11	1643	0.1557	29.0213	0.2707	0	1.3563	0.0037	0.0069	0.0102	0	45.2548	0	0.0476	0.028	0.0482	73.2033	-0.0109
12	1644	0.4287	30.3077	0.1052	0.0027	1.5066	0.0128	0.0181	0	0	42.9207	0.0728	0.0319	0.0381	0.008	75.4533	-0.0018
13	1691	0.8586	2.282	0.5417	0.0246	4.0406	0.0371	0	0.0019	0	67.8656	0.055	0.0674	0.0116		75.7861	
14																	
15	2391	0.0183	0.0254	1.6782	0.1296	14.8626	45.2619	0.1821	0.0168	1.3453	22.4013	0	0.2202	0.2186	0.0305	86.3908	-0.0069
16																	
17	1841	0.1908	39.407	0.0406	0	3.7782	0.0369	0	51.108	0.041	0.3795	0	0.053	0		95.035	
18	1871	0	41.971	0	0.0505	0	0.06	0	56.5469	0.0732	0.6518	0	0.019	0.0126	0.0237	99.4086	-0.0053
19	1881	0.038	42.1443	0.0085	0	0.052	0	0	56.8195	0.0707	0.0794	0	0.0292	0		99.2415	
20																	
21	2161	0.0436	26.6315	0.0579	0	24.1313	0	0	1.008	0	3.7031	0	0.0533	0	0.0036	55.6322	-0.0008
22	2191	0.3043	25.1818	1.5513	0	27.8884	0.8272	0.0087	0.8646	0	3.0322	0.1156	0.0677	0.3081	0.0356	60.1855	-0.008

	R	S	T	U	V	W	X	Y	Z	AA	AB	AC	AD	AE	AF	AG
1	slide/ring/no.	Cations	S	P	Si	Ti	Al	Cr	Mg	Ca	Mn	Fe	Ni	Na	K	Total
2																
3	1211		0.0023	0.0015	6.9262	0.0003	5.9447	0.0013	0.0318	0.0094	0	0.2906	0	0.5159	1.2551	14.9792
4	12121		0.0044	0.0013	8.4396	0	4.4947	0	0.0272	0.0199	0	0.0712	0.0045	0.2309	0.2364	13.53
5																
6	1561		0.0669	5.2633	0.0021	0	3.0255	0.0027	0	5.8332	0.0491	0.1953	0	0.0282	0.0058	14.472
7																
8	1631		0.6298	1.7046	1.9567	0.0164	6.0168	0	0.1589	0.1872	0.0165	4.4623	0.0015	0.0247	0.048	15.2235
9	1641		0.0468	5.9088	0.0463	0	0.3685	0	0	0.0058	0.0001	8.4165	0.0072	0.0063	0.0042	14.8103
10	1642		0.0491	5.9077	0.0416	0	0.3744	0	0.0092	0.0096	0	8.3996	0.0038	0.0046	0.007	14.8066
11	1643		0.028	5.886	0.0649	0	0.383	0.0007	0.0025	0.0026	0	8.4657	0	0.0221	0.0085	14.8639
12	1644		0.0742	5.9185	0.0243	0.0005	0.4096	0.0023	0.0062	0	0	8.2796	0.0135	0.0142	0.0112	14.7542
13	1691		0.2149	0.6445	0.1087	0.0062	1.5886	0.0098	0	0.0007	0	18.9329	0.0148	0.0436	0.0049	21.6416
14																
15	2391		0.0032	0.005	0.3868	0.0225	4.0368	8.247	0.0626	0.0042	0.2626	4.3174	0	0.0984	0.0643	17.5105
16																
17	1841		0.0236	5.4916	0.0067	0	0.733	0.0048	0	9.0137	0.0057	0.0522	0	0.0169	0	15.3483
18	1871		0	5.677	0	0.0061	0	0.0076	0	9.6796	0.0099	0.0871	0	0.0059	0.0026	15.4757
19	1881		0.0045	5.6926	0.0014	0	0.0098	0	0	9.7129	0.0096	0.0106	0	0.009	0	15.4503
20																
21	2161		0.0076	5.2295	0.0134	0	6.5967	0	0	0.2505	0	0.7183	0	0.024	0	12.84
22	2191		0.0493	4.6	0.3347	0	7.0921	0.1411	0.0028	0.1999	0	0.5472	0.0201	0.0283	0.0848	13.1002

	A	B	C	D	E	F	G	H	I	J
1	slide/ring/mineo	TiO2	Al2O3	Fe2O3	Total	Cations	Ti	Al	Fe	Total
2	Hematite									
3	441	0.1314	0.5306	95.4625	96.1245					
4	442	0.2768	1.8977	93.9954	96.1839					
5	443	1.0521	0.0289	59.691	60.7721					
6	444	0.4241	5.5319	93.1727	99.1286					
7	451	0.5624	1.9052	93.2236	95.7114					
8	452	0.2639	0.4443	97.0784	97.7866					
9	453	0.9397	1.7507	97.0153	99.7116					
10	454	0.5392	11.4948	84.299	96.333					
11										
12	1011	0.5564	1.2184	98.367	100.1459					
13	1012	0.565	0.3999	98.9922	99.9571					
14	1021	0.5847	0.8391	97.6533	99.0771					
15	1022	0.8983	0.9782	94.7803	96.6762					
16	1031	0.4107	0.1473	99.1444	99.7024					
17	1032	0.4786	0.5312	97.698	98.7165					
18										
19	1171	2.2328	0.1654	97.2847	99.6839					
20	1172	1.3641	0.2189	98.6389	100.2219					
21	1173	2.034	0.0799	98.9058	101.0197					
22	1174	1.0478	0.0811	99.6646	100.7945					
23										
24	1241	0.7941	0.3404	99.0612	100.2171		0.0158	0.0106	1.9681	1.9949
25	1251	0.6317	1.0336	98.1585	99.854		0.0125	0.0322	1.9505	1.9961
26	1261	0.5649	0.3775	98.56	99.5149		0.0113	0.0118	1.9728	1.9964
27	1262	0.7048	0.2714	99.736	100.7613		0.0139	0.0084	1.9722	1.9958
28	12121	0.6362	1.7919	96.0107	98.4388		0.0128	0.0563	1.9267	1.9957
29	12131	0.5248	2.3743	95.1275	98.0378		0.0105	0.0747	1.911	1.9966
30										
31	1511	0	0.5089	98.2825	98.8338		0	0.0161	1.9832	2.0003
32	15151	0	0.5146	96.7465	97.3015		0	0.0165	1.9825	2.0005
33	1552	0	0.2266	99.1636	99.3932		0	0.0071	1.9928	2
34	1553	0	0.2562	98.2279	98.4937		0	0.0081	1.9916	2.0001
35	1561	0.0239	0.6048	95.3705	96.0402		0.0005	0.0197	1.979	2.0002
36	1562	0.0002	0.6229	95.2208	95.8796		0	0.0203	1.979	2.0004
37	1563	0.0161	0.3866	97.0591	97.4617		0.0003	0.0124	1.9872	1.999
38	1564	0	0.3253	96.2466	96.579		0	0.0105	1.9893	2.0001
39	1565	0.0189	0.4198	96.8052	97.2714		0.0004	0.0135	1.9856	2.0001
40	1571	0	0.6588	97.9977	98.6761		0	0.0208	1.9786	2.0003
41	1591	0.2638	0.5574	97.0164	97.8592		0.0054	0.0178	1.9745	1.9985
42	1592	0.0457	0.2868	98.4524	98.7879		0.0009	0.0091	1.9896	1.9997
43										
44	1862	0.1754	0.6705	98.4332	99.279		0.0035	0.0211	1.9743	1.9988
45	1871	0.2624	0.9157	97.8336	99.0328		0.0053	0.0288	1.9639	1.9984
46	1881	0.0121	0.4553	98.294	98.7958		0.0002	0.0144	1.9844	2.0004

Se-Te cations

sample	S	Se	Cu	Ag	Te	Au	Hg	Pb	Bi
181	0.07		0.77	63.52	34.33	0	0.15	1.16	0
182	1.05		1.57	63.3	33.32	0.1	0.16	0.36	0.13
183	0.27		0.96	63.88	34.42	0.1	0.23	0.15	0
161	11.27	42.8			0.2			45.51	
171	9.83	40.96			0.32			48.68	
172	10.28	40.4			0.31			48.82	
174	10.34	40.57			0.31			48.56	
131	5.87	45.06			0.09			48.77	
132	6.9	45.13			0.21			47.53	
133	6.01	45.09			0.2			48.46	

	A	B	C	D	E	F	G	H	I
1	chalcopyrite								
2		S	Fe	Cu	As	Sb	Ni	Pb	total
3	1171	33.274	30.451	36.377					100.21
4	1172	33.824	30.272	35.995					100.116
5	1173	33.788	30.562	36.228					100.618
6	1174	33.685	30.652	36.166					100.529
7	1175	33.7	30.708	36.322					100.777
8	1176	33.772	30.605	36.09					100.608
9	1179	34.096	29.586	36.303					100.146
10	tetrahedrite								
11	1177	25.862	2.975	42.124	7.945	17.37			96.276
12	1178	25.659	2.547	42.052	7.814	18.127			96.2
13	11710	25.77	2.592	41.651	7.454	17.167			95.74
14	11711	25.82	2.702	42.084	8.998	15.795			96.107
15	pyrite								
16	1641	51.36	45.414		0		0.082	0.059	97.036
17	1642	51.207	46.001		0		0.036	0.08	97.359
18	1643	51.308	46.367		0		0.185	0.134	98.004
19	1644	50.696	45.725		0		0.315	0.107	96.905
20	1645	50.757	46.006		0		0.334	0.061	97.21
21	1691	50.4	46.256		0		0.108	0.112	96.902
22	16101	51.293	46.012		0		0.375	0.15	97.848

bornite-cpy cations

sample	S	Fe	Cu	Ag	Se
122	45.71	7.8	45.75	0.11	0.61
123	45.14	8.26	44.92	0.11	1.55
124	45.17	7.46	46.01	0.13	1.21
125	45.44	9.27	44.61	0.13	0.54
126	45.05	4.05	50.1	0.13	0.62
127	45.65	6.44	47.14	0.15	0.59
141	45.19	2.79	51.47	0.08	0.44
142	46.58	23.55	29.24	0.11	0.49
143	46.33	23.5	30.05	0.04	0.04
151	45.16	5.82	48.35	0.21	0.45
152	46.48	16.14	37.2	0.05	0.12
161	43.57	1.52	54.29	0.08	0.52
162	45.88	17.22	36.39	0.06	0.44
163	46.26	13.34	40.08	0.06	0.24
164	44.79	8.46	46.46	0.08	0.19
181	44.89	1.62	53.04	0.13	0.31
182	46.21	17.96	35.67	0.12	0.01

	A	B	C	D	E	F	G	H
1	SAMPLE	Y	LA	SM	YB	HF	LOG(Y/HF)	LOG(LA/YB)
2	1811	0.112	0.009	0.001	0.064	1.055	-0.97403444	-0.85193746
3	1821	0.001	0.003	0.003	0.006	1.36	-3.13353891	-0.30103
4	1831	0.001	0.002	0.001	0.04	1.38	-3.13987909	-1.30103
5	2011	0.0206	0.0031	0.0052	0.0321	1.1404	-1.74318999	-1.01514334
6	2021	0.0353	0.001	0.0057	0.0159	0.1763	-0.69847761	-1.20139712
7	2031	0.001	0.0012	0.0004	0.005	0.094	-1.97312785	-0.61978876
8	2041	0.001	0.001	0.0032	0.0497	1.567	-3.195069	-1.69635639
9	2042	0.001	0.0015	0.0071	0.0242	1.0398	-3.01694981	-1.20772411
10	2111	0.0597	0.0018	0.002	0.0415	1.3741	-1.36204401	-1.36277559
11	2121	0.1027	0.001	0.0068	0.0577	1.4458	-1.14853778	-1.76117581
12	2122	0.3786	0.001	0.0097	0.1326	1.6319	-0.63451293	-2.12254352
13	2311	0.0243	0.001	0.0025	0.0346	1.3786	-1.753832	-1.5390761
14	2321	0.001	0.001	0.0077	0.0214	1.2198	-3.08628863	-1.33041377
15	2331	0.0247	0.0036	0.0029	0.0331	1.1761	-1.6777473	-0.96352549
16	2341	0.0088	0.0027	0.001	0.0307	1.2478	-2.15166231	-1.05577461
17	2351	0.001	0.001	0.0031	0.0202	1.4348	-3.15679137	-1.30535137
18	2361	0.001	0.0029	0.0002	0.0176	1.0656	-3.02759421	-0.78311467
19	2511	0.2733	0.0142	0.0211	0.1081	0.8169	-0.47552926	-0.88153735
20	2531	0.0983	0.0125	0.0077	0.0471	0.7078	-0.85735704	-0.57611089
21	2541	0.1392	0.0004	0.001	0.3081	0.1128	0.09133014	-2.88663171
22	2551	0.1412	0.0043	0.0028	0.0525	1.184	-0.92351701	-1.08669085
23	2561	0.0285	0.0057	0.0046	0.0328	0.7643	-1.428419	-0.75999899
24	2562	0.6304	0.0024	0.1052	0.0987	0.7255	-0.06102121	-1.61410591
25	2711	0.1048	0.0133	0.0147	0.0483	0.7668	-0.86432082	-0.56009549
26	2721	0.0071	0.0069	0.0145	0.0174	0.518	-1.86307141	-0.40170016
27	2731	0.0471	0.0079	0.0116	0.0271	0.4216	-0.9518797	-0.5353422
28	2741	0.1137	0.0123	0.0071	0.0704	1.4017	-1.09089461	-0.75766755
29	2751	0.001	0.0058	0.0026	0.0119	1.3213	-3.12100143	-0.31211897
30	2761	0.001	0.001	0.0075	0.0146	1.1633	-3.06569173	-1.16435286
31	3011	0.014	0.0039	0.001	0.0207	1.3888	-1.99651167	-0.72490574
32	3021	0.1572	0.001	0.009	0.0679	1.1063	-0.84742037	-1.83186977
33	3031	0.1595	0.0007	0.0022	0.0715	1.1059	-0.84095517	-2.009208
34	3211	0.12	0.001	0.001	0.037	1.469	-1.08784055	-1.56820172
35	3221	0.08	0.001	0.006	0.049	1.174	-1.16657811	-1.69019608
36	3231	0.001	0.001	0.001	0.024	1.188	-3.07481644	-1.38021124
37	3241	0.061	0.003	0.007	0.05	1.138	-1.27081243	-1.22184875
38	3251	0.001	0.001	0.001	0.003	1.432	-3.15594302	-0.47712125
39	3261	0.001	0.004	0.001	0.028	1.438	-3.15775889	-0.84509804
40	3711	0.0057	0.0036	0.0069	0.0093	0.2575	-1.65490238	-0.41218045
41	3721	0.0032	0.001	0.001	0.0298	1.3492	-2.62492635	-1.47421626

REE analyses from zircons

APPENDIX IV

XRD Analyses

Jan

report on your Samples

☐ Account

☐ Typing

R. Bottrill, 8359

1/11/91

. R. Berry,
ODES Key Centre,
ni. of Tasm.,

ear Sir,

XRD Analysis: NL 12

Sample NL 12, stated to be from Lyell Tharsis, was eceived for mineralogical identification by XRD. The results are, pproximately:

Quartz: 40-45%
Haematite: 30-35%
Muscovite: 10-15%
Pyrophyllite: 5-10%
Chlorite: 5-10%
Barite: ~1%
?Gorceixite: ~1% $BaPO_4$

ur costs of $70 for this work comes under the CODES/Mines Dept. in- ind agreement.

Yours Sincerely,
R. Bottrill
Mineralogist/Petrologist

Table. 1. XRD mineralogy for Ian Hart, CODES (approx. wt. %).

Sample No.	Quartz	Mica	Goethite
NL69	85	10	5
NL70	45	30	25
NL96*	90	5	nd

Instrument settings: Cu/Ni; 40kV/30 mA; 40 mm/° 2-theta; 0.01°/sec; Time constant = 5.

nd: not detected
* probably includes ~ 5% carbonaceous material (peroxide test).

DEPARTMENT OF
MINES
TASMANIA

Date: 16/12/92

To:	
Name:	**Ian Hart**
Company:	**CODES**
Phone:	
Fax:	**232547**

From:	
Name:	**Ralph Bottrill**
Company:	**Petrology**
Phone:	**(002) 338359**
Fax:	**(002) 442117**

Total number of pages including cover: 1

Message/subject

XRDs:

	Quartz	mica	goethite
NL69	85	10	5
NI70	45	30	25
NL96*	90	5	-

* Treatment with H_2O_2 suggests the presence of ~5% carbonaceous material.

P.O. Box 56, Rosny Park, Tasmania, 7018
Gordons Hill Rd, Rosny Park

TASMANIA
Department of Res. Mines & Energy
DIVISION OF MINES & MINERAL RESOURCES

Enquiries: R.S. Bottrill
Phone: 30 8359
Your ref:
Our file: RSB89.91:AT

28 NOV 1991

Mr I. Hart
CODES Key Centre
University of Tasmania
GPO Box 252C
HOBART TAS 7001

Dear Sir

XRD ANALYSES: NL 19 & NL 36

Two samples, stated to be from the North Lyell area, were received for mineralogical identification by XRD. The results are, approximately:

Reg. No.	Sample No.	% Quartz	%Muscovite	% Kaolinite
G400896	NL 19	50	50	<5
G400897	NL 36	65	30	5

Our costs of $120 for this work comes under the CODES/Mines Dept. in-kind agreement.

Yours faithfully

R. Bottrill
MINERALOGIST/PETROLOGIST

APPENDIX V

Thermodynamic simulations

T (°C)	P (bars)	a(H+)	pH	TotMix	log f(O2)	bornite (m)	% Cu as borni	bornite (g)	chalcopy (m)	u deposited as	chalcopy (g)	muscovit (m)	muscovit (g)	quartz (m)	quartz (g)
300	500	3.34E-05	4.48	0.00E+00	-30.32	1.96E-05	0.00	9.85E-03	2.90E-05	0.00	5.33E-03	1.01E-07	4.02E-05	4.92E-07	2.96E-05
300	500	3.28E-05	4.48	1.00E-02	-30.33		supersaturated	fluid!	2.58E-06	2.48	4.73E-04	9.86E-06	3.93E-03	9.31E-05	5.60E-03
300	500	3.22E-05	4.49	2.00E-02	-30.34				2.54E-06	4.93	4.66E-04	9.86E-06	3.93E-03	9.31E-05	5.60E-03
300	500	3.16E-05	4.5	3.00E-02	-30.34				2.50E-06	7.34	4.59E-04	9.86E-06	3.93E-03	9.31E-05	5.60E-03
300	500	3.10E-05	4.51	4.00E-02	-30.35				2.46E-06	9.71	4.51E-04	9.86E-06	3.93E-03	9.31E-05	5.60E-03
300	500	3.05E-05	4.52	5.00E-02	-30.36				2.42E-06	12.03	4.43E-04	9.86E-06	3.93E-03	9.31E-05	5.60E-03
300	500	2.99E-05	4.52	6.00E-02	-30.36				2.37E-06	14.31	4.35E-04	9.86E-06	3.93E-03	9.31E-05	5.60E-03
300	500	2.93E-05	4.53	7.00E-02	-30.37				2.33E-06	16.55	4.27E-04	9.86E-06	3.93E-03	9.31E-05	5.60E-03
300	500	2.88E-05	4.54	8.00E-02	-30.38				2.28E-06	18.75	4.18E-04	9.86E-06	3.93E-03	9.31E-05	5.60E-03
300	500	2.82E-05	4.55	9.00E-02	-30.38				2.23E-06	20.90	4.09E-04	9.86E-06	3.93E-03	9.31E-05	5.60E-03
300	500	2.77E-05	4.56	1.00E-01	-30.39				2.18E-06	23.00	4.00E-04	9.86E-06	3.93E-03	9.31E-05	5.60E-03
300	500	2.71E-05	4.57	1.10E-01	-30.4				2.13E-06	25.05	3.91E-04	9.86E-06	3.93E-03	9.31E-05	5.60E-03
300	500	2.66E-05	4.58	1.20E-01	-30.4				2.08E-06	27.05	3.81E-04	9.86E-06	3.93E-03	9.31E-05	5.60E-03
300	500	2.60E-05	4.58	1.30E-01	-30.41				2.03E-06	29.00	3.72E-04	9.86E-06	3.93E-03	9.31E-05	5.60E-03
300	500	2.55E-05	4.59	1.40E-01	-30.42				1.97E-06	30.90	3.62E-04	9.86E-06	3.93E-03	9.31E-05	5.60E-03
300	500	2.50E-05	4.6	1.50E-01	-30.42				1.92E-06	32.74	3.52E-04	9.86E-06	3.93E-03	9.31E-05	5.60E-03
300	500	2.45E-05	4.61	1.60E-01	-30.43				1.86E-06	34.54	3.41E-04	9.86E-06	3.93E-03	9.31E-05	5.60E-03
300	500	2.40E-05	4.62	1.70E-01	-30.44				1.80E-06	36.27	3.31E-04	9.86E-06	3.93E-03	9.31E-05	5.60E-03
300	500	2.35E-05	4.63	1.80E-01	-30.45				1.75E-06	37.95	3.20E-04	9.86E-06	3.93E-03	9.31E-05	5.60E-03
300	500	2.30E-05	4.64	1.90E-01	-30.45				1.69E-06	39.58	3.10E-04	9.86E-06	3.93E-03	9.31E-05	5.60E-03
300	500	2.25E-05	4.65	2.00E-01	-30.46				1.63E-06	41.15	2.99E-04	9.86E-06	3.93E-03	9.31E-05	5.60E-03
300	500	2.21E-05	4.66	2.10E-01	-30.47				1.24E-06	42.35	2.28E-04	9.86E-06	3.93E-03	9.31E-05	5.60E-03
300	500	2.18E-05	4.66	2.20E-01	-30.47				1.05E-06	43.36	1.93E-04	9.86E-06	3.93E-03	9.31E-05	5.60E-03
300	500	2.15E-05	4.67	2.30E-01	-30.48				1.03E-06	44.35	1.89E-04	9.86E-06	3.93E-03	9.31E-05	5.60E-03
300	500	2.12E-05	4.67	2.40E-01	-30.48				1.01E-06	45.33	1.85E-04	9.86E-06	3.93E-03	9.31E-05	5.60E-03
300	500	2.09E-05	4.68	2.50E-01	-30.49				9.86E-07	46.28	1.81E-04	9.86E-06	3.93E-03	9.31E-05	5.60E-03
300	500	2.06E-05	4.69	2.60E-01	-30.49				9.62E-07	47.20	1.77E-04	9.86E-06	3.93E-03	9.31E-05	5.60E-03
300	500	2.03E-05	4.69	2.70E-01	-30.5				9.39E-07	48.11	1.72E-04	9.86E-06	3.93E-03	9.31E-05	5.60E-03
300	500	2.00E-05	4.7	2.80E-01	-30.5				9.15E-07	48.99	1.68E-04	9.86E-06	3.93E-03	9.31E-05	5.60E-03
300	500	1.97E-05	4.71	2.90E-01	-30.51				8.91E-07	49.84	1.63E-04	9.86E-06	3.93E-03	9.31E-05	5.60E-03
300	500	1.94E-05	4.71	3.00E-01	-30.52				8.67E-07	50.68	1.59E-04	9.86E-06	3.93E-03	9.31E-05	5.60E-03
300	500	1.91E-05	4.72	3.10E-01	-30.52				8.42E-07	51.49	1.55E-04	9.86E-06	3.93E-03	9.31E-05	5.60E-03
300	500	1.88E-05	4.73	3.20E-01	-30.53				8.18E-07	52.28	1.50E-04	9.86E-06	3.93E-03	9.31E-05	5.60E-03
300	500	1.87E-05	4.73	3.30E-01	-30.53				1.70E-07	52.44	3.12E-05	9.87E-06	3.93E-03	8.39E-05	5.04E-03
300	500	1.87E-05	4.73	3.40E-01	-30.53				6.16E-08	52.50	1.13E-05	9.87E-06	3.93E-03	8.23E-05	4.94E-03
300	500	1.87E-05	4.73	3.50E-01	-30.53				6.13E-08	52.56	1.12E-05	9.87E-06	3.93E-03	8.23E-05	4.94E-03
300	500	1.87E-05	4.73	3.60E-01	-30.53				6.10E-08	52.62	1.12E-05	9.87E-06	3.93E-03	8.23E-05	4.94E-03
300	500	1.87E-05	4.73	3.70E-01	-30.53				6.07E-08	52.68	1.11E-05	9.87E-06	3.93E-03	8.23E-05	4.94E-03
300	500	1.87E-05	4.73	3.80E-01	-30.52				6.04E-08	52.74	1.11E-05	9.87E-06	3.93E-03	8.23E-05	4.94E-03
300	500	1.87E-05	4.73	3.90E-01	-30.52				6.00E-08	52.79	1.10E-05	9.87E-06	3.93E-03	8.23E-05	4.94E-03
300	500	1.87E-05	4.73	4.00E-01	-30.52				5.97E-08	52.85	1.10E-05	9.87E-06	3.93E-03	8.23E-05	4.94E-03
300	500	1.87E-05	4.73	4.10E-01	-30.52				5.94E-08	52.91	1.09E-05	9.87E-06	3.93E-03	8.23E-05	4.94E-03
300	500	1.87E-05	4.73	4.20E-01	-30.52				5.91E-08	52.96	1.09E-05	9.87E-06	3.93E-03	8.23E-05	4.94E-03
300	500	1.87E-05	4.73	4.30E-01	-30.52				5.89E-08	53.02	1.08E-05	9.87E-06	3.93E-03	8.23E-05	4.94E-03
300	500	1.87E-05	4.73	4.40E-01	-30.52				5.86E-08	53.08	1.07E-05	9.87E-06	3.93E-03	8.23E-05	4.94E-03
300	500	1.87E-05	4.73	4.50E-01	-30.52				5.83E-08	53.13	1.07E-05	9.87E-06	3.93E-03	8.23E-05	4.94E-03
300	500	1.87E-05	4.73	4.60E-01	-30.52				5.80E-08	53.19	1.06E-05	9.87E-06	3.93E-03	8.23E-05	4.94E-03
300	500	1.88E-05	4.73	4.70E-01	-30.52				5.77E-08	53.25	1.06E-05	9.87E-06	3.93E-03	8.23E-05	4.94E-03
300	500	1.88E-05	4.73	4.80E-01	-30.52				5.74E-08	53.30	1.05E-05	9.87E-06	3.93E-03	8.23E-05	4.94E-03
300	500	1.88E-05	4.73	4.90E-01	-30.52				5.71E-08	53.36	1.05E-05	9.87E-06	3.93E-03	8.23E-05	4.94E-03
								bornite			chalcopyrite		muscovite		quartz

Simulation 1 - equilibration of Fluid 1 with felsic volcanics

T (°C)	P (bars)	a(H+)	pH	TotMix	log f(O2)	bornite (m)	% Cu as borni	bornite (g)	chalcopy (m)	u deposited as	chalcopy (g)	muscovit (m)	muscovit (g)	quartz (m)	quartz (g)	apat-chl (m)	apat-chl (g)	talc (m)
300	500	3.34E-05	4.48	0.00E+00	-30.32	1.96E-05	0.00	9.85E-03	2.90E-05	0.00	5.33E-03	1.01E-07	4.02E-05	4.92E-07	2.96E-05			
300	500	3.02E-05	4.52	1.00E-02	-30.36		supersaturated in fluid!		1.36E-05	13.12	2.50E-03	8.49E-06	3.38E-03	6.72E-05	4.04E-03			
300	500	2.71E-05	4.57	2.00E-02	-30.4				1.23E-05	24.94	2.25E-03	8.48E-06	3.38E-03	6.72E-05	4.04E-03			
300	500	2.42E-05	4.62	3.00E-02	-30.44				1.07E-05	35.26	1.97E-03	8.47E-06	3.37E-03	6.72E-05	4.04E-03			
300	500	2.18E-05	4.66	4.00E-02	-30.47				8.18E-06	43.14	1.50E-03	8.47E-06	3.37E-03	6.72E-05	4.04E-03	1.55E-06	8.05E-04	
300	500	2.01E-05	4.7	5.00E-02	-30.5				5.37E-06	48.31	9.86E-04	8.47E-06	3.37E-03	6.72E-05	4.04E-03	4.64E-06	2.42E-03	
300	500	1.87E-05	4.73	6.00E-02	-30.53				3.95E-06	52.11	7.25E-04	8.47E-06	3.38E-03	5.67E-05	3.40E-03	3.60E-06	1.88E-03	2.47E-06
300	500	1.87E-05	4.73	7.00E-02	-30.53				2.89E-07	52.39	5.30E-05	8.51E-06	3.39E-03	7.33E-06	4.40E-04			1.40E-05
300	500	1.87E-05	4.73	8.00E-02	-30.52				2.82E-07	52.66	5.18E-05	8.51E-06	3.39E-03	7.32E-06	4.40E-04			1.40E-05
300	500	1.87E-05	4.73	9.00E-02	-30.52				2.76E-07	52.93	5.06E-05	8.51E-06	3.39E-03	7.30E-06	4.39E-04			1.40E-05
300	500	1.88E-05	4.73	1.00E-01	-30.52				2.69E-07	53.18	4.94E-05	8.51E-06	3.39E-03	7.29E-06	4.38E-04			1.40E-05
300	500	1.88E-05	4.73	1.10E-01	-30.52				2.54E-07	53.43	4.66E-05	8.51E-06	3.39E-03	7.29E-06	4.38E-04			1.40E-05
300	500	1.88E-05	4.73	1.20E-01	-30.52				2.34E-07	53.65	4.30E-05	8.51E-06	3.39E-03	7.31E-06	4.39E-04			1.40E-05
300	500	1.88E-05	4.73	1.30E-01	-30.52				2.29E-07	53.88	4.21E-05	8.51E-06	3.39E-03	7.30E-06	4.38E-04			1.40E-05
300	500	1.88E-05	4.73	1.40E-01	-30.52				2.25E-07	54.09	4.12E-05	8.51E-06	3.39E-03	7.29E-06	4.38E-04			1.40E-05
300	500	1.88E-05	4.73	1.50E-01	-30.52				2.20E-07	54.30	4.03E-05	8.51E-06	3.39E-03	7.28E-06	4.37E-04			1.40E-05
300	500	1.88E-05	4.73	1.60E-01	-30.52				2.15E-07	54.51	3.95E-05	8.51E-06	3.39E-03	7.27E-06	4.37E-04			1.40E-05
300	500	1.88E-05	4.73	1.70E-01	-30.52				2.11E-07	54.71	3.87E-05	8.51E-06	3.39E-03	7.26E-06	4.36E-04			1.40E-05
300	500	1.88E-05	4.73	1.80E-01	-30.52				2.06E-07	54.91	3.79E-05	8.51E-06	3.39E-03	7.26E-06	4.36E-04			1.40E-05
300	500	1.88E-05	4.73	1.90E-01	-30.53				2.02E-07	55.11	3.71E-05	8.51E-06	3.39E-03	7.25E-06	4.36E-04			1.40E-05
300	500	1.88E-05	4.72	2.00E-01	-30.53				1.98E-07	55.30	3.63E-05	8.51E-06	3.39E-03	7.24E-06	4.35E-04			1.40E-05
300	500	1.89E-05	4.72	2.10E-01	-30.53				1.94E-07	55.48	3.56E-05	8.51E-06	3.39E-03	7.24E-06	4.35E-04			1.40E-05
300	500	1.89E-05	4.72	2.20E-01	-30.53				1.90E-07	55.67	3.49E-05	8.51E-06	3.39E-03	7.23E-06	4.34E-04			1.40E-05
300	500	1.89E-05	4.72	2.30E-01	-30.53				1.86E-07	55.85	3.42E-05	8.51E-06	3.39E-03	7.22E-06	4.34E-04			1.40E-05
300	500	1.89E-05	4.72	2.40E-01	-30.53				1.82E-07	56.02	3.35E-05	8.51E-06	3.39E-03	7.22E-06	4.34E-04			1.40E-05
300	500	1.89E-05	4.72	2.50E-01	-30.53				1.79E-07	56.19	3.28E-05	8.51E-06	3.39E-03	7.21E-06	4.33E-04			1.40E-05
300	500	1.89E-05	4.72	2.60E-01	-30.53				1.75E-07	56.36	3.22E-05	8.51E-06	3.39E-03	7.20E-06	4.33E-04			1.40E-05
300	500	1.89E-05	4.72	2.70E-01	-30.53				1.72E-07	56.53	3.15E-05	8.51E-06	3.39E-03	7.20E-06	4.33E-04			1.40E-05
300	500	1.89E-05	4.72	2.80E-01	-30.53				1.69E-07	56.69	3.09E-05	8.51E-06	3.39E-03	7.19E-06	4.32E-04			1.40E-05
300	500	1.89E-05	4.72	2.90E-01	-30.53				1.65E-07	56.85	3.03E-05	8.51E-06	3.39E-03	7.19E-06	4.32E-04			1.39E-05
300	500	1.89E-05	4.72	3.00E-01	-30.53				1.62E-07	57.01	2.97E-05	8.51E-06	3.39E-03	7.18E-06	4.32E-04			1.39E-05
300	500	1.89E-05	4.72	3.10E-01	-30.53				1.59E-07	57.16	2.92E-05	8.51E-06	3.39E-03	7.18E-06	4.31E-04			1.39E-05
300	500	1.90E-05	4.72	3.20E-01	-30.53				1.56E-07	57.31	2.86E-05	8.51E-06	3.39E-03	7.17E-06	4.31E-04			1.39E-05
300	500	1.90E-05	4.72	3.30E-01	-30.53				1.53E-07	57.46	2.81E-05	8.51E-06	3.39E-03	7.17E-06	4.31E-04			1.39E-05
300	500	1.90E-05	4.72	3.40E-01	-30.54				4.89E-08	57.50	8.98E-06	8.51E-06	3.39E-03	8.30E-06	4.99E-04			1.37E-05
300	500	1.90E-05	4.72	3.50E-01	-30.54					57.50		8.51E-06	3.39E-03	8.86E-06	5.32E-04			1.36E-05
300	500	1.90E-05	4.72	3.60E-01	-30.54					57.50		8.51E-06	3.39E-03	8.87E-06	5.33E-04			1.36E-05
300	500	1.90E-05	4.72	3.70E-01	-30.54					57.50		8.51E-06	3.39E-03	8.87E-06	5.33E-04			1.36E-05
300	500	1.90E-05	4.72	3.80E-01	-30.54					57.50		8.51E-06	3.39E-03	8.88E-06	5.34E-04			1.36E-05
300	500	1.90E-05	4.72	3.90E-01	-30.54					57.50		8.51E-06	3.39E-03	8.89E-06	5.34E-04			1.36E-05
300	500	1.90E-05	4.72	4.00E-01	-30.54					57.50		8.51E-06	3.39E-03	8.89E-06	5.34E-04			1.36E-05
300	500	1.90E-05	4.72	4.10E-01	-30.54					57.50		8.51E-06	3.39E-03	8.90E-06	5.35E-04			1.36E-05
300	500	1.90E-05	4.72	4.20E-01	-30.54					57.50		8.51E-06	3.39E-03	8.91E-06	5.35E-04			1.36E-05
300	500	1.90E-05	4.72	4.30E-01	-30.54					57.50		8.51E-06	3.39E-03	8.91E-06	5.35E-04			1.36E-05
300	500	1.90E-05	4.72	4.40E-01	-30.54					57.50		8.51E-06	3.39E-03	8.92E-06	5.36E-04			1.36E-05
300	500	1.90E-05	4.72	4.50E-01	-30.54					57.50		8.51E-06	3.39E-03	8.93E-06	5.36E-04			1.36E-05
300	500	1.90E-05	4.72	4.60E-01	-30.54					57.50		8.51E-06	3.39E-03	8.93E-06	5.37E-04			1.36E-05
300	500	1.90E-05	4.72	4.70E-01	-30.54					57.50		8.51E-06	3.39E-03	8.94E-06	5.37E-04			1.36E-05
300	500	1.90E-05	4.72	4.80E-01	-30.54					57.50		8.51E-06	3.39E-03	8.94E-06	5.37E-04			1.36E-05
300	500	1.90E-05	4.72	4.90E-01	-30.54					57.50		8.51E-06	3.39E-03	8.95E-06	5.38E-04			1.36E-05

Simulation 2 - equilibration of Fluid 1 with mafic volcanics

talc (g)	minneso* (m)	minneso* (g)	barite (m)	deposited as	barite (g)	pyrite (m)	deposited as	pyrite (g)
				0.00			0.00	
				0.00			0.00	
				0.00			0.00	
				0.00			0.00	
				0.00			0.00	
				0.00			0.00	
9.36E-04	1.70E-07	8.07E-05		0.00			0.00	
5.31E-03	9.71E-07	4.60E-04		0.00			0.00	
5.31E-03	9.76E-07	4.63E-04		0.00			0.00	
5.31E-03	9.81E-07	4.65E-04		0.00			0.00	
5.31E-03	9.85E-07	4.67E-04		0.00			0.00	
5.31E-03	9.90E-07	4.69E-04	9.68E-07	0.03	8.60E-05		0.00	
5.31E-03	9.94E-07	4.71E-04	9.59E-07	0.09	2.24E-04		0.00	
5.31E-03	9.98E-07	4.73E-04	9.60E-07	0.16	2.24E-04		0.00	
5.30E-03	1.00E-06	4.75E-04	9.60E-07	0.23	2.24E-04		0.00	
5.30E-03	1.01E-06	4.77E-04	9.61E-07	0.30	2.24E-04		0.00	
5.30E-03	1.01E-06	4.79E-04	9.61E-07	0.36	2.24E-04		0.00	
5.30E-03	1.02E-06	4.82E-04	9.62E-07	0.43	2.24E-04		0.00	
5.30E-03	1.02E-06	4.84E-04	9.62E-07	0.50	2.25E-04		0.00	
5.30E-03	1.02E-06	4.86E-04	9.62E-07	0.57	2.25E-04		0.00	
5.30E-03	1.03E-06	4.88E-04	9.63E-07	0.63	2.25E-04		0.00	
5.30E-03	1.03E-06	4.89E-04	9.63E-07	0.70	2.25E-04		0.00	
5.30E-03	1.04E-06	4.91E-04	9.64E-07	0.77	2.25E-04		0.00	
5.30E-03	1.04E-06	4.93E-04	9.64E-07	0.84	2.25E-04		0.00	
5.30E-03	1.04E-06	4.95E-04	9.64E-07	0.91	2.25E-04		0.00	
5.29E-03	1.05E-06	4.97E-04	9.65E-07	0.97	2.25E-04		0.00	
5.29E-03	1.05E-06	4.99E-04	9.65E-07	1.04	2.25E-04		0.00	
5.29E-03	1.06E-06	5.01E-04	9.65E-07	1.11	2.25E-04		0.00	
5.29E-03	1.06E-06	5.02E-04	9.66E-07	1.18	2.25E-04		0.00	
5.29E-03	1.06E-06	5.04E-04	9.66E-07	1.25	2.25E-04		0.00	
5.29E-03	1.07E-06	5.06E-04	9.66E-07	1.31	2.26E-04		0.00	
5.29E-03	1.07E-06	5.07E-04	9.67E-07	1.38	2.26E-04		0.00	
5.29E-03	1.07E-06	5.09E-04	9.67E-07	1.45	2.26E-04		0.00	
5.29E-03	1.08E-06	5.11E-04	9.67E-07	1.52	2.26E-04		0.00	
5.19E-03	1.06E-06	5.00E-04	6.81E-07	1.57	1.59E-04	1.26E-06	0.01	1.51E-04
5.14E-03	1.04E-06	4.93E-04	5.42E-07	1.60	1.27E-04	1.88E-06	0.02	2.25E-04
5.14E-03	1.03E-06	4.90E-04	5.40E-07	1.64	1.26E-04	1.88E-06	0.03	2.26E-04
5.14E-03	1.03E-06	4.88E-04	5.39E-07	1.68	1.26E-04	1.89E-06	0.04	2.27E-04
5.15E-03	1.02E-06	4.86E-04	5.37E-07	1.72	1.25E-04	1.90E-06	0.05	2.27E-04
5.15E-03	1.02E-06	4.83E-04	5.36E-07	1.76	1.25E-04	1.90E-06	0.06	2.28E-04
5.15E-03	1.02E-06	4.81E-04	5.34E-07	1.79	1.25E-04	1.91E-06	0.07	2.29E-04
5.15E-03	1.01E-06	4.79E-04	5.32E-07	1.83	1.24E-04	1.92E-06	0.08	2.30E-04
5.15E-03	1.01E-06	4.76E-04	5.31E-07	1.87	1.24E-04	1.92E-06	0.09	2.31E-04
5.15E-03	1.00E-06	4.74E-04	5.29E-07	1.90	1.24E-04	1.93E-06	0.10	2.31E-04
5.15E-03	9.96E-07	4.72E-04	5.28E-07	1.94	1.23E-04	1.93E-06	0.12	2.32E-04
5.15E-03	9.91E-07	4.70E-04	5.26E-07	1.98	1.23E-04	1.94E-06	0.13	2.33E-04
5.15E-03	9.86E-07	4.67E-04	5.25E-07	2.02	1.22E-04	1.95E-06	0.14	2.34E-04
5.16E-03	9.82E-07	4.65E-04	5.23E-07	2.05	1.22E-04	1.95E-06	0.15	2.34E-04
5.16E-03	9.77E-07	4.63E-04	5.21E-07	2.09	1.22E-04	1.96E-06	0.16	2.35E-04
5.16E-03	9.73E-07	4.61E-04	5.20E-07	2.13	1.21E-04	1.97E-06	0.17	2.36E-04

T (°C)	P (bars)	a(H+)	pH	TotMix	log f(O2)	barite (m)	barite (g)	muscovit (m)	muscovit (g)	pyrite (m)	pyrite (g)	quartz (m)	quartz (g)	talc (m)	talc (g)	hematite (m)	hematite (g)
300	500	1.88E-05	4.73	0.00E+00	-30.53	6.69E-08	1.56E-05	4.25E-05	1.69E-02	2.05E-05	2.46E-03	5.55E-05	3.33E-03	7.02E-05	2.66E-02		
300	500	1.86E-05	4.73	5.00E-02	-30.52			6.46E-06	2.57E-03	2.00E-05	2.40E-03	7.37E-04	4.43E-02	3.00E-06	1.14E-03		
300	500	1.87E-05	4.73	1.00E-01	-30.52			6.46E-06	2.57E-03	1.94E-05	2.33E-03	7.36E-04	4.42E-02	3.13E-06	1.19E-03		
300	500	1.87E-05	4.73	1.50E-01	-30.52			6.46E-06	2.57E-03	1.89E-05	2.27E-03	7.36E-04	4.42E-02	3.27E-06	1.24E-03		
300	500	1.87E-05	4.73	2.00E-01	-30.51			6.46E-06	2.57E-03	1.84E-05	2.20E-03	7.35E-04	4.42E-02	3.40E-06	1.29E-03		
300	500	1.87E-05	4.73	2.50E-01	-30.51			6.46E-06	2.57E-03	1.78E-05	2.14E-03	7.35E-04	4.41E-02	3.54E-06	1.34E-03		
300	500	1.87E-05	4.73	3.00E-01	-30.5			6.46E-06	2.57E-03	1.73E-05	2.07E-03	7.34E-04	4.41E-02	3.68E-06	1.39E-03		
300	500	1.86E-05	4.73	3.50E-01	-30.5			6.46E-06	2.57E-03	1.67E-05	2.01E-03	7.34E-04	4.41E-02	3.81E-06	1.45E-03		
300	500	1.86E-05	4.73	4.00E-01	-30.49			6.46E-06	2.57E-03	1.62E-05	1.94E-03	7.33E-04	4.40E-02	3.95E-06	1.50E-03		
300	500	1.86E-05	4.73	4.50E-01	-30.49			6.46E-06	2.57E-03	1.56E-05	1.88E-03	7.33E-04	4.40E-02	4.08E-06	1.55E-03		
300	500	1.86E-05	4.73	5.00E-01	-30.48			6.46E-06	2.57E-03	1.51E-05	1.81E-03	7.32E-04	4.40E-02	4.22E-06	1.60E-03		
300	500	1.86E-05	4.73	5.50E-01	-30.48			6.46E-06	2.57E-03	1.46E-05	1.75E-03	7.31E-04	4.39E-02	4.35E-06	1.65E-03		
300	500	1.85E-05	4.73	6.00E-01	-30.47			6.46E-06	2.57E-03	1.41E-05	1.69E-03	7.31E-04	4.39E-02	4.48E-06	1.70E-03		
300	500	1.85E-05	4.73	6.50E-01	-30.46			6.46E-06	2.57E-03	1.35E-05	1.63E-03	7.30E-04	4.39E-02	4.61E-06	1.75E-03		
300	500	1.85E-05	4.73	7.00E-01	-30.45			6.46E-06	2.57E-03	1.30E-05	1.56E-03	7.30E-04	4.39E-02	4.74E-06	1.80E-03		
300	500	1.84E-05	4.73	7.50E-01	-30.45			6.46E-06	2.57E-03	1.25E-05	1.50E-03	7.29E-04	4.38E-02	4.86E-06	1.84E-03		
300	500	1.84E-05	4.73	8.00E-01	-30.44			6.46E-06	2.57E-03	1.21E-05	1.45E-03	7.29E-04	4.38E-02	4.98E-06	1.89E-03		
300	500	1.84E-05	4.74	8.50E-01	-30.43			6.46E-06	2.57E-03	1.16E-05	1.39E-03	7.28E-04	4.38E-02	5.10E-06	1.94E-03		
300	500	1.84E-05	4.74	9.00E-01	-30.43	2.34E-08	5.46E-06	6.46E-06	2.57E-03	2.70E-06	3.24E-04	7.47E-04	4.49E-02	4.97E-07	1.88E-04	1.18E-05	1.89E-03
300	500	1.84E-05	4.73	9.50E-01	-30.43	2.81E-07	6.56E-05	6.46E-06	2.57E-03	2.49E-08	2.98E-06	7.49E-04	4.50E-02			1.43E-05	2.29E-03
300	500	1.85E-05	4.73	1.00E+00	-30.43	2.82E-07	6.57E-05	6.46E-06	2.57E-03	2.38E-08	2.86E-06	7.49E-04	4.50E-02			1.43E-05	2.29E-03
300	500	1.86E-05	4.73	1.05E+00	-30.43	2.82E-07	6.59E-05	6.46E-06	2.57E-03	2.28E-08	2.73E-06	7.49E-04	4.50E-02			1.43E-05	2.29E-03
300	500	1.86E-05	4.73	1.10E+00	-30.42	2.83E-07	6.60E-05	6.46E-06	2.57E-03	2.17E-08	2.61E-06	7.49E-04	4.50E-02			1.43E-05	2.29E-03
300	500	1.87E-05	4.73	1.15E+00	-30.42	2.83E-07	6.61E-05	6.46E-06	2.57E-03	2.07E-08	2.48E-06	7.49E-04	4.50E-02			1.43E-05	2.29E-03
300	500	1.87E-05	4.73	1.20E+00	-30.42	2.84E-07	6.63E-05	6.46E-06	2.57E-03	1.97E-08	2.36E-06	7.49E-04	4.50E-02			1.43E-05	2.29E-03
300	500	1.88E-05	4.73	1.25E+00	-30.42	2.84E-07	6.64E-05	6.46E-06	2.57E-03	1.86E-08	2.24E-06	7.49E-04	4.50E-02			1.43E-05	2.29E-03
300	500	1.88E-05	4.72	1.30E+00	-30.42	2.85E-07	6.65E-05	6.46E-06	2.57E-03	1.76E-08	2.11E-06	7.49E-04	4.50E-02			1.43E-05	2.29E-03
300	500	1.89E-05	4.72	1.35E+00	-30.42	2.86E-07	6.67E-05	6.46E-06	2.57E-03	1.66E-08	1.99E-06	7.49E-04	4.50E-02			1.43E-05	2.29E-03
300	500	1.90E-05	4.72	1.40E+00	-30.42	2.86E-07	6.68E-05	6.46E-06	2.57E-03	1.56E-08	1.87E-06	7.49E-04	4.50E-02			1.43E-05	2.29E-03
300	500	1.90E-05	4.72	1.45E+00	-30.41	2.87E-07	6.69E-05	6.46E-06	2.57E-03	1.46E-08	1.75E-06	7.49E-04	4.50E-02			1.43E-05	2.29E-03
300	500	1.91E-05	4.72	1.50E+00	-30.41	2.87E-07	6.70E-05	6.46E-06	2.57E-03	1.36E-08	1.63E-06	7.49E-04	4.50E-02			1.43E-05	2.29E-03
300	500	1.91E-05	4.72	1.55E+00	-30.41	2.88E-07	6.72E-05	6.46E-06	2.57E-03	1.26E-08	1.51E-06	7.49E-04	4.50E-02			1.43E-05	2.29E-03
300	500	1.92E-05	4.72	1.60E+00	-30.41	2.88E-07	6.73E-05	6.46E-06	2.57E-03	1.16E-08	1.39E-06	7.49E-04	4.50E-02			1.43E-05	2.29E-03
300	500	1.92E-05	4.72	1.65E+00	-30.41	2.89E-07	6.74E-05	6.46E-06	2.57E-03	1.06E-08	1.27E-06	7.49E-04	4.50E-02			1.43E-05	2.29E-03
300	500	1.93E-05	4.71	1.70E+00	-30.41	2.89E-07	6.76E-05	6.46E-06	2.57E-03	9.63E-09	1.16E-06	7.49E-04	4.50E-02			1.43E-05	2.29E-03
300	500	1.94E-05	4.71	1.75E+00	-30.41	2.90E-07	6.77E-05	6.46E-06	2.57E-03	8.66E-09	1.04E-06	7.49E-04	4.50E-02			1.43E-05	2.28E-03
300	500	1.94E-05	4.71	1.80E+00	-30.4	2.91E-07	6.78E-05	6.46E-06	2.57E-03	7.69E-09	9.23E-07	7.49E-04	4.50E-02			1.43E-05	2.28E-03
300	500	1.95E-05	4.71	1.85E+00	-30.4	2.91E-07	6.79E-05	6.46E-06	2.57E-03	6.73E-09	8.08E-07	7.49E-04	4.50E-02			1.43E-05	2.28E-03
300	500	1.95E-05	4.71	1.90E+00	-30.4	2.92E-07	6.81E-05	6.46E-06	2.57E-03	5.78E-09	6.93E-07	7.49E-04	4.50E-02			1.43E-05	2.28E-03
300	500	1.96E-05	4.71	1.95E+00	-30.4	2.92E-07	6.82E-05	6.46E-06	2.57E-03	4.82E-09	5.79E-07	7.49E-04	4.50E-02			1.43E-05	2.28E-03
300	500	1.96E-05	4.71	2.00E+00	-30.4	2.93E-07	6.83E-05	6.46E-06	2.57E-03	3.88E-09	4.65E-07	7.49E-04	4.50E-02			1.43E-05	2.28E-03
300	500	1.97E-05	4.71	2.05E+00	-30.4	2.93E-07	6.84E-05	6.46E-06	2.57E-03	2.94E-09	3.52E-07	7.49E-04	4.50E-02			1.43E-05	2.28E-03
300	500	1.98E-05	4.7	2.10E+00	-30.4	2.94E-07	6.85E-05	6.46E-06	2.57E-03	2.00E-09	2.40E-07	7.49E-04	4.50E-02			1.43E-05	2.28E-03
300	500	1.98E-05	4.7	2.15E+00	-30.4	2.94E-07	6.87E-05	6.46E-06	2.57E-03	1.07E-09	1.29E-07	7.49E-04	4.50E-02			1.43E-05	2.28E-03
300	500	1.99E-05	4.7	2.20E+00	-30.39	2.95E-07	6.88E-05	6.46E-06	2.57E-03	1.46E-10	1.75E-08	7.49E-04	4.50E-02			1.43E-05	2.28E-03
300	500	1.99E-05	4.7	2.25E+00	-30.39	2.95E-07	6.89E-05	6.46E-06	2.57E-03			7.49E-04	4.50E-02			1.43E-05	2.28E-03
300	500	2.00E-05	4.7	2.30E+00	-30.39	2.96E-07	6.90E-05	6.46E-06	2.57E-03			7.49E-04	4.50E-02			1.43E-05	2.28E-03
300	500	2.00E-05	4.7	2.35E+00	-30.39	2.96E-07	6.91E-05	6.46E-06	2.57E-03			7.49E-04	4.50E-02			1.43E-05	2.28E-03
300	500	2.01E-05	4.7	2.40E+00	-30.39	2.96E-07	6.91E-05	6.46E-06	2.57E-03			7.49E-04	4.50E-02			1.43E-05	2.28E-03
300	500	2.01E-05	4.7	2.45E+00	-30.39	2.97E-07	6.92E-05	6.46E-06	2.57E-03			7.49E-04	4.50E-02			1.43E-05	2.28E-03
300	500	2.02E-05	4.69	2.50E+00	-30.39	2.97E-07	6.93E-05	6.46E-06	2.57E-03			7.49E-04	4.50E-02			1.43E-05	2.28E-03

Simulation 3 - equilibration of Fluid 2 with Owen Conglomerate 1
(85% quartz, 10% hematite and 5% kaolinite)

T (°C)	P (bars)	a(H+)	pH	TotMlx	log f(O2)	bornite (m)	deposited as b	bornite (g)	chalcopy (m)	u deposited as	chalcopy (g)	muscovit (m)	muscovit (g)	quartz (m)	quartz (g)	pyrite (m)	deposited as	pyrite (g)
300	500	3.34E-05	4.48	0.00E+00	-30.32	1.96E-05	0.00	9.85E-03	2.90E-05	0.00	5.33E-03	1.01E-07	4.02E-05	4.92E-07	2.96E-05		0.00	
295	500	3.68E-05	4.43	0.00E+00	-30.69	2.22E-06	10.68	1.11E-03		0.00		1.76E-07	7.02E-05	3.71E-04	2.23E-02		0.00	
290	500	4.05E-05	4.39	0.00E+00	-31.05	1.85E-06	19.61	9.31E-04		0.00		1.53E-07	6.08E-05	3.73E-04	2.24E-02		0.00	
285	500	4.46E-05	4.35	0.00E+00	-31.42	1.58E-06	27.24	7.95E-04		0.00		1.32E-07	5.25E-05	3.72E-04	2.24E-02		0.00	
280	500	4.91E-05	4.31	0.00E+00	-31.8	1.37E-06	33.85	6.89E-04		0.00		1.14E-07	4.54E-05	3.69E-04	2.22E-02		0.00	
275	500	5.39E-05	4.27	0.00E+00	-32.18	1.20E-06	39.62	6.01E-04		0.00		9.88E-08	3.93E-05	3.64E-04	2.19E-02		0.00	
270	500	5.90E-05	4.23	0.00E+00	-32.57	1.05E-06	44.65	5.24E-04		0.00		8.60E-08	3.42E-05	3.57E-04	2.14E-02		0.00	
265	500	6.55E-05	4.18	0.00E+00	-32.96		44.65		5.15E-06	4.96	9.46E-04	7.01E-08	2.79E-05	3.49E-04	2.10E-02		0.00	
260	500	7.23E-05	4.14	0.00E+00	-33.36		44.65		4.84E-06	9.63	8.89E-04	6.00E-08	2.39E-05	3.40E-04	2.04E-02		0.00	
255	500	8.06E-05	4.09	0.00E+00	-33.76		44.65		3.12E-06	12.63	5.73E-04	4.68E-08	1.87E-05	3.29E-04	1.98E-02	6.65E-06	0.04	7.98E-04
250	500	9.25E-05	4.03	0.00E+00	-34.17		44.65		1.54E-07	12.78	2.82E-05	2.47E-08	9.83E-06	3.19E-04	1.92E-02	2.31E-05	0.17	2.77E-03
245	500	1.05E-04	3.98	0.00E+00	-34.59		44.65		2.61E-07	13.03	4.78E-05	1.64E-08	6.55E-06	3.08E-04	1.85E-02	2.25E-05	0.30	2.70E-03
240	500	1.19E-04	3.92	0.00E+00	-35.02		44.65		3.95E-07	13.41	7.25E-05	1.07E-08	4.25E-06	2.97E-04	1.78E-02	2.11E-05	0.42	2.53E-03
235	500	1.33E-04	3.88	0.00E+00	-35.46	2.31E-07	45.76	1.16E-04		13.41		6.81E-09	2.71E-06	2.85E-04	1.71E-02	1.93E-05	0.52	2.31E-03
230	500	1.47E-04	3.83	0.00E+00	-35.91	2.65E-07	47.04	1.33E-04		13.41		5.16E-09	2.05E-06	2.74E-04	1.65E-02	1.69E-05	0.62	2.02E-03
225	500	1.61E-04	3.79	0.00E+00	-36.37	2.61E-07	48.30	1.31E-04		13.41		5.05E-09	2.01E-06	2.63E-04	1.58E-02	1.42E-05	0.70	1.71E-03
220	500	1.75E-04	3.76	0.00E+00	-36.85	2.49E-07	49.50	1.25E-04		13.41		5.77E-09	2.30E-06	2.52E-04	1.51E-02	1.16E-05	0.77	1.39E-03
215	500	1.87E-04	3.73	0.00E+00	-37.33	2.31E-07	50.61	1.16E-04		13.41		6.71E-09	2.67E-06	2.41E-04	1.45E-02	9.11E-06	0.82	1.09E-03
210	500	2.00E-04	3.7	0.00E+00	-37.82	2.08E-07	51.61	1.04E-04		13.41		7.46E-09	2.97E-06	2.31E-04	1.39E-02	6.99E-06	0.86	8.39E-04
205	500	2.12E-04	3.67	0.00E+00	-38.33	1.83E-07	52.50	9.20E-05		13.41		7.77E-09	3.10E-06	2.21E-04	1.33E-02	5.28E-06	0.89	6.33E-04
200	500	2.24E-04	3.65	0.00E+00	-38.84	1.58E-07	53.26	7.95E-05		13.41		7.57E-09	3.01E-06	2.11E-04	1.27E-02	3.96E-06	0.91	4.75E-04
195	500	2.35E-04	3.63	0.00E+00	-39.36	1.35E-07	53.91	6.76E-05		13.41		6.87E-09	2.74E-06	2.02E-04	1.22E-02	2.97E-06	0.93	3.56E-04
190	500	2.47E-04	3.61	0.00E+00	-39.9	1.13E-07	54.45	5.67E-05		13.41		5.72E-09	2.28E-06	1.93E-04	1.16E-02	2.23E-06	0.94	2.68E-04
185	500	2.59E-04	3.59	0.00E+00	-40.44	9.37E-08	54.90	4.70E-05		13.41		4.15E-09	1.65E-06	1.85E-04	1.11E-02	1.70E-06	0.95	2.04E-04
180	500	2.70E-04	3.57	0.00E+00	-41	7.70E-08	55.27	3.87E-05		13.41		2.13E-09	8.49E-07	1.77E-04	1.06E-02	1.30E-06	0.96	1.56E-04
175	500	2.82E-04	3.55	0.00E+00	-41.57	6.27E-08	55.58	3.15E-05		13.41				1.70E-04	1.02E-02	1.01E-06	0.96	1.21E-04
170	500	2.94E-04	3.53	0.00E+00	-42.15	5.06E-08	55.82	2.54E-05		13.41				1.62E-04	9.76E-03	7.83E-07	0.97	9.40E-05
165	500	3.07E-04	3.51	0.00E+00	-42.74		55.82			13.41				1.56E-04	9.35E-03	6.52E-07	0.97	7.83E-05
160	500	3.19E-04	3.5	0.00E+00	-43.35		55.82			13.41				1.49E-04	8.96E-03	5.12E-07	0.97	6.14E-05
155	500	3.32E-04	3.48	0.00E+00	-43.97		55.82			13.41				1.43E-04	8.59E-03	3.98E-07	0.97	4.77E-05
150	500	3.45E-04	3.46	0.00E+00	-44.61		55.82			13.41				1.37E-04	8.23E-03	3.10E-07	0.98	3.72E-05
145	500	3.59E-04	3.45	0.00E+00	-45.26		55.82			13.41				1.31E-04	7.88E-03	2.44E-07	0.98	2.93E-05
140	500	3.72E-04	3.43	0.00E+00	-45.93		55.82			13.41				1.26E-04	7.55E-03	1.91E-07	0.98	2.29E-05
135	500	3.85E-04	3.41	0.00E+00	-46.62		55.82			13.41				1.20E-04	7.23E-03	1.48E-07	0.98	1.77E-05
130	500	3.99E-04	3.4	0.00E+00	-47.32		55.82			13.41				1.15E-04	6.92E-03	1.14E-07	0.98	1.36E-05
125	500	4.12E-04	3.39	0.00E+00	-48.04		55.82			13.41				1.10E-04	6.61E-03	8.66E-08	0.98	1.04E-05
120	500	4.28E-04	3.37	0.00E+00	-48.78		55.82			13.41				1.05E-04	6.32E-03	6.30E-08	0.98	7.56E-06
115	500	4.43E-04	3.35	0.00E+00	-49.53		55.82			13.41				1.00E-04	6.02E-03	4.83E-08	0.98	5.79E-06
110	500	4.57E-04	3.34	0.00E+00	-50.31		55.82			13.41				9.54E-05	5.73E-03	3.66E-08	0.98	4.39E-06
105	500	4.71E-04	3.33	0.00E+00	-51.11		55.82			13.41				9.06E-05	5.44E-03	2.74E-08	0.98	3.28E-06
100	500	4.85E-04	3.31	0.00E+00	-51.93		55.82			13.41				8.59E-05	5.16E-03	2.02E-08	0.98	2.42E-06

Simulation 6 - cooling of Fluid 1 to 100 degrees C

acanthit (m)	deposited as a	acanthit (g)	kaolinit (m)	kaolinit (g)	covellit (m)	deposited as c	covellit (g)	galena (m)	deposited as c	galena (g)	sphaleri (m)	deposited as	sphaleri (g)	barite (m)	deposited as	barite (g)
	0.00					0.00			0.00			0.00				
	0.00					0.00			0.00			0.00				
	0.00					0.00			0.00			0.00				
	0.00					0.00			0.00			0.00				
	0.00					0.00			0.00			0.00				
	0.00					0.00			0.00			0.00				
	0.00					0.00			0.00			0.00				
	0.00					0.00			0.00			0.00				
	0.00					0.00			0.00			0.00				
	0.00					0.00			0.00			0.00				
	0.00					0.00			0.00			0.00				
	0.00					0.00			0.00			0.00				
	0.00					0.00			0.00			0.00				
	0.00					0.00			0.00			0.00				
	0.00					0.00			0.00			0.00				
	0.00					0.00			0.00			0.00				
	0.00					0.00			0.00			0.00				
	0.00					0.00			0.00			0.00				
	0.00					0.00			0.00			0.00				
	0.00					0.00			0.00			0.00				
	0.00					0.00			0.00			0.00				
	0.00					0.00			0.00			0.00				
	0.00					0.00			0.00			0.00				
	0.00					0.00			0.00			0.00				
	0.00					0.00			0.00			0.00				
1.65E-08	3.30	4.10E-06				0.00			0.00			0.00				
1.01E-07	23.45	2.50E-05	2.55E-08	6.58E-06		0.00			0.00			0.00				
7.78E-08	38.98	1.93E-05	2.01E-08	5.19E-06	2.17E-07	0.21	2.07E-05		0.00			0.00				
5.99E-08	50.95	1.49E-05	1.20E-08	3.09E-06	2.22E-07	0.42	2.13E-05		0.00			0.00				
4.61E-08	60.16	1.14E-05	2.42E-10	6.26E-08	1.53E-07	0.57	1.47E-05	6.81E-07	13.35	1.63E-04		0.00				
3.58E-08	67.31	8.87E-06			1.05E-07	0.67	1.01E-05	1.06E-06	34.20	2.54E-04		0.00				
2.81E-08	72.93	6.96E-06			7.16E-08	0.74	6.84E-06	8.22E-07	50.31	1.97E-04		0.00				
2.23E-08	77.37	5.52E-06			4.81E-08	0.79	4.60E-06	6.31E-07	62.68	1.51E-04		0.00				
1.79E-08	80.94	4.42E-06			3.20E-08	0.82	3.06E-06	4.81E-07	72.12	1.15E-04		0.00				
1.45E-08	83.84	3.60E-06			2.10E-08	0.84	2.01E-06	3.65E-07	79.28	8.73E-05		0.00				
1.20E-08	86.24	2.98E-06			1.36E-08	0.85	1.30E-06	2.75E-07	84.68	6.59E-05		0.00				
1.01E-08	88.25	2.50E-06			8.62E-09	0.86	8.24E-07	1.99E-07	88.58	4.76E-05	3.27E-06	20.45	3.19E-04			
8.65E-09	89.98	2.14E-06			5.44E-09	0.86	5.20E-07	1.52E-07	91.56	3.63E-05	2.78E-06	37.87	2.71E-04			
7.49E-09	91.48	1.86E-06			3.34E-09	0.87	3.19E-07	1.15E-07	93.82	2.75E-05	2.21E-06	51.72	2.16E-04			
6.53E-09	92.78	1.62E-06			1.95E-09	0.87	1.86E-07	8.62E-08	95.51	2.06E-05	1.75E-06	62.64	1.70E-04			
5.71E-09	93.92	1.42E-06			1.04E-09	0.87	9.90E-08	6.40E-08	96.76	1.53E-05	1.37E-06	71.18	1.33E-04			

T (°C)	P (bars)	a(H2)	pH	TotMix	log f(O2)	barite (m)	barite (g)	muscovit (m)	muscovit (g)	pyrite (m)	deposited as	pyrite (g)	quartz (m)	% qtz dep	quartz (g)	talc (m)	talc (g)	chalcopy (m)
300	500	1.88E-05	4.73	0.00E+00	-30.53	6.69E-08	1.56E-05	4.25E-05	1.69E-02	2.05E-05	0.00	2.46E-03	5.55E-05	3.81E+00	3.33E-03	7.02E-05	2.66E-02	
295	500	2.00E-05	4.7	0.00E+00	-30.9			2.37E-07	9.45E-05	3.21E-06	1.48	3.85E-04	3.71E-04	7.63E+00	2.23E-02			1.27E-06
290	500	2.17E-05	4.66	0.00E+00	-31.28			2.13E-07	8.47E-05	5.88E-06	4.19	7.06E-04	3.73E-04	1.14E+01	2.24E-02			1.24E-06
285	500	2.39E-05	4.62	0.00E+00	-31.65			1.86E-07	7.40E-05	8.88E-06	8.27	1.07E-03	3.72E-04	1.52E+01	2.24E-02			8.48E-07
280	500	2.67E-05	4.57	0.00E+00	-32.03			1.59E-07	6.32E-05	1.15E-05	13.55	1.38E-03	3.69E-04	1.90E+01	2.22E-02			5.81E-07
275	500	3.01E-05	4.52	0.00E+00	-32.41			1.33E-07	5.31E-05	1.36E-05	19.81	1.63E-03	3.64E-04	2.26E+01	2.19E-02			3.98E-07
270	500	3.41E-05	4.47	0.00E+00	-32.8			1.10E-07	4.39E-05	1.53E-05	26.84	1.83E-03	3.57E-04	2.62E+01	2.14E-02			2.75E-07
265	500	3.89E-05	4.41	0.00E+00	-33.19			9.00E-08	3.58E-05	1.64E-05	34.39	1.97E-03	3.49E-04	2.97E+01	2.10E-02			2.00E-07
260	500	4.43E-05	4.35	0.00E+00	-33.59			7.29E-08	2.90E-05	1.70E-05	42.20	2.04E-03	3.40E-04	3.30E+01	2.04E-02			1.63E-07
255	500	5.05E-05	4.3	0.00E+00	-33.99			5.87E-08	2.34E-05	1.70E-05	50.01	2.04E-03	3.30E-04	3.63E+01	1.98E-02			1.57E-07
250	500	5.74E-05	4.24	0.00E+00	-34.4			4.72E-08	1.88E-05	1.64E-05	57.56	1.97E-03	3.19E-04	3.95E+01	1.92E-02			1.78E-07
245	500	6.49E-05	4.19	0.00E+00	-34.83			3.82E-08	1.52E-05	1.53E-05	64.61	1.84E-03	3.08E-04	4.25E+01	1.85E-02			2.17E-07
240	500	7.28E-05	4.14	0.00E+00	-35.26			3.12E-08	1.24E-05	1.38E-05	70.94	1.65E-03	2.97E-04	4.54E+01	1.78E-02			2.67E-07
235	500	8.10E-05	4.09	0.00E+00	-35.7			2.60E-08	1.04E-05	1.19E-05	76.40	1.42E-03	2.85E-04	4.82E+01	1.71E-02			3.19E-07
230	500	8.93E-05	4.05	0.00E+00	-36.15			2.21E-08	8.82E-06	9.83E-06	80.92	1.18E-03	2.74E-04	5.09E+01	1.65E-02			3.64E-07
225	500	9.78E-05	4.01	0.00E+00	-36.61			1.90E-08	7.56E-06	8.03E-06	84.62	9.64E-04	2.63E-04	5.35E+01	1.58E-02			
220	500	1.06E-04	3.97	0.00E+00	-37.08			1.66E-08	6.60E-06	6.24E-06	87.49	7.49E-04	2.52E-04	5.60E+01	1.51E-02			
215	500	1.15E-04	3.94	0.00E+00	-37.56			1.45E-08	5.76E-06	4.73E-06	89.67	5.68E-04	2.41E-04	5.84E+01	1.45E-02			
210	500	1.23E-04	3.91	0.00E+00	-38.05			1.25E-08	4.98E-06	3.52E-06	91.29	4.23E-04	2.31E-04	6.06E+01	1.39E-02			
205	500	1.32E-04	3.88	0.00E+00	-38.55			1.06E-08	4.23E-06	2.60E-06	92.49	3.12E-04	2.21E-04	6.28E+01	1.33E-02			
200	500	1.41E-04	3.85	0.00E+00	-39.06			8.79E-09	3.50E-06	1.92E-06	93.37	2.31E-04	2.11E-04	6.49E+01	1.27E-02			
195	500	1.50E-04	3.82	0.00E+00	-39.57			7.01E-09	2.79E-06	1.43E-06	94.03	1.72E-04	2.02E-04	6.68E+01	1.22E-02			
190	500	1.59E-04	3.8	0.00E+00	-40.1			5.28E-09	2.10E-06	1.08E-06	94.53	1.30E-04	1.94E-04	6.87E+01	1.16E-02			
185	500	1.69E-04	3.77	0.00E+00	-40.64			3.60E-09	1.43E-06	8.25E-07	94.91	9.90E-05	1.85E-04	7.06E+01	1.11E-02			
180	500	1.78E-04	3.75	0.00E+00	-41.19			1.86E-09	7.41E-07	6.38E-07	95.20	7.66E-05	1.77E-04	7.23E+01	1.06E-02			
175	500	1.88E-04	3.73	0.00E+00	-41.76			1.41E-10	5.63E-08	5.00E-07	95.43	6.00E-05	1.70E-04	7.40E+01	1.02E-02			
170	500	1.99E-04	3.7	0.00E+00	-42.34					3.91E-07	95.61	4.70E-05	1.63E-04	7.56E+01	9.76E-03			
165	500	2.10E-04	3.68	0.00E+00	-42.93					3.10E-07	95.76	3.72E-05	1.56E-04	7.71E+01	9.35E-03			
160	500	2.21E-04	3.66	0.00E+00	-43.53					2.70E-07	95.88	3.24E-05	1.49E-04	7.85E+01	8.96E-03			
155	500	2.32E-04	3.63	0.00E+00	-44.15					2.17E-07	95.98	2.61E-05	1.43E-04	7.99E+01	8.59E-03			
150	500	2.44E-04	3.61	0.00E+00	-44.78					1.74E-07	96.06	2.09E-05	1.37E-04	8.13E+01	8.23E-03			
145	500	2.55E-04	3.59	0.00E+00	-45.43					1.39E-07	96.13	1.66E-05	1.31E-04	8.26E+01	7.88E-03			
140	500	2.67E-04	3.57	0.00E+00	-46.1					1.10E-07	96.18	1.32E-05	1.26E-04	8.38E+01	7.55E-03			
135	500	2.79E-04	3.55	0.00E+00	-46.78					8.36E-08	96.21	1.00E-05	1.20E-04	8.50E+01	7.23E-03			
130	500	2.93E-04	3.53	0.00E+00	-47.47					6.52E-08	96.24	7.83E-06	1.15E-04	8.61E+01	6.92E-03			
125	500	3.06E-04	3.51	0.00E+00	-48.19					5.15E-08	96.27	6.18E-06	1.10E-04	8.72E+01	6.62E-03			
120	500	3.18E-04	3.5	0.00E+00	-48.93					4.02E-08	96.29	4.82E-06	1.05E-04	8.82E+01	6.32E-03			
115	500	3.31E-04	3.48	0.00E+00	-49.68					3.09E-08	96.30	3.71E-06	1.00E-04	8.92E+01	6.02E-03			
110	500	3.43E-04	3.46	0.00E+00	-50.46					2.35E-08	96.31	2.82E-06	9.54E-05	9.01E+01	5.73E-03			
105	500	3.55E-04	3.45	0.00E+00	-51.25					1.76E-08	96.32	2.11E-06	9.06E-05	9.10E+01	5.45E-03			
100	500	3.66E-04	3.44	0.00E+00	-52.07					1.31E-08	96.33	1.57E-06	8.59E-05	9.10E+01	5.16E-03			

Simulation 7 - cooling of Fluid 2 to 100 degrees C

u deposited as	chalcopy (g)	bornite (m)	deposited as b	bornite (g)	acanthit (m)	deposited as a	acanthit (g)	galena (m)	deposited as g	galena (g)	covellit (m)	deposited as c	covellit (g)	sphaleri (m)	eposited as sp	sphaleri (g)
0.00			0.00									0.00			0.00	
10.22	2.33E-04		0.00									0.00			0.00	
20.20	2.27E-04		0.00									0.00			0.00	
27.04	1.56E-04		0.00									0.00			0.00	
31.71	1.07E-04		0.00									0.00			0.00	
34.92	7.29E-05		0.00									0.00			0.00	
37.14	5.05E-05		0.00									0.00			0.00	
38.75	3.67E-05		0.00									0.00			0.00	
40.06	2.98E-05		0.00									0.00			0.00	
41.33	2.88E-05		0.00									0.00			0.00	
42.76	3.26E-05		0.00									0.00			0.00	
44.51	3.98E-05		0.00									0.00			0.00	
46.66	4.90E-05		0.00									0.00			0.00	
49.23	5.85E-05		0.00									0.00			0.00	
52.16	6.67E-05		0.00									0.00			0.00	
52.16		1.52E-07	6.12	7.64E-05								0.00			0.00	
52.16		1.49E-07	12.09	7.46E-05								0.00			0.00	
52.16		1.35E-07	17.53	6.79E-05								0.00			0.00	
52.16		1.21E-07	22.39	6.07E-05								0.00			0.00	
52.16		1.06E-07	26.66	5.33E-05								0.00			0.00	
52.16		9.20E-08	30.36	4.61E-05								0.00			0.00	
52.16		7.87E-08	33.52	3.95E-05								0.00			0.00	
52.16		6.67E-08	36.20	3.35E-05								0.00			0.00	
52.16		5.60E-08	38.45	2.81E-05								0.00			0.00	
52.16		4.66E-08	40.32	2.34E-05	6.69E-08	13.36	1.66E-05		0.00			0.00			0.00	
52.16		3.84E-08	41.87	1.93E-05	8.32E-08	29.97	2.06E-05		0.00			0.00			0.00	
52.16		3.13E-08	43.13	1.57E-05	6.50E-08	42.95	1.61E-05	5.77E-07	11.30	1.38E-04		0.00			0.00	
52.16		2.54E-08	44.15	1.27E-05	5.09E-08	53.12	1.26E-05	9.64E-07	30.16	2.31E-04		0.00			0.00	
52.16			44.15		4.02E-08	61.16	9.97E-06	7.74E-07	45.32	1.85E-04	1.15E-07	0.92	1.10E-05		0.00	
52.16			44.15		3.19E-08	67.53	7.91E-06	6.18E-07	57.41	1.48E-04	1.15E-07	1.84	1.10E-05		0.00	
52.16			44.15		2.55E-08	72.61	6.31E-06	4.90E-07	67.00	1.17E-04	7.94E-08	2.48	7.59E-06		0.00	
52.16			44.15		2.05E-08	76.71	5.08E-06	3.86E-07	74.55	9.24E-05	5.43E-08	2.92	5.19E-06		0.00	
52.16			44.15		1.67E-08	80.05	4.15E-06	3.03E-07	80.48	7.24E-05	3.68E-08	3.21	3.51E-06		0.00	
52.16			44.15		1.38E-08	82.80	3.42E-06	2.29E-07	84.95	5.47E-05	2.44E-08	3.41	2.33E-06	2.07E-06	12.92	2.02E-04
52.16			44.15		1.17E-08	85.13	2.89E-06	1.78E-07	88.43	4.25E-05	1.61E-08	3.54	1.54E-06	2.78E-06	30.26	2.71E-04
52.16			44.15		1.00E-08	87.13	2.48E-06	1.40E-07	91.17	3.35E-05	1.06E-08	3.62	1.01E-06	2.28E-06	44.53	2.23E-04
52.16			44.15		8.72E-09	88.87	2.16E-06	1.09E-07	93.30	2.61E-05	6.76E-09	3.68	6.46E-07	1.86E-06	56.13	1.81E-04
52.16			44.15		7.67E-09	90.40	1.90E-06	8.42E-08	94.95	2.01E-05	4.19E-09	3.71	4.01E-07	1.50E-06	65.49	1.46E-04
52.16			44.15		6.79E-09	91.76	1.68E-06	6.44E-08	96.21	1.54E-05	2.48E-09	3.73	2.37E-07	1.20E-06	72.97	1.17E-04
52.16			44.15		6.04E-09	92.97	1.50E-06	4.88E-08	97.16	1.17E-05	1.33E-09	3.74	1.27E-07	9.51E-07	78.91	9.27E-05
52.16			44.15		5.38E-09	94.04	1.33E-06	3.67E-08	97.88	8.79E-06	5.73E-10	3.74	5.48E-08	7.50E-07	83.59	7.31E-05

T (°C)	P (bars)	a(H2)	pH	TotMix	log f(O2)	barite (m)	deposited as	barite (g)	muscovit (m)	muscovit (g)	pyrite (m)	deposited as	pyrite (g)	quartz (m)	quartz (g)	talc (m)	talc (g)	chalcopy (m)
300	500	1.81E-05	4.74	0.00E+00	-30.54	1.27E-08	0.00	2.96E-06	4.93E-05	1.97E-02	4.11E-06	1.93	4.93E-04	4.15E-04	2.49E-02	1.26E-05	4.79E-03	
295	500	1.93E-05	4.72	0.00E+00	-30.92		0.00		2.42E-07	9.62E-05	2.65E-06	3.17	3.17E-04	3.71E-04	2.23E-02			1.74E-06
290	500	2.09E-05	4.68	0.00E+00	-31.29		0.00		2.16E-07	8.62E-05	5.90E-06	5.94	7.08E-04	3.73E-04	2.24E-02			1.19E-06
285	500	2.30E-05	4.64	0.00E+00	-31.67		0.00		1.89E-07	7.54E-05	8.81E-06	10.07	1.06E-03	3.72E-04	2.24E-02			8.20E-07
280	500	2.56E-05	4.59	0.00E+00	-32.05		0.00		1.62E-07	6.45E-05	1.13E-05	15.39	1.36E-03	3.69E-04	2.22E-02			5.64E-07
275	500	2.88E-05	4.54	0.00E+00	-32.43		0.00		1.36E-07	5.42E-05	1.34E-05	21.67	1.61E-03	3.64E-04	2.19E-02			3.89E-07
270	500	3.27E-05	4.49	0.00E+00	-32.81		0.00		1.13E-07	4.48E-05	1.50E-05	28.70	1.80E-03	3.57E-04	2.14E-02			2.72E-07
265	500	3.71E-05	4.43	0.00E+00	-33.2		0.00		9.22E-08	3.67E-05	1.60E-05	36.21	1.92E-03	3.49E-04	2.10E-02			2.00E-07
260	500	4.23E-05	4.37	0.00E+00	-33.6		0.00		7.49E-08	2.98E-05	1.65E-05	43.96	1.98E-03	3.40E-04	2.04E-02			1.64E-07
255	500	4.82E-05	4.32	0.00E+00	-34.01		0.00		6.06E-08	2.41E-05	1.64E-05	51.67	1.97E-03	3.29E-04	1.98E-02			1.58E-07
250	500	5.47E-05	4.26	0.00E+00	-34.42		0.00		4.90E-08	1.95E-05	1.58E-05	59.08	1.90E-03	3.19E-04	1.92E-02			1.75E-07
245	500	6.17E-05	4.21	0.00E+00	-34.84		0.00		3.98E-08	1.59E-05	1.47E-05	65.96	1.76E-03	3.08E-04	1.85E-02			2.10E-07
240	500	6.92E-05	4.16	0.00E+00	-35.27		0.00		3.28E-08	1.30E-05	1.31E-05	72.10	1.57E-03	2.97E-04	1.78E-02			2.55E-07
235	500	7.69E-05	4.11	0.00E+00	-35.71		0.00		2.74E-08	1.09E-05	1.12E-05	77.37	1.35E-03	2.85E-04	1.71E-02			3.01E-07
230	500	8.48E-05	4.07	0.00E+00	-36.16		0.00		2.33E-08	9.27E-06	9.22E-06	81.70	1.11E-03	2.74E-04	1.65E-02			3.41E-07
225	500	9.28E-05	4.03	0.00E+00	-36.62		0.00		1.99E-08	7.94E-06	7.49E-06	85.21	8.99E-04	2.63E-04	1.58E-02			
220	500	1.01E-04	4	0.00E+00	-37.09		0.00		1.73E-08	6.88E-06	5.78E-06	87.92	6.93E-04	2.52E-04	1.51E-02			
215	500	1.09E-04	3.96	0.00E+00	-37.57		0.00		1.50E-08	5.96E-06	4.35E-06	89.97	5.22E-04	2.41E-04	1.45E-02			
210	500	1.17E-04	3.93	0.00E+00	-38.06		0.00		1.28E-08	5.11E-06	3.23E-06	91.48	3.87E-04	2.31E-04	1.39E-02			
205	500	1.26E-04	3.9	0.00E+00	-38.55		0.00		1.08E-08	4.30E-06	2.38E-06	92.60	2.85E-04	2.21E-04	1.33E-02			
200	500	1.34E-04	3.87	0.00E+00	-39.06		0.00		8.86E-09	3.53E-06	1.75E-06	93.42	2.10E-04	2.11E-04	1.27E-02			
195	500	1.43E-04	3.84	0.00E+00	-39.58		0.00		7.01E-09	2.79E-06	1.30E-06	94.03	1.56E-04	2.02E-04	1.22E-02			
190	500	1.52E-04	3.82	0.00E+00	-40.11		0.00		5.25E-09	2.09E-06	9.82E-07	94.49	1.18E-04	1.94E-04	1.16E-02			
185	500	1.61E-04	3.79	0.00E+00	-40.64		0.00		3.56E-09	1.42E-06	7.51E-07	94.85	9.01E-05	1.85E-04	1.11E-02			
180	500	1.71E-04	3.77	0.00E+00	-41.2		0.00		1.84E-09	7.31E-07	5.81E-07	95.12	6.97E-05	1.77E-04	1.06E-02			
175	500	1.81E-04	3.74	0.00E+00	-41.76		0.00		1.80E-10	7.18E-08	4.56E-07	95.33	5.47E-05	1.70E-04	1.02E-02			
170	500	1.91E-04	3.72	0.00E+00	-42.33		0.00				3.55E-07	95.50	4.26E-05	1.63E-04	9.76E-03			
165	500	2.02E-04	3.69	0.00E+00	-42.92		0.00				2.85E-07	95.63	3.42E-05	1.56E-04	9.35E-03			
160	500	2.13E-04	3.67	0.00E+00	-43.53		0.00				2.49E-07	95.75	2.99E-05	1.49E-04	8.96E-03			
155	500	2.24E-04	3.65	0.00E+00	-44.15		0.00				2.00E-07	95.84	2.41E-05	1.43E-04	8.59E-03			
150	500	2.35E-04	3.63	0.00E+00	-44.78		0.00				1.61E-07	95.92	1.93E-05	1.37E-04	8.23E-03			
145	500	2.46E-04	3.61	0.00E+00	-45.43		0.00				1.28E-07	95.98	1.54E-05	1.31E-04	7.88E-03			
140	500	2.58E-04	3.59	0.00E+00	-46.09		0.00				1.02E-07	96.03	1.22E-05	1.26E-04	7.55E-03			
135	500	2.71E-04	3.57	0.00E+00	-46.77		0.00				7.66E-08	96.06	9.19E-06	1.20E-04	7.23E-03			
130	500	2.84E-04	3.55	0.00E+00	-47.47		0.00				6.10E-08	96.09	7.32E-06	1.15E-04	6.92E-03			
125	500	2.97E-04	3.53	0.00E+00	-48.19		0.00				4.82E-08	96.12	5.79E-06	1.10E-04	6.61E-03			
120	500	3.09E-04	3.51	0.00E+00	-48.92		0.00				3.76E-08	96.13	4.51E-06	1.05E-04	6.32E-03			
115	500	3.21E-04	3.49	0.00E+00	-49.68		0.00				2.89E-08	96.15	3.47E-06	1.00E-04	6.02E-03			
110	500	3.33E-04	3.48	0.00E+00	-50.45		0.00				2.20E-08	96.16	2.64E-06	9.54E-05	5.73E-03			
105	500	3.45E-04	3.46	0.00E+00	-51.25		0.00				1.65E-08	96.16	1.98E-06	9.06E-05	5.44E-03			
100	500	3.56E-04	3.45	0.00E+00	-52.07		0.00				1.23E-08	96.17	1.47E-06	8.59E-05	5.16E-03			

Simulation 8 - cooling of Fluid 3 to 100 degrees C

u deposited as	chalcopy (g)	bornite (m)	deposited as	bornite (g)	acanthit (m)	deposited as a	acanthit (g)	galena (m)	deposited as g	galena (g)	covellit (m)	deposited as c	covellit (g)	sphaleri (m)	eposited as sp	sphaleri (g)
0.00			0.00									0.00			0.00	
14.06	3.20E-04		0.00									0.00			0.00	
23.69	2.19E-04		0.00									0.00			0.00	
30.30	1.50E-04		0.00									0.00			0.00	
34.84	1.03E-04		0.00									0.00			0.00	
37.97	7.14E-05		0.00									0.00			0.00	
40.17	5.00E-05		0.00									0.00			0.00	
41.78	3.68E-05		0.00									0.00			0.00	
43.11	3.01E-05		0.00									0.00			0.00	
44.38	2.89E-05		0.00									0.00			0.00	
45.79	3.22E-05		0.00									0.00			0.00	
47.48	3.86E-05		0.00									0.00			0.00	
49.54	4.67E-05		0.00									0.00			0.00	
51.96	5.52E-05		0.00									0.00			0.00	
54.71	6.25E-05		0.00									0.00			0.00	
54.71		1.37E-07	5.50	6.86E-05								0.00			0.00	
54.71		1.41E-07	11.16	7.07E-05								0.00			0.00	
54.71		1.28E-07	16.32	6.43E-05								0.00			0.00	
54.71		1.14E-07	20.91	5.74E-05								0.00			0.00	
54.71		1.00E-07	24.95	5.04E-05								0.00			0.00	
54.71		8.71E-08	28.45	4.37E-05								0.00			0.00	
54.71		7.46E-08	31.45	3.74E-05								0.00			0.00	
54.71		6.33E-08	34.00	3.18E-05								0.00			0.00	
54.71		5.32E-08	36.14	2.67E-05								0.00			0.00	
54.71		4.43E-08	37.92	2.22E-05	8.11E-08	16.20	2.01E-05		0.00			0.00			0.00	
54.71		3.67E-08	39.39	1.84E-05	7.95E-08	32.08	1.97E-05		0.00			0.00			0.00	
54.71		2.98E-08	40.59	1.49E-05	6.21E-08	44.47	1.54E-05	9.09E-07	17.79	2.17E-04		0.00			0.00	
54.71		2.43E-08	41.57	1.22E-05	4.90E-08	54.24	1.21E-05	8.86E-07	35.13	2.12E-04		0.00			0.00	
54.71			41.57		3.87E-08	61.98	9.60E-06	7.14E-07	49.10	1.71E-04	1.10E-07	0.89	1.05E-05		0.00	
54.71			41.57		3.08E-08	68.13	7.63E-06	5.71E-07	60.26	1.37E-04	1.10E-07	1.77	1.05E-05		0.00	
54.71			41.57		2.46E-08	73.04	6.10E-06	4.54E-07	69.14	1.09E-04	7.64E-08	2.39	7.30E-06		0.00	
54.71			41.57		1.99E-08	77.02	4.93E-06	3.58E-07	76.15	8.57E-05	5.23E-08	2.81	5.00E-06		0.00	
54.71			41.57		1.63E-08	80.27	4.04E-06	2.81E-07	81.66	6.73E-05	3.54E-08	3.09	3.39E-06		0.00	
54.71			41.57		1.35E-08	82.96	3.33E-06	2.11E-07	85.78	5.04E-05	2.34E-08	3.28	2.24E-06	2.89E-06	18.05	2.82E-04
54.71			41.57		1.14E-08	85.24	2.83E-06	1.67E-07	89.05	4.00E-05	1.56E-08	3.40	1.49E-06	2.61E-06	34.33	2.54E-04
54.71			41.57		9.86E-09	87.21	2.44E-06	1.32E-07	91.63	3.15E-05	1.02E-08	3.49	9.75E-07	2.15E-06	47.72	2.09E-04
54.71			41.57		8.60E-09	88.93	2.13E-06	1.03E-07	93.64	2.46E-05	6.52E-09	3.54	6.24E-07	1.75E-06	58.62	1.70E-04
54.71			41.57		7.59E-09	90.44	1.88E-06	7.94E-08	95.20	1.90E-05	4.04E-09	3.57	3.86E-07	1.41E-06	67.42	1.37E-04
54.71			41.57		6.73E-09	91.79	1.67E-06	6.09E-08	96.39	1.46E-05	2.37E-09	3.59	2.27E-07	1.13E-06	74.48	1.10E-04
54.71			41.57		6.00E-09	92.98	1.49E-06	4.62E-08	97.29	1.11E-05	1.26E-09	3.60	1.21E-07	8.96E-07	80.05	8.73E-05
54.71			41.57		5.35E-09	94.05	1.33E-06	3.48E-08	97.97	8.34E-06	5.24E-10	3.61	5.01E-08	7.07E-07	84.46	6.89E-05

T (°C)	P (bars)	a(H+)	pH	TotMix	log f(O2)	hematite (m)		hematite (g)	pyrite (m)	deposited as	pyrite (g)	talc (m)	talc (g)	chalcopy (m)	u deposited as	chalcopy (g)	muscovit (m)
300	500	1.83E-05	4.74	0.00E+00	-30.43	3.13E-05	12.96	5.00E-03	3.38E-13	0.00	4.05E-11	1.94E-12	7.37E-10		0.00		
295	500	1.95E-05	4.71	0.00E+00	-30.81				4.25E-06	0.88	5.10E-04			9.79E-07	7.89	1.80E-04	2.27E-07
290	500	2.12E-05	4.67	0.00E+00	-31.18				6.83E-06	2.29	8.20E-04			1.24E-06	17.89	2.28E-04	2.16E-07
285	500	2.35E-05	4.63	0.00E+00	-31.56				1.02E-05	4.40	1.22E-03			8.28E-07	24.57	1.52E-04	1.89E-07
280	500	2.63E-05	4.58	0.00E+00	-31.93				1.32E-05	7.13	1.58E-03			5.42E-07	28.94	9.95E-05	1.61E-07
275	500	2.98E-05	4.53	0.00E+00	-32.31				1.58E-05	10.40	1.90E-03			3.41E-07	31.68	6.25E-05	1.34E-07
270	500	3.41E-05	4.47	0.00E+00	-32.69				1.80E-05	14.12	2.16E-03			1.99E-07	33.29	3.66E-05	1.10E-07
265	500	3.92E-05	4.41	0.00E+00	-33.07				1.98E-05	18.21	2.37E-03			1.04E-07	34.13	1.92E-05	8.88E-08
260	500	4.53E-05	4.34	0.00E+00	-33.47				2.11E-05	22.57	2.53E-03			4.88E-08	34.52	8.95E-06	7.04E-08
255	500	5.24E-05	4.28	0.00E+00	-33.86				2.19E-05	27.11	2.63E-03			2.86E-08	34.75	5.25E-06	5.47E-08
250	500	6.06E-05	4.22	0.00E+00	-34.27				2.23E-05	31.73	2.68E-03			4.20E-08	35.09	7.71E-06	4.16E-08
245	500	6.97E-05	4.16	0.00E+00	-34.7				2.22E-05	36.33	2.67E-03			8.71E-08	35.79	1.60E-05	3.09E-08
240	500	7.99E-05	4.1	0.00E+00	-35.13				2.16E-05	40.81	2.60E-03			1.60E-07	37.08	2.94E-05	2.23E-08
235	500	9.09E-05	4.04	0.00E+00	-35.58				2.05E-05	45.06	2.47E-03			2.56E-07	39.15	4.71E-05	1.56E-08
230	500	1.02E-04	3.99	0.00E+00	-36.06				1.90E-05	48.98	2.27E-03			3.68E-07	42.11	6.75E-05	1.07E-08
225	500	1.14E-04	3.94	0.00E+00	-36.55				1.69E-05	52.48	2.03E-03			4.86E-07	46.03	8.91E-05	7.49E-09
220	500	1.26E-04	3.9	0.00E+00	-37.08				1.44E-05	55.45	1.72E-03			6.02E-07	50.88	1.10E-04	5.74E-09
215	500	1.38E-04	3.86	0.00E+00	-37.65				1.14E-05	57.80	1.37E-03			7.08E-07	56.58	1.30E-04	5.34E-09
210	500	1.50E-04	3.83	0.00E+00	-38.26				8.04E-06	59.47	9.65E-04			7.88E-07	62.94	1.45E-04	6.08E-09
205	500	1.60E-04	3.8	0.00E+00	-38.92				4.69E-06	60.44	5.63E-04			8.15E-07	69.51	1.50E-04	7.36E-09
200	500	1.70E-04	3.77	0.00E+00	-39.63				2.11E-06	60.88	2.53E-04			7.62E-07	75.65	1.40E-04	8.12E-09
195	500	1.80E-04	3.75	0.00E+00	-40.36				7.33E-07	61.03	8.80E-05			6.49E-07	80.87	1.19E-04	7.69E-09
190	500	1.90E-04	3.72	0.00E+00	-41.11				2.42E-07	61.08	2.90E-05			5.23E-07	85.09	9.60E-05	6.31E-09
185	500	2.00E-04	3.7	0.00E+00	-41.86				2.32E-07	61.12	2.78E-05			4.12E-07	88.41	7.56E-05	4.36E-09
180	500	2.10E-04	3.68	0.00E+00	-42.61				5.82E-07	61.25	6.99E-05			3.20E-07	90.99	5.87E-05	1.88E-09
175	500	2.21E-04	3.65	0.00E+00	-43.36				1.38E-06	61.53	1.65E-04			2.44E-07	92.96	4.48E-05	
170	500	2.34E-04	3.63	0.00E+00	-44.1				2.66E-06	62.08	3.19E-04			1.83E-07	94.43	3.36E-05	
165	500	2.47E-04	3.61	0.00E+00	-44.83				4.18E-06	62.94	5.01E-04			1.37E-07	95.54	2.52E-05	
160	500	2.61E-04	3.58	0.00E+00	-45.54				5.59E-06	64.10	6.71E-04			1.05E-07	96.38	1.92E-05	
155	500	2.77E-04	3.56	0.00E+00	-46.24				6.67E-06	65.48	8.00E-04			8.23E-08	97.05	1.51E-05	
150	500	2.93E-04	3.53	0.00E+00	-46.94				7.42E-06	67.01	8.90E-04			6.63E-08	97.58	1.22E-05	
145	500	3.10E-04	3.51	0.00E+00	-47.65				7.92E-06	68.65	9.50E-04				97.58		
140	500	3.27E-04	3.48	0.00E+00	-48.36				8.38E-06	70.39	1.01E-03				97.58		
135	500	3.48E-04	3.46	0.00E+00	-48.97				1.25E-05	72.98	1.50E-03				97.58		
130	500	3.69E-04	3.43	0.00E+00	-49.61				1.15E-05	75.35	1.38E-03				97.58		
125	500	3.89E-04	3.41	0.00E+00	-50.25				1.06E-05	77.55	1.27E-03				97.58		
120	500	4.09E-04	3.39	0.00E+00	-50.92				9.81E-06	79.58	1.18E-03				97.58		
115	500	4.29E-04	3.37	0.00E+00	-51.61				9.01E-06	81.44	1.08E-03				97.58		
110	500	4.48E-04	3.35	0.00E+00	-52.31				8.22E-06	83.14	9.86E-04				97.58		
105	500	4.66E-04	3.33	0.00E+00	-53.04				7.45E-06	84.68	8.94E-04				97.58		
100	500	4.84E-04	3.32	0.00E+00	-53.78				6.72E-06	86.07	8.06E-04				97.58		
								total Fe in fluid		total pyrite pos	total Fe in fluid				total cpy poss	total Cu in fluid	
								2.70E-02		2.61E-02	2.70E-02				2.28E-03	7.91E-04	

Simulation 9 - cooling of Fluid 4 to 100 degrees C

muscovit (g)	quartz (m)	quartz (g)	gold (m)	Cl2 deposited	gold (g)	acanthit (m)	deposited as ac	acanthit (g)	bornite (m)	deposited as b	bornite (g)	graphite (m)	graphite (g)	galena (m)	deposited as g	galena (g)
	7.49E-04	4.50E-02		0.00						0.00						
9.04E-05	3.71E-04	2.23E-02		0.00						0.00						
8.62E-05	3.73E-04	2.24E-02		0.00						0.00						
7.52E-05	3.72E-04	2.24E-02		0.00						0.00						
6.41E-05	3.69E-04	2.22E-02		0.00						0.00						
5.36E-05	3.64E-04	2.19E-02		0.00						0.00						
4.39E-05	3.57E-04	2.14E-02		0.00						0.00						
3.54E-05	3.49E-04	2.10E-02		0.00						0.00						
2.80E-05	3.40E-04	2.04E-02		0.00						0.00						
2.18E-05	3.30E-04	1.98E-02		0.00						0.00						
1.66E-05	3.19E-04	1.92E-02		0.00						0.00						
1.23E-05	3.08E-04	1.85E-02		0.00						0.00						
8.87E-06	2.97E-04	1.78E-02		0.00						0.00						
6.22E-06	2.85E-04	1.71E-02		0.00						0.00						
4.27E-06	2.74E-04	1.65E-02		0.00						0.00						
2.98E-06	2.63E-04	1.58E-02		0.00						0.00						
2.29E-06	2.52E-04	1.51E-02		0.00						0.00						
2.13E-06	2.41E-04	1.45E-02		0.00						0.00						
2.42E-06	2.31E-04	1.39E-02	3.50E-10	5.80	6.89E-08					0.00						
2.93E-06	2.21E-04	1.33E-02	5.30E-10	14.60	1.04E-07					0.00						
3.24E-06	2.11E-04	1.27E-02	4.27E-10	21.69	8.42E-08					0.00						
3.06E-06	2.02E-04	1.22E-02	3.55E-10	27.57	6.99E-08					0.00						
2.51E-06	1.94E-04	1.16E-02	3.04E-10	32.62	6.00E-08					0.00						
1.74E-06	1.85E-04	1.11E-02	2.68E-10	37.07	5.28E-08					0.00						
7.51E-07	1.77E-04	1.06E-02	2.42E-10	41.08	4.76E-08		0.00			0.00					0.00	
	1.70E-04	1.02E-02	2.23E-10	44.79	4.40E-08		0.00			0.00					0.00	
	1.63E-04	9.76E-03	2.11E-10	48.28	4.15E-08	3.38E-08	6.76	8.39E-06		0.00					0.00	
	1.56E-04	9.35E-03	2.00E-10	51.59	3.94E-08	9.91E-08	26.56	2.46E-05		0.00					0.00	
	1.49E-04	8.96E-03	1.88E-10	54.72	3.71E-08	7.64E-08	41.81	1.89E-05		0.00					0.00	
	1.43E-04	8.59E-03	1.75E-10	57.63	3.45E-08	5.95E-08	53.70	1.48E-05		0.00					0.00	
	1.37E-04	8.23E-03	1.61E-10	60.30	3.17E-08	4.68E-08	63.05	1.16E-05		0.00					0.00	
	1.31E-04	7.88E-03	1.46E-10	62.73	2.88E-08	3.71E-08	70.47	9.20E-06	1.11E-08	0.45	5.57E-06				0.00	
	1.26E-04	7.55E-03	1.32E-10	64.91	2.60E-08	2.95E-08	76.36	7.31E-06	1.18E-08	0.92	5.94E-06	6.16E-07	7.40E-06		0.00	
	1.20E-04	7.23E-03	1.28E-10	67.04	2.53E-08	2.24E-08	80.83	5.55E-06	8.23E-09	1.25	4.13E-06	1.29E-05	1.55E-04		0.00	
	1.15E-04	6.92E-03	1.10E-10	68.87	2.18E-08	1.85E-08	84.53	4.58E-06	6.80E-09	1.53	3.41E-06	1.05E-05	1.26E-04	5.61E-07	10.99	1.34E-04
	1.10E-04	6.62E-03	9.34E-11	70.42	1.84E-08	1.52E-08	87.57	3.78E-06	5.60E-09	1.75	2.81E-06	8.68E-06	1.04E-04	6.18E-07	23.09	1.48E-04
	1.05E-04	6.32E-03	7.80E-11	71.72	1.54E-08	1.25E-08	90.07	3.10E-06	4.56E-09	1.93	2.29E-06	7.29E-06	8.76E-05	5.52E-07	33.89	1.32E-04
	1.00E-04	6.02E-03	6.43E-11	72.78	1.27E-08	1.02E-08	92.11	2.53E-06	3.69E-09	2.08	1.85E-06	6.19E-06	7.43E-05	4.88E-07	43.45	1.17E-04
	9.54E-05	5.73E-03	5.23E-11	73.65	1.03E-08	8.30E-09	93.76	2.06E-06	2.96E-09	2.20	1.49E-06	5.29E-06	6.36E-05	4.29E-07	51.84	1.03E-04
	9.06E-05	5.45E-03	4.19E-11	74.35	8.26E-09	6.71E-09	95.10	1.66E-06	2.36E-09	2.30	1.19E-06	4.55E-06	5.47E-05	3.74E-07	59.15	8.94E-05
	8.59E-05	5.16E-03	3.31E-11	74.90	6.53E-09	5.38E-09	96.18	1.33E-06	1.87E-09	2.37	9.39E-07	3.93E-06	4.73E-05	3.23E-07	65.48	7.73E-05
					total Au in fluid		total acanthite	total Ag in fluid		total bornite p	total Cu in fluid				total galena po	total Pb in fluid
					8.73E-07		1.24E-04	1.08E-04		1.25E-03	7.91E-04				1.22E-03	1.06E-03

T (°C)	P (bars)	a(H+)	pH	TotMix	log f(O2)	apat-chl (m)	apat-chl (g)	calcite (m)	calcite (g)	muscovit (m)	muscovit (g)	phlogopi (m)	phlogopi (g)	chalcopy (m)
300	500	1.81E-06	5.74	0.00E+00	-31.58	8.67E-13	4.51E-10	4.24E-04	4.25E-02	6.35E-06	2.53E-03	1.55E-07	6.49E-05	
295	500	2.05E-06	5.69	0.00E+00	-31.94					2.08E-06	8.29E-04			6.34E-09
290	500	2.31E-06	5.64	0.00E+00	-32.31					1.62E-06	6.46E-04			7.76E-08
285	500	2.60E-06	5.59	0.00E+00	-32.68					1.26E-06	5.01E-04			1.30E-07
280	500	2.92E-06	5.54	0.00E+00	-33.06					9.73E-07	3.88E-04			1.66E-07
275	500	3.26E-06	5.49	0.00E+00	-33.44					7.51E-07	2.99E-04			1.84E-07
270	500	3.64E-06	5.44	0.00E+00	-33.83					5.79E-07	2.30E-04			1.84E-07
265	500	4.06E-06	5.39	0.00E+00	-34.22					4.45E-07	1.77E-04			1.74E-07
260	500	4.52E-06	5.34	0.00E+00	-34.62					3.41E-07	1.36E-04			1.54E-07
255	500	5.04E-06	5.3	0.00E+00	-35.03									1.31E-07
250	500	5.61E-06	5.25	0.00E+00	-35.44					1.79E-07	7.12E-05			2.51E-08
245	500	6.24E-06	5.2	0.00E+00	-35.86					1.28E-07	5.09E-05			1.53E-08
240	500	6.94E-06	5.16	0.00E+00	-36.29					1.02E-07	4.06E-05			1.47E-08
235	500	7.71E-06	5.11	0.00E+00	-36.72					8.11E-08	3.23E-05			1.43E-08
230	500	8.56E-06	5.07	0.00E+00	-37.16					6.46E-08	2.57E-05			1.40E-08
225	500	9.48E-06	5.02	0.00E+00	-37.61					5.15E-08	2.05E-05			1.39E-08
220	500	1.05E-05	4.98	0.00E+00	-38.06					4.12E-08	1.64E-05			1.38E-08
215	500	1.16E-05	4.94	0.00E+00	-38.53					3.30E-08	1.31E-05			1.38E-08
210	500	1.28E-05	4.89	0.00E+00	-39					2.65E-08	1.06E-05			1.39E-08
205	500	1.42E-05	4.85	0.00E+00	-39.48					2.13E-08	8.49E-06			1.39E-08
200	500	1.56E-05	4.81	0.00E+00	-39.98					1.72E-08	6.84E-06			1.38E-08
195	500	1.71E-05	4.77	0.00E+00	-40.48					1.39E-08	5.52E-06			
190	500	1.88E-05	4.73	0.00E+00	-40.99					1.12E-08	4.46E-06			
185	500	2.06E-05	4.69	0.00E+00	-41.52					9.05E-09	3.60E-06			
180	500	2.26E-05	4.65	0.00E+00	-42.06					7.30E-09	2.91E-06			
175	500	2.47E-05	4.61	0.00E+00	-42.61					5.86E-09	2.33E-06			
170	500	2.69E-05	4.57	0.00E+00	-43.17					4.68E-09	1.86E-06			
165	500	2.93E-05	4.53	0.00E+00	-43.75					3.70E-09	1.47E-06			
160	500	3.18E-05	4.5	0.00E+00	-44.34					2.89E-09	1.15E-06			
155	500	3.44E-05	4.46	0.00E+00	-44.95					2.21E-09	8.79E-07			
150	500	3.72E-05	4.43	0.00E+00	-45.57					1.63E-09	6.51E-07			
145	500	4.01E-05	4.4	0.00E+00	-46.21					1.15E-09	4.57E-07			
140	500	4.31E-05	4.37	0.00E+00	-46.87					7.27E-10	2.90E-07			
135	500	4.63E-05	4.33	0.00E+00	-47.54					3.53E-10	1.41E-07			
130	500	4.95E-05	4.31	0.00E+00	-48.23					9.40E-13	3.75E-10			
125	500	5.27E-05	4.28	0.00E+00	-48.94									
120	500	5.60E-05	4.25	0.00E+00	-49.66									
115	500	5.94E-05	4.23	0.00E+00	-50.41									
110	500	6.26E-05	4.2	0.00E+00	-51.18									
105	500	6.59E-05	4.18	0.00E+00	-51.97									
100	500	6.90E-05	4.16	0.00E+00	-52.79									
							apat-chl (g)		calcite (g)		muscovit (g)		phlogopi (g)	
							4.51E-10		4.25E-02		6.06E-03		6.49E-05	

Simulation 10 - cooling of Fluid 5 to 100 degrees C

Cu deposited as	chalcopy (g)	galena (m)	deposited as g	galena (g)	witherit (m)	witherit (g)	sphaleri (m)	deposited as sp	sphaleri (g)	micr-max (m)	micr-max (g)	pyrite (m)	deposited as	pyrite (g)
0.00								0.00					0.00	
0.37	1.16E-06	6.67E-07		1.60E-04	4.31E-05	8.51E-03		0.00					0.00	
4.95	1.42E-05	6.16E-07		1.47E-04	3.02E-05	5.96E-03		0.00					0.00	
12.59	2.38E-05	5.41E-07		1.30E-04	1.98E-05	3.91E-03		0.00					0.00	
22.36	3.04E-05	4.70E-07		1.12E-04	1.22E-05	2.40E-03		0.00					0.00	
33.23	3.38E-05	4.04E-07		9.66E-05	6.42E-06	1.27E-03	1.27E-07	0.41	1.24E-05				0.00	
44.09	3.38E-05	3.40E-07		8.14E-05	1.59E-06	3.13E-04	1.68E-06	5.82	1.63E-04				0.00	
54.35	3.19E-05	2.88E-07		6.90E-05			1.49E-06	10.64	1.45E-04				0.00	
63.46	2.83E-05	2.43E-07		5.80E-05			1.31E-06	14.88	1.28E-04				0.00	
71.17	2.40E-05	2.05E-07		4.89E-05			1.16E-06	18.62	1.13E-04	7.97E-07	2.22E-04		0.00	
72.66	4.61E-06	1.70E-07		4.06E-05			1.00E-06	21.86	9.78E-05			1.42E-06	18.36	1.70E-04
73.56	2.80E-06	1.45E-07		3.48E-05			9.03E-07	24.78	8.79E-05			1.28E-06	34.85	1.53E-04
74.42	2.69E-06	1.25E-07		3.00E-05			8.16E-07	27.41	7.95E-05			9.98E-07	47.76	1.20E-04
75.26	2.61E-06	1.08E-07		2.58E-05			7.39E-07	29.80	7.20E-05			7.59E-07	57.57	9.11E-05
76.09	2.57E-06	9.34E-08		2.23E-05			6.71E-07	31.97	6.54E-05			5.63E-07	64.85	6.76E-05
76.91	2.55E-06	8.09E-08		1.94E-05			6.09E-07	33.93	5.94E-05			4.10E-07	70.16	4.92E-05
77.72	2.54E-06	7.03E-08		1.68E-05			5.55E-07	35.72	5.41E-05			2.95E-07	73.98	3.54E-05
78.54	2.54E-06	6.13E-08		1.47E-05			5.06E-07	37.36	4.93E-05			2.10E-07	76.70	2.52E-05
79.36	2.55E-06	5.35E-08		1.28E-05			4.61E-07	38.85	4.50E-05			1.49E-07	78.63	1.79E-05
80.18	2.55E-06	4.69E-08		1.12E-05			4.21E-07	40.21	4.10E-05			1.06E-07	80.00	1.27E-05
80.99	2.54E-06	4.13E-08		9.88E-06			3.84E-07	41.45	3.75E-05			7.57E-08	80.98	9.08E-06
80.99		3.65E-08		8.72E-06			3.51E-07	42.58	3.42E-05			6.22E-08	81.78	7.47E-06
80.99		3.23E-08		7.73E-06			3.20E-07	43.61	3.11E-05			4.64E-08	82.38	5.56E-06
80.99		2.88E-08		6.89E-06			2.91E-07	44.55	2.84E-05			3.63E-08	82.85	4.35E-06
80.99		2.58E-08	0.51	6.16E-06			2.64E-07	45.41	2.58E-05			2.90E-08	83.23	3.48E-06
80.99		2.32E-08	0.96	5.54E-06			2.40E-07	46.18	2.33E-05			2.37E-08	83.53	2.85E-06
80.99		2.09E-08	1.37	5.00E-06			2.16E-07	46.88	2.11E-05			1.97E-08	83.79	2.36E-06
80.99		1.89E-08	1.74	4.53E-06			1.95E-07	47.51	1.90E-05			1.66E-08	84.00	1.99E-06
80.99		1.72E-08	2.08	4.12E-06			1.74E-07	48.59	1.70E-05			1.40E-08	84.18	1.68E-06
80.99		1.57E-08	2.39	3.75E-06			1.55E-07	49.55	1.51E-05			1.20E-08	84.34	1.43E-06
80.99		1.43E-08	2.66	3.42E-06			1.38E-07	50.40	1.34E-05			1.02E-08	84.47	1.23E-06
80.99		1.30E-08	2.92	3.11E-06			1.22E-07	51.15	1.19E-05			8.77E-09	84.58	1.05E-06
80.99		1.18E-08	3.15	2.82E-06			1.07E-07	51.81	1.04E-05			7.56E-09	84.68	9.07E-07
80.99		1.07E-08	3.36	2.55E-06			9.29E-08	52.39	9.05E-06			6.78E-09	84.77	8.13E-07
80.99		9.57E-09	3.55	2.29E-06			8.04E-08	52.89	7.84E-06			5.56E-09	84.84	6.67E-07
80.99		8.53E-09	3.71	2.04E-06			6.92E-08	53.32	6.74E-06			4.51E-09	84.90	5.41E-07
80.99		7.53E-09	3.86	1.80E-06			5.91E-08	53.69	5.76E-06			3.62E-09	84.95	4.35E-07
80.99		6.58E-09	3.99	1.57E-06			5.01E-08	54.00	4.88E-06			2.88E-09	84.98	3.45E-07
80.99		5.67E-09	4.10	1.36E-06			4.22E-08	54.27	4.11E-06			2.26E-09	85.01	2.71E-07
80.99		4.83E-09	4.19	1.15E-06			3.53E-08	54.49	3.44E-06			1.75E-09	85.04	2.10E-07
80.99		4.04E-09	4.27	9.67E-07			2.94E-08	54.67	2.86E-06			1.34E-09	85.05	1.60E-07
total cpy poss.			total galena po	total Pb in fluid				total sphal pos	total Zn in fluid				total pyrite pos	total Fe in sys
2.28E-03	total Cu in fluid		1.22E-03	0.0010584		witherit (g)		1.56E-03	0.0010476		micr-max (g)		2.56E-02	0.000432
	0.000108			1.22E-03		2.24E-02			1.55E-03		2.22E-04			7.89E-04

quartz (m)	quartz (g)	acanthit (m)	deposited as ac	acanthit (g)	bornite (m)	deposited as b	bornite (g)	covellit (m)	deposited as cc	covellit (g)
						0.00			0.00	
						0.00			0.00	
						0.00			0.00	
						0.00			0.00	
						0.00			0.00	
						0.00			0.00	
						0.00			0.00	
						0.00			0.00	
						0.00			0.00	
						0.00			0.00	
1.44E-04	8.67E-03					0.00			0.00	
3.08E-04	1.85E-02					0.00			0.00	
2.97E-04	1.78E-02					0.00			0.00	
2.86E-04	1.72E-02					0.00			0.00	
2.74E-04	1.65E-02	2.08E-08	4.16	5.16E-06		0.00			0.00	
2.63E-04	1.58E-02	7.15E-08	18.44	1.77E-05		0.00			0.00	
2.52E-04	1.51E-02	5.91E-08	30.24	1.46E-05		0.00			0.00	
2.41E-04	1.45E-02	4.88E-08	39.99	1.21E-05		0.00			0.00	
2.31E-04	1.39E-02	4.03E-08	48.03	9.98E-06		0.00			0.00	
2.21E-04	1.33E-02	3.32E-08	54.66	8.23E-06		0.00			0.00	
2.12E-04	1.27E-02	2.74E-08	60.13	6.79E-06		0.00			0.00	
2.02E-04	1.22E-02	2.27E-08	64.66	5.61E-06	5.84E-09	1.72	2.93E-06		0.00	
1.94E-04	1.16E-02	1.88E-08	68.41	4.66E-06	6.49E-09	3.63	3.26E-06		0.00	
1.85E-04	1.11E-02	1.57E-08	71.54	3.88E-06	5.67E-09	5.30	2.85E-06		0.00	
1.77E-04	1.07E-02	1.32E-08	74.17	3.27E-06	4.91E-09	6.74	2.47E-06		0.00	
1.70E-04	1.02E-02	1.12E-08	76.41	2.78E-06	4.21E-09	7.98	2.12E-06		0.00	
1.63E-04	9.77E-03	9.69E-09	78.35	2.40E-06	3.58E-09	9.03	1.79E-06		0.00	
1.56E-04	9.36E-03	8.53E-09	80.05	2.11E-06	2.99E-09	9.91	1.50E-06		0.00	
1.49E-04	8.96E-03	7.65E-09	81.58	1.89E-06	2.45E-09	10.64	1.23E-06		0.00	
1.43E-04	8.59E-03	7.00E-09	82.97	1.73E-06	1.96E-09	11.21	9.83E-07		0.00	
1.37E-04	8.23E-03	6.52E-09	84.28	1.62E-06	1.50E-09	11.65	7.51E-07		0.00	
1.31E-04	7.89E-03	6.18E-09	85.51	1.53E-06	1.06E-09	11.96	5.32E-07		0.00	
1.26E-04	7.55E-03	5.93E-09	86.70	1.47E-06	6.34E-10	12.15	3.18E-07		0.00	
1.20E-04	7.23E-03	5.74E-09	87.84	1.42E-06		12.15		5.25E-09	0.31	5.02E-07
1.15E-04	6.92E-03	5.57E-09	88.96	1.38E-06		12.15		4.82E-09	0.59	4.61E-07
1.10E-04	6.62E-03	5.41E-09	90.04	1.34E-06		12.15		2.67E-09	0.75	2.55E-07
1.05E-04	6.32E-03	5.24E-09	91.08	1.30E-06		12.15		1.06E-09	0.81	1.02E-07
1.00E-04	6.02E-03	5.04E-09	92.09	1.25E-06		12.15			0.81	
9.54E-05	5.73E-03	4.80E-09	93.05	1.19E-06		12.15			0.81	
9.06E-05	5.45E-03	4.53E-09	93.95	1.12E-06		12.15			0.81	
8.59E-05	5.16E-03	4.23E-09	94.80	1.05E-06		12.15			0.81	
em			total acanthite	total Ag in fluid		total bornite p	total Cu in fluid		total covellite p	total Cu in fluic
	quartz (g)		1.24E-04	0.000108		1.25E-03	0.000108		1.19E-03	0.000108
	3.30E-01			1.18E-04			2.07E-05			1.32E-06

T (°C)	P (bars)	a(H+)	pH	TotMix	log f(O2)	bornite (m)	deposited as b	bornite (g)	chalcopy (m)	chalcopy (g)	muscovit (m)	muscovit (g)	quartz (m)
300	116.34	3.33E-05	4.48	0.00E+00	-30.32	1.95E-05	0.00	9.79E-03	2.98E-05	5.46E-03	1.01E-07	4.01E-05	6.26E-07
295	93.49	2.83E-05	4.55	0.00E+00	-30.7	3.25E-06	14.48	1.63E-03			1.65E-07	6.56E-05	4.81E-04
290	81.41	2.64E-05	4.58	0.00E+00	-31.06	1.39E-06	20.68	6.99E-04			1.75E-07	6.97E-05	4.93E-04
285	73.08	2.61E-05	4.58	0.00E+00	-31.42	7.65E-07	24.09	3.84E-04			1.71E-07	6.81E-05	4.85E-04
280	66.45	2.66E-05	4.57	0.00E+00	-31.77	5.37E-07	26.48	2.69E-04			1.58E-07	6.28E-05	4.70E-04
275	60.78	2.77E-05	4.56	0.00E+00	-32.13	4.61E-07	28.53	2.31E-04			1.41E-07	5.60E-05	4.52E-04
270	55.74	2.92E-05	4.54	0.00E+00	-32.49	4.49E-07	30.53	2.25E-04			1.23E-07	4.90E-05	4.33E-04
265	51.19	3.09E-05	4.51	0.00E+00	-32.86	4.64E-07	32.59	2.33E-04			1.06E-07	4.24E-05	4.14E-04
260	47.02	3.28E-05	4.48	0.00E+00	-33.23	4.86E-07	34.76	2.44E-04			9.17E-08	3.65E-05	3.94E-04
255	43.18	3.49E-05	4.46	0.00E+00	-33.61	5.06E-07	37.01	2.54E-04			7.87E-08	3.14E-05	3.74E-04
250	39.62	3.71E-05	4.43	0.00E+00	-34	5.20E-07	39.33	2.61E-04			6.76E-08	2.69E-05	3.55E-04
245	36.32	3.94E-05	4.4	0.00E+00	-34.4	5.24E-07	41.66	2.63E-04			5.80E-08	2.31E-05	3.36E-04
240	33.26	4.18E-05	4.38	0.00E+00	-34.81	5.18E-07	43.96	2.60E-04			4.99E-08	1.99E-05	3.18E-04
235	30.41	4.43E-05	4.35	0.00E+00	-35.22	5.03E-07	46.20	2.52E-04			4.30E-08	1.71E-05	3.00E-04
230	27.77	4.68E-05	4.33	0.00E+00	-35.65	4.79E-07	48.33	2.40E-04			3.71E-08	1.48E-05	2.83E-04
225	25.31	4.93E-05	4.31	0.00E+00	-36.09	4.49E-07	50.33	2.25E-04			3.21E-08	1.28E-05	2.67E-04
220	23.02	5.18E-05	4.29	0.00E+00	-36.53	4.15E-07	52.18	2.08E-04			2.79E-08	1.11E-05	2.52E-04
215	20.91	5.43E-05	4.27	0.00E+00	-36.99	3.78E-07	53.86	1.90E-04			2.42E-08	9.66E-06	2.37E-04
210	18.94	5.67E-05	4.25	0.00E+00	-37.45	3.40E-07	55.38	1.71E-04			2.11E-08	8.42E-06	2.23E-04
205	17.12	5.91E-05	4.23	0.00E+00	-37.93	3.03E-07	56.73	1.52E-04			1.85E-08	7.36E-06	2.10E-04
200	15.44	6.14E-05	4.21	0.00E+00	-38.42	2.67E-07	57.91	1.34E-04			1.62E-08	6.44E-06	1.98E-04
195	13.89	6.36E-05	4.2	0.00E+00	-38.92	2.34E-07	58.96	1.17E-04			1.42E-08	5.65E-06	1.87E-04
190	12.47	6.58E-05	4.18	0.00E+00	-39.43	2.03E-07	59.86	1.02E-04			1.25E-08	4.97E-06	1.76E-04
185	11.15	6.80E-05	4.17	0.00E+00	-39.95	1.76E-07	60.65	8.83E-05			1.10E-08	4.37E-06	1.66E-04
180	9.95	7.01E-05	4.15	0.00E+00	-40.49	1.51E-07	61.32	7.60E-05			9.67E-09	3.85E-06	1.56E-04
175	8.85	7.21E-05	4.14	0.00E+00	-41.04	1.30E-07	61.90	6.50E-05			8.53E-09	3.40E-06	1.47E-04
170	7.85	7.41E-05	4.13	0.00E+00	-41.6	1.10E-07	62.39	5.54E-05			7.53E-09	3.00E-06	1.39E-04
165	6.93	7.60E-05	4.12	0.00E+00	-42.18	9.33E-08	62.80	4.68E-05			6.65E-09	2.65E-06	1.31E-04
160	6.1	7.79E-05	4.11	0.00E+00	-42.77	7.84E-08	63.15	3.93E-05			5.86E-09	2.33E-06	1.23E-04
155	5.35	7.98E-05	4.1	0.00E+00	-43.37	6.54E-08	63.44	3.28E-05			5.12E-09	2.04E-06	1.16E-04
150	4.68	8.18E-05	4.09	0.00E+00	-43.99	5.39E-08	63.68	2.70E-05			4.38E-09	1.74E-06	1.10E-04
145	4.07	8.38E-05	4.08	0.00E+00	-44.63	4.45E-08	63.88	2.23E-05			3.78E-09	1.51E-06	1.03E-04
140	3.53	8.57E-05	4.07	0.00E+00	-45.28	3.65E-08	64.04	1.83E-05			3.20E-09	1.27E-06	9.75E-05
135	3.04	8.77E-05	4.06	0.00E+00	-45.95	2.97E-08	64.18	1.49E-05			2.60E-09	1.04E-06	9.17E-05
130	2.61	8.96E-05	4.05	0.00E+00	-46.64	2.40E-08	64.28	1.20E-05			1.95E-09	7.78E-07	8.63E-05
125	2.23	9.16E-05	4.04	0.00E+00	-47.34	1.93E-08	64.37	9.67E-06			1.22E-09	4.85E-07	8.11E-05
120	1.9	9.36E-05	4.03	0.00E+00	-48.06	1.54E-08	64.44	7.72E-06			3.32E-10	1.32E-07	7.61E-05
115	1.6	9.56E-05	4.02	0.00E+00	-48.81	1.22E-08	64.49	6.13E-06					7.13E-05
110	1.35	9.77E-05	4.01	0.00E+00	-49.57	9.64E-09	64.53	4.84E-06					6.66E-05
105	1.13	9.98E-05	4	0.00E+00	-50.35	7.57E-09	64.57	3.80E-06					6.22E-05
100	0.94	1.02E-04	3.99	0.00E+00	-51.16	5.93E-09	64.59	2.98E-06					5.78E-05

Simulation 11 - boiling of Fluid 1 as it is cooled to 100 degrees C

	quartz (g)	barite (m)	deposited as	barite (g)	gold (m)	Cl2 deposited	gold (g)	acanthit (m)	deposited as a	acanthit (g)
0.01	3.76E-05		0.00			0.00				
4.94	2.89E-02		0.00			0.00				
9.99	2.96E-02	7.41E-06	0.52	1.73E-03		0.00				
14.96	2.91E-02	5.75E-06	0.93	1.34E-03		0.00				
19.78	2.82E-02	4.26E-06	1.23	9.94E-04		0.00				
24.41	2.72E-02	3.23E-06	1.45	7.53E-04		0.00				
28.85	2.60E-02	2.47E-06	1.63	5.76E-04	5.39E-10	8.93	1.06E-07			
33.09	2.49E-02	1.90E-06	1.76	4.43E-04	1.01E-09	25.69	1.99E-07			
37.13	2.37E-02	1.46E-06	1.86	3.41E-04	7.36E-10	37.89	1.45E-07			
40.96	2.25E-02	1.12E-06	1.94	2.62E-04	5.45E-10	46.93	1.07E-07			
44.60	2.13E-02	8.62E-07	2.00	2.01E-04	4.08E-10	53.69	8.04E-08			
48.04	2.02E-02	6.64E-07	2.05	1.55E-04	3.09E-10	58.81	6.08E-08			
51.29	1.91E-02	5.16E-07	2.09	1.20E-04	2.36E-10	62.72	4.64E-08			
54.37	1.80E-02	4.08E-07	2.11	9.52E-05	1.81E-10	65.73	3.57E-08			
57.27	1.70E-02	3.32E-07	2.14	7.76E-05	1.40E-10	68.05	2.76E-08			
60.00	1.60E-02	2.83E-07	2.16	6.61E-05	1.09E-10	69.86	2.14E-08			
62.58	1.51E-02	2.55E-07	2.18	5.95E-05	8.50E-11	71.27	1.67E-08			
65.01	1.42E-02	2.44E-07	2.19	5.69E-05	6.66E-11	72.37	1.31E-08			
67.30	1.34E-02	2.47E-07	2.21	5.76E-05	5.23E-11	73.24	1.03E-08			
69.46	1.26E-02	2.62E-07	2.23	6.12E-05	4.12E-11	73.92	8.12E-09			
71.49	1.19E-02	2.88E-07	2.25	6.73E-05	3.26E-11	74.46	6.41E-09			
73.40	1.12E-02	3.24E-07	2.27	7.56E-05	2.57E-11	74.89	5.07E-09			
75.21	1.06E-02	3.69E-07	2.30	8.61E-05	2.04E-11	75.23	4.01E-09			
76.91	9.96E-03	4.23E-07	2.33	9.86E-05	1.61E-11	75.49	3.18E-09			
78.51	9.39E-03	4.84E-07	2.36	1.13E-04	1.28E-11	75.71	2.52E-09			
80.02	8.85E-03	5.54E-07	2.40	1.29E-04	1.01E-11	75.87	1.99E-09			
81.44	8.34E-03	6.31E-07	2.44	1.47E-04	7.98E-12	76.01	1.57E-09			
82.78	7.87E-03	7.14E-07	2.49	1.67E-04	6.29E-12	76.11	1.24E-09			
84.05	7.42E-03	8.02E-07	2.55	1.87E-04	4.94E-12	76.19	9.73E-10			
85.24	7.00E-03	8.93E-07	2.61	2.08E-04	3.87E-12	76.26	7.62E-10	1.84E-08	3.71	4.56E-06
86.37	6.60E-03	9.79E-07	2.68	2.29E-04	3.03E-12	76.31	5.96E-10	9.82E-08	23.51	2.43E-05
87.43	6.22E-03	1.08E-06	2.76	2.51E-04	2.34E-12	76.34	4.61E-10	7.92E-08	39.49	1.96E-05
88.43	5.86E-03	1.17E-06	2.84	2.74E-04	1.80E-12	76.37	3.55E-10	6.37E-08	52.34	1.58E-05
89.37	5.51E-03	1.27E-06	2.93	2.95E-04	1.38E-12	76.40	2.72E-10	5.10E-08	62.62	1.26E-05
90.25	5.18E-03	1.35E-06	3.03	3.16E-04	1.05E-12	76.41	2.07E-10	4.06E-08	70.81	1.01E-05
91.08	4.87E-03	1.43E-06	3.13	3.34E-04	7.93E-13	76.43	1.56E-10	3.23E-08	77.32	8.00E-06
91.86	4.57E-03	1.50E-06	3.23	3.50E-04	5.93E-13	76.44	1.17E-10	2.56E-08	82.48	6.33E-06
92.59	4.28E-03	1.55E-06	3.34	3.63E-04	4.40E-13	76.45	8.67E-11	2.02E-08	86.54	4.99E-06
93.27	4.00E-03	1.60E-06	3.45	3.72E-04	3.23E-13	76.45	6.37E-11	1.58E-08	89.74	3.93E-06
93.91	3.73E-03	1.62E-06	3.57	3.79E-04	2.35E-13	76.45	4.63E-11	1.24E-08	92.24	3.08E-06
94.50	3.48E-03	1.63E-06	3.68	3.81E-04	1.69E-13	76.46	3.33E-11	9.70E-09	94.20	2.40E-06